



HAL
open science

Multiscale investigation of caking phenomenon of lactose powders : from physico-chemical aspects to industrial applications

Zahra Afrassiabian

► To cite this version:

Zahra Afrassiabian. Multiscale investigation of caking phenomenon of lactose powders : from physico-chemical aspects to industrial applications. Theoretical and/or physical chemistry. Université de Technologie de Compiègne, 2019. English. NNT : 2019COMP2475 . tel-02182904

HAL Id: tel-02182904

<https://theses.hal.science/tel-02182904>

Submitted on 13 Jul 2019

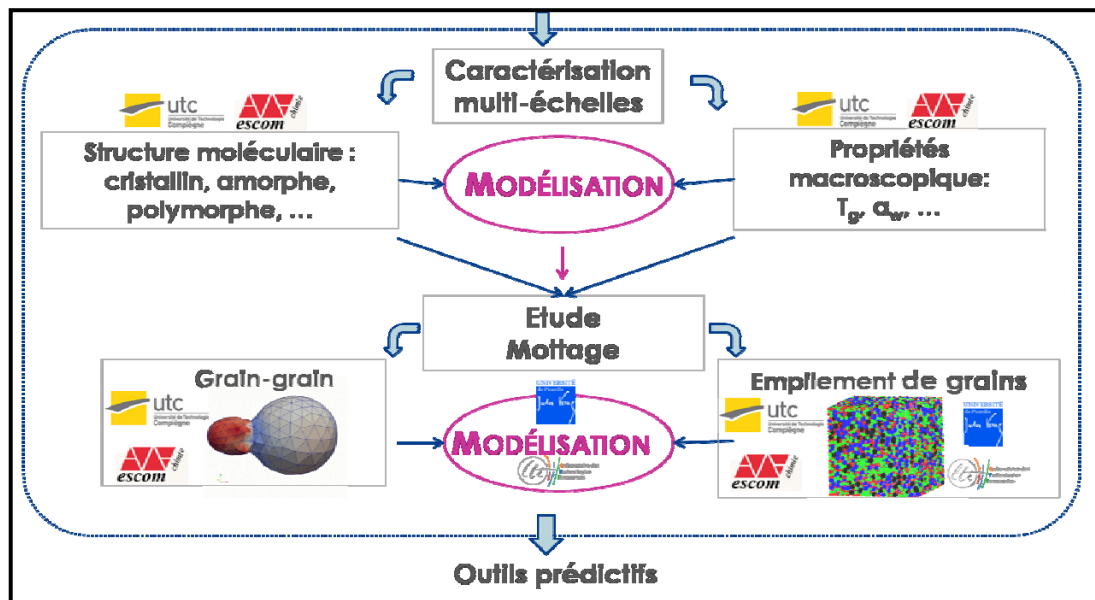
HAL is a multi-disciplinary open access archive for the deposit and dissemination of scientific research documents, whether they are published or not. The documents may come from teaching and research institutions in France or abroad, or from public or private research centers.

L'archive ouverte pluridisciplinaire **HAL**, est destinée au dépôt et à la diffusion de documents scientifiques de niveau recherche, publiés ou non, émanant des établissements d'enseignement et de recherche français ou étrangers, des laboratoires publics ou privés.

Par Zahra AFRASSIABIAN

Multiscale investigation of caking phenomenon of lactose powders: from physico-chemical aspects to industrial applications

Thèse présentée
 pour l'obtention du grade
 de Docteur de l'UTC



Soutenue le 13 mars 2019

Spécialité : Génie des Procédés Industriels : Transformations intégrées de la matière renouvelable (EA-4297)

D2475

MULTISCALE INVESTIGATION OF CAKING PHENOMENON OF LACTOSE
POWDERS: FROM PHYSICO-CHEMICAL ASPECTS TO INDUSTRIAL
APPLICATIONS

ETUDE MULTI-ECHELLES DU PHENOMENE DE MOTTAGE DES POUDRES
DU LACTOSE : DE LA PHYSICO-CHIMIE DES MATERIAUX AUX
APPLICATIONS INDUSTRIELLES

THESE

présentée et soutenue publiquement le 13 mars 2019
pour l'obtention du

Doctorat en Sciences de l'Ingénieur

Spécialité : Génie des Procédés Industriels

par

Zahra AFRASSIABIAN

Devant le jury composé de :

Professeur Pierre TCHORELOFF, Université de Bordeaux	(rapporteur)
Docteur Christelle TURCHIULI, Agroparistech, Massy	(rapporteur)
Docteur Erwann GUENIN, Université de Technologie de Compiègne	(examineur)
Docteur Hervé MUHR, Université de Lorraine, Nancy	(examineur)
Docteur Willy LECLERC, LTI-UPJV, Amiens	(membre invité)
Docteur Mohammed BENALI, Université de Technologie de Compiègne	(co-directeur de thèse)
Professeur Mohammed GUESSASMA, LTI-UPJV, Amiens	(co-directeur de thèse)
Professeur Khashayar SALEH, Université de Technologie de Compiègne	(directeur de thèse)

Acknowledgment

This work has been carried out in the laboratory TIMR-EA 4297; within the framework of the "Mottamorph" project, led by Professor Saleh and financed by région HdF and FEDER.

This doctoral thesis is in its current form due to the assistance and encouragement of several people.

It is a pleasure to express my sincere thanks to all those who helped me for the success of this study and made it an unforgettable experience. I would like to express my special appreciation and thanks to my advisor Professor Khashayar SALEH, you have been a tremendous mentor for me. I would like to thank you for encouraging my research and for allowing me to grow as a research scientist.

I would also like to thank my co-directors professor Mohammed GUESSASMA and doctor Mohammed BENALI and my committee members, professor Pierre TOCHORELOFF, doctor Christelle TURCHIULI, doctor Erwann GUENIN, doctor Hervé MUHR, doctor Willy LECLERC and all for serving as my committee members even at hardship. I would like also to thank you for letting my defense be an enjoyable moment, and for your brilliant comments and suggestions.

I would like to thank all people in our laboratory for their all support and kindness, especially, Veronique, Qi, Lorine, and my best friend Narges.

I express my sincere thanks to my dearest parents for all blessing, love, confidence, encouragement, affection and kindness during my study and my whole life. Without the inspiration, drive, and sustained support that you have given me, I might not be the person I am today

I am extremely fortunate to have such amazing, caring and loving family, parents, sisters, brothers, and nieces in my life.

Table of contents

General Introduction	1
Chapter I: Literature Survey	9
I.1 Introduction	10
I.2 Powders, characteristics and behavior	10
I.3 Interparticle forces within granular media	11
I.4 Classification and Mechanisms of caking	15
I.4.1 Mechanical (Pressure induced) caking	16
I.4.2 Wet (Relative Humidity induced) caking	17
I.4.2.1 Capillary condensation	19
I.4.2.2 Pendular capillary (liquid bridge) forces	21
I.4.2.3 Insoluble powders	22
I.4.2.4 Non deliquescent water soluble powders	23
I.4.2.5 Deliquescent powders	23
I.4.3 Thermal (temperature induced) caking	30
I.4.4 Chemical (reaction induced) caking (phase transition)	34
I.5 Caking testing methods	36
I.6 Molecular structure of materials in relation with caking	37
I.6.1 Polymorphism	38
I.6.2 Phase and phase transitions in materials	38
I.6.2.1 Amorphous structure	41
I.6.2.2 Semi-crystalline structure	41
I.6.2.3 Crystalline structure	41
I.6.3 Phase Transitions	42
I.6.3.1 First-order transition	43
I.6.3.2 Second-order transition	43
I.6.3.3 Glass Transition Phenomenon	44
I.6.4 Rheology of amorphous materials	52
I.6.4.1 Glass transition, rheology and stickiness of powders	53

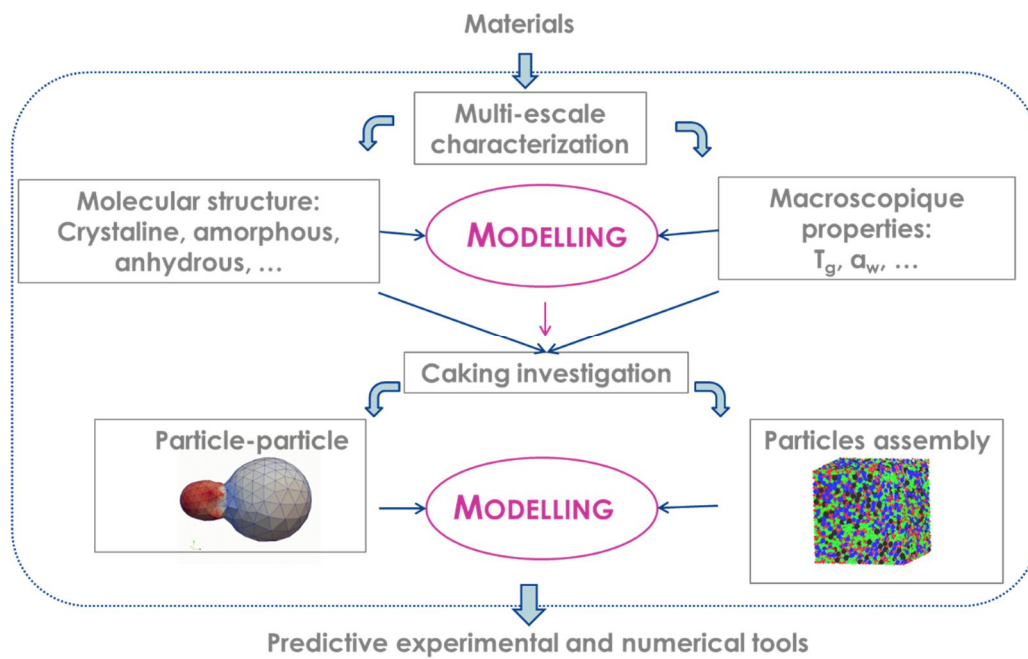
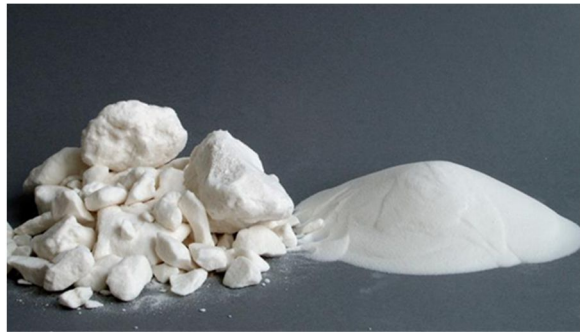
I.7	Lactose	55
I.7.1	Lactose, structure, properties and characterization	55
I.7.1.1	Lactose molecule	56
I.7.1.2	Lactose in binary aqueous solutions	56
I.7.1.3	Solid forms of lactose	58
I.7.1.4	Lactose solubility in water	62
I.7.1.5	Lactose crystallization and crystallization rate	65
I.7.1.6	Glass Transition Temperature	67
I.7.2	State diagram of lactose	67
I.8	Conclusion	69
	References	70
 Chapter II: Materials & Methods		75
II.1	Introduction	76
II.2	Analytical Techniques	76
II.2.1	ESEM images	76
II.2.2	Particle size analysis	76
	II.2.2.1 Laser granulometry	76
	II.2.2.2 Morpho-granulometry analysis	78
II.2.3	Density measurements	79
II.2.4	Specific surface area measurements	80
II.2.5	Differential Scanning Calorimetry (DSC)	82
II.2.6	Dynamic Vapor Sorption	83
	II.2.6.1 Dynamic vapor sorption from SMS	83
	II.2.6.2 SPS instrument from ProUmid	83
II.2.7	X-ray Diffraction	84
II.3	Caking experiments	85
II.3.1	Closed-loop air flow (CLAIR) caking device	86
II.3.2	Open-loop air flow (OLAF) caking device	87
II.3.3	Caking cells and preparation of samples	89
II.3.4	Post-caking analysis	90

II.3.4.1	Mechanical resistance tests	90
II.3.4.2	Sieving testing method	91
II.4	Lactose samples	92
II.4.1	Monohydrate lactose powders	92
II.4.2	Anhydrous lactose powder	92
II.4.3	Amorphous lactose samples	93
II.4.3.1	Freeze drying	94
II.4.3.2	Spray drying	95
II.5	Conclusion	96
	References	97
 Chapter III: The role of amorphous amount in caking of Monohydrate Lactose		99
III.1	Introduction	100
III.2	Materials and methods	107
III.3	Results and discussion	108
III.3.1	Sample characterization	108
III.3.2	Water sorption and crystallization kinetics	110
III.3.3	Caking experiments	117
III.3.3.1	Preliminary experiments in CLAIR caking Device	117
III.3.3.2	Choice of a proper yield strength test	119
III.3.3.3	Influencing parameters	121
III.3.3.4	Parametric study of caking using OLAF caking Device	126
III.4	Conclusion	129
	References	131
 Chapter IV: Caking of anhydrous Lactose powder under humid conditions		135
IV.1	Introduction	136
IV.2	Materials and methods	137
IV.2.1	Raw materials and physical properties	137
IV.2.2	Thermal Analyses: Differential Scanning Calorimetry	139
IV.2.3	X-ray Diffraction	140

IV.2.4	Specific surface analysis by gas adsorption (BET)	141
IV.2.5	Dynamic Vapor Sorption	141
IV.3	Kinetic study of hydration, crystallization and dehydration of anhydrous lactose	143
IV.3.1	Dynamic water vapor sorption experiments	143
IV.3.2	Typical example of hydration kinetics	144
IV.3.3	Effect of the particle size	149
IV.3.4	Effect of the relative humidity	150
IV.3.5	Effect of temperature	153
IV.4	Caking experiments	157
IV.4.1	Experimental results and discussion	157
	IV.4.1.1 Preliminary experiments in CLAIR caking Device	157
	IV.4.1.2 Kinetic study of caking	160
IV.5	Conclusion	165
	References	166
 Chapter V: Phenomenological modelling and Numerical simulation of mechanical resistance of caked powders		169
V.1	Introduction	170
V.2	"Grain-bulk" model of capillary condensation within a granular medium	173
V.2.1	Binary contact	174
V.2.2	Influencing parameters	178
	V.2.2.1 Binary agglomerate	179
	V.2.2.2 Assembly of particles	184
V.2.3	Partial conclusions on "grain-bulk" model	188
V.3	Discrete Element Method (DEM)	190
V.3.1	DEM simulation of mechanical strength of cakes due to capillary (liquid) and solid bridges	190
V.3.2	Discrete simulations of capillary effects at a REV scale	194
V.3.3	Modeling of densification on regular packings under the effect of capillary bridges	195
V.3.4	Mechanical behavior of powder compacts in the presence of capillary bridges	196

V.3.5	Mechanical behavior of powder compacts in the presence of solid bridges	199
	V.3.5.1 Calibration of beam properties and stress state at particle scale	200
	V.3.5.2 Brazilian test	202
	V.3.5.3 Shear test	203
V.4	Conclusion	204
	References	206
	General conclusions and perspectives	209

General Introduction



Powdered products are a significant part of finished or intermediate products encountered in the various industrial sectors. Their economic importance is undeniable and has been growing steadily for many years. Indeed, nowadays it is an obvious fact that powders are omnipresent in our daily lives. This ubiquity results, certainly, from the fact that many of these products are originally in divided form, but mainly because of the advantages that an implementation in powder form presents in terms of [1, 2]:

- Handling, transport and storage
- Reduced deterioration and phytosanitary risks due to lack of water
- Reduction of the volumes to be treated

The industrial context of the powdery products sector is tightly connected to the key factors that govern the chemical industry in general. In fact, faced with an increasingly competitive global context and, in order to maintain its leadership over emerging competitors, the chemical industry in all industrial countries has been forced to progressively integrate a quality approach based on customer satisfaction and the development of innovative products with higher added-value. Nowadays, these products must be more elaborated, more functional and, sometimes, more fanciful. For example, a milk powder must have good physical, chemical and biological stability, good flowability, adequate organoleptic and nutritional properties, good reconstitution ability, *etc.*

However, despite the numerous benefits of powders, their handling and storage often cause some severe problems (*i.e.*, explosion, clogging, dust generation, *etc.*). This could lead to a destruction of products and even their corresponding manufacturing units or to deterioration of the expected functionalities of products. Among these issues, caking is undoubtedly one of the most important. Generally speaking, caking corresponds to spontaneous and undesired formation of a coherent mass from individual grains. This unwanted agglomeration of particles of a powder, illustrated in [Figure 1](#), is often irreversible and difficult to predict.



Figure 1 : Illustration of caking

Caking is a common root of many problems encountered when handling powders and can lead to spurious shutdowns, client's claims and product recycling/rejection due to clogging of conveying lines, feeding devices and storage silos. From a product quality point of view, caked products have a penalizing appearance and a poor flowability. In addition to these problems related to the appearance and handling of powders, caking leads, in most cases, to a degradation of the end-use properties of powders. In this case, the powder responds no longer to the product/process specifications, becomes unusable, and is returned by customers, sometimes by whole cargoes.

Caking phenomenon occurs as a result of formation of material bonds at the points of contact between particles. These links, whose fundamental mechanisms of appearance are still poorly understood, are reinforced by pressure, the migration of matter and variations in humidity and temperature. In addition to the problems caused by the recycling of degraded products (if however this is possible), the negative impacts of these incidents can be significant. The costs related to the caking can sometimes be important when the destruction of the product is unavoidable, and much more if one also takes into account the assumption of the expenses of the recovery of the incriminated product.

However, the solutions proposed to avoid caking are far from satisfactory and have a rather curative character (sieving, crumbling, declogging, *etc.*). The rare preventive actions require the implementation of complex formulations based on anti-caking agents. In addition to the direct costs related to the purchase of these additives, these solutions require the implementation of additional operations (storage, transport, mixing, coating, *etc.*) as well as a preliminary development step to optimize the proposed formulation. Moreover, depending on the nature of the products used and the target sector, these solutions are not always

applicable or require a phase of homologation, often very long and expensive (*e.g.* food, phytosanitary or pharmaceutical products).

This situation is essentially due to the fact that the theoretical aspects of the physicochemical phenomena occurring during the caking of the powders have not yet been completely elucidated. However, this knowledge is essential to bring reasoned, rational and sustainable solutions to this problem.

Caking is usually induced by one or more of the following factors:

- increase in pressure
- increase in temperature beyond the melting temperature or the softening temperature of materials
- presence of moisture in the granular medium

Although the presence of water, in one form or another, affects considerably the caking process, the underlying elementary mechanisms of caking may be substantially different: capillary condensation, dissolution/recrystallization, deliquescence/efflorescence, phase transition, *etc.* Indeed, for crystalline powders, the process of formation of agglomerates has been the subject of much research. The research carried out within the IMid group of the TIMR laboratory has significantly contributed to a better understanding of the intimate phenomena of caking and have made it possible to improve the means of combating this phenomenon [3-13]. On the other hand, only few studies have been conducted on the caking due to phase transition *i.e.* amorphous to crystalline or crystalline to crystalline transformations.

This PhD thesis is part of a multi-partner project, entitled Motamorph, including TIMR laboratory of UTC, LTI laboratory of UPJV and Momentive Company (became Synthomer recently). The project focuses on the fundamental problem of powder caking due to phase transition mechanisms. The project, was funded by the Région Picardie and FEDER (Fonds Européen de Développement Régional).

The project aims to study the caking of powders due to phase transition of polymorphic materials. The objectives of the study are to:

- Understand and highlight the fundamental mechanisms behind caking
- Model the process of caking at the micro, meso and macroscopic scale
- Establish predictive tools (laboratory tests and/or mathematical and numerical models) to describe the caking behavior of powders
- Propose preventive solutions according to the physicochemical properties of materials, their compositions and the conditions of their storage.

More generally, the project aims to study the impact of intrinsic factors (molecular structure of materials, physical and/or physicochemical properties, *etc.*) or environmental factors (storage conditions or process parameters) on the stability of the structure of powders. The scientific knowledge developed in this project must help to control and preserve the quality of powders under optimal conditions during the manufacturing, storage and transport steps by acting judiciously on the possible levers for action: the formulation of the product, process parameters or storage conditions.

In this project, we propose a multi-scale study (micro, meso, macro) of the caking process of polymorphic powders based on a coupling of experimental study and modelling of the phenomena. Two categories of powders have been used: several forms of lactose as a model product and several types of real industrial products. However, only the results relative to lactose are presented in this report.

The thesis includes 5 chapters:

- Chapter I provides first a literature review on the general aspects involved in caking. It focuses then on some more specific aspects such as caking mechanisms, interparticle forces and caking tests. Special attention is paid to lactose, used as the main support of our study, and its properties.
- The second chapter presents the material and methods used in this work. This concerns both classical analysis and characterization techniques and experimental installations, specially designed and implemented for the caking study in our laboratory.

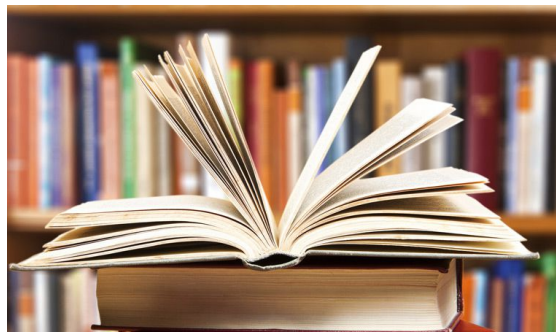
- In the third chapter, the results of an experimental study on caking of lactose monohydrate powders containing varying amounts of amorphous lactose are presented and commented. The role of operating conditions and the main mechanisms of caking are presented.
- The fourth chapter presents the results of an investigation on the caking of anhydrous lactose powders. Experiments were conducted to establish kinetics data for the main mechanism of caking, which was found to be anhydrous lactose crystallization.
- The last chapter deals with modelling and simulation of the mechanical strength of cakes. This chapter includes two sections. In the first section, a phenomenological model based on the fundamental laws of Kelvin and Laplace is presented. The model is used to study the tensile strength of wet cakes due to capillary condensation phenomenon. In the second section, the mechanical resistance (yield, tensile and shear strengths) of wet and dry compacts was simulated by Discrete Element Method.

References

1. Saleh, K. and P. Guigon, *Caractérisation et analyse des poudres Propriétés physiques des solides divisés*. Techniques de l'ingénieur Principes de formulation, 2009. **base documentaire : TIB489DUO**(ref. article : j2251).
2. Saleh, K. and P. Guigon, *Caractérisation et analyse des poudres Propriétés comportementales des solides divisés*. Techniques de l'ingénieur Principes de formulation, 2009. **base documentaire : TIB489DUO**(ref. article : j2252).
3. Rondeau, X., *Processus Physicochimiques intervenant dans le phénomène de mottage de solides divisés*. 2000, Université de Technologie de Compiègne. p. 259.
4. Affolter, C., *Etude des modes d'action d'additifs sur les phénomènes de dissolution et de cristallisation de sels hygroscopiques : application au mottage du nitrate d'ammonium*. 2003, Université de Technologie de Compiègne.
5. Rondeau, X., C. Affolter, L. Komunjer, D. Clause and P. Guigon, *Experimental determination of capillary forces by crushing strength measurements*. Powder Technology, 2003. **130**(1): p. 124-131.
6. Komunjer, L. and C. Affolter, *Absorption–evaporation kinetics of water vapor on highly hygroscopic powder: Case of ammonium nitrate*. Powder Technology, 2005. **157**(1): p. 67-71.
7. Dupas-Langlet, M., *De la déliquescence au mottage des poudres cristallines: cas du chlorure de sodium*. 2013, Université de Technologie de Compiègne. p. 226.
8. Dupas-Langlet, M., M. Benali, I. Pezron, K. Saleh and L. Metlas-Komunjer, *Deliquescence lowering in mixtures of NaCl and sucrose powders elucidated by modeling the water activity of corresponding solutions*. Journal of Food Engineering, 2013. **115**(3): p. 391-397.

9. Dupas-Langlet, M., M. Benali, I. Pezron, K. Saleh and L. Metlas-Komunjer, *The impact of deliquescence lowering on the caking of powder mixtures*. Powder Technology, 2015. **270**, Part B: p. 502-509.
10. Dupas-Langlet, M., M. Benali, I. Pezron and K. Saleh, *Characterization of saturated solutions and establishment of "aw-phase diagram" of ternary aqueous inorganic-organic and organic-organic systems*. Journal of Food Engineering, 2017. **201**: p. 42-48.
11. Samain, S., M. Dupas-Langlet, M. Leturia, M. Benali and K. Saleh, *Caking of sucrose: Elucidation of the drying kinetics according to the relative humidity by considering external and internal mass transfer*. Journal of Food Engineering, 2017. **212**: p. 298-308.
12. Samain, S., *Caractérisation multi-échelle de l'efflorescence et du mottage du saccharose*, in *Génie des Procédés Industriels*. 2018, Université de Technologie de Compiègne: Compiègne, France.
13. Samain, S., M. Leturia, S. Mottelet, M. Benali and K. Saleh, *Characterization of caking for crystalline materials: comparison and statistical analysis of three mechanical tests*. Chemical Engineering Science, 2018.

Chapter 1: Literature Survey



Caking arises from physico-chemical interactions taking place in micro or meso-scale at particles surface or contact points between particles. The main cause of caking is the appearance of attractive forces following these interactions. In this chapter, we present the principal forces as well as the main mechanisms responsible for caking.

1 Introduction

Whether crystalline or amorphous, it is proven that caking of granular materials results from variations in environmental conditions, in particular those of temperature and relative humidity (the two parameters being linked elsewhere). These parameters vary with the weather (day/night, summer/winter) and the geographical location where the product is stored and transported. These variations are sometimes significant and can largely exceed the limit conditions necessary for a good conservation of the product (*e.g.*, the critical relative humidity of deliquescence, DRH, or the glass transition temperature, T_g).

However, beyond these macroscopic and general aspects, the elementary mechanisms underlying the caking phenomenon differ substantially according to the physical properties (*e.g.*, particles shape and size distribution), the molecular structure and, in particular, the solubility and the crystallinity of materials.

This section aims to introduce the main powder characteristics and the basic mechanisms responsible for caking of powders.

2 Powders, characteristics and behavior

A powder is an assembly of heterogeneous solid particles dispersed in a continuous gaseous phase between which a multitude of interactions exist (van der Waals, capillaries, electrostatic, *etc.*). The overall behavior of a powder depends directly on these interactions and the characteristics of the solid particles. Thus, the characterization of a particulate system includes three levels [1, 2]:

- The intrinsic characteristics of particles (size, density, shape, porosity, hygroscopicity, softening point, *etc.*);
- The properties related to a population of particles (size distribution, bulk density, homogeneity, *etc.*);
- Behavioral properties that reflect, globally and macroscopically, the existing interactions within the particulate medium or between the

powder particles and their environment. These are therefore collective characters translating the behavior of the powder in various circumstances and/or environments. The caking ability of powders can be classified in this category.

Many reference works have described the properties of the first two categories of properties (*e.g.*, [3-5]). In this part, we focus on the properties and mechanisms directly related to the caking phenomenon, such as the origin of forces and the thermodynamic aspects of this process.

3 Interparticle forces within granular media

The caking phenomenon occurs when the interparticle adhesion forces are predominant forces within granular media. According to Rumpf [6], the presence or absence of material bridges can be considered as the overriding criterion for classifying these forces. Accordingly, forces that can cause the coalescence of particles can be divided into two families: forces existing in the absence of material bridges and forces including material bridges.

The formation of non-material agglomerates can be attributed to four categories of forces:

- The forces of entanglement and mechanical attachment. This type of bond is observed when using excipients with particular structures (filamentous or fibrous structure).
- The attractive forces of van der Waals type. These forces of electromagnetic origin are omnipresent. On the other hand, their field of action is restricted. The particles must be closely spaced (<50 nm) and very small (<100 μm), so that the intermolecular forces can prevail against the gravity.

Van der Waals forces arises from intermolecular forces (dipole/dipole, dipole/non-polar and non-polar/non-polar) exerting at molecular scale. The mean van der Waals force between macroscopic bodies could be obtained by integrating the pair potentials over the contact surface. For two unequal-sized spherical particles, with radius R_1 and R_2 , the van der Waals forces are given by [7]:

$$F_{vdw} = \frac{C}{8\pi Z^2} \left(\frac{R_1 \cdot R_2}{R_1 + R_2} \right) \quad (I-1)$$

where C is the so-called Hamaker constant and Z is the gap between particles.

- Electrostatic forces. They usually exist in systems where particles are in motion. They appear when electrostatic charges are present. The particles in contact create a potential of contact, which generates the electrostatic forces. The importance of these forces decreases sharply with increasing temperature or ambient humidity.
- Magnetic forces. These forces intervene only when using metallic and magnetic powders.

As for the forces with material links, they are also divided into four categories:

- Adhesion forces in static or liquid bridges with restricted mobility. These forces are due to the presence of adsorbed layers on the particles surface. These are mono or multi-molecular layers of the liquid strongly bonded to the surface by van der Waals forces. In this case, the activity of the adsorbed liquid, which represents the ratio between the liquid vapor pressure in equilibrium with the solid and its vapor pressure, is less than 0.4 and the binding energy is high.
- Interfacial forces and capillary pressure on mobile liquid bridges. In wet granulation, the tensile strength of the granule depends on the quantity of liquid present in the interparticle space of the particle cluster, *i.e.* the degree of saturation. The latter is defined as the volume fraction of the interstitial space of the granule occupied by the liquid phase. The extent of capillary forces in these different states will be detailed later (section §4).
- Adhesion forces due to solid bridges. Solid bridges are formed by crystallization or by drying of dissolved substance present in liquid bridges. Little attention has been paid to the theoretical description of solid bridges, and in most cases the importance of these forces is estimated experimentally. However, the

formation of this type of bond depends primarily on the strength and stability of liquid bridges. Since solid bridges have a much higher strength, if the liquid bridges are strong enough to withstand the breaking forces of the medium, so will solid bridges.

- Adhesion forces due to sintered bridges. These bridges result from creep or partial melting of the solid handled on its surface during high temperature operations. In general, a temperature above the glass transition temperature and/or 60% of the melting point of particles must be attained. This type of bond, which is considered to be responsible for the caking of amorphous products, leads to the formation of very resistant agglomerates.

Seville *et al.* [8] provided a review on interparticle forces and discussed the relative importance of above-mentioned forces. Corresponding theoretical curves are presented in [Figure I-1](#). Theoretically, both van der Waals and capillary forces increase with the square of particle size. On the other hand, the gravity force, which is considered as the main force of rupture, increases with the particles volume, then, with the cube of the particle size. The intersection between attractive forces and disruptive (gravity) forces corresponds to the size limit from which the attraction forces are no longer sufficient to ensure the cohesion of a binary agglomerate. According to this diagram, for the van der Waals forces, this theoretical limit is around 1000 μm . However, this conclusion contrasts with the experimental observations, which show that beyond a size of about 100 μm , the cohesion of powders becomes negligible: “Particles of 100- μm sizes are commonly found adhering to surfaces and resisting the force of gravity; 1-mm particles are not!” as stated by Seville *et al.* [8]. In order to explain this contradiction, Seville *et al.* suggested that the importance of that intermolecular forces depends more on the particle surface properties than on the mean particle size. Therefore, it may be more plausible to use the size of asperities and the surface roughness to determine the local curvature at contact points ([Figure I-2](#)). The van der Waals forces then depend on this local curvature and are independent of R. The resulting curves obtained by applying this hypothesis are also plotted in [Figure I-1](#) (dashed lines), and suggests, for the set of variables chosen by these authors, that spherical particles of diameter of order 100 μm should exhibit interparticle van der Waals forces to equal their single particle weight.

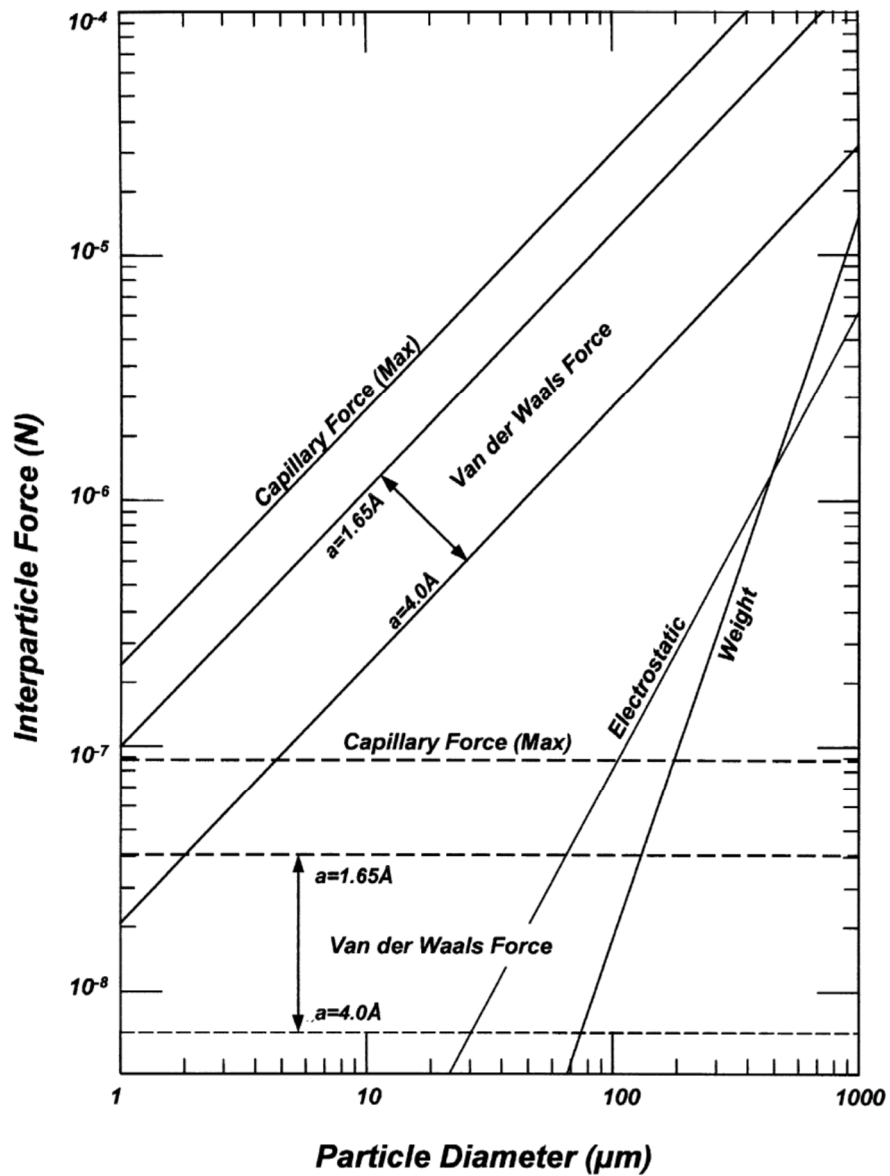


Figure I-1: Comparison of the theoretical magnitude of interparticle forces for single-point contact between equal spheres in air, with particle weight plotted for comparison (Seville *et al.* [8])

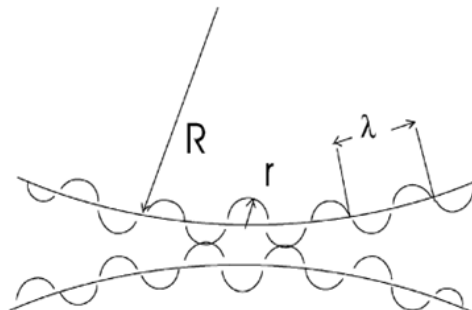


Figure I-2: A schematic drawing of two rough-surfaced particles in contact

4 Classification and Mechanisms of caking

Many investigations, rather recent, focused on the phenomenon of caking. The main caking mechanisms have been the subject of several bibliographical reviews. In his book entitled "Cake formation in particulate systems", Griffith [9] gave a rather qualitative description of these mechanisms. He distinguished four main classes of caking based on the involved binding forces, namely: mechanical caking, plastic flow caking, chemical caking and electrical caking. Cleaver also provided an overview of the responsible mechanisms of powder caking [10]. More recently, Zafar *et al.* [11] established a review on the caking of powders synthesizing more than one hundred works on this subject. More specifically, Hartmann and Palzer [12] focused on the caking of amorphous powders. They described the dynamics of the process based on a plastic creep of amorphous materials beyond their glass transition temperature. Finally, in a recent work, *Carpin et al.* [13] drew up a critical review on the caking of lactose.

A synthesis of these studies shows that it is difficult to establish a universal classification for the different types of caking. Indeed, the caking phenomenon is multi-dimensional and can be seen according to different criteria:

- The nature of the materials concerned, which may be amorphous, polymorphous, semi-crystalline, crystalline, *etc.*
- The interparticle forces that are at the origin of the particles agglomeration. Several forces can be present together in the granular medium; it is to identify the main force.
- The initiating factors of caking (pressure, relative humidity, temperature). However, it is important to distinguish between the main factor and other influencing factors. For example, in the case of a hygroscopic product, the main factor initiating the caking is the relative humidity and the temperature come in play through its effect on RH. On the other hand, in the case of a plastic creep (as is the case of amorphous products), the main factor is the temperature and the humidity plays a role by its effect on the viscosity of the material. In this regard, it is important to highlight the special role of water. Generally, whatever the main mechanism of caking is, the presence of water either in vapor, liquid, adsorbed or absorbed state could largely accentuate the caking process.

However, this effect arises from processes that can be completely different by nature. For example, in the case of insoluble materials, caking occurs as a result of water condensation at contact points between particles whereas for amorphous materials, the presence of absorbed water decreases the glass transition temperature, T_g , at a level lower than the storage temperature, bringing the material to a rubbery state which is subject to caking [12, 14-17]. However, in this case, the process should not be considered as “wet” but as “thermal” caking. The water will then act as a plasticizer in case of amorphous materials, as a binder for insoluble solids or as a solvent for crystalline powders.

- The phenomenology of the process and the different steps involved (capillary condensation, dissolution/drying, deliquescence/efflorescence, fusion/solidification, *etc.*).

Other criteria exist but they are of lesser importance. In what follows, we establish our classification based on the main factor triggering the caking. This choice was made because this classification best corresponds to the nature of the materials used in the present study and to the results that will be presented in the following chapters.

4.1 Mechanical (Pressure induced) caking

This type of caking can be included in the broader category of caking in the absence of material bridges. In this case, the caking occurs following the rearrangement and consolidation of powder under pressure (weight, compression, *etc.*). The cohesion of the cake is ensured by the forces without material link, the most important of which are the van der Waals forces. This process is similar to the early stages of dry granulation in which the interparticle distance decreases and the number of contacts as well as the contact area between the particles increases. This results in a decrease in the void fraction and an increase in the cohesion of the powder (Figure I-3). However, the pressures involved are much lower than those exerted during dry granulation and the compaction and consolidation levels obtained are significantly lower. Only rearrangement and dense packing stages illustrated in Figure I-3 are present during dry caking.

Generally, any variable that affects van der Waals forces (gap, contact surface area) or number of contacts (*e.g.*, particle shape and size distribution, packing, pressure, deformability, roughness, *etc.*) plays a role on dry caking. Furthermore, environmental conditions (RH, T) or additional forces (*e.g.*, electrostatic or capillary) could accentuate the caking.

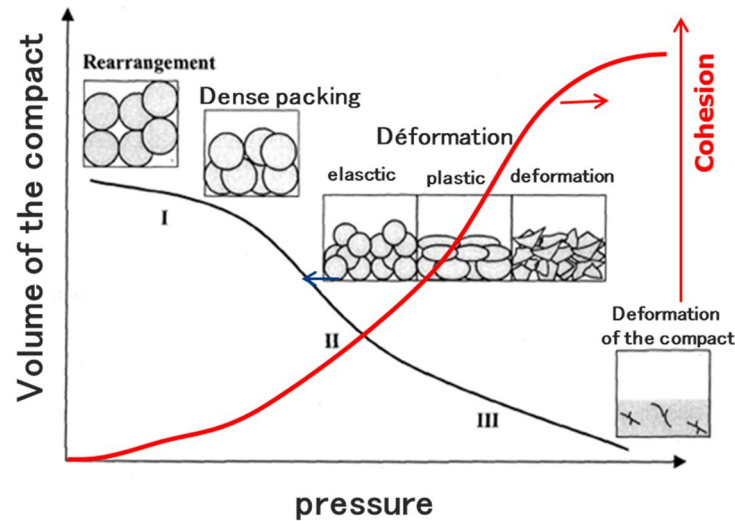


Figure I-3: Different stages of dry compaction

4.2 Wet (Relative Humidity induced) caking

This category includes all cases where moisture is directly involved in the process. They may appear due to formation of liquid bridges following to adsorption and capillary condensation phenomena, or the appearance of solid bridges following the dissolution and drying of the solid if the latter is hydrosoluble. In fact, the behavior of powders during their storage or their handling could be largely affected by the presence of water in vapor or liquid form. Particularly, the presence of water in adsorbed or condensed form could affect the flowability of powders and lead to caking.

The common basis of this kind of caking is water adsorption at the solids surface and capillary condensation. Indeed, like any vapor, the water vapor from the surrounding air could be fixed on the surface of particles by adsorption due to intermolecular interactions. The amount of adsorbed water in equilibrium with the relative humidity of air is given by the sorption isotherm, where the water content of solid is plotted against the water activity (*i.e.*

relative humidity at equilibrium). A typical example of a sorption isotherm is shown in [Figure I-4](#).

At low water activities (*i.e.* at early stages of adsorption - generally between 5%-40%) the solids surface is covered by a few layer of water molecules. This phase is characterized by a linear and slight increase in water sorption isotherm and can be modelled by classical BET or GAB models (for more details please refer to appendix A). Indeed, the amount of adsorbed water in this zone is low but even these small amounts of water could reinforce vdw forces because of strong interactions between water and solid molecules. However, as long as the adsorption takes place in this zone, the main caking mechanism remains similar to dry caking except that the extent of vdw forces are higher than for dry powder.

At higher water activities, water molecules become mobile enough to form liquid bridges. In addition, a capillary condensation phenomenon occurs leading to filling of small gaps at contact points between particles. In this zone, all spaces that could be considered as mesopores, (pore size < 50 nanometers) such as particle porosity and asperities are filled. A typical example of liquid bridge formation due to capillary condensation is shown in [Figure I-4](#).

Note that the presence of free liquid water and the subsequent capillary forces is the main cause of wet caking but its effect depends also on the wettability and solubility of powders. In what follows, we present, first, the theoretical basics of the capillary condensation and capillary forces. Then, the main mechanisms of wet caking for different types of particles are described. Three categories of solids in the ascending order of their affinity with respect to water are distinguished, namely insoluble, soluble (but not deliquescent) and hygroscopic (deliquescent) solids.

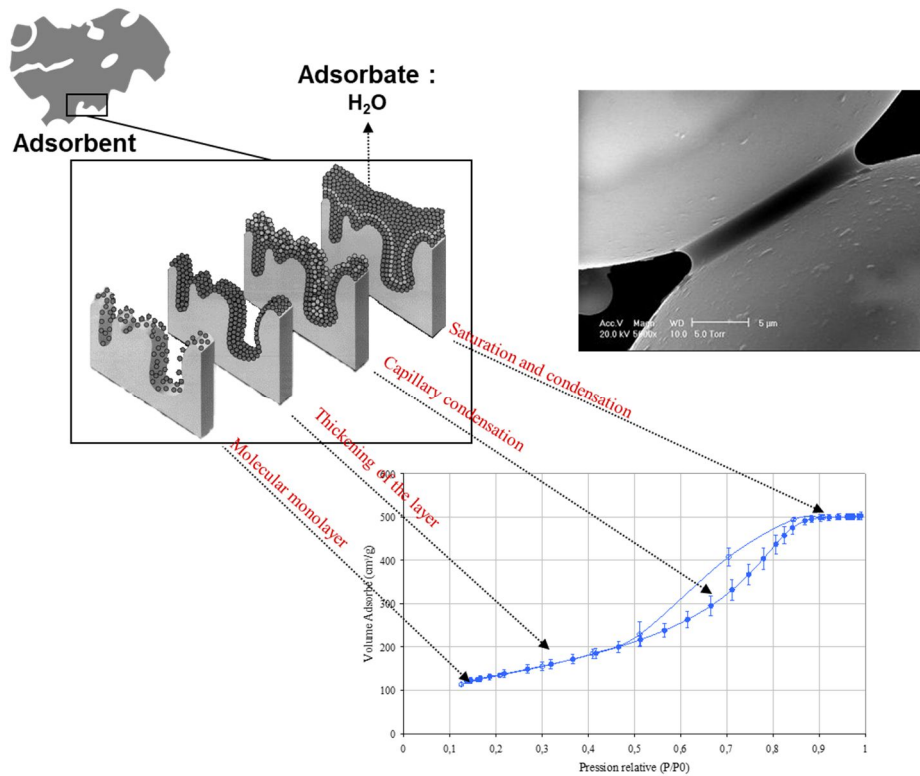


Figure I-4: A typical example of a water sorption isotherm and a liquid bridge formation due to capillary condensation (ESEM image: SAPC/UTC)

4.2.1 Capillary condensation

Capillary condensation phenomenon occurs in very confined spaces of nanometric size, such as internal porosities (mesopores), contact points between particles or surface roughnesses. Indeed, it is well established that at a given temperature, a vapor phase present in such a space can condensate at a partial pressure lower than its normal vapor pressure. In other words, the vapor pressure of the water at equilibrium inside the pores is less than that measured in a wide space.

Note that the ratio between the equilibrium vapor pressure in the pores and the normal vapor pressure represents the activity of the water. This decrease in vapor pressure can be related to the equivalent pore radius, r_k , by the Kelvin model:

$$\ln \frac{p_v}{p_v^*} = \frac{-2v_L \sigma_{LV} \cos \theta}{r_k RT} \quad (I-2)$$

where:

- p_v is the equilibrium vapor pressure
- p_v^* is the normal vapor pressure at saturation
- r_k is mean equivalent capillary size
- σ_{LV} is the liquid/vapor surface tension
- v_L is the liquid molar volume
- R is the ideal gas constant
- T is the absolute temperature

According to this model, for a wetting system which is characterized by $\cos \theta > 0$, in a confined space, a vapor could condensate at vapor pressures lower than its normal vapor pressure and then at water activities smaller than unity. This relation shows that the activity of the water inside pores decreases exponentially with the reduction of the pore radius and with the increase of the wettability of the solid with respect to the liquid. For example, [Figure I-5](#) shows the variation of water activity as a function of pore radius (assumed to be cylindrical) for different values of $\frac{\sigma_{LV} \cos \theta}{T}$ [18, 19].

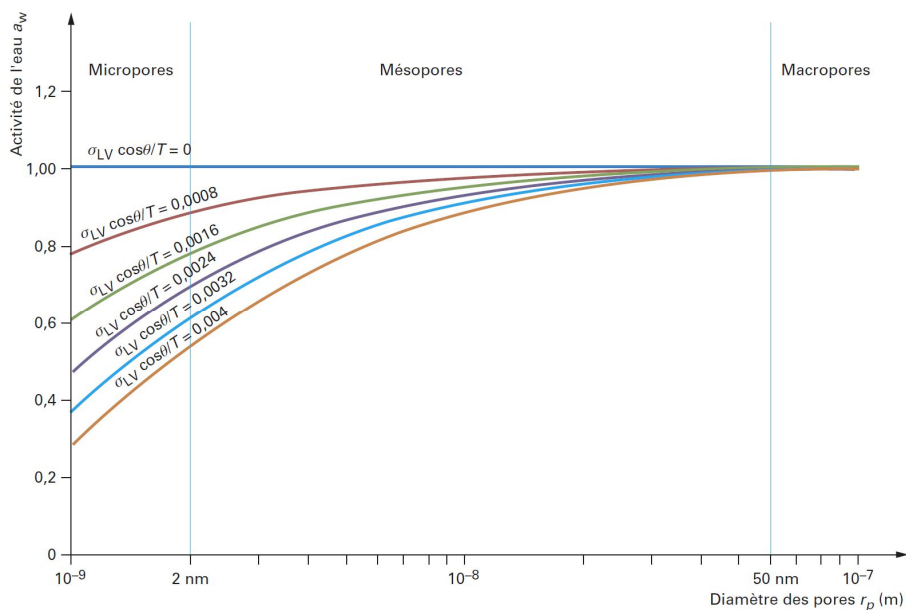


Figure I-5: variation of water activity as a function of pore radius for different $\frac{\sigma_{LV} \cos \theta}{T}$

We can note that the activity is very affected in the field of micropores (<2 nm) and a part of the mesopores (2 to 20 nm). On the other hand, macropores (> 50 nm) are only slightly (not to say not) affected by capillary condensation phenomenon.

Thus, if, for example, at room temperature, the water vapor begins to condensate at a relative humidity of 100%, in a pore of 10 nm in a completely hydrophilic solid ($\theta = 0$) it condenses from a relative humidity as low as 80%.

4.2.2 Pendular capillary (liquid bridge) forces

The presence of liquid water bridges between particles results in capillary forces, which are attractive for hydrophilic systems and repulsive for hydrophobic ones. These forces are amenable to a theoretical description for simple geometries by applying the Laplace theory for capillary forces. According to this theory, for the case of two equal-sized spherical particles distant of $2h$ joined by a liquid bridge shown in [Figure I-6](#), , the total attractive force between the two particles including both the capillary and the surface tension components is given by [6, 20-23]:

$$F = 4\pi R\gamma \sin(\psi) \left[\sin(\psi + \theta) + \frac{R}{2} \sin \psi \left(\frac{1}{\varrho_1} + \frac{1}{\varrho_2} \right) \right] \quad (1-3)$$

where ϱ_1 and ϱ_2 are the principle radii of curvature given by :

$$\varrho_1 = -\frac{R(1 - \cos \psi) + h}{\cos(\psi + \theta)} \quad (1-4)$$

$$\varrho_2 = R \sin \psi - \varrho_1 [1 - \sin(\psi + \theta)] \quad (1-5)$$

in which ψ is the filling angle and θ is the liquid-solid contact angle as shown in [Figure I-6](#).

More details on capillary condensation and capillary forces are provided in chapter V.

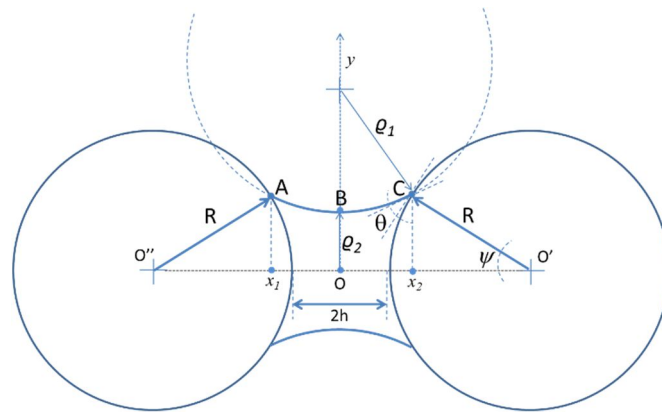


Figure I-6: Schematic representation of a pendular liquid bridge between two equal-sized particles

4.2.3 Insoluble powders

The main cause of caking for insoluble solids including a large variety of mineral powders (talc, calcite, mica, alumina, *etc.*) is the formation of liquid bridges due to capillary condensation. The ESEM images presented in [Figure I-7](#) illustrate an example of capillary condensation in a sample of hydrophilic particles. As we can see, this phenomenon leads to formation of liquid bridges between particles. The intensity and range of the connection forces induced by these bridges being several orders of magnitude greater than those of the van der Waals forces, this leads to a wet clogging of the powder. The role of capillary condensation and consequent liquid bridges will be discussed in detail later in chapter V.

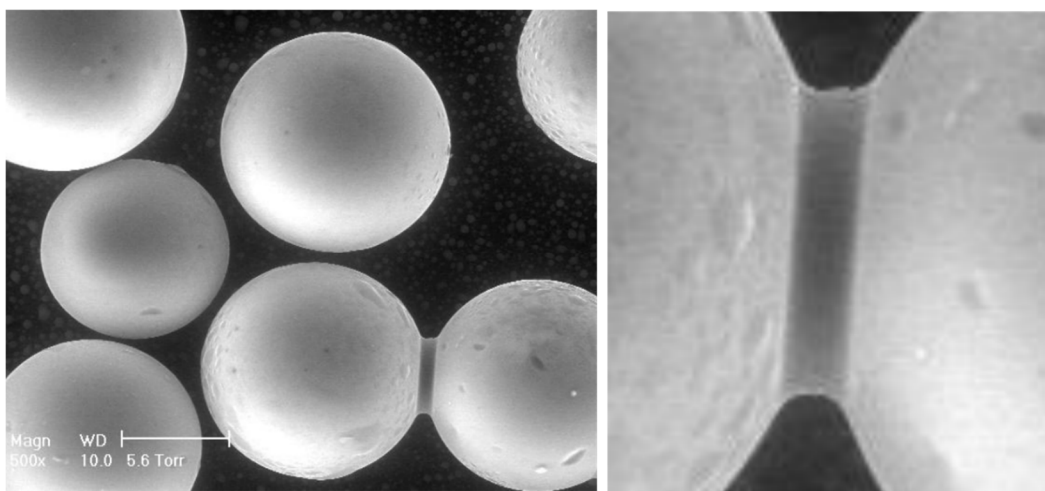


Figure I-7: capillary condensation in contact points between particles

4.2.4 Non deliquescent water soluble powders

For hydrosoluble solids, local liquid bridges appeared after capillary condensation could dissolve a part of solids and form solid bridges after solidification by drying or recrystallization.

An example of this kind of caking has been reported by Cleaver *et al.* [24] for Boric acid which is a soluble but not too much hygroscopic solid. As we can see from the adsorption isotherm shown in Figure I-8-a, the quantity of adsorbed vapor is not very high. However, the exposure of boric acid to humid air could result to partial dissolution and then recrystallization of the solid. An example given by these authors is presented in Figure I-8-b, which illustrates the crystallization phenomenon at particle-particle contact points and a macroscopic view of the cake Figure I-8-c.

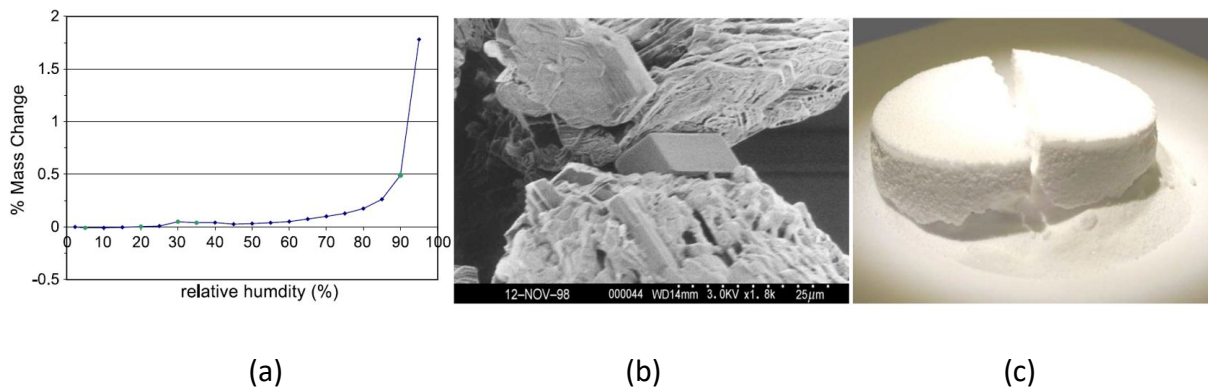


Figure I-8 : Equilibrium water sorption isotherm (25°C) for boric acid (a), solid bridge formation due to crystallization (b) and subsequent cake formation (c) (from Cleaver *et al.* [24])

4.2.5 Deliquescent powders

Problems are accentuated for soluble hygroscopic solids. In fact, an important but not universal feature of crystalline solids is the existence, sometimes, of a critical (deliquescence) relative humidity, DRH, also called the point of deliquescence. This point corresponds to the relative humidity from which the solid absorbs substantial amounts of water vapor. Generally, deliquescence refers to the conversion of a solid substance into a liquid as a result of absorption of moisture or water vapor from the air.

Typical examples of this kind of solids are sodium chloride, NaCl, and sucrose, the sorption isotherms of which are shown in Figure I-9. Other examples of solids of this type are KCl, and ammonium nitrate.

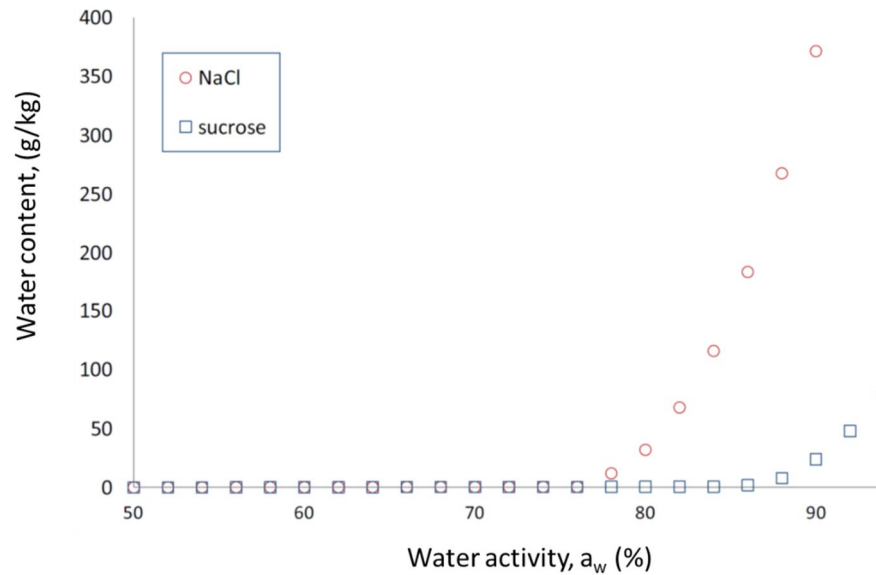


Figure I-9 : water sorption isotherms of two typical deliquescent solids (NaCl: DRH=76% and sucrose: DRH=85%) at 25°C.

If we focus on these sorption isotherms, we can see that a sharp increase on water uptake happens at 76% for NaCl and at 85% for sucrose. Substantial amounts of water are sorbed at these respective critical RH (DRH) until the solid is completely dissolved. Beyond deliquescence, water vapor is absorbed by a liquid solution of NaCl or sucrose.

In general, the storage of water-soluble crystals at relative humidity below their critical relative humidity, DRH, does not present major problems. On the other hand, an oscillation of the relative humidity around the DRH can lead to caking by the following elementary steps:

- capillary condensation followed by the dissolution of the solid during humidification which can go as far as the deliquescence,
- evaporation and recrystallization (efflorescence) during drying

Figure I-10 illustrate these different steps through a sequence of ESEM images taken during a humidification/drying cycle of NaCl crystals. In addition, Figure I-11 shows a superposition of the images of Figure I-10 on the water sorption isotherm of NaCl.

As can be seen, three segments are distinguished during the sorption step:

- Until DRH (76% RH), there is no significant water uptake and only multilayer molecular adsorption and capillary condensation at very narrow spaces takes place at this zone.

- From 76% to 77% RH, deliquescence happens and a sharp increase of water uptake is observed. The equilibrium point at 77% RH is an aqueous solution with a concentration of 340 gNaCl/kg water which is very close to the solubility value of 350 gNaCl/kg at 25 °C reported in the literature as the solubility of NaCl in water.
- Above DRH, the aqueous solution of NaCl is diluted while increasing RH.

During the desorption step, three particular branches are also distinguished:

- From 93% until 77% RH, desorption points overlap the dilution curve until reaching the saturation. Below 77% RH, evaporation of water continues and the solution becomes supersaturated. The decrease is smooth and no sharp variation in water uptake is observed, suggesting that no recrystallization occurs. In fact, for crystallization to occur, the solution must reach the state of supersaturation.
- Between 66% and 65% RH, the desorption curve undergoes a sharp decrease due to efflorescence of NaCl. The water is completely eliminated and there is no residual water in solids.

Consequently, starting from a dispersed powder, this procedure leads to a mass of particles linked by the appearance of solid bridges. It should be noted that in practice, these hydration/dehydration cycles could come from variations in atmospheric conditions.

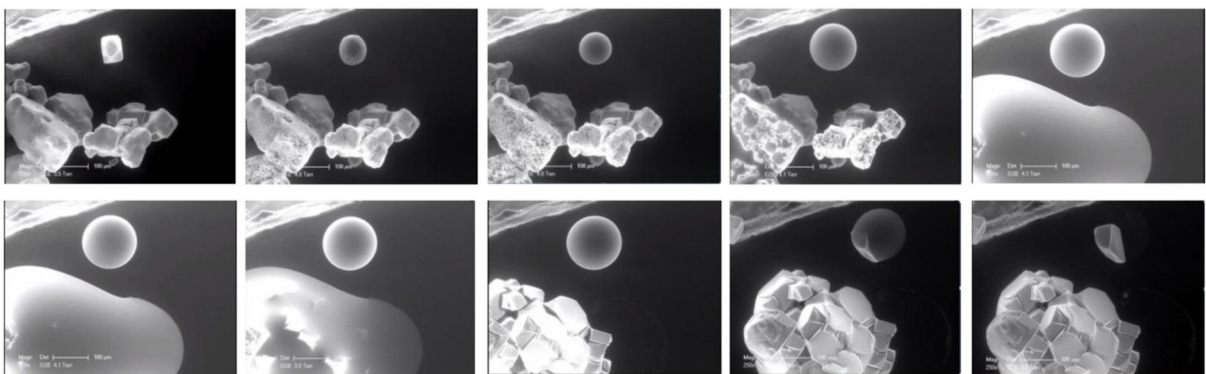


Figure I-10: Time sequence of ESEM images of the deliquescence of NaCl crystals (upper images) followed by their efflorescence (lower images) (Langlet *et al.* [25])

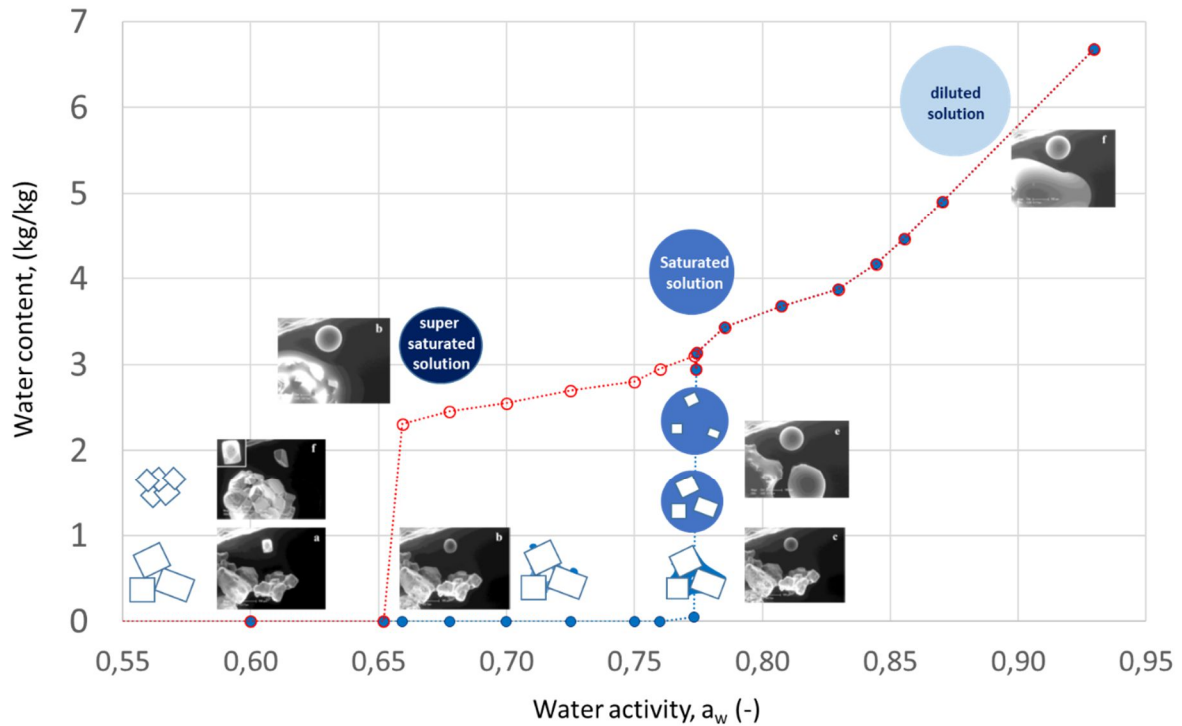
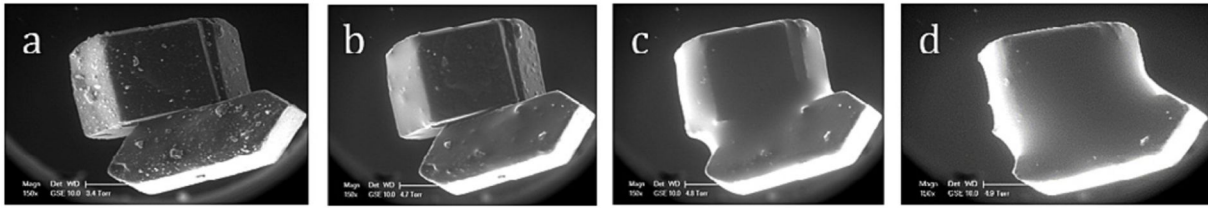
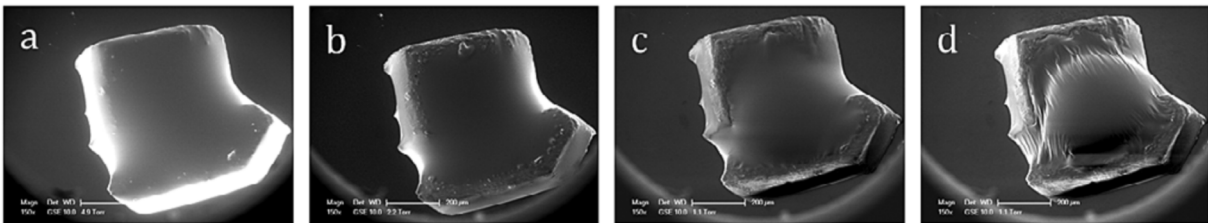


Figure I-11: Sorption isotherm of NaCl at 25 °C, and the sequence of deliquescence/efflorescence.

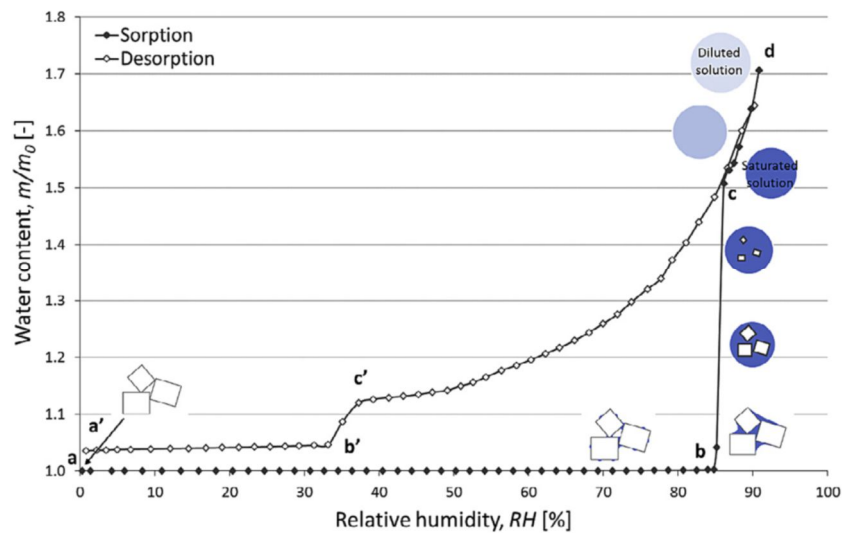
It is also important to note that some solids could form amorphous phases during the drying. This is specially the case for viscous solutions. A good example of this type of solid is sucrose. We can see in [Figure I-12](#), taken from the investigations of Samain *et al.* [26] that deliquescence of sucrose proceeds in the same manner as NaCl. However, its behavior is very different during the drying phase because the solution becomes viscous and water is entrapped within the solid matrix. Therefore, in this case, departing from a well crystalline and dispersed state, the product becomes a cake, which is partly amorphous.



a) Sorption and deliquescence



b) Desorption and efflorescence



c) Sorption isotherm of sucrose at 25°C

Figure I-12: Time sequence of ESEM images of sucrose deliquescence (a) and efflorescence (b) together with sorption isotherm of sucrose (c) (from Samain *et al.* [26])

The situation becomes more complicated when the mixtures of two or more deliquescent components are involved. Several works [25, 27-30] have pointed out the existence of a Mutual Deliquescence Relative Humidity (MDRH). For example, Figure I-13, taken from the work of Dupas-Langlet *et al.* [27], shows the mutual deliquescence of binary mixtures of NaCl and sucrose (50% w/w). It can be seen that the mutual deliquescence takes

place at a RH lower than DRH of both salt and sucrose that was equal to 76% for salt and 85% for sucrose, respectively.

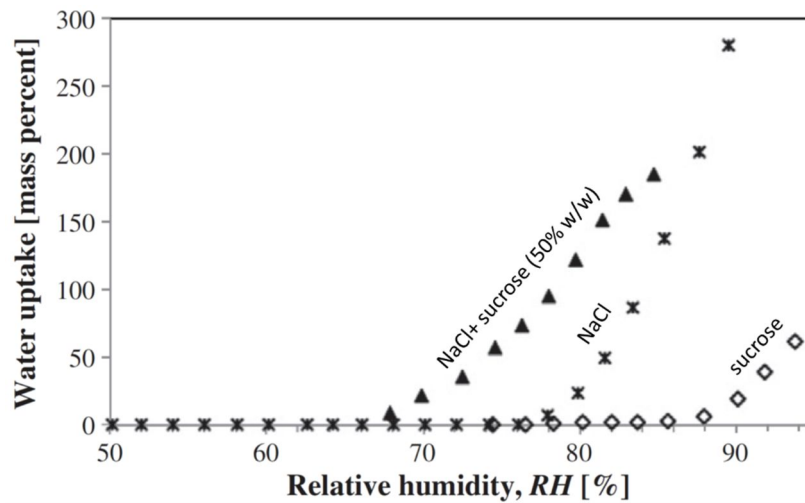


Figure I-13: Water uptake after 6 hours by pure sucrose (\diamond), pure NaCl (\times) and by the mixture of NaCl-sucrose $f_{\text{NaCl/sucrose}}=50$ (w/w) (\blacktriangle) at varying relative humidity (from [27]).

This singular phenomenon which is known as “Deliquescence lowering”, can be explained by some thermodynamic concepts to describe the water activity (a_w) in aqueous solutions of electrolytes or of organic substances. For regular solutions, Norrish’s model predicts quite well the water activity in binary systems (solute + water) [30]:

$$a_w = x_w \exp(\alpha x_{\text{solute}}^2) \quad (I-6)$$

where x_w is the molar fraction of water. Actually, the Norrish model could be extended to the case of ternary mixtures with the following general form [30]:

$$a_w = x_w \exp(\alpha_1 x_1^2 + \alpha_2 x_2^2 + \alpha_{12} x_1 x_2) \quad (I-7)$$

where x_1 and x_2 are the mole fractions of solute 1 and 2. Parameters α_1 , α_2 and α_{12} are interaction parameters of the model and must be identified by regression by use of

experimental data. Figure I-14 shows a set of data fitted by Dupas-Langlet *et al.* for the ternary system of NaCl-sucrose-water.

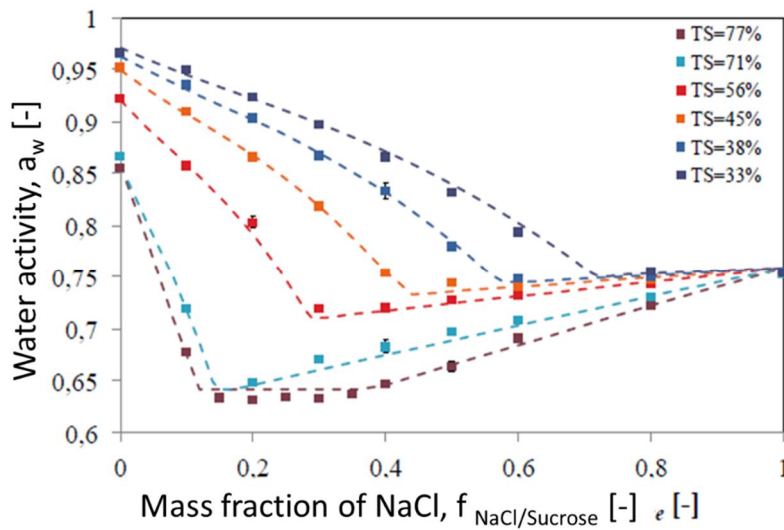


Figure I-14 : Phase diagram of critical water activity at 25 °C for NaCl-sugar-water system as a function of composition fitted with the model of regular solutions [30] (TS: Total Solid content)

A good agreement between the experimental data and predictions of the model is observed. Finally, using this model, these authors established a general phase diagram for this type of ternary systems (Figure I-15).

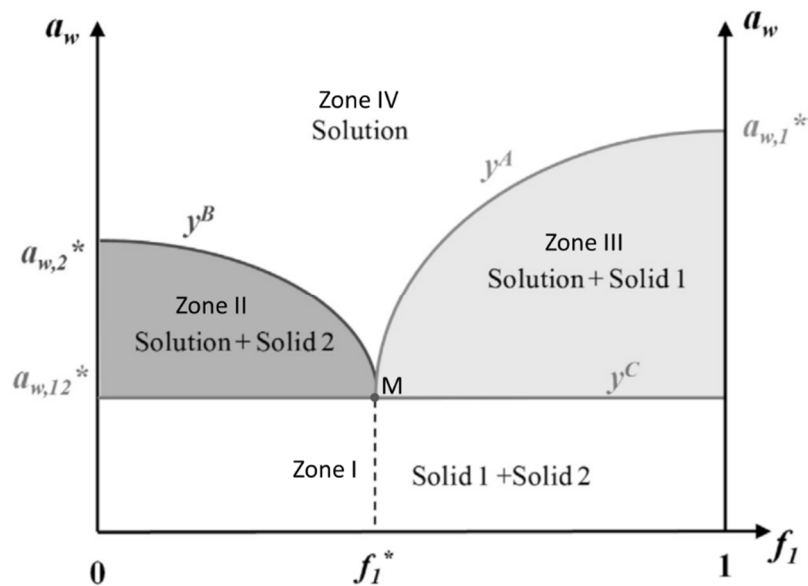


Figure I-15: Schematic phase diagram of water activity as a function of the mass solid composition [30].

The lower horizontal border in this diagram corresponds to solubility limits of solutes. Below this line (zone I), both solutes are in solid state. In zone IV, the two solutes are completely dissolved in water and only a solution of sucrose and NaCl exists. However, there are two other regions where one of solutes is only partially dissolved. In region II, solutions of solute 1 + solute 2 with some undissolved solute 2 coexists whereas in the opposite side (zone III), a solution containing some solute 1 in solid state exists. The intersection of the branches corresponds to the limit of saturation with respect to both solutes, *i.e.* to the *eutonic point*, represented by the point M in this diagram.

Note that regarding the caking, the main problem is that during mutual deliquescence, the exact composition of the solution is not known. However, whatever the composition of the solution is, the critical RH of the mixture is lower than that for the major component and even both components. For example, small amounts of salt in a sucrose solution could lower significantly the critical RH. The maximum effect is obtained at the eutonic point which is reached at 16% [30].

4.3 Thermal (temperature induced) caking

Another common caking mechanism is thermal caking. Involved mechanisms are:

- solid phase diffusion (the same involved in sandstone formation) which accelerates with temperature
- phase transition mechanisms like melting, softening, change of crystalline phase

Note that almost all kind of solids are involved. The common thermodynamic base for this kind of caking is the lowering of surface energy. Indeed, it is well known that if two objects, which are free to move, are brought into contact, the system will tend to minimum energy. This is for example what happens during the coalescence of two liquid droplets. Therefore, any factor that could make a solid flow goes toward this evolution.

One of these mechanisms is solid phase diffusion. This type of caking is very similar to solid phase sintering. The main mechanisms are presented in [Figure I-16](#) [31, 32].

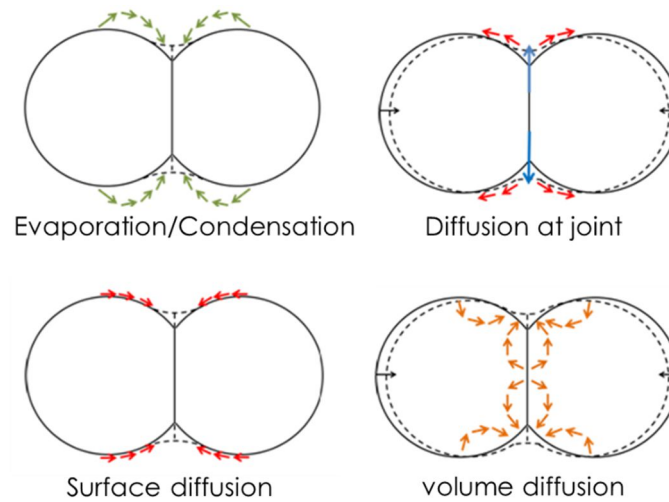


Figure I-16: mechanisms of solid sintering

All these mechanisms are limited by the molecular diffusivity that is highly temperature dependent. Using a simple rule of thumb from literature, the time necessary for an atom to travel 1mm is 300 years at 25°C but only 10 days at 900°C. Fortunately, this is a too high temperature with respect to storage conditions and so, this kind of caking is rarely encountered in practice.

However, for solids with a low melting point, even at ordinary temperatures, a partial melting of solid could occur which increases the diffusivity and then accelerates considerably the caking. It is for example the case for cocoa powder whose melting temperature is low enough and could cake under thermal stress even at 30 °C.

Another (and very important) class of thermal caking concerns amorphous powders. Unlike crystalline materials, amorphous materials do not have critical relative humidity. Their water content increases gradually with moisture but at a much lower level than that encountered for crystals. Although we cannot completely rule out the possibility of humid caking for water-soluble amorphous powders (capillary condensation, partial dissolution, drying and solidification), these mechanisms are not sufficient to explain the advent of caking of amorphous powders. Many studies show that for amorphous materials, it is actually the temperature that is the key factor. Indeed, a remarkable feature of amorphous materials is the existence of a so-called glass transition temperature, T_g , corresponding to the transition between the vitreous (glass) state and the rubbery state. Remind that an amorphous solid above its glass transition temperature, T_g , is a soft solid (or hard liquid). In this so-called

rubbery state, volume and surface diffusion mechanisms are accelerated. Thus, on the basis of these arguments, the idea was born that the caking of amorphous powders was analogous to the solid sintering process which is well-known in the field of metallurgy and plastics. It is indeed a process of agglomeration under the effect of heat at temperatures below the melting temperature of the material.

In this case, the extent of sintering is characterized by the ratio of the radius of the bridge to the particle radius (Figure I-17).

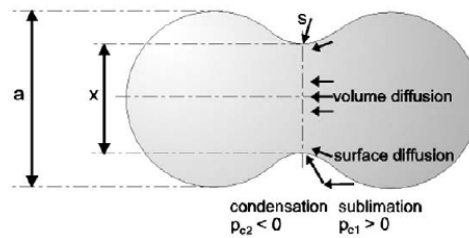


Figure I-17: Schematic presentation of sintering (from Hartmann and Palzer [12])

A simple model to describe the kinetics of caking for two equal-sized particles was established by Rumpf's model, which considers the surface tension and the external pressure as the driving force of caking and the viscosity as the opposing force [12, 16, 17]:

$$\left(\frac{x}{a}\right)^2 = \left(\frac{4}{5} \cdot \frac{\gamma}{a} + \frac{2F_t}{5\pi a^2}\right) \frac{t}{\mu} \quad (I-8)$$

where γ is the surface tension of rubbery material, μ is the viscosity, F_t is the external force and t is time.

Note that more accurate models have been also proposed considering unequal sized or multiparticle systems but their resolution requires the use of sophisticated numerical methods [33, 34].

As far as amorphous powders are concerned, we have to keep in mind two crucial phenomena:

- First of all, it is well established that the glass transition temperature decreases with the water content of solid (§6)

- In addition, the viscosity of a material in rubbery state decreases sensibly with the difference between T and T_g (§6)

Therefore, on the one hand, a solid which is exposed to the relative humidity of surrounding air could adsorb water until equilibrium (the amount of which is given by sorption isotherm). On the other hand, an increase in the water content of solid could decrease the glass transition temperature. Therefore, we can expect that even at constant storage temperature, the T_g could change due to RH and fall down to storage temperature and the caking could take place. For example, [Figure I-18](#) shows the water sorption isotherm (inside box) as well as the variations of the T_g as a function of the water content for a maltodextrin powder [14].

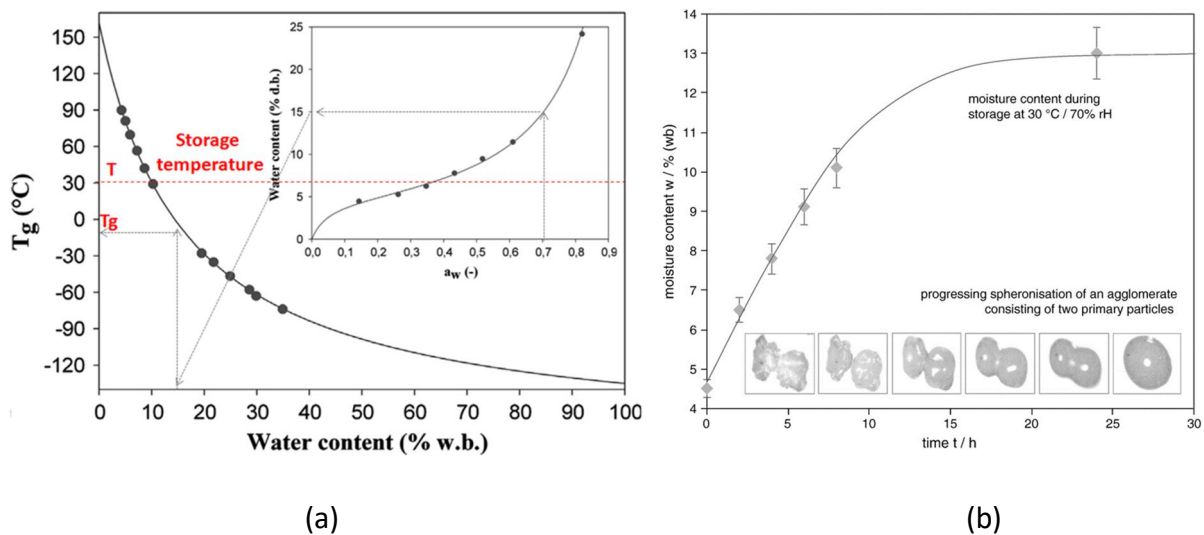


Figure I-18: Glass transition vs water content and the sorption isotherm of a maltodextrin (DE21) (a) and images of sintering of two dextrose syrup particles (DE 21) stored at 30 °C and 70% RH (b)

As can be seen, the presence of water, even in small quantities leads to a sustained decay in T_g for this product. For example, if an initially dry sample is exposed to moist air at 50% RH, its equilibrium water content would be about 10% which would lead to a sharp decrease in T_g ; from 160 ° C (dry solid) to 30°C (see the path of the arrows in [Figure I-18-a](#)). Storage above this temperature would be detrimental to the quality of the product. [Figure I-18-b](#) taken from the work of Hartman and Palzer [12] illustrates this possibility. We can see that the exposure of a sample of dextrose to humid air with a RH equal to 70% results in vapor sorption and subsequent agglomeration of the two particles. This phenomenon could be

described by the fact that at a relative humidity of 70%, the water content could attain up to 15% and for such a water content, the glass transition is even negative whereas for dry air the T_g is about 160°C. So combining T_g curve and sorption isotherm constitutes a useful tool to determine the proper conditions for storage of an amorphous powder. These issues will be discussed in more details for lactose in the following sections.

However, this knowledge, although very useful, is not sufficient to fully describe the caking phenomenon. Indeed, they only give a static view of the phenomenon because they are based solely on thermodynamic equilibria. In reality, caking is a dynamic process that progresses slowly out of equilibrium. Nevertheless, the current state of knowledge on the subject does not allow predicting the time that a powder would put to cake once the environmental conditions are favorable. Similarly, the role of the mechanical stresses on the powder is not taken into account in this approach. To answer these questions, we need a detailed knowledge of the dynamics of the mechanisms involved at different scales (particles, agglomerates, heaps) with a view to their coupling in a dynamic model.

Indeed, it is only very recently that these dynamic aspects have been subject of in-depth studies.

4.4 Chemical (reaction induced) caking (phase transition)

Caking can occur also due to chemical bonding at contact points between particles. The chemical bond could result from a chemical reaction with oxygen or water (*e.g.* cement) or from a change of crystallinity of the solid. Ammonium nitrate is a very good example of this latter mechanism. Ammonium nitrate is a crystalline powder with several possible structures [9]. This is a hygroscopic salt with a DRH about 61% at 25°C but one singularity of this product is that it can cake at RH lower than DRH. The reason is that Ammonium nitrate could undergo several phase transitions one of which occurs at room temperature (Figure I-19).

More precisely, it is the transition between form III and form IV of this substance that is important. This transition is reversible and happens between 32 and 56 °C according to the water content of the solid. So, the product could undergo phase transitions, sometimes several times per day. The problem is that this transition is accompanied by an important change of the density of the product (graph at the top left of Figure I-19). In addition, the

transition temperature varies with the water content of the product (graph at the top right of Figure I-19). Consequently, at constant storage volume, the product could cake under pressure when its density increases. This phenomenon could generate dust and fine particles because of the fracture of particles, which is also a negative point in regard of caking.

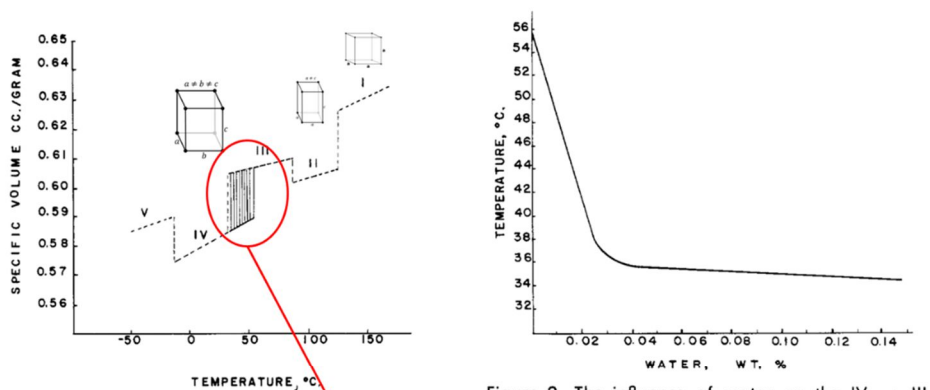


Figure 1. The specific volume of ammonium nitrate demonstrates the unlimited number of paths between Form IV and Form III when Form IV is heated

Figure 2. The influence of water on the IV → III transition of pure ammonium nitrate

phase	Temperature (°C)	state
-	>170	liquid
NH ₄ NO ₃ (I)	125/170	cubic
NH ₄ NO ₃ (II)	84/125	tetragonal
NH ₄ NO ₃ (III)	32/84	orthorhombic
NH ₄ NO ₃ (IV)	-18/32	orthorhombic
NH ₄ NO ₃ (V)	< -18	orthorhombic

Figure I-19: Phase diagram of ammonium nitrate [9]

It should be noted that most polymorphic products may present caking risks due to phase changes. Indeed, during these changes, links can be created at the contact surfaces between particles. In addition, water can be released during amorphous to crystalline transition or from the dehydration reaction leading to formation of liquid bridges. Lactose and other hydrated sugars or salts, cocoa and many of pharmaceutical products are good examples of this kind of product.

5 Caking testing methods

A multitude of methods has been reported in the literature to characterize the propensity of powders to cake. The test methods reported in the literature range from very basic tests (drop test) to much more sophisticated tests such as shear tests.

The common point of all these methods is that they include two stages:

- The first step consists in placing the powder under conditions such that bonds will form between the particles. This can be done by applying a stress (formation of van der Waals bonds or solid bonds), by humidifying the powder (liquid bridges) or by subjecting the powder to a moisture and/or temperature cycle (formation of solid bridges)
- Once the powder has been caked, the sample can then be characterized mechanically by methods such as shear, compression, traction and indentation, which will be detailed below.

In a recent PhD thesis, Samain [35] provided an extensive review of the caking tests by crossing the methods to prepare the caked samples and those used to characterize the cakes. Zafar *et al.* [11] and Carpin *et al.* [13] reviewed the different tests reported in the literature. These authors made a classification of tests based on the method used to measure the mechanical resistance of cakes. They distinguish mechanical test methods including shear cell, uniaxial compression, tensile, ICI, penetration and powder rheometer testings as well as alternative tests (sensory, sieving, sticky point measurement, blow tester, microscopic observations, *etc.*). Because the caking is a slow process, the preparation of cakes is generally accelerated by prior wetting of powders or by using an air current instead of stagnant air.

In this work, two specific caking devices were manufactured for caking of powders and several characterization methods (radial compression, uniaxial compression and shearing) were tested to determine the caking behavior of powders. Detailed information about these devices will be provided in chapter II.

6 Molecular structure of materials in relation with caking

The vast majority of organic materials are composed of a mix of polymeric chains ranging from the shortest (dimers such as lactose, maltose) to the longest (macromolecules: proteins, polysaccharides such as cellulose or starch, DNA, chromosome). For example, food matrices such as dairy powders are biopolymer complexes constituted mainly of sugars, amino acids and lipids [36]. The physical state and stability of foods are tightly related to their molecular mobility and molecular interactions. Such products can exist either in stable crystalline state or in metastable amorphous state, or in an intermediate state between them (*e.g.* [37-39]). Although its physical reality is not formally proven (since for some compounds, no crystalline form has ever been observed), the "amorphous state" is considered to be thermodynamically metastable with respect to a crystalline form. Amorphous materials are then supposed to evolve through the stable crystalline form with kinetic rates that are specific to their nature and physical conditions. In addition, most of materials are polymorphic and then can exist in more than one form or crystal structure.

It is also well known that above their glass transition temperature, T_g , amorphous materials can flow and then undergo shape changes under mechanical or physico-chemical stresses (*e.g.*, pressure, gravity, surface tension, *etc.*). They exhibit a pseudo-fluid behavior with a tacky appearance whose intensity depends on the rheological properties of the material.

These phenomena have a significant impact on the material properties (*e.g.* solubility, wettability, hygroscopicity, stability, hardness, *etc.*) and must be explained for a better understanding of the mechanisms taking place during the caking process.

6.1 Polymorphism

In materials science, polymorphism designates the ability of a solid material to form more than one molecular structure. Potentially, any crystalline material including pure elements¹, polymers, minerals, and metals can be polymorphic.

Several types of polymorphism could exist:

- *packing polymorphism* which results from a difference in crystal packing,
- *conformational polymorphism* which results from the existence of different conformers of the same molecule,
- *pseudopolymorphism* or *solvomorphism* in which the different crystal types are the result of hydration or solvation.

Lactose, used as the support material in this study, is a good example of an organic polymorph, which can exist in several forms including either conformational polymorphism or solvomorphism. The polymorphs of lactose will be described in more detail in the following section.

6.2 Phase and phase transitions in materials

Let's first note that it is difficult to find a consensus on the use of the terms "*form*", "*phase*" and "*state*" in the literature. These words have been used indifferently as well to designate the various states of condensation of a material (solid, liquid, gas) as its ordered (crystalline) or disordered (amorphous) structure. Indeed, the classical classification, which consists of distinguishing the three conventional phases (gas, liquid and solid) by the degree of mobility and the density of atoms and/or molecules, is too limiting to cover the diversity of states observed for complex materials. Moreover, Tager [40] used the word "form" to distinguish these cases and reserved the word "phase" for a classification of materials according to a structural and / or thermodynamic criterion (Figure I-20):

¹ The specific case of polymorphism of pure elements is called allotropy, from Greek ἄλλος (*allos*), meaning "other", and τρόπος (*tropos*), meaning "form". For example, diamond, graphite, graphene and fullerenes are the different allotropes of carbon.

- from a thermodynamic point of view, a phase corresponds to a portion of a system, which is (thermodynamically) stable and separable from the rest of the system through the existence of an interface.
- In structural terms, the phases can be differentiated by the mutual arrangement of their molecules. Following this order of arrangement, some distinguish three phases: (i) crystalline, (ii) amorphous (including liquids) and (iii) gaseous.



Figure I-20: “Phase” and “state” from thermodynamic (left) and structural (right) point of view

Furthermore, from a kinematic point of view, a classification based on the level of molecular motions and the corresponding activation energies is also possible (§6.3.3).

Under terrestrial conditions, the pure components of small molecular (or atomic) dimensions are in one of three well-known forms: gas, solid, liquid. The most stable state and the equilibrium between phases can be straightforwardly described as a function of the intensive state variables of the system (*e.g.* T and P). The most familiar example of this type of component is water the *phase diagram* of which is perfectly known. If liquid water is cooled at constant pressure, once the freezing temperature is reached, it is transformed to ice (solid) phase. Due to small dimension of water molecules and then their subsequent high mobility, they have time to organize into a well-structured network to form crystals. However, for more complex materials composed of (mixtures of) long chains, the material can exist in a state outside thermodynamic equilibrium. This is a purely dynamic phenomenon, which occurs

when the mobility of molecules is highly reduced because of their excessive length or the high viscosity of liquid. Almost all materials can be obtained in amorphous form if they are cooled quickly enough until a fairly low temperature. The whole question is to cross the temperature range where the material could crystallize without allowing it to do so. This range goes from T_f (melting temperature) to T_g (glass transition temperature below which the viscosity no longer allows structural rearrangements). Any spatially heterogeneous material will fit into this definition insofar as these spatial heterogeneities will result in internal constraints thus implying a thermodynamically unstable state. Nevertheless, the relaxation time of such systems can reach durations so long that they are unobservable experimentally (up to several tens of thousands of years). Among these materials are many systems of soft matter, neither solid nor liquid, such as glasses, gels or pastes. For those materials, it is no longer possible to talk about a phase diagram (referring to a thermodynamically stable state of matter), the term used then being that of a *state diagram*. State diagrams unifying the behavior of condensed materials have been established for many systems including binary aqueous solutions of lactose that will be presented later. At the macromolecular scale, these condensed materials essentially have three different structures (Figure I-21):

- The amorphous state, which is characterized by a ball-like structure in which no large-scale order is distinguished;
- The crystalline state that is characterized by a long-range order
- The intermediate (semi-crystalline) state.

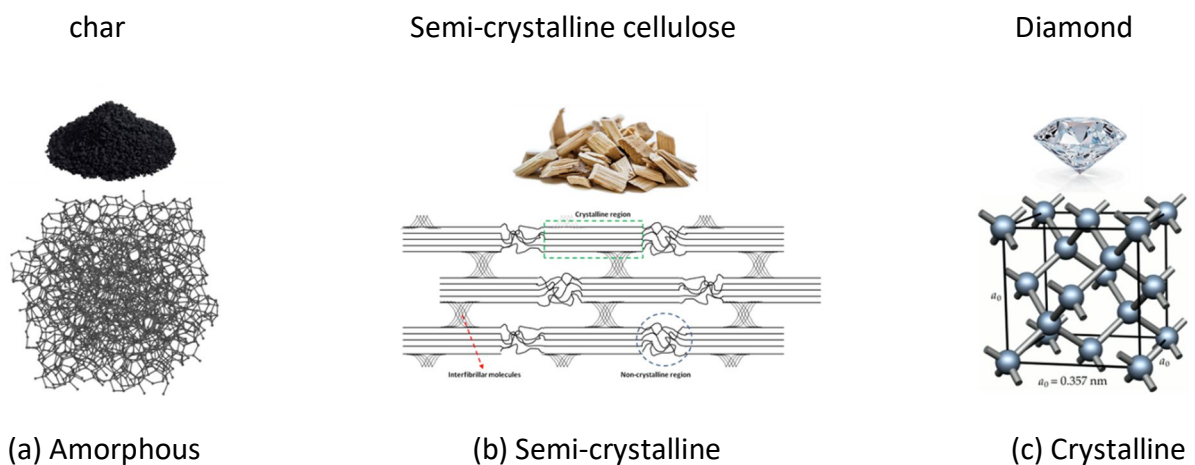


Figure I-21: Different states of condensed materials

6.2.1 Amorphous structure

The so-called "amorphous" form corresponds to a structure comparable to that of liquids characterized by the absence of order at large scales with respects to the molecular dimension. There is no constant distance between the molecules and no regularity in the arrangement and orientation of these in submicron areas. Macromolecules can form physical entanglement points that are inevitable from a certain length of the molecular chains, very often attained in commercial polymers. The length of the segments between entanglements is generally large enough for the segments to behave as individual strings. The chain segments are able to create some molecular mobility if free spaces exist throughout the volume of the material. These spaces constitute the *free volume* of the material, which determines the mobility of the molecules and their ability to change conformation.

6.2.2 Semi-crystalline structure

Under certain conditions, ordered zones following a periodic network may appear within the material. However, depending on the physical conditions, the crystallization may not be complete. The semi-crystalline morphology occurs locally as a set of crystalline lamellae, separated from each other by an amorphous phase. In this case, segments of molecular chains called link molecules bond the two phases together. A representative example of this category of structure is cellulose, which can exist in both crystalline or semi-crystalline state.

6.2.3 Crystalline structure

A crystalline solid is a highly ordered network constituted by the periodic repetition of an atomic or molecular pattern, called *unit cell*, in the three dimensions of space. The unit cell constitutes the smallest repeating unit having the full symmetry of the crystal structure. Its geometry is described by a parallelepiped, providing six lattice parameters taken as the lengths of the cell edges (a , b , c) and the angles between them (α , β , γ). Diamond, salts (NaCl, KCl, *etc.*) as well as some sugars (fructose, glucose, sucrose, *etc.*) constitutes good examples of this category of structure.

6.3 Phase Transitions

The term transition refers to the change in the physical state that is caused by a change in temperature or pressure [41]. In this work, we will use the word "*transition*" in the sense defined by Tager [40], which includes all the changes involving variations in the arrangement of the molecular structure and/or in the thermodynamic properties (*e.g.* density, heat capacity, viscosity, or textural characteristics) of a system. From a thermodynamic point of view, the Gibbs energy or the chemical potential of a system can be used in the classification of phase transitions. In 1933, Ehrenfest [42] was the first to establish such classification of phase transitions based on discontinuities observed in the state functions at the transition temperatures. According to this classification, transitions can be classified into two main categories, *i.e.* first-order and second-order transitions ([38, 43, 44]). Figure I-22 gives an example of these two categories of transitions allowing the change from the liquid state to the solid state. It should be pointed out that the cooling rate, r ($^{\circ}\text{C}/\text{min}$) is one of the determining factors either to favor or to avoid a transition compared to another [45]. Amorphous state is obtained at high cooling rates whereas crystal formation requires a low cooling rate so that the molecules have time enough to form a regular structure.

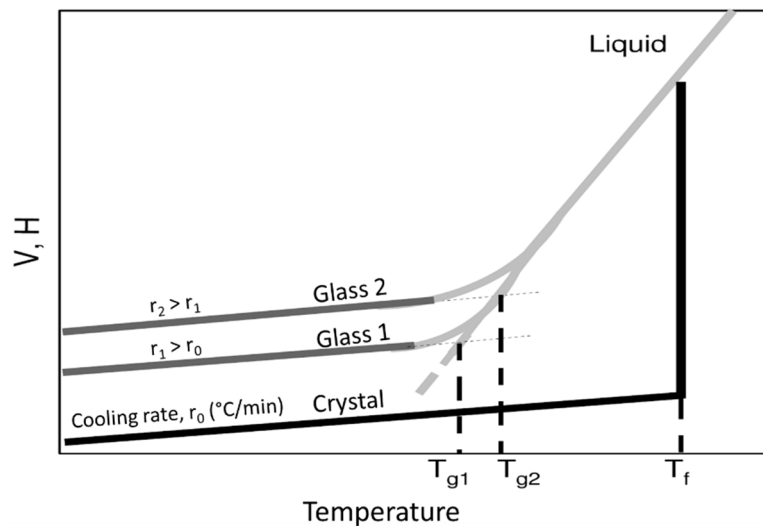


Figure I-22: Qualitative representation of first- and second-order transitions

6.3.1 First-order transition

The Ehrenfest classification of phase transitions is then based on changes in chemical potential or Gibbs energy. At equilibrium, the thermodynamic potentials of the two phases are equal. At a first-order transition temperature, the thermodynamic potential and Gibbs energy vary continuously but their first derivative undergo a discontinuity [40]. This type of transition is then characterized by a discontinuous change in certain characteristics such as enthalpy, entropy or the specific volume of the system (Figure I-22-Black line). This transition generates the absorption or generation of heat (transition energy). Among these transitions are fusion, vaporization and sublimation [40, 46, 47].

6.3.2 Second-order transition

According to the Ehrenfest classification of phase transitions [42], for second-order phase transitions, it is the second (and not the first) derivative of the chemical potential or Gibbs energy that becomes discontinuous at the transition temperature. In this case, the change of enthalpy, entropy and volume is continuous and smooth (Figure I-22-grey lines). This means that for a first-order transition, H, S and V will change abruptly, whereas for a second-order transition, these changes will be detected only on properties such as the specific heat, C_p , or the thermal coefficient of volume expansion, respectively defined as following:

$$C_p = \left(\frac{\partial H}{\partial T} \right)_p \quad (I-9)$$

and

$$\alpha = \frac{1}{V} \left(\frac{\partial V}{\partial T} \right)_p \quad (I-10)$$

Hence, a second-order transition has no latent heat, *i.e.* the energy required remains low, even very negligible, compared to that of a first-order transition [40]. On the other hand, the specific heat undergoes a remarkable variation with a discontinuity at the transition temperature. The heat capacity is different in the two phases but does not undergo a jump at the transition temperature while this is the case for first-order transitions.

Taking into account these details, from a thermodynamic point of view, the glass transition described in the following section could be considered as a second-order transition.

6.3.3 Glass Transition Phenomenon

A large variety of materials including both organics and minerals are present in an amorphous form. This corresponds to an unstable state that can exist at temperatures below the equilibrium melting temperature of the material. Indeed, in the food industry, the production process of most solids contains a drying operation. Starting from a more or less complex fluid (solution, suspension, paste), the drying aims to reduce the water content of the product to a target value. If the drying kinetics (or heating rate) is lower than that of solid crystallization (*i.e.* mild drying conditions) the solid phase molecules have time to organize into well structured networks to form a crystalline phase which is a first order phase transition. In most cases, however, the evaporation rate of water is high with respect to crystallization rate so that the drying operation results in formation of a highly concentrated and viscous solution (or suspension). In this case, according to the temperature and the water content, the material can exist either in a viscoelastic “rubbery” state or in a glassy solid form.

Note that the same sequences could be observed when an under-saturated solution is rapidly cooled (quenching) until the limit of solubility is exceeded. In fact, if the cooling rate is much higher than the re-orientation time of the solute molecules (also called the *relaxation time*), they are unable to volumetrically relax, therefore, excess free volume is “stored” inside the material. Elliott *et al.* [48] listed a number of other methods that could be used to produce amorphous materials.

The transition between the hard and relatively brittle form and the rubbery form of an amorphous material (or a semi-crystalline material with amorphous regions) is a reversible phenomenon, which is known as the “*glass transition*” phenomenon. Accordingly, the corresponding temperature at which this transformation occurs is called “*glass transition temperature*”, T_g , which is one of the most important characteristics of amorphous solids.

Globally, the theoretical models launched to describe T_g can be classified into three main categories, namely thermodynamic, kinematic and free volume theories. It is beyond the scope of this work to present a detailed description of these theories that are well documented in several references (*e.g.* [41]). In what follows, we limit our presentation to

some basic concepts that are necessary to understand the behavior of amorphous solids as well as the characterization of T_g .

From the molecular structure point of view, the glass transition can be explained by molecular motions. These movements can be classified, in the decreasing order of the activation energies involved, into four main categories:

- 1) Translation of whole molecules that allows (fluid like) flow.
- 2) Bending and twisting combined segments (40 to 50 atoms) of carbon molecules that lead to the elasticity of the material (restoring force).
- 3) Movement of a few atoms along the main chain or beside the functional groups.
- 4) Vibration of atoms around their equilibrium position.

The glass transition temperature is highly related to segmental chain motion. In crystalline solids, only the fourth category of motion exists. This is also the case for amorphous solids below T_g although unlike the crystalline networks, atoms do not have regular equilibrium positions within the amorphous structure. However, for amorphous solids above T_g the material has enough energy to activate also the movements of third (and even second) type. Nevertheless, because the energy distribution follows a Boltzmann distribution, even at $T < T_g$, it happens that type 1 and 2 movements occur also if the observation time is long enough.

From a thermodynamic point of view, as mentioned in previous section, the glass transition is acknowledged to be a second order-transition. This signifies that the transition involves a change in heat capacity but does not include a latent heat. This has been already illustrated in [Figure I-22](#) which shows the characteristic evolution of the thermodynamic properties (H, S, V) of a system during the cooling of a liquid with different cooling rates. As shown in this figure, the glass transition has some characteristic features of a second-order thermodynamic transition. The first-order derivatives of the free enthalpy G as well as that of V and H vary continuously during the decrease of T , showing a change of slope at T_g , which corresponds to the discontinuity of the properties of the second-order such that the heat capacity, C_p , and isobaric dilatation coefficient, α . Indeed, because the motion of molecules is greatly increased above T_g , generally, amorphous solids have a higher heat capacity and dilatation coefficient above the glass transition temperature than they do below it.

However, different contradictions observed experimentally, and more particularly the fact that T_g increases with the cooling rate (*i.e.* faster cooling rates lead to a higher T_g : $T_{g2} > T_{g1}$ in Figure I-22), show that the glass transition cannot be considered as a thermodynamic transition in the strict sense of the term.

It is also important to note that despite the glass transition is well known since a while, this phenomenon is not yet well understood and is still one of the mysteries of materials science. Significant efforts to describe this phenomenon have been done but a unique theoretical description of T_g has not yet been established. In fact, the glass transition, T_g , is not an intrinsic property of materials and could vary with their composition (*e.g.* water content). The history of the material in terms of process and storage conditions play also a significant role through its influence on the supramolecular structure of the material [14].

6.3.3.1 Composition and Glass Transition Temperature, T_g

Most real industrial products have a complex composition. For example, food substances are matrices made up of mixtures of several biomolecules such as sugars, protein lipids and water. One of the major issues concerning the glass transition is the determination of the T_g from the molecular structure and/or the composition of materials.

For low molecular weight polymers with known structures, numerical simulations using the molecular dynamics method can calculate the glass transition temperature satisfactorily [49, 50]. However, so far, these methods are very time consuming and are limited to the short chain lengths and pure components.

For more complex molecules, more practical approaches (*e.g.* Group Contribution Method) for a rough estimation of T_g have been proposed but their application is limited to organic compounds with well-defined structure.

Based on the mathematical expressions developed in the polymer science, several attempts have been made to predict the value of T_g as a function of the main components. The vast majority of work has focused on binary mixtures. The results of these attempts show that the approach could be satisfactory for several food matrices. Table I-1 summarizes the expressions allowing the prediction of T_g of binary mixtures from the individual contribution

of each constituent. The molecules involved in these cases are mainly biopolymers of soya and some soluble proteins [38, 46].

Table I-1: Somme correlations for estimation of glass transition temperature of mixtures as a function of individual data of compenents

Author(s)	Equation	comments	[Ref.]
Gordon & Taylor (1952)	$T_g = \frac{x_1 T_{g1} + kx_2 T_{g2}}{x_1 + kx_2}$	k is a constant $0 < a_w < 0.5$	[43, 46, 51, 52]
Couchman & Karasz (1978)	$T_g = \frac{x_1 \Delta c_{p1} T_{g1} + x_2 \Delta c_{p2} T_{g2}}{x_1 \Delta c_{p1} + x_2 \Delta c_{p2}}$	Analogous to G&T with: $k = \Delta c_{p2} / \Delta c_{p1}$	[46, 52]
Couchman & Karasz (1978)	$\ln(T_g) = \frac{x_1 \ln(T_{g1}) + kx_2 \ln(T_{g2})}{x_1 + kx_2}$	Adapted from C&K with mathematical simplifications	[46]
Kwei (1984)	$T_g = \frac{x_1 T_{g1} + kx_2 T_{g2}}{x_1 + kx_2} + qx_1 x_2$	k, q : constants	[46, 53]
Kalichewski & Blanshard (1992)	$T_g = \frac{x_1 \Delta c_{p1} T_{g1} + x_2 \Delta c_{p2} T_{g2} + x_3 \Delta c_{p3} T_{g3}}{x_1 \Delta c_{p1} + x_2 \Delta c_{p2} + x_3 \Delta c_{p3}}$	Ternary mixtures	[46, 54-56]
Fox (1952)	$\frac{1}{T_g} = \frac{x_1}{T_{g1}} + \frac{x_2}{T_{g2}}$	Underestimate T_g	[46, 57]
Linear	$T_g = x_1 T_{g1} + x_2 T_{g2}$	Overestimates T_g	[46, 57]
Pochan-Beahy-Hinman (1978)	$\ln(T_g) = x_1 \ln(T_{g1}) + x_2 \ln(T_{g2})$	Less used for foods	[46]
Huang (1993)	$T_g = \frac{x_1 \Delta c_{p1} (T_{g1} + T_{g2}) + 2x_2 \Delta c_{p2} T_{g2}}{x_1 \Delta c_{p1} (T_{g1} + T_{g2}) + 2x_2 \Delta c_{p2} T_{g1}} T_{g1}$	Suitable for hydrocarbons	[46]

Among the models presented in [Table I-1](#), the one proposed by Gordon and Taylor is among the most popular. As we can see from this table, the number of models for the prediction of the T_g according to the composition is quite important. However, the mathematical analysis of certain equations shows that, with some simplifying assumptions, some can be deduced from the others. Note that the parameter Δc_p , involved in some expressions, can be measured experimentally by DCS analysis. The values reported in the literature are not always identical, even when it concerns the same product (Rahman 1995, Roos 1995a). For example, the Δc_p values reported for amorphous water vary between 0.14 and 1.94 J.g⁻¹.°C⁻¹ [38]. For example, the variable k , in the Gordon and Taylor equation, can be expressed according to some measurable parameters. Several experiments have been carried out to find a meaning for k . The most used relation is that involving the variations of the specific heat of the two components of the mixture at glass transition [38, 46, 55]:

$$k = \frac{\Delta c_{p2}}{\Delta c_{p1}} \quad (I-11)$$

Roos [46] suggests that in the case of some sugars, the prediction of the constant k can be done using the value of the T_g of sugar in the anhydrous state:

$$k = 0.0293 T_g + 3.61 \quad (I-12)$$

When the T_g measurement method is based on the coefficient of expansion, other parameters are associated with constant k . Indeed, Bueche ([58] cited by [55]), proposes the combined effect of density and expansion coefficient on this constant:

$$k = \frac{\rho_1 \Delta \alpha_2}{\rho_2 \Delta \alpha_1} \quad (I-13)$$

Figure I-23 which provides a comparison between the predictions of different models for glucose shows that the models of Gordon and Taylor and Couchman and Karasz remain the most satisfactory. It is also evident that the accuracy of each model depends on the system to which it is applied. Thus, for a rigorous prediction of T_g , it is recommended to determine the model parameters experimentally.

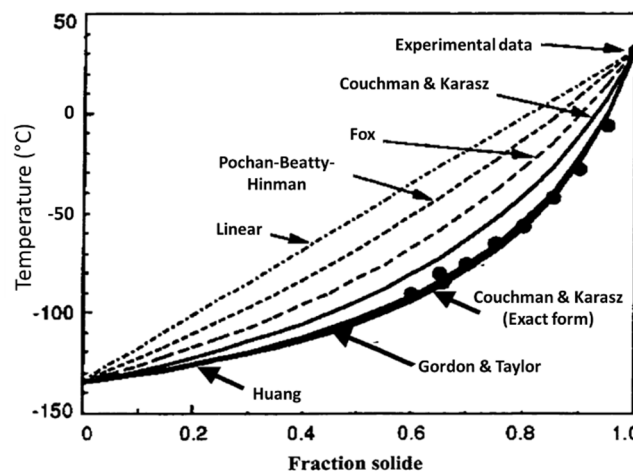


Figure I-23: A comparison between the predictions of different models for T_g of glucose

6.3.3.2 Factors affecting T_g

Among the parameters that influence the glass transition temperature, T_g , the most important one is undoubtedly the chemical composition of materials. As already mentioned, the theoretical approaches to describe T_g have not yet reached the required level of maturity.

As a first approximation, the molar mass of the materials can be used as a criterion for a rough description of the molecular structure. It has been reported that the glass transition temperature T_g increases with molecular weight and asymptotically approaches a maximum value. In polymer chemistry, the Flory–Fox equation relates the number-average molecular mass M_n of a polymer to its glass transition temperature, T_g :

$$T_g = T_g^\infty + \frac{K}{M_n} \quad (I-14)$$

where T_g^∞ is the maximum glass transition temperature that can be achieved at a theoretical infinite molecular weight and K is an empirical parameter that is related to the free volume present in the polymer sample. Parameters K and T_g^∞ differ from one material to another but can be obtained experimentally by a plot of T_g vs $\frac{1}{M_n}$.

Another important parameter influencing the T_g is the water activity and more precisely, the water content of materials. As mentioned in previous section, the presence of low T_g compounds depresses the T_g of a binary mixture. Because the glass transition temperature of water is very low (around -130°C), its presence in solid matrix affects significantly the T_g . The best known example of this effect is in the food field where the lowering effect of water is known since a while [38, 46, 57]. Indeed, dehydrated foods can be considered as binary mixtures consisting of a fraction of water and another fraction of dry matter.

This phenomenon of lowering of the glass transition temperature is known as the *plasticizer effect* of water [38, 40, 46, 59]. More generally, in polymer science, a plasticizer is defined by a nonvolatile solvent remaining in the matrix in the state of its initial use [59]. On the molecular level, the plasticizer is usually seen as a lubricant [57]. Indeed, it has generally a low molecular weight, which allows lubricating adjacent polymer chains having a high molecular weight [57]. This will facilitate the mobility of these chains. Theoretically, a plasticizer acts essentially by altering the viscosity of the system, increasing the flexibility of its molecules and increasing molecular mobility [38, 46].

Finally, some investigators have proposed models to describe T_g as a function of water activity. Some of these authors use linear regression to directly predict the T_g value as a function of water activity (aw):

$$T_g = a + b a_w \quad (I-15)$$

The physical signification of constants, a and b , is :

- a represents the glass transition temperature of the dry solid fraction (T_g).
- b represents the temperature difference ($T_g - T_{gs}$), with T_{gs} , denoting the glass transition temperature of water.

However, this correlation should be used with caution. It is not valid for $a_w > 0.75$ and does not always give good results using corresponding T_g values of water. Thus, some authors do not take into account the meaning of the parameters a and b and use them as the adjustable parameters of the model.

Lloyd *et al.* [60] studied the phenomenon of glass transition for the case of spray dried lactose and proposed a third-order polynomial for the relation between T_g and a_w ($0 < a_w < 0.35$) is:

$$T_g = -410a_w^3 + 720.7a_w^2 - 406.3 a_w + 101.4 \quad (I-16)$$

Note finally that according to Roos and Karel [46] the relation between T_g and a_w could be considered as linear when the values of a_w are between 0.1 and 0.8. However, they specify that the relation that would cover all the values of a_w would be a sigmoidal function.

6.3.3.3 Techniques of measuring T_g

Despite some numerical methods have been proposed to evaluate T_g , experimental measurement remains the only universal approach for determining T_g .

As explained earlier, there is a discontinuity of thermodynamic properties at a second-order phase transition. More specifically, the glass transition is characterized by the change of slope of specific volume, the change of the specific heat as well as the vanishing of the self-diffusion coefficient and the divergence of the shear viscosity. Consequently, experimental measurements of changes in heat capacity by Differential Scanning Calorimetry (DSC) analysis and thermal expansion can be used for determination of second-order transition temperatures. DSC remains however the most common technique. Carter and Schmidt [61] reported the main thermal analysis used for T_g determination (Table II-2).

Table II-2: Classification of Thermal analysis methods for T_g measurements according to Carter and Schmidt [61]

Common thermal analysis methods used to investigate the glass transition, the technique or concept of each method, and the event that signals the glass transition.

Method	Technique	Event signalling glass transition
Thermal mechanical analysis (TMA)	Volumetric	Increased penetration or dimension change
Dynamic thermal analysis (DMTA)	Mechanical	Decrease in storage modulus and maximum in loss modulus
Dielectric thermal analysis (DETA)	Mechanical	Dielectric loss constant goes through a maxima
Differential thermal analysis (DTA)	Thermodynamic	Temperature of sample differs from reference temperature
Differential scanning calorimetry (DSC)	Thermodynamic	Step change in the heat capacity

Besides thermal analysis techniques (DMA, DEA and DSC), sensitive determinations of thickness-dependent glass transitions in thin polymer films can be accomplished using ellipsometry [62], X-ray or neutron reflectivity, fluorescence spectroscopy [63], Brillouin light scattering [64], or positron annihilation lifetime spectroscopy (PALS) [65]. The latter techniques are all sensitive to properties related with the change in polymer density at T_g . In most cases, the accuracy of estimates will strongly depend on the thermal history of the testing material. It might be more helpful to use modulated-temperature experimental conditions (*e.g.*, MTDSC instead of conventional DSC).

6.4 Rheology of amorphous materials

As we mentioned before, caking of amorphous powders results from the balance between two types of forces:

- The surface tension forces that act as the driving force for deformation of particles and their consequent coalescence;
- the viscous forces that oppose flow and deformation and slow down the process.

The knowledge of the rheology of amorphous materials is then essential to a better description of the phenomena occurring during the caking.

From a kinetic point of view, one of the principal criteria for characterizing a material is by its *relaxation time*, which corresponds to the time required for gradual disappearance of stresses from a medium after it has been deformed. In this respect, three classes of material could be distinguished (Figure I-24): gases ($<10^{-6}$ s); liquids (10^{-6} - 10^2 s) and solids ($>10^2$ s).

Another way of classifying materials rheology is by the terms viscous, elastic or viscoelastic. An ideal viscous fluid is reversibly deformed when subjected to stress. It flows and the deformation energy is dissipated as heat, resulting in a rise of temperature. Hence, a viscous material is unable to store any deformation energy and has no memory of its form. This is mainly the case of fluids, gas or liquid. A viscous fluid can therefore be described as a fluid that resists the act of deformation but not the state of deformation.

Solids on the other hand, are normally considered as elastic materials. An ideal elastic material stores all imposed deformation energy and will consequently recover totally upon release of stress. Hence, an elastic material resists the act as well as the state of deformation. A number of materials show viscous as well as elastic properties, *i.e.* they store some of the deformation energy in their structure while some is lost by flow. These materials are called viscoelastic. Most food powders and especially those that are amorphous belongs to the category of viscoelastic materials.

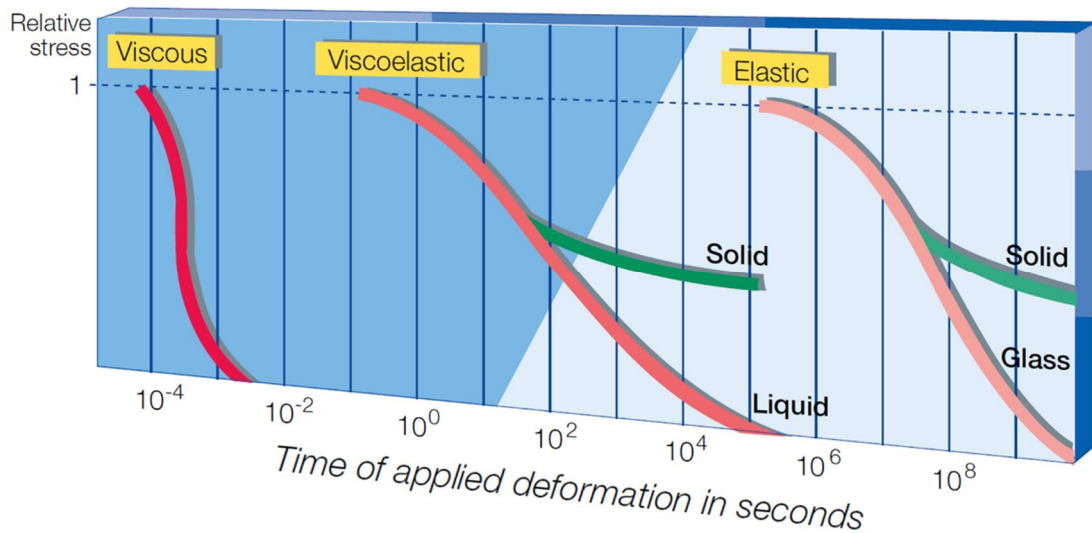


Figure I-24: Classification of materials according to their relaxation time (source [[66]])

6.4.1 Glass transition, rheology and stickiness of powders

The Glass Transition Temperature is recognized as being responsible for the stickiness and subsequent caking of amorphous powders above T_g . Indeed, below T_g , an amorphous material behaves like a brittle solid. In the contrary, above T_g , the material becomes rubbery-like and can be considered as a pseudo-liquid with a very high viscosity. The associated threshold viscosity value is reported to be about 10^{12} Pa s [17, 67-70]. In the rubbery zone, the viscosity of the material sharply decreases with increasing temperature. This reduction in viscosity causes the material to flow and results in formation of viscous bridges between particles leading to caking. It has been found that this mechanism is viscosity related. In fact, based on investigations carried out on some simple sugars (amorphous glucose, galactose, sucrose, maltose and fructose) as well as on lactose, it has been found that the extent of sticking does not depend directly to the temperature but on the excess of temperature with respect to the Glass Transition Temperature (*i.e.* $T-T_g$). Substantial efforts have been made to relate the viscosity of amorphous materials in rubbery zone to the glass transition temperature, or more specifically to $(T-T_g)$.

Williams, Landel and Ferry [71] were the first to establish a model to describe the dependency of the viscosity (η) on the temperature above the T_g :

$$\log_{10} \left(\frac{\eta}{\eta_g} \right) = \frac{-C_1(T - T_g)}{C_2 + (T - T_g)} \quad (I-17)$$

Williams *et al.* [71] reported so-called "universal" constants values of 17.44 and 51.60 for C_1 and C_2 , respectively. These values are the averages of the coefficients obtained on several synthetic polymers and have been exploited to predict the evolution of the viscosity of various carbohydrates. However, Ferry, one of the authors of the WLF model, cautioned about using these "universal" coefficients, as it is more appropriate to determine them for each study system.

Similar types of models with different constants have been proposed by other workers (Aguilera *et al.* [72]; Haque and Roos, [73]; Jouppila and Roos [74]; Jouppila *et al.* [75]; Paterson *et al.* [76]; Roos [69]; Roos and Karel [43]; Carter and Schmidt [61]). Some examples are given in [Table I-3](#).

Table I-3: Main models for the viscosity of amorphous powders in rubbery zone as a function of temperature

	Equation	[Ref.]
Arrhenius law	$\ln \left(\frac{\eta}{\eta_0} \right) = \frac{E}{RT}$	[40]
Williams-Landel-Ferry	$\log_{10} \left(\frac{\eta}{\eta_g} \right) = \frac{-C_1(T - T_g)}{C_2 + (T - T_g)}$	[71]
Vogel-Tamman-Fulcher	$\ln \left(\frac{\eta}{\eta_0} \right) = \frac{DT_g}{T - T_g}$	[77]
Power law	$\eta = A(T - T_g)^B$	[46]

7 Lactose

In this section, we present a literature survey on the principal properties of lactose, which was used as the main support material in this study. Lactose² is one of the most cited products in the scientific literature. A quick overview of the literature shows that rarely a product has been the subject of as much interest and studies as lactose. For example, Figure I-25 shows the number of publications found on Science Direct and Scopus databases using the single word of *Lactose* as the keyword. Obviously, such a mass of information cannot be analyzed in this report. We will therefore limit our survey to those aspects that are related to the caking phenomenon.

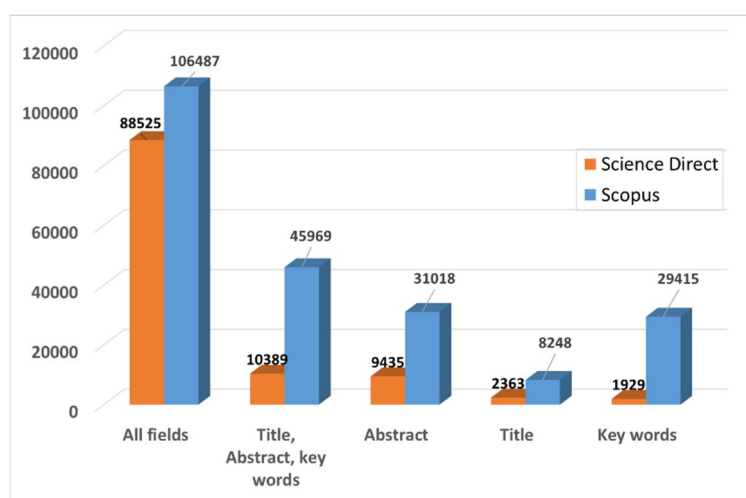


Figure I-25: Number of references found in Science Direct and in Scopus for “Lactose”

7.1 Lactose, structure, properties and characterization

Lactose is a by-product of the dairy industry widely used in a large variety of products and applications. With an average increase of around 1% per year during the last decade, its annual global production has increased from 1.12 million MT in 2011 to 1.38 million MT in 2015. The global market is expected to continue to grow at the same pace with an expected production of 1.65 million MT in 2020, which corresponds to about USD 1.5 billion in 2020

² Word meaning "milk sugar" composed by Marcellin Berthelot (1855), from Latin: *lac, lactis* ("milk") and *ose* (sugar).

[78-80]. The main uses of lactose are in the food and infant formula (accounting together for about 75-79%) as well as in the pharmaceutical industry and animal feed [78, 79, 81].

Lactose is a natural sugar found in milk as well as in its by-products such as whey. Free lactose constitutes more than 80% of milk hydrocarbons, the quantity of which can in turn reach 10% of the total mass of milk [82].

7.1.1 Lactose molecule

From a chemical structure point of view, lactose is a carbohydrate and more specifically a disaccharide composed of galactose and glucose with a chemical formula of $C_{12}H_{22}O_{11}$ (Figure I-26). According to IUPAC, the systematic name of lactose is β -D-galactopyranosyl-(1 \rightarrow 4)-D-glucose.

The hydroxyl group at carbon number 1 of the hemiacetal group can take two different positions (Figure I-26). Depending on the spatial arrangement of this hydroxyl group, lactose can exist in α and β stereoisomer forms (Figure I-26). In aqueous solutions of lactose, the reversible conversion from one isomer to the other, known as *mutarotation*, takes place permanently and spontaneously whereas in solid phase, this transformation is insignificant due to reduced mobility of molecules in solid phase.

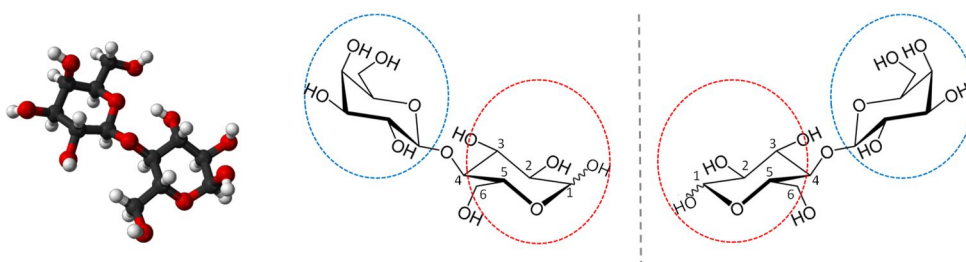


Figure I-26: Molecular structure of Lactose

7.1.2 Lactose in binary aqueous solutions

In aqueous phase, the galactose ring is unstable and opens up at the carbon number 1 so that the spatial arrangement of the hydroxyl group of the carbon number 1 changes constantly from one isomer to the other (phenomenon known as *mutarotation*):

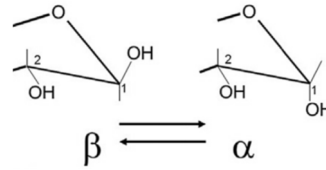


Figure I-27: Mutarotation reaction

The rate of mutarotation depends on the temperature, the pH and the impurities in the aqueous solution. At equilibrium, the ratio of the concentration of α to β isomers is represented by the equilibrium constant, K :

$$K = \frac{k_1}{k_2} = \frac{[C_\beta]}{[C_\alpha]} \quad (I-18)$$

where k_1 and k_2 correspond to the rate constants of the reversible mutarotation mechanism. These constants vary with temperature, pH and impurities. The temperature dependence of the rate constants, k_1 and k_2 , obeys the Arrhenius Law:

$$k_i = k_{i,0} e^{-\frac{E_i}{RT}} \quad i = 1 \text{ or } 2 \quad (I-19)$$

On the other hand, the kinetic rate depends on pH and follows a U-shape trend (Figure I-28): the mutarotation remains almost constant in the pH range between 3.0 and 6.0 whereas it increases sharply outside of this range [80].

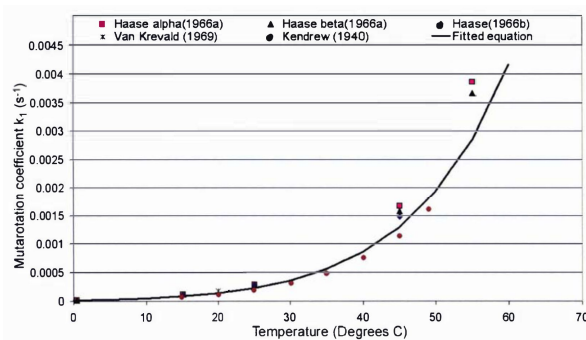


Figure 2-6 The effect of temperature on the lactose mutarotation rate

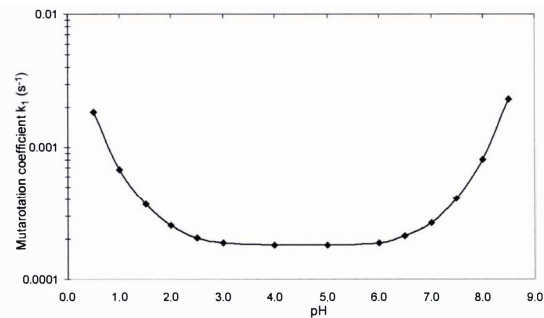


Figure 2-7- The relationship between pH and the lactose mutarotation rate in water at 25 °C (Troy & Sharp, 1930)

Figure I-28: Temperature and pH dependency of mutarotation kinetics (Source [80])

However, according to the literature, unlike the transformation rate, the equilibrium constant is not sensitive to pH and varies only slightly with temperature. For example,

Roetman and Buma [83] using three different methods to quantify the equilibrium constant on the temperature range from 0°C to 100°C established the following correlation for the equilibrium constant:

$$K = 1.6353 - 0.0024 T \quad (I-20)$$

with T in K. For example, AT 20°C, the equilibrium corresponds to 63% β -lactose and 37% α -lactose.

7.1.3 Solid forms of lactose

In solid state, lactose could exist in both amorphous (disordered arrangement of molecules) and crystalline (highly ordered lattice) forms. In addition, lactose is a polymorphic product and can exist in several crystalline forms. According to the literature, there are at least five different crystalline forms of lactose (Table I-4). One of them only is hydrated and the others are anhydrous being stable or unstable. Kirk *et al.* [84] reported five well accepted crystalline forms, including the hydrated form (α -lactose monohydrate), anhydrous β -lactose, stable anhydrous α -lactose and unstable (hygroscopic) anhydrous α -lactose. Note that some other investigators [13, 78] distinguished also a sixth form corresponding to Compound β/α lactose.

However, the most commonly used types in industrial applications are amorphous lactose as well as crystalline α -lactose monohydrate and β -lactose anhydrous. Therefore, in this work, only these three types of lactose whose properties will be described in the following paragraphs were used.

Table I-4: Different forms of solid lactose (from Carpin *et al.* [13])

Currently known forms of lactose (from Listiohadi *et al.* (2005b))

Crystalline	Monohydrate	α -lactose
	Anhydrous	Unstable α -lactose
		Stable α -lactose
		β -lactose
		Compound β/α lactose
Amorphous	Mixture of α -lactose and β -lactose	

7.1.3.1 α -lactose monohydrate

α -lactose monohydrate is the most commonly used form of lactose. This form of lactose is generally obtained through crystallization of supersaturated aqueous solutions below 93.5°C. Indeed, although in aqueous solution both α and β anomers are simultaneously present, only α -lactose crystallizes spontaneously below 93.5°C [24]. During crystallization, the water is incorporated in the crystalline structure of the solid and develops Hydrogen bonds with the central oxygen atoms of lactose. The crystal structure of α -lactose monohydrate has been the subject of many studies and is now well described. The first scheme appeared in the early seventies and was revisited recently for a more accurate description of the molecular network and the crystalline structure [85]. The molecular arrangement is described by a sophisticated 3D H-bond network in which each water molecule is H-bonded to four α -lactose molecules through their central oxygen atom (Figure I-29). According to this arrangement, each α -lactose molecule is in turn involved in 14 intermolecular H-bonds (more detailed description of the crystallographic orientation of α -lactose and water can be found in Garnier *et al.* [85, 86]).

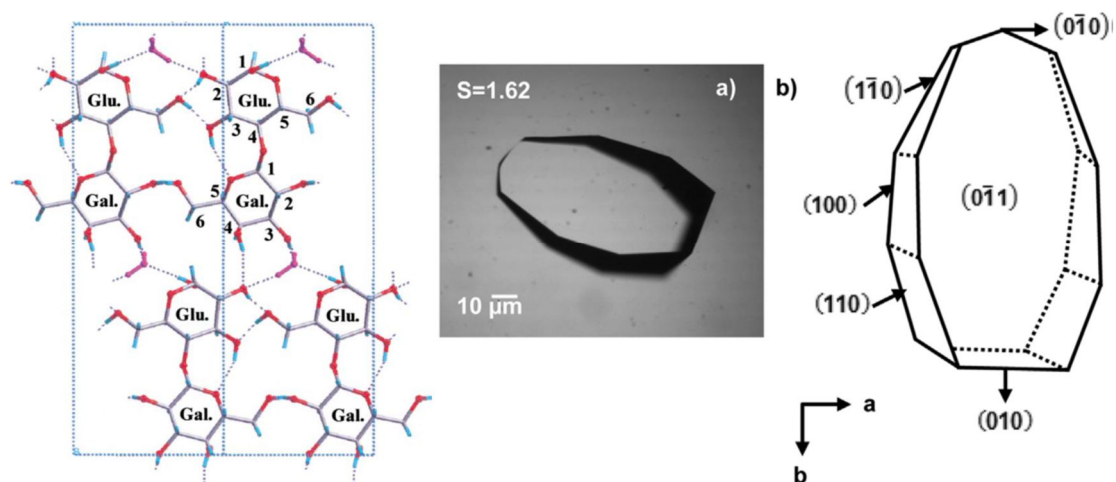


Figure I-29: Crystallographic orientation of α -lactose and water molecules [85] and nucleated α -lactose monohydrate crystal with tomahawk morphology [87]

This structure confers to crystals the well-known “tomahawk-like” shape which is explained by the specific adsorption of β -lactose molecules on 0-1-1 faces during the growth in aqueous medium making this face unavailable for growth [85]. However, recently Parimaladevi and Srinivasan [87] found that the influence of β -lactose depends very much on

the level of supersaturation generated within the mother liquor. Depending on the supersaturation range and evaporating and cooling conditions, other morphologies of crystals shown in Figure I-30 could be obtained.

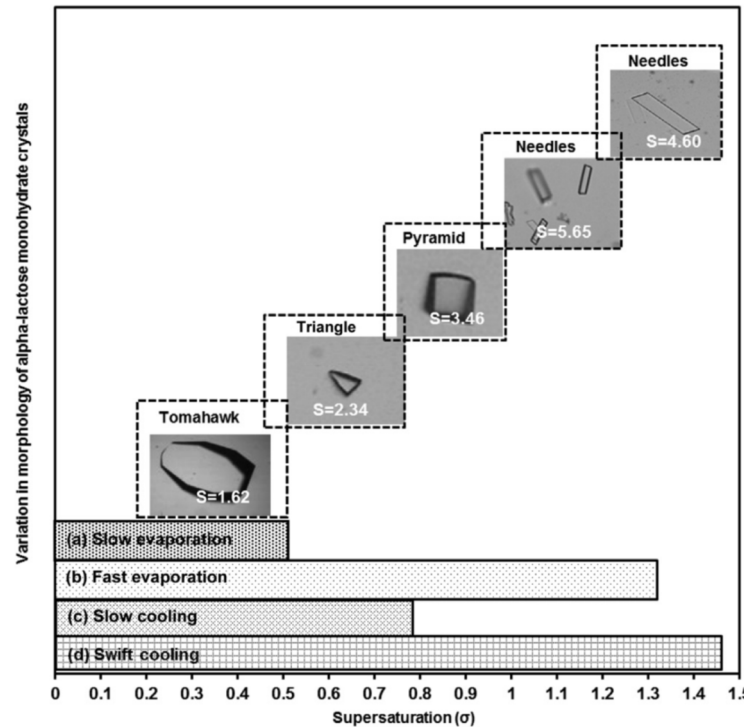


Figure I-30: Change in morphology at different supersaturation ranges generated by four different processes (a) slow evaporation, (b) slow cooling, (c) fast evaporation and (d) swift cooling.

It is important to note that because of strong H-bonds involved in its crystalline structure, α -lactose monohydrate is the most stable form of solid lactose. This form of lactose is not hygroscopic and remains stable below 95% Relative Humidity.

7.1.3.2 Anhydrous β -lactose

Crystallization of lactose containing solutions at temperatures higher than 94°C leads to formation of anhydrous β -lactose, which is the only form of the β anomer in crystalline form. Although less stable than lactose monohydrate, this variety of solid lactose remains stable below 95% RH at room temperature. According to the liquid solvent used for crystallization, the process leads to either uneven-sided diamonds (aqueous solutions) or to curved needle-like prisms (crystallization from alcohols) [88]. In industry, this process is achieved through

roller drying. Note that pure anhydrous β -lactose cannot be isolated and commercially available grades could contain more than 20% of α -lactose.

Anhydrous β -lactose is more soluble than lactose monohydrate so it is suitable for applications where large-scale dissolution is required. Anhydrous lactose is brittle in nature and fractures upon compaction, thereby exposing a larger surface area. This results in additional binding sites and improved compactability. It is therefore used extensively in tableting. The crystals of β -lactose exhibit a characteristic kite-shape.

Table I-5 compares some principal characteristics of these two types of lactose polymorphs.

Table I-5: Main characteristics of α -L-H₂O and β -L (From [80]).

	Units	α -lactose monohydrate	β -lactose anhydride
Molecular weight	g/mol	360.3	342.3
Melting point	°C	202	252
Density	g/ml	1.545	1.59
Specific optical rotation	α_{589}^{20}	+91.55	+33.5
Heat of solution	J/g	-50.2	-9.6
Solubility in water (20°C)	g/100 ml	7.4	50.00

7.1.3.3 Amorphous lactose

The amorphous form of lactose is obtained through rapid drying (*e.g.* spray-drying, freeze-drying) of aqueous lactose. This process causes a sharp increase in viscosity, which prevents crystallization to take place. Spray-dried lactose commonly contains a mixture of amorphous and hydrated lactose. Generally, the product consists of lactose crystals covered by a thin layer and bound together by solid bridges formed by amorphous lactose (Figure I-31). So far, only Freeze-drying process allows reaching higher amounts of amorphous lactose. Note also that crystalline products contain also some amorphous lactose, which often appears in thin layers or in fine fragments following washing/drying or milling operations, respectively.

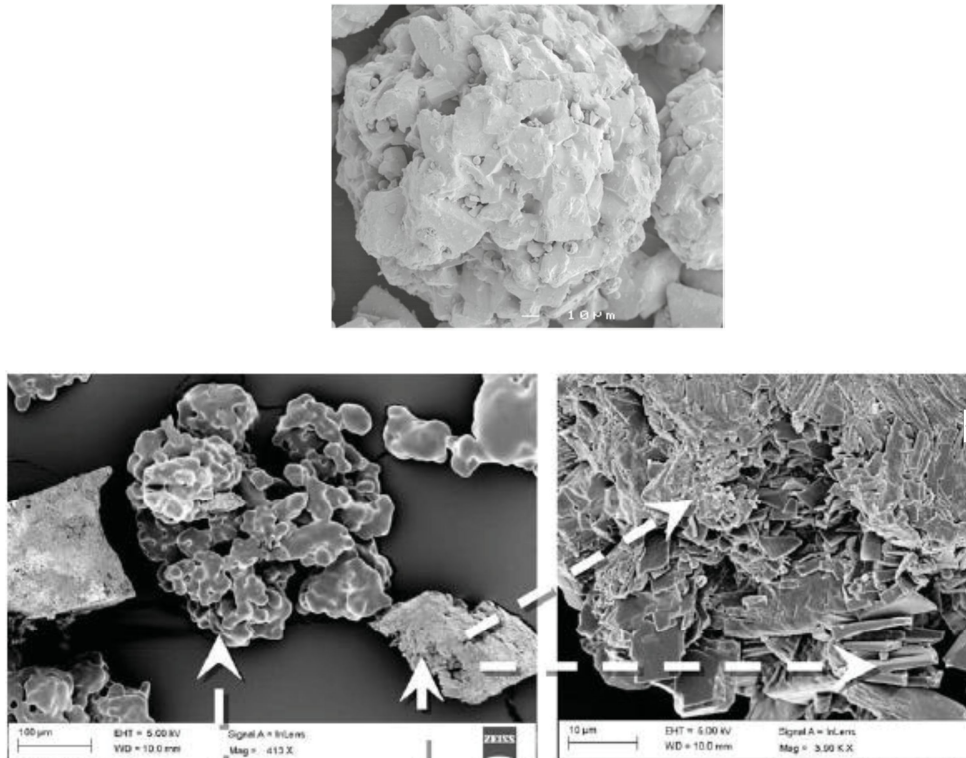


Figure I-31: SEM images of spray-dried lactose top image from [89] and bottom image from [90]

Amorphous lactose is highly hygroscopic. Alike hydrated and anhydrous lactose, the primary use for amorphous lactose is in tablet manufacturing and in dairy food powders. In these applications, the presence of some amorphous form is intentionally sought. For example, due to higher dissolution rate of amorphous lactose, its presence in powdered and instant milk is suitable and helps to reconstitution of dairy formulations. On the other hand, because of its high ductileness and compressibility, during tableting, the amorphous phase makes the spray dried lactose highly compactable. This is beneficial to the tableting process and yields tablets with a convenient tensile strength. Then, a post-crystallization of the amorphous fraction leads to reach higher tableting strengths.

7.1.4 Lactose solubility in water

The solubility of lactose in water is much lower than other sugars. For example, at 25°C the solubility of lactose is about 22 g per 100 g water, which is about fivefold lower than the solubility of sucrose at the same conditions. [Figure I-32](#) compares the solubility of lactose to some common sugars.

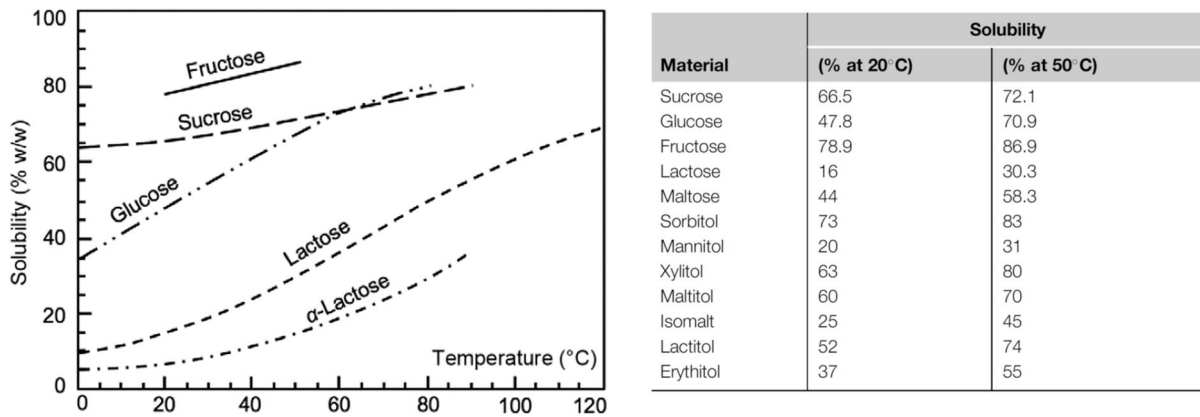


Figure I-32: Solubility of lactose compared to some other common food component sugars as a function of temperature [46].

The equilibrium solubility of lactose in water has been extensively investigated in the literature. Two methods are generally used: dissolving lactose into undersaturated solutions until the dissolution is stopped or crystallizing lactose from supersaturated solutions. It is a well established fact that because of the co-existence of two anomeric forms (α and β), the initial and the final (equilibrium) solubility of α - and β -lactose isomers are different. Indeed, when $L\alpha\text{-H}_2\text{O}$ is dissolved, a part of it is transformed spontaneously and simultaneously to $L\beta$ through mutarotation mechanism. Then, further dissolving of $L\alpha\text{-H}_2\text{O}$ continues until the equilibrium between the two forms, *i.e.* the final solubility, is reached. However, the presence of β -lactose depresses the solubility of α -lactose. The dissolution rate of $L\alpha\text{-H}_2\text{O}$ is higher than both mutarotation and β -lactose dissolution rate. Therefore, depending on temperature, the process is controlled either by mutarotation rate below 93.5°C or by β -lactose solubility above 93.5°C [91]. The discontinuity at 93.5°C arises from the change of stable form of lactose at this temperature [92].

Generally, an exponential law can suitably represent the equilibrium solubility of lactose in water, C_s :

$$C_s = A \cdot e^{B \cdot T} \quad (\text{I-21})$$

where C_s is the total solubility of lactose, T is the temperature in K and A and B are constants. Several authors have investigated the solubility of lactose and established the numerical values for A and B from their experimental data. Some of them are gathered in [Table I-6](#).

Regarding the solubility of $L\alpha\text{-H}_2\text{O}$ itself, as it was already mentioned, the presence of the β anomer in the solution (like other polysaccharides and sugars) depresses the dissolution of $L\alpha\text{-H}_2\text{O}$. This effect is taken into account by means of a depression factor defined as:

$$C_{\alpha s} = \frac{C_s - FK_e(C - C_s)}{K_e + 1} \quad (I-22)$$

where C is the total lactose concentration (anhydrous lactose $\text{g}100 \text{g}^{-1}$ water), $C_{\alpha s}$ is the actual $L\alpha\text{-H}_2\text{O}$ concentration and K_e is the equilibrium constant (Eq. I-20).

Consequently, the βL concentration at saturation can be obtained from the equilibrium constant and the corresponding $L\alpha\text{-H}_2\text{O}$ concentration:

$$C_{\beta s} = K_e \cdot C_{\alpha s} \quad (I-23)$$

Table I-6 summarizes some useful correlations reported in the literature for these different parameters.

Table I-6: Correlations for solubility, C_s , equilibrium constant, K_e , and depression factor, F

Parameter	Correlation	remarks
Final solubility, C_s	$C_s = A \cdot e^{B \cdot T}$ [93]: $A = 0.0035$ & $B = 0.0295$ [94]: $A = 0.0041$ & $B = 0.0287$ [87]: $A = 0.0037$ & $B = 0.0293$ [95]: $A = 0.0052$ & $B = 0.028$ (for $T < 366.65$ K) $A = 0.0589$ & $B = 0.015$ (for $T > 366.65$ K)	T in K C_s in anhydrous lactose $\text{g} \cdot 100\text{g}^{-1}$ water
Equilibrium constant, K_e	$K_e = \frac{k_1}{k_2} = \frac{[\beta]^*}{[\alpha]^*}$ [93] $K_e = 2.01268 - 0.002286 T$ $K_e = 1.644 - 0.0026 T$	
Depression factor, F	[95]: $F = 0.0159 - 0.00023 \theta^{1.36}$ [96]: $F = \exp\left(\frac{-2374.6}{T} + 4.5683\right)$	θ Temperature in $^{\circ}\text{C}$ T Temperature in K

Furthermore, it should be noted that impurities could affect the equilibrium solubility of lactose but pH does not seem to have an effect [97]. Certain salts and sugars, alcohols and whey components can decrease the equilibrium solubility whereas the presence of structurally related additives (SRAs) increases slightly the solubility [85].

Finally, note that under cold conditions the solubility of lactose decreases drastically, it is only about 12 g/100 g of water at 0°C and decreases further towards almost insolubility below the freezing temperature of water (Nickerson, 1974).

7.1.5 Lactose crystallization and crystallization rate in liquid phase

As far as the caking process is concerned, the crystallization in liquid phase is of secondary importance compared to phase transition in liquid phase. However, during the storage of powders under humid conditions, the capillary condensation leads to appearance of free liquid, which could dissolve a part of the solute at the solids surface. The drying of this solution leads to formation of solid bridges due to crystallization.

Numerous studies have been carried out in the area of lactose crystallization kinetics. McLeod [80] provided a critical review of some relevant works reported in literature and noticed that a global conclusion as a collective body of knowledge cannot be drawn definitely. However, all these works highlight the supersaturation, the temperature and the mixing rate as key factors governing the crystallization process.

According to the literature, both crystal morphology (Figure I-30) and crystallization rate depend strongly to the supersaturation level. A rapid overview of literature indicates, as a rough rule of thumb, that the crystal growth rate (G in $\mu\text{m}\cdot\text{min}^{-1}$) varies according to a power law with supersaturation, $G \propto (C - C_s)^n$. Reported values of n vary between 1.3 and 2.5.

The effect of temperature is more controversy and almost the majority of the data reported by different authors indicates that the temperature does not influence significantly the growth rate. This can be explained by the mixing conditions that may be different from one investigation to another. Indeed, the mixing conditions could play a substantial role if the rate-limiting step of growth is the mass transfer to the crystal surface.

Jelen and Coulter [98] studied the crystallization kinetics of lactose at different absolute supersaturations ranging from 10 to 25 (g lactose/100g water) and at varying temperatures from 30°C to 70°C. These authors used a power law model to correlate their experimental data:

$$G = a(C - C_s)^b \quad (I-24)$$

where G is the crystal growth rate ($\text{mg}\cdot\text{m}^{-2}\cdot\text{min}^{-1}$), C is the actual concentration and C_s the concentration at saturation (g lactose/100g water). The C_s values used by these authors were conveniently represented (relative error $< \pm 1.0\%$) by the correlation of Butler [95] or that of Herrington [94] presented in Table I-6. Constants a and b found to be temperature dependent (Table I-7).

Table I-7: constants of crystal growth rate (Eq. I-24)

Temperature, °C	a	b
30	0.148	2.52
50	0.862	2.15
60	1.371	2.05
70	0.839	2.17

Butler [95] reported also the following power law equation to represent the crystal growth rate:

$$G = k_g(C_\alpha - C_{\alpha s})^2 \quad (I-25)$$

$$k_g = 0.00013 T \quad (I-26)$$

The above-mentioned temperature dependency of k_g suggested by Butler was however inconsistent with other works.

McLeod [80] carried out a kinetic study of lactose crystallization and proposed the following correlation:

$$G = 0.0173(C_\alpha - C_{\alpha s})^{1.31} \quad (I-27)$$

This author found that the temperature has only an insignificant effect through its role in solubility.

Note that despite the abundance of work done on this subject, there is unfortunately no study conducted on the nucleation and crystalline growth of lactose in the absence of agitation, a condition that corresponds most to that of efflorescence and consequent caking.

In addition, one may distinguish between conventional crystallization in solution phase and solid-phase crystallization which appears at the presence of low water contents for some amorphous materials. A review on solid-phase crystallization of amorphous lactose will be presented in chapter III. For the moment, let's just mention that it is generally assumed that the crystallization rate is directly related to the viscosity of the medium and must, logically, follow the same evolution with the temperature deviation ($T - T_g$). The corresponding relation is similar to that presented previously (Eq. I-17) except that η and η_g are replaced by crystallization time, t_{cr} , and crystallization time at T_g , respectively.

7.1.6 Glass Transition Temperature

The glass transition temperature of pure amorphous lactose has been reported in many works (*e.g.* [46, 47, 74, 80, 99, 100]). The reported values of the T_g vary between 97 to 110°C. The T_g of humid samples of lactose changes with their water content. Generally, the GT model is convenient to predict the T_g of binary aqueous mixtures of lactose. Remind however that T_g is not an intrinsic property of solids and could vary according to the history of the material and the process conditions (cooling or evaporation rates). The presence of impurities could also affect the value of T_g .

7.2 State diagram of lactose

According to Roos [38, 46, 47, 51], a state diagram consists of a "map" which describes conditions at which amorphous systems appear as solid glasses or as super-cooled liquids at various water contents and temperatures. State diagrams gather the information on concentration dependence of the glass transition of solutes, the solubility and, the solvent crystallization (ice formation).

State diagrams have been established by several authors for lactose, milk powders with various fat contents and with hydrolyzed lactose [69, 74, 101], lactose protein mixtures [102] and lactose–salt systems [103]. It should be noted, however, that the delimitation between the different zones of a state diagram remains approximate and rather qualitative. This is mainly due to the difficulty of measuring the T_g and the materials properties at the glass transition, the experimental errors as well as the accuracy of the correlations used to extrapolate the experimental results. These diagrams remain nevertheless very powerful tools for better understanding and interpreting the experimental results.

In this work, a state diagram for lactose was established based on the main correlations presented in this chapter for the prediction of the T_g and the solubility. The diagram as well as the specific data and correlations used are given in [Figure I-33](#).

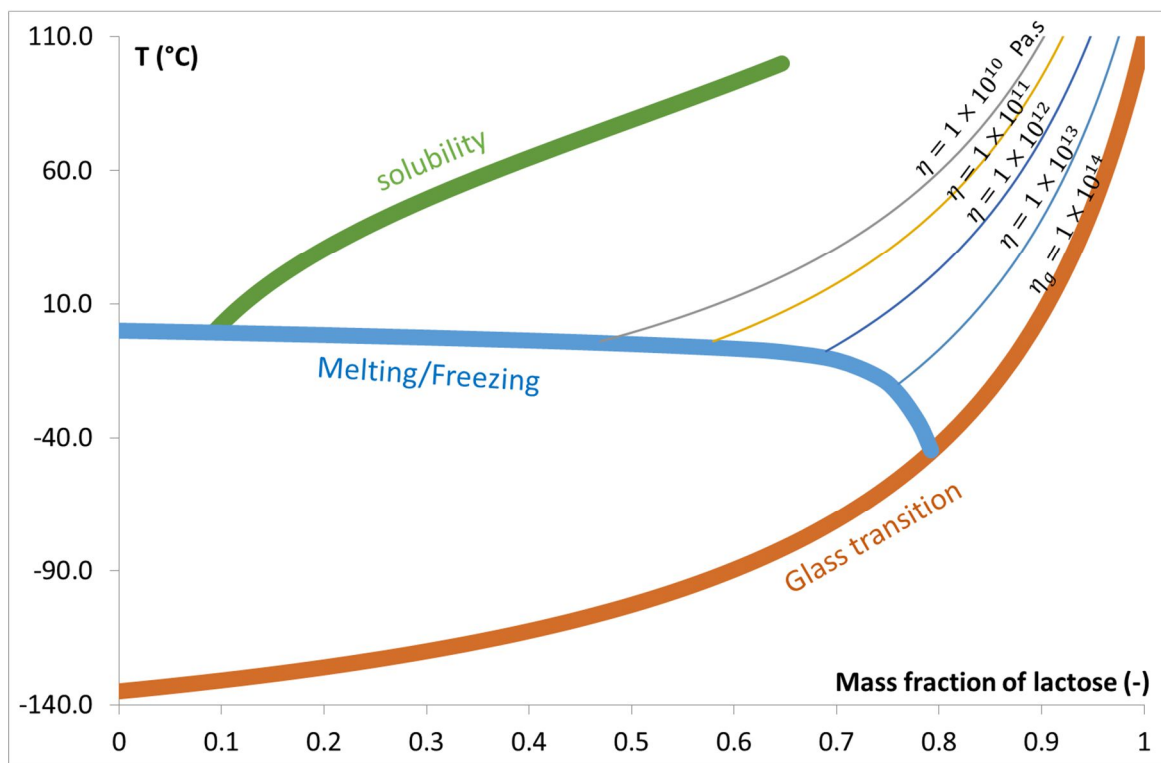


Figure I-33: State diagram of lactose after bibliographic data

8 Conclusion

In this chapter, we presented a bibliographic study on the phenomenon of powder caking. First, some generalities on the caking process were described. Then, the different elementary mechanisms and the interparticle forces that could be at the origin of this phenomenon were commented. A classification of different types of caking was then made. The different types of tests proposed in the literature to quantify the ability of powders to cake were also discussed. The last two sections of the chapter have focused on the structural aspect of the materials concerned. First of all, a general presentation of the structure of materials and phenomena of polymorphism was presented, then a particular focus was made on lactose which is the main support used in the case of our work. This last section was concretized by the establishment of a state diagram for lactose from a synthesis of bibliographic work.

References

1. Saleh, K. and P. Guigon, *Caractérisation et analyse des poudres Propriétés physiques des solides divisés*. Techniques de l'ingénieur Principes de formulation, 2009. **base documentaire : TIB489DUO**(ref. article : j2251).
2. Saleh, K. and P. Guigon, *Caractérisation et analyse des poudres Propriétés comportementales des solides divisés*. Techniques de l'ingénieur Principes de formulation, 2009. **base documentaire : TIB489DUO**(ref. article : j2252).
3. Allen, T., *Powder Sampling and Particle Size Determination*, ed. T. Allen. 2003, Amsterdam: Elsevier. 660.
4. Fayed, M.E. and L. Otten, *Handbook of powder science and Technology*. 2nd Edition ed. 1997: Springer.
5. McGlinchey, D., *Characterisation of Bulk Solids*. 2005: Blackwell Publishing Ltd.
6. Rumpf, H., *Particle Technology*. 1990: Chapman and Hall.
7. Saleh, K. and P. Guigon, *Chapter 7 Coating and encapsulation processes in powder technology*, in *Handbook of Powder Technology*, M.J.H. A.D. Salman and J.P.K. Seville, Editors. 2007, Elsevier Science B.V. p. 323-375.
8. Seville, J.P.K., C.D. Willett and P.C. Knight, *Interparticle forces in fluidisation: a review*. Powder Technology, 2000. **113**(3): p. 261-268.
9. Griffith, E.J., *Cake formation in particulate systems*. 1991: VCH Publishers.
10. Cleaver, J., *Powder Caking – An Overview of the Responsible Mechanisms*. 2007. **79**(9): p. 1387.
11. Zafar, U., V. Vivacqua, G. Calvert, M. Ghadiri and J.A.S. Cleaver, *A review of bulk powder caking*. Powder Technology, 2017. **313**: p. 389-401.
12. Hartmann, M. and S. Palzer, *Caking of amorphous powders — Material aspects, modelling and applications*. Powder Technology, 2011. **206**(1–2): p. 112-121.
13. Carpin, M., H. Bertelsen, J.K. Bech, R. Jeantet, J. Risbo and P. Schuck, *Caking of lactose: A critical review*. Trends in Food Science & Technology, 2016. **53**: p. 1-12.
14. Descamps, N., S. Palzer, Y.H. Roos and J.J. Fitzpatrick, *Glass transition and flowability/caking behavior of maltodextrin DE 21*. Journal of Food Engineering, 2013. **119**(4): p. 809-813.
15. Descamps, N., S. Palzer and U. Zuercher, *The amorphous state of spray-dried maltodextrin: sub-sub-Tg enthalpy relaxation and impact of temperature and water annealing*. Carbohydr Res, 2009. **344**(1): p. 85-90.
16. Descamps, N., E. Schreyer and S. Palzer, *Modeling the sintering of water soluble amorphous particles*, in *PARTEC*. 2007.
17. Palzer, S., *The effect of glass transition on the desired and undesired agglomeration of amorphous food powders*. Chemical Engineering Science, 2005. **60**(14): p. 3959-3968.
18. François, G. and S. Khashayar, *Mise en œuvre des poudres Séchage par atomisation. Procédé*. Techniques de l'ingénieur Mise en forme des médicaments, 2012. **base documentaire : TIB611DUO**(ref. article : j2257).
19. François, G. and S. Khashayar, *Mise en forme des poudres Séchage par atomisation. Principes*. Techniques de l'ingénieur Opérations unitaires : évaporation et séchage, 2012. **base documentaire : TIB316DUO**(ref. article : j2256).
20. Afrassiabian, Z., M. Leturia, M. Benali, M. Guessasma and K. Saleh, *An overview of the role of capillary condensation in wet caking of powders*. Chemical Engineering Research and Design, 2016. **110**: p. 245-254.
21. Guessasma, M., H. Silva Tavares, Z. Afrassiabian and K. Saleh. *Numerical modelling of powder caking at REV scale by using DEM*. in *EPJ Web of Conferences*. 2017.
22. Khashayar, S. and G. Pierre, *Mise en œuvre des poudres Granulation humide : bases et théorie*. Techniques de l'ingénieur Cosmétiques, 2009. **base documentaire : TIB634DUO**(ref. article : j2253).

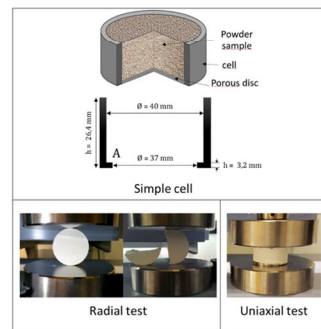
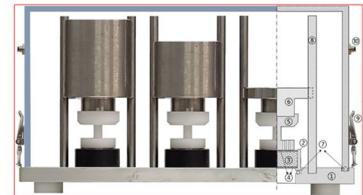
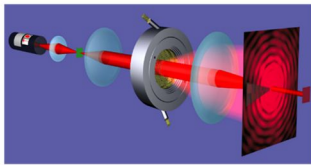
23. Khashayar, S. and G. Pierre, *Mise en œuvre des poudres Techniques de granulation humide et liants*. Techniques de l'ingénieur Mise en forme des médicaments, 2009. **base documentaire : TIB611DUO**(ref. article : j2254).
24. Cleaver, J.A.S., G. Karatzas, S. Louis and I. Hayati, *Moisture-induced caking of boric acid powder*. Powder Technology, 2004. **146**(1): p. 93-101.
25. Langlet, M., F. Nadaud, M. Benali, I. Pezron, K. Saleh, P. Guigon and L. Metlas-Komunjier, *Kinetics of Dissolution and Recrystallization of Sodium Chloride at Controlled Relative Humidity*. KONA Powder and Particle Journal, 2011. **29**: p. 168-179.
26. Samain, S., M. Dupas-Langlet, M. Leturia, M. Benali and K. Saleh, *Caking of sucrose: Elucidation of the drying kinetics according to the relative humidity by considering external and internal mass transfer*. Journal of Food Engineering, 2017. **212**: p. 298-308.
27. Langlet, M., M. Benali, I. Pezron, K. Saleh, P. Guigon and L. Metlas-Komunjier, *Caking of sodium chloride: Role of ambient relative humidity in dissolution and recrystallization process*. Chemical Engineering Science, 2013. **86**: p. 78-86.
28. Mauer, L.J. and L.S. Taylor, *Deliquescence of pharmaceutical systems*. Pharmaceutical Development and Technology, 2010. **15**(6): p. 582-594.
29. Mauer, L.J. and L.S. Taylor, *Water-Solids Interactions: Deliquescence*. Annual Review of Food Science and Technology, 2010. **1**(1): p. 41-63.
30. Dupas-Langlet, M., M. Benali, I. Pezron and K. Saleh, *Characterization of saturated solutions and establishment of "aw-phase diagram" of ternary aqueous inorganic-organic and organic-organic systems*. Journal of Food Engineering, 2017. **201**: p. 42-48.
31. Martin, S., M. Guessasma, J. Léchelle, J. Fortin, K. Saleh and F. Adenot, *Simulation of sintering using a Non Smooth Discrete Element Method. Application to the study of rearrangement*. Computational Materials Science, 2014. **84**: p. 31-39.
32. Martin, S., R. Parekh, M. Guessasma, J. Léchelle, J. Fortin and K. Saleh, *Study of the sintering kinetics of bimodal powders. A parametric DEM study*. Powder Technology, 2015. **270, Part B**: p. 637-645.
33. Kamyabi, M., K. Saleh, R. Sotudeh-Gharebagh and R. Zarghami, *Simulation of Viscous-Flow Agglomerate Sintering Process: Effect of Number of Particles and Coordination Number*. Particuology.
34. Kamyabi, M., R. Sotudeh-Gharebagh, R. Zarghami and K. Saleh, *Principles of viscous sintering in amorphous powders: A critical review*. Chemical Engineering Research and Design, 2017. **125**: p. 328-347.
35. Samain, S., *Caractérisation multi-échelle de l'efflorescence et du mottage du saccharose*. 2017, Université de Technologie de Compiègne.
36. Achenta, S. and M.R. Okos, *Impact of drying on the biological product quality*, in *Food preservation by moisture control. Fundamentals and applications*, G.V. Barbosa-Canovas and J. Welti-Chanes, Editors. 1995, Technomic Publishing: Lancaster, PA. p. 637.
37. Karmas, R., M.P. Buera and M. Karel, *Effect of glass transition on rates of nonenzymatic browning in food systems*. J. Agric. Food Chem. , 1992. **40**: p. 873-879.
38. Slade, L. and H. Levine, *Beyond water activity: recent advances based on an alternative approach to the assessment of food quality and safety*. Crit. Rev. Food Sci. Nutr. , 1991. **30**: p. 115-360.
39. Schenz, T.W., *Glass transitions and product stability—an overview*. Food Hydrocolloids, 1995. **9**(4): p. 307-315.
40. Tager, A., *Physical chemistry of polymers. Second edition*. 1978, Moscow: Mir Publishers.
41. Roos, Y. and S. Drusch, *Phase Transitions in Foods: Second Edition*. 2015. 1-367.
42. Ehrenfest, P., *Phasenumwandlungen im ueblichen und erweiterten Sinn, classifiziert nach dem entsprechenden Singularitaeten des thermodynamischen Potentiales*. Communications from the Physical Laboratory of the University of Leiden, Supplement No. 75b, 1933.
43. Roos, Y. and M. Karel, *Phase Transitions of Mixtures of Amorphous Polysaccharides and Sugars*. Biotechnology Progress, 1991. **7**(1): p. 49-53.

44. Billmeyer, F.W., *Textbook of Polymer science*. 2nd Edition ed. 1971, New York: Wiley-Interscience.
45. Simatos, D., M. Le Meste, D. Petroff and B. Halphen, *Use of electron spin resonance for the study of solute mobility in relation to moisture content in model food systems.*, in *Water Activity: Influences on Food Quality*, L.B. Rockland and G.F. Stewart, Editors. 1981, Academic Press: New York. p. 319-346.
46. Roos, Y.H. and S. Drusch, *Phase Transitions in Foods.*, ed. S. Edition. 2016.
47. Roos, Y.H., *Solid and Liquid States of Lactose*, in *Advanced Dairy Chemistry: Volume 3: Lactose, Water, Salts and Minor Constituents*, P. McSweeney and P.F. Fox, Editors. 2009, Springer New York: New York, NY. p. 17-33.
48. Elliott Stephen, R., C.N.R. Rao and M. Thomas John, *The Chemistry of the Noncrystalline State*. *Angewandte Chemie International Edition in English*, 1986. **25**(1): p. 31-46.
49. Schnell, B., *Etude par simulation numérique de la transition vitreuse et de l'état vitreux de polymères denses amorphes : propriétés mécaniques et phénomène de cavitation*. 2006, Université Louis Pasteur Strasbourg I. p. 206.
50. Caffarena, E.R. and J.R. Grigera, *Glass transition in aqueous solutions of glucose. Molecular dynamics simulation*. *Carbohydrate Research*, 1997. **300**(1): p. 51-57.
51. Roos, Y. and M. Karel, *Applying State Diagrams to Food Processing and Development*. *Food Technology*, 1991. **45**(107): p. 66-70.
52. Arvanitoyannis, I. and J.M.V. Blanshard, *Calorimetric Study of the Glass Transition Occuring in Aqueous Glucose : Fructose Solutions*. *Journal of Science of Food and Agriculture*, 1993. **63**: p. 177-188.
53. Rahman, M.S., *Food Properties Handbook*. 1995, Florida: CRP Press Inc.
54. Rahman, T., P.J. Resnick and B. Harry, *Anders Breivik: Extreme Beliefs Mistaken for Psychosis*. *J Am Acad Psychiatry Law*, 2016. **44**(1): p. 28-35.
55. Arvanitoyannis, I., J.M.V. Blanshard, M.J. Izzard, P.J. Lillford and S. Ablett, *Calorimetric study of the glass transition occurring in aqueous glucose: Fructose solutions*. *Journal of the Science of Food and Agriculture*, 1993. **63**(2): p. 177-188.
56. Pierre, S., B. Eric, D. Anne, M. Serge, O. Evelyne and J. Romain, *Water activity and glass transition in dairy ingredients*. *Lait*, 2005. **85**: p. 295-304.
57. Genin, N. and F. René, *Analyse du Rôle de la Transition Vitreuse dans les Procédés de Conservation Agroalimentaires*. *Journal of Food Engineering*, 1995. **26**: p. 391-408.
58. F., B., in *Physical Properties of Polymers*, K.R. E, Editor. 1979, Publishing Co, Huntington, A.P.: New York, USA. p. 210.
59. Rodriguez, F.J., *Principles of polymer systems*. Second edition ed. 1983, Singapore.
60. Lioyd, R.J., X.D. Chen and J.B. Hargreaves, *Glass Transition and Caking of Spray-Dried Lactose*. *International Journal of Food Science and Technology* 1996. **31**: p. 305-311.
61. Carter, B.P. and S.J. Schmidt, *Developments in glass transition determination in foods using moisture sorption isotherms*. *Food Chemistry*, 2012. **132**(4): p. 1693-1698.
62. Priestley, R.D., C.J. Ellison, L.J. Broadbelt and J.M. Torkelson, *Structural Relaxation of Polymer Glasses at Surfaces, Interfaces, and In Between*. *Science*, 2005. **309**(5733): p. 456.
63. Brady, R.F. and J.M. Charlesworth, *Fluorescence cure studies of amino-epoxy systems*. *Progress in Organic Coatings*, 1994. **24**(1): p. 1-9.
64. Forrest, J.A., K. Dalnoki-Veress and J.R. Dutcher, *Interface and chain confinement effects on the glass transition temperature of thin polymer films*. *Physical Review E*, 1997. **56**(5): p. 5705-5716.
65. DeMaggio, G.B., W.E. Frieze, D.W. Gidley, M. Zhu, H.A. Hristov and A.F. Yee, *Interface and Surface Effects on the Glass Transition in Thin Polystyrene Films*. *Physical Review Letters*, 1997. **78**(8): p. 1524-1527.
66. Bylund, G., *Dairy processing handbook*. 2nd, rev. ed. ed. 2003: Lund : Tetra Pak.
67. Wallack David, A. and C.J. King, *Sticking and Agglomeration of Hygroscopic, Amorphous Carbohydrate and Food Powders*. *Biotechnology Progress*, 1988. **4**(1): p. 31-35.

68. Fitzpatrick, J.J., K. Barry, P.S.M. Cerqueira, T. Iqbal, J. O'Neill and Y.H. Roos, *Effect of composition and storage conditions on the flowability of dairy powders*. International Dairy Journal, 2007. **17**(4): p. 383-392.
69. Roos, Y.H., *Importance of glass transition and water activity to spray drying and stability of dairy powders*. Lait, 2002. **82**(4): p. 475-484.
70. Adhikari, B., T. Howes, B.J. Wood and B.R. Bhandari, *The effect of low molecular weight surfactants and proteins on surface stickiness of sucrose during powder formation through spray drying*. Journal of Food Engineering, 2009. **94**(2): p. 135-143.
71. Williams, M.L., R.F. Landel and J.D. Ferry, *The Temperature Dependence of Relaxation Mechanisms in Amorphous Polymers and Other Glass-forming Liquids*. Journal of the American Chemical Society, 1955. **77**(14): p. 3701-3707.
72. Aguilera, J., J. del Valle and M. Karel, *Caking phenomena in amorphous food powders*. Trends in Food Science & Technology, 1995. **6**(5): p. 149-155.
73. Haque, M.K. and Y.H. Roos, *Crystallization and X-ray diffraction of spray-dried and freeze-dried amorphous lactose*. Carbohydrate Research, 2005. **340**(2): p. 293-301.
74. Jouppila, K. and Y.H. Roos, *Water Sorption and Time-Dependent Phenomena of Milk Powders*. Journal of Dairy Science, 1994. **77**(7): p. 1798-1808.
75. Jouppila, K., J. Kansikas and Y.H. Roos, *Glass Transition, Water Plasticization, and Lactose Crystallization in Skim Milk Powder*. Journal of Dairy Science, 1997. **80**(12): p. 3152-3160.
76. Paterson, A.H.J., G.F. Brooks, J.E. Bronlund and K.D. Foster, *Development of stickiness in amorphous lactose at constant T-T_g levels*. International Dairy Journal, 2005. **15**(5): p. 513-519.
77. Rault, J., *Origin of the Vogel-Fulcher-Tammann law in glass-forming materials: the α - β bifurcation*. Journal of Non-Crystalline Solids, 2000. **271**(3): p. 177-217.
78. Carpin, M., *Lactose caking: Understanding the mechanisms as a route to prevention*, in INRA-Agrocampus Ouest, *Science and Technology of Milk and Eggs (STLO)*, Rennes, France. 2018, European University of Brittany.
79. Affertsholt, T. and D. Pedersen, *Whey Book 2016 - The Global Market for Whey and Lactose Ingredients 2016-2020*. . 2016: 3A Business Consulting.
80. Mcleod, J., *Nucleation and growth of alpha Lactose Monohydrate*, in *Process Engineering*. 2007, Massey University: New Zeland.
81. Alais, C., *Science du lait - Principes des techniques laitières - 3ème Edition*. 1974.
82. Urashima, T., K. Fukuda and M. Messer, *Evolution of milk oligosaccharides and lactose: a hypothesis*. Animal. , 2012. **6**(3): p. 369-374.
83. Roetman, K. and T.J. Buma, *Temperature dependence of the equilibrium β/α ratio of lactose in aqueous solution*. Netherlands Milk and Dairy Journal, 1974. **28**: p. 155-165.
84. Kirk, J.H., S.E. Dann and C.G. Blatchford, *Lactose: A definitive guide to polymorph determination*. International Journal of Pharmaceutics, 2007. **334**(1): p. 103-114.
85. Garnier, S., S. Petit and G. Coquerel, *Influence of supersaturation and structurally related additives on the crystal growth of α -lactose monohydrate*. Journal of Crystal Growth, 2002. **234**(1): p. 207-219.
86. Garnier, S., S. Petit and G. Coquerel, *Dehydration Mechanism and Crystallization Behavior of Lactose*. Journal of Thermal Analysis and Calorimetry, 2002. **68**(2): p. 489-502.
87. Parimaladevi, P. and K. Srinivasan, *Influence of supersaturation level on the morphology of α -lactose monohydrate crystals*. International Dairy Journal, 2014. **39**(2): p. 301-311.
88. Holsinger, V.H., *Physical and chemical properties of lactose*, in *Advanced Dairy Chemistry*, F.P. F., Editor. 1997. p. 1-38.
89. *Amorphous lactose. Origins and measurement*, D. Pharma, Editor.
90. Whiteside, P., S. Luk, C. Madden-Smith, P. Turner, N. Patel and M. W George, *Detection of Low Levels of Amorphous Lactose using H/D Exchange and FT-Raman Spectroscopy*. Vol. 25. 2008. 2650-6.
91. Walstra, P. and R. Jenness, *Dairy Chemistry and Physics*. 1984, New York: John Wiley.

92. Hudson, C.S., *The hydration of milk-sugar in solution*. . Journal of the American Chemical Society, 1904(26): p. 1065-1082.
93. Visser, R.A., *Supersaturation of alpha-lactose in aqueous solutions in mutarotation equilibrium*. Netherlands Milk and Dairy Journal, 1982. **36**: p. 89-101.
94. Herrington, B.L., *Some physico-chemical properties of lactose. VII. Transformations of α -hydrate in organic solvents and at high temperatures.*, in *Borden Award Address, 114th Meeting of the Association of the American Medical Colleges*. 1948: Portland, OR, USA.
95. Butler, B., *Modelling Industrial Lactose Crystallization*. . 1998, University of Queensland: Queensland.
96. Wong, S.Y., R.K. Bund, R.K. Connelly and R.W. Hartel, *Designing a lactose crystallization process based on dynamic metastable limit*. Journal of Food Engineering, 2012. **111**(4): p. 642-654.
97. Smart, J.B., *Effect of Whey Components on the Rate of Crystallization and Solubility of α -Lactose Monohydrate*. New Zealand Journal of Dairy Science and Technology, 1988. **23**: p. 275-289.
98. Jelen, P. and S.T. Coulter, *Effects of supersaturation and temperature on the growth of lactose crystals*. Journal of Food Science, 1973. **38**(7): p. 1182-1185.
99. Clark, Z., A.H.J. Paterson, R. Joe and J.S. McLeod, *Amorphous lactose crystallization kinetics*. International Dairy Journal, 2016. **56**: p. 22-28.
100. Ronkart, S.N., C.S. Blecker, C. Deroanne and M. Paquot, *Phénomène de la transition vitreuse appliquée aux glucides alimentaires amorphes à l'état de poudre*. Biotechnologie, Agronomie, Société et Environnement, 2009. **13**(1): p. 177-186.
101. Vuataz, G., *The phase diagram of milk: a new tool for optimising the drying process*. Lait, 2002. **82**(4): p. 2002.
102. Haque, M.K. and Y.H. Roos, *Differences in the physical state and thermal behavior of spray-dried and freeze-dried lactose and lactose/protein mixtures*. Innovative Food Science & Emerging Technologies, 2006. **7**(1): p. 62-73.
103. Omar, A.M.E. and Y.H. Roos, *Water sorption and time-dependent crystallization behavior of freeze-dried lactose-salt mixtures*. LWT - Food Science and Technology, 2007. **40**(3): p. 520-528.

Chapter 2: Materials & Methods



1 Introduction

This chapter presents the materials and methods used in in this work to study the caking behavior of powders. It first presents the analytical techniques and experimental tools used and then the products experimented in this study. A set of typical results is also presented and discussed.

2 Analytical Techniques

2.1 ESEM images

The surface of powders was examined by using Environmental Scanning Electronic Microscopy (Philips XL30 ESEM-FEG). This instrument has the performance of a conventional SEM but has the advantage that practically any material can be examined in its natural state in dry or humid environment at pressures as high as 1330 Pa (10 Torr). Due to the multiple pressure limiting apertures (PLA) and its environmental secondary electron detectors (GSED), the microscope can offer high-resolution images in a saturated water vapor environment keeping the sample in its original wet state (minimum 4.6 Torr at 0°C). Dehydration and hydration in the ESEM is a question of temperature and vacuum pressure: a Peltier cooled specimen stage offers the possibility to maintain water on the samples inside and to investigate samples between -5 and +60°C.

2.2 Particle size analysis

The Particle Size Distribution (PSD) was measured using two equipment, both of which are manufactured by Malvern Instruments: laser diffraction (Malvern 2000) which provides volume-based distributions and image analyses (Malvern Morpho G3) which gives number-based information.

2.2.1 Laser granulometry

The laser diffraction technique is based on the diffraction pattern (rings) which appears when a particle is illuminated by a coherent and monochromatic laser beam ([Figure II-1](#)).

According to Fraunhofer's approximation of the Mie theory, the intensity of the diffracted radiation is a function of the diameter of the particles: The finer the particles, the greater the angle of diffraction. For large opaque particles, only the diffracted part of the light is significant and the results can be analysed based on Fraunhofer theory, which is a simplified form of the general theory established by Mie [1]. The Fraunhofer theory is applicable only if the particles size is significantly larger than the wavelength of the laser beam ($d_p > 10 \lambda$). In the opposite case, it is necessary to use the general theory of Mie, which takes into account the light scattering as well. This theory requires however the knowledge of refraction indices of the materials. The diffraction particle size analysis is sensitive to the volume of the particles and measures the diameter of the equivalent sphere having the same light scattering properties as the particle analysed. This technique is fast, allows the analysis of a large quantity of sample and, ensures a good repeatability.

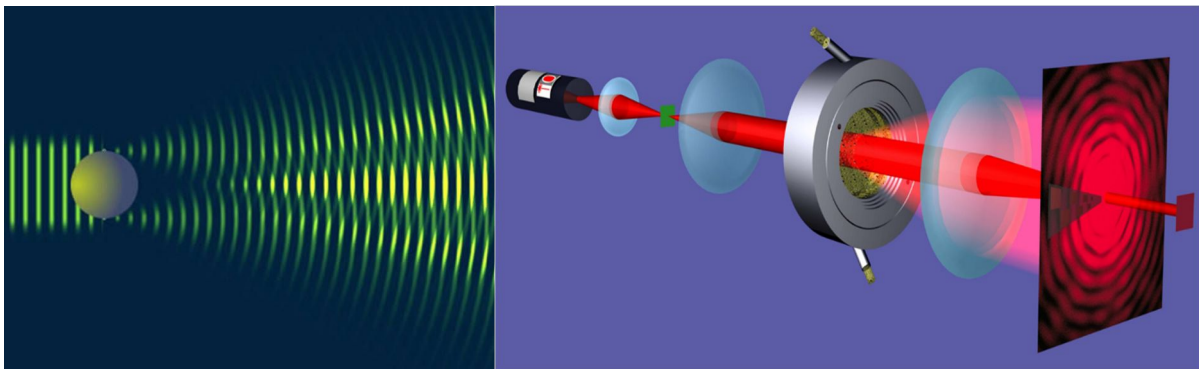


Figure II-1: Idealized scattering of a spherical particle (left-
<http://www.horiba.com/scientific/products/particle-characterization/technology/laser-diffraction/>)
and the principle of laser diffraction particle size analysis (right-Malvern documentation)

In this work, laser diffraction measurements were carried out using a Mastersizer 2000 from Malvern Instruments. This equipment allows to measure sizes between 0.02 μm and 2000 μm and can operate in dry or liquid conditions. The measurements were carried out in the dry phase using the Sirocco sampler (Malvern Instruments) which allows to:

- control the sample feed rate through a vibrating hopper;
- control the dispersion pressure in a range from 0 to 4 bar. The dispersion is then achieved by suspending the particles within an air stream.

Each test requires only a few grams of sample. Measurements were repeated at least three times for each sample. The data processing was then carried out using the "Mastersizer" software to obtain the various desired parameters:

- d_{32} : average surface-volume diameter (or Sauter diameter);
- $d_{x\%}$: diameter such that x percent of the particles (in volume) are smaller than $d_{x\%}$. In this case, three diameters $d_{10\%}$, $d_{50\%}$, $d_{90\%}$ were chosen. Note also that $d_{50\%}$ corresponds to the median of the particle size distribution;
- the "span" that characterizes the broadness of the particle size distribution:

$$span = \frac{d_{90\%} - d_{10\%}}{d_{50\%}}$$

2.2.2 Morpho-granulometry analysis

Combined shape and size analyses were carried out by image analysis using a Morpho G3 from Malvern Instruments. The "MorphologIG3" (Figure II-2) is an advanced characterization tool for measuring particle size and shape from 0.5 microns to several millimetres. This technique is often used in conjunction with laser granulometry, to deepen the knowledge of the product or the behavior of the process.

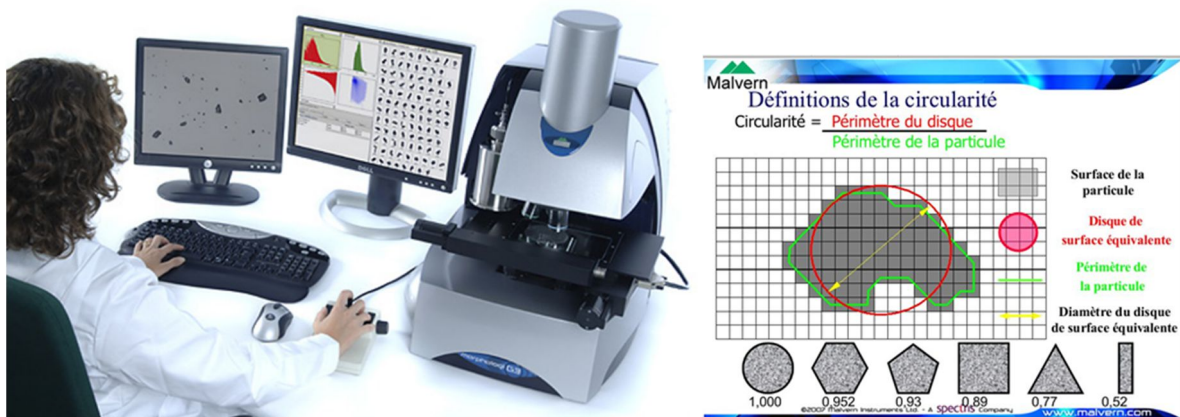


Figure II-2: MorphologIG3 size and shape analyzer

MorphologIG3 measures the particle size and shape distribution of particles using static image analysis. There are three essential steps in the measurement process:

- Preparation and dispersion of the sample. This step is critical to getting good results. The goal is to obtain a physical separation of individual particles and agglomerates. The MorphologIG3 has an integrated dry powder dispersion system that makes the preparation of dry powder samples simple and reproducible. A range of accessories is also available for the preparation of samples in the form of liquid-phase suspensions or membrane filters.
- Image Capturing. The instrument captures images of individual particles by scrolling the sample under the microscope's lenses while keeping the focus on the particles. The MorphologIG3 can illuminate the sample from above or below, while precisely controlling the level of illumination.
- Data analysis. The instrument measures a range of morphological parameters for each particle. The software's advanced graphing and data classification options allows to extract relevant data from collected data. Images are stored individually for each particle to allow qualitative verification of quantitative results.

The measuring range of the device is between 0.5 μm and 10 mm (depending on the sample). From the image analysis, different size parameters can be determined:

- Size parameter: EC diameter (Equivalent Circle), length, width, perimeter, area, max distance, *etc.*
- Shape Parameters: Aspect Ratio, Circularity, Convexity, Elongation HS Circularity, Strength, Mean Intensity, Standard Deviation of Intensity »

A more detailed description of these parameters are given in Appendix A.

2.3 Density measurements

The true (skeletal) density of samples was measured by gas pycnometry (AccuPyc 1330 from Micromeritics) using a 10 cm^3 sample module and helium as filling gas (99.995% pure) (Figure II-3). This technique is based on the determination of the volume of a well-known amount of product. Due to its very small molecular size, helium is capable of filling all

accessible (open) pores within the solids. By measuring the pressure change of helium in two previously calibrated volumes [2], the volume of sample is determined. According to the supplier (Micromeritics) the accuracy of measurements can be estimated to $\pm 0.03\%$ of reading plus $\pm 0.03\%$ of nominal full-scale cell volume.

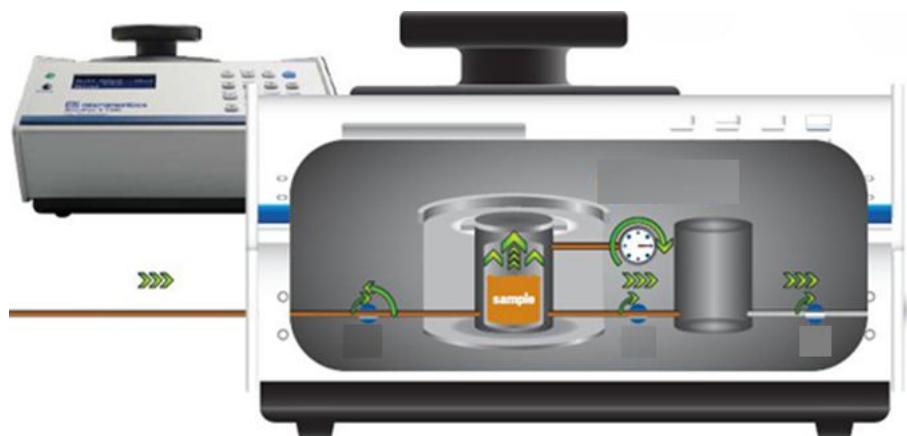


Figure II-3: He pycnometer AccuPyc 1330 from Micromeritics

In this study, density measurements were carried out on approximately 1g of solids. After having accurately measured their mass, the samples were placed in the pycnometer. Prior to each measurement, a series of 5 purges (cycles of cell filling/expulsion of helium) were carried out to remove air and moisture from the chamber. Then, 10 successive density measurements were made and the corresponding average value was determined.

2.4 Specific surface area measurements

The specific surface measurements were performed using an ASAP 2010 device from Micromeritics (Figure II-4-a). Gaseous adsorption (here N_2) allows determination of the specific surface area of the solid particles, including the surface of the open pores, without modifying the geometrical texture of the sample (Figure II-4-b). This technique is limited to the analysis of micro (<2 nm) and meso-pores (2-50 nm). The specific surface area calculation is based on the experimentally determined analytical adsorption treatment, so it is possible to calculate, from the BET theory, the quantity of gas necessary to cover the surface of solids by a monomolecular layer, so the specific surface of the powder.

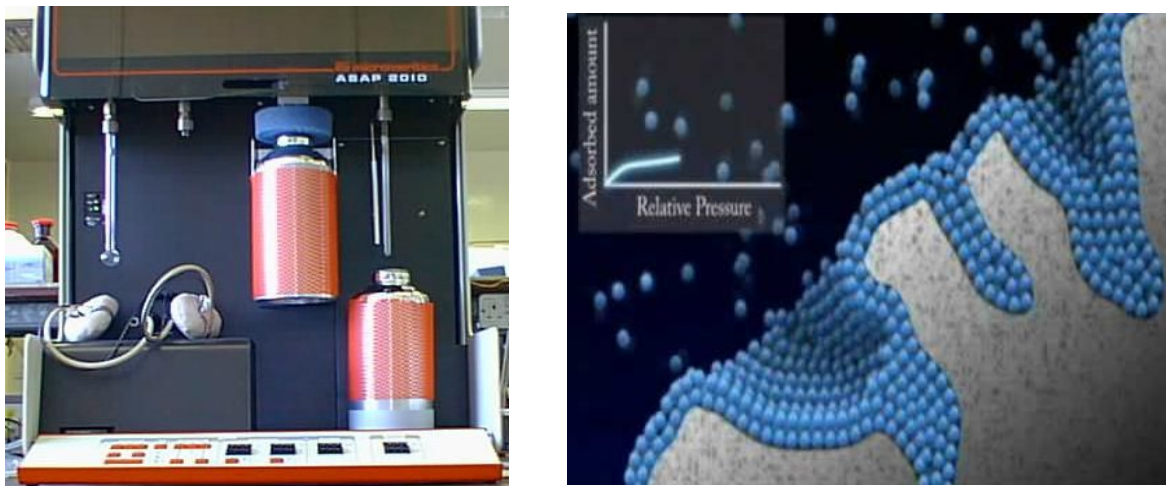


Figure II-4: Surface characterization by gas adsorption: ASAP 2010 instrument (left) and principle of analysis (right)

A specific surface measurement requires the following different handling steps:

- Preparation of the sample to evacuate the water or CO₂ molecules deposited on the sample. This step is carried out under vacuum and high temperature for several hours. In the case of lactose, in order not to alter the product, the temperature is kept below 100 °C. Degassing is preceded by a desiccation step at 20 °C for one week using silica gel.
- Once the sample is prepared, the sample holder is placed on the analysis station, and is immersed in a cooling bath of liquid nitrogen.
- Incremental injections of the adsorbate (N₂) at its normal boiling point. The apparatus uses volumetric measurements to determine the quantities of adsorbed gas as a function of the equilibrium pressure.

Concretely, the sorption isotherm is determined by the sequential introduction of known amounts of adsorbate into the sample holder. At each stage, gas adsorption by the sample occurs and at the pressure in the isolated volume falls until the adsorbate and the remaining gas are in equilibrium. The amount of nitrogen adsorbed at each equilibrium pressure is determined by the difference between the amount of gas initially introduced and that remaining effectively gaseous at equilibrium. These successive measurements of adsorbed quantity and equilibrium pressure allows the establishment of the sorption isotherm

and the corresponding value of the specific surface area and the micro and meso porosity of samples is obtained by applying appropriate theories (*i.e.* BET, GAB, BJH, *etc.*) [3].

2.5 Differential Scanning Calorimetry (DSC)

Differential scanning calorimetry, (DSC), is a thermoanalytical technique in which the difference in the heat flow required to increase the temperature of a sample and a reference pan is measured as a function of temperature. Both the sample and the reference pan are maintained at nearly the same temperature. Generally, the temperature is programmed such that the sample holder temperature increases linearly as a function of time but other programs are also available.

The differential Scanning Calorimeter used in this study to characterise the thermal behavior of materials was a DSC Q100 from TA Instruments (Figure II-5). Given that the thermograms of anhydrous and monohydrate lactose are different [4], the technique allows detecting of eventual transformations during caking. Between 8 and 12mg of powder from each sample was loaded into 40 μ L aluminium pans. The pans were then sealed with an aluminium lid and placed into the autosampler. Samples were analysed over a temperature range of -40°C to 200°C, using a heating rate of 5°C/min. The maximum temperature was limited to 200°C to avoid decomposition of the sample which could damage the heating cell.

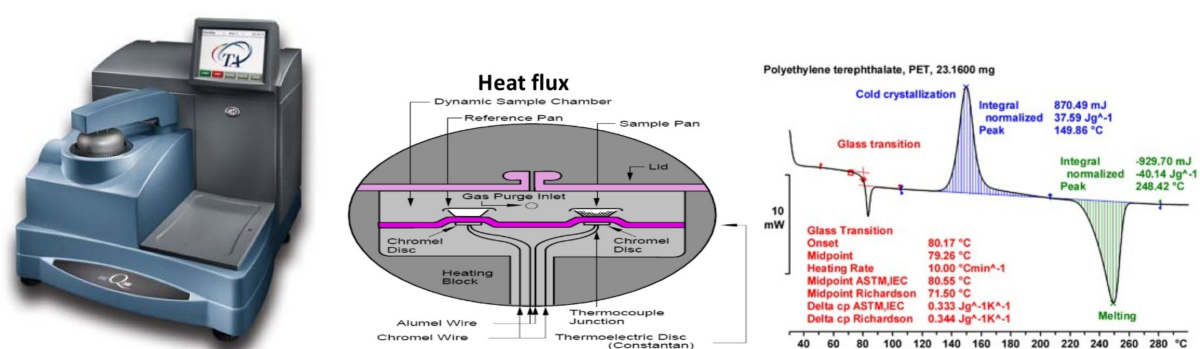


Figure II-5: DSC Q100 from TA Instruments (left) and a sketch of the measuring chamber (middle) and a typical result (right)

2.6 Dynamic Vapor Sorption

Two different instruments were used to measure the water uptake and sorption isotherms of samples: DVS from SMS and SPS from ProUmid GmbH.

2.6.1 Dynamic vapor sorption from SMS

DVS from SMS is a gravimetric water vapor sorption analyzer that measures sorption and desorption isotherms over a broad range of humidity and temperature. A schematic representation of the apparatus is shown in Figure II-6. The apparatus measures uptake and loss of moisture by flowing a carrier gas at a specified relative humidity over a sample suspended from the weighing mechanism of an ultrasensitive recording microbalance. Samples, typically of 10 to 50 mg, are submitted to the continuous gas flow of 200 cm³/min containing pure nitrogen and water-vapor-saturated nitrogen in proportion corresponding to the desired relative humidity. Mass variations due to the uptake of water from the gas phase are measured by an accurate microbalance system with a precision of 0.1 µg. The average mass variation with respect to time, dm/dt , is calculated on a lapse of time of 10 min with an acquisition every minute. Temperature and relative humidity are controlled to 0.1°C and 0.5%, respectively.

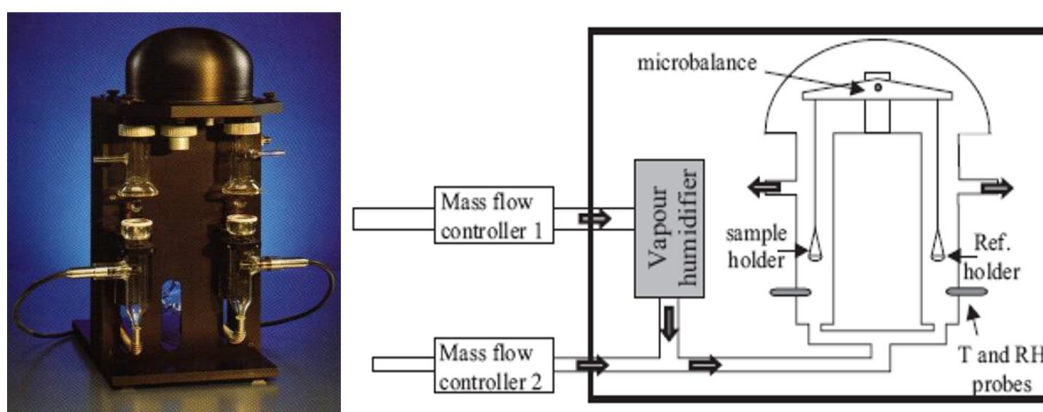


Figure II-6: DVS instrument from Surface Measurement Systems

2.6.2 SPS instrument from ProUmid

The SPS instrument is a multisample Gravimetric Sorption Analyzer, capable of simultaneous measurement of water sorption isotherms on up to 11 samples for the SPS11 versions, with a possibility of upgrade up to 23 samples for SPS23 (Figure II-7). All samples

together with a reference pan are placed on a tray inside a temperature and humidity controlled chamber under a laminar air flow ($20^{\circ}\text{C} < T < 50^{\circ}\text{C}$; $0\% < \text{RH} < 95\%$). The samples are sequentially weighed using a high precision microbalance connected to a computer. Weight variations of each sample are thus recorded every 5 min during the whole experiment through instrument-specific software, as well as air temperature and RH profiles. Additional non-weighed sample positions allow conditioning of material for alternative analysis techniques.



Figure II-7: SPS instrument from ProUmid

2.7 X-ray Diffraction

About 50 mg of each sample was analysed in a Bruker D8 Advance diffractometer equipped with a Lynxeye-XE detector using the $\text{CuK}\alpha$ radiation (Ni filter, $\lambda = 1.5418 \text{ \AA}$). The X-ray powder diffraction (XRD) pattern was recorded from 10° to 50° (2θ) with a step size of 0.02° and counting time of 5 sec/step. The position of peaks in the diffractograms (2θ) was used to determine the interplanar distances following Bragg's law:

$$2d \sin \theta = n\lambda \quad (\text{II-1})$$

where n is a positive integer and λ is the wavelength of the incident wave. The Miller indices, referred as d, h, k, l values were then calculated and compared to standard powder diffraction data in the literature (ICDD PDF4 + database).

3 Caking experiments

Generally, a caking experiment includes three successive stages:

- preparation and preliminary characterization of the samples,
- caking test itself, which must be in as controlled conditions as possible.
- characterization of cakes obtained.

In the present work, the caking of lactose powders were carried out using two principal items of equipment:

- Closed-loop air flow device that we will call "*CLAIR*". It allows accelerated caking experiments by forced-convection in a temperature and RH regulated cabinet. The airflow passing through the samples circulates in closed circuit. However, the airflow is neither measured nor controlled.
- Open-loop air flow equipment, which will be called "*OLAF*". This equipment is controlled in temperature. A flow of air at controlled temperature and RH cross the samples in an open circuit mode with a controlled flowrate.

Both of these experimental devices are home-made facilities that have been designed and developed within our laboratory. The main concept of these two devices is quite close. They will be described in detail in the following paragraphs. They have been designed to accelerate the caking process that might normally take weeks or months to occur. Very briefly, the basic idea is to accelerate the caking phenomenon by forced convection under controlled and evenly distributed conditions. The main difference between the two devices lies in the regulation and irrigation systems used in each of them.

Both devices are multi-cell and can process up to 6 samples at a time. Specially designed sample-holder cells (§2.3) can be used independently with either device. The experiments were carried out depending on the required accuracy and the availability of each these two items of equipment. OLAF provides more reliable results while CLAIR is easier to use and more convenient for preliminary investigations.

For both instruments, the operating temperature was maintained at 25°C and tests were carried out over different time periods ranging from 6 to 96 hours. The standard length of test was 24 hours.

3.1 Closed-loop air flow (CLAIR) caking device

The CLAIR setup can accommodate up to six samples, which are held in place on a rack onto which various pressures can be applied via a perforated junction piece and different weights (Figure II-8). The samples are prepared following a rigorously established procedure using special sample-holder cells (§2.3). The cells are placed on the rack and desired pressures are applied by placing appropriate weights on to them. The base of the sample holder is fixed on a location provided with a sealing ring to ensure the closure between the upper part and the lower part and guarantee that the air passing through the caking cell necessarily crosses the bed of powder. The plastic perforated junction piece is placed between the weight and the sample to ensure that the sample remains exposed to the required environmental conditions throughout the experiment. The range of pressures used was 5, 10, 15, 20 and 25kPa. Once the pressure is applied, the cell can be hermetically closed using a transparent plastic enclosure. A rubber seal placed between the cover and the rack ensures the airtight closure of the chamber. The assembly is then placed inside an enclosure with regulated temperature and RH. A control unit controls the relative humidity (0-90%) and the temperature inside the chamber. The cap of the multi-cell box is equipped with one air inlet in each side for circulating an airflow taken directly from the regulated chamber supplied with a pump. The only possible outlet for the airflow is through the lower porous disc after passing through the bed of powder.

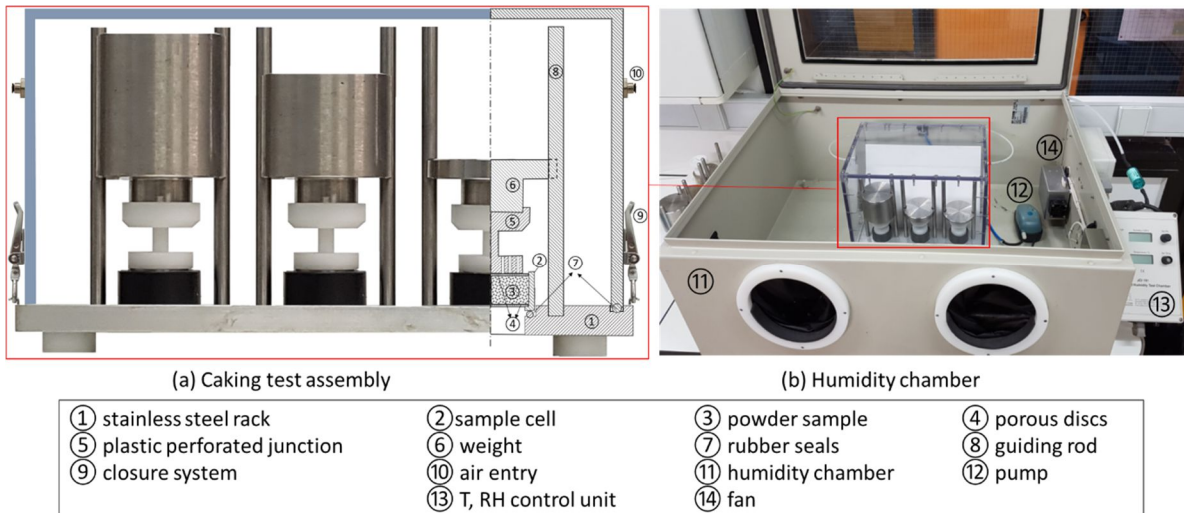


Figure II-8: Closed-Loop AIR flow (CLAIR) caking device

3.2 Open-loop air flow (OLAF) caking device

The OLAF device (Figure II-9) is a homemade instrument consisting of six cylindrical chambers that can each accommodate independently one sample of powder. The cylinders are held in place on a rack, which is placed inside a thermostatically-controlled cabinet (Figure II-9-a). Different pressures may be applied to the samples by putting various weights onto them as a similar way than for CLAIR device. However, here each sample cell can be isolated independently using a cylindrical tube hermetically closed by a lid (Figure II-9-b). The range of pressures used was the same as for CLAIR device (5, 10, 15, 20 and 25kPa).

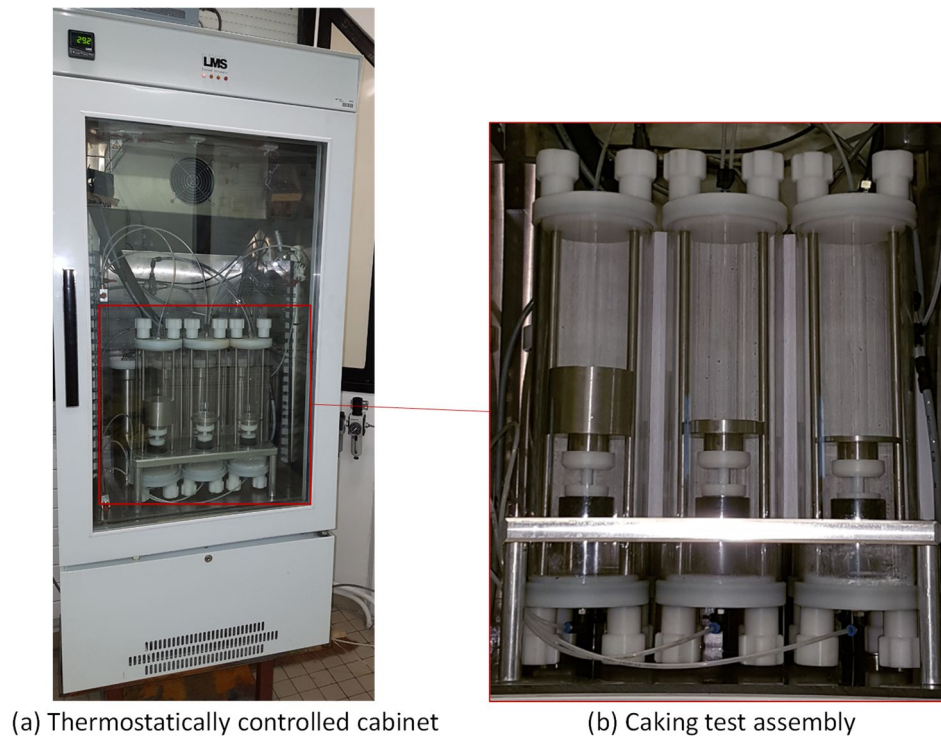


Figure II-9: Multi-cell caking device: thermostatically-controlled chamber (left) and sample holder rack (right)

A forced convective airflow with a specified relative humidity, temperature and flow rate enters the top of each cylinder, passes through the samples and exits via the bottom of the cylinder. The flow of the air can be manipulated between 0 and 15 L/min. The required humidity is generated by mixing a stream of dry air and a stream of air saturated with water vapor. The humidified air stream is obtained by bubbling dry air through distilled water. The available range of relative humidity is 0-95%. A combination of a control unit and software package allows for the modification and monitoring of all variables in the process. For each experimental run, three samples were installed to the caking device, either at the same conditions to evaluate the repeatability or with a different pressure applied to each sample. A schematic diagram of the air humidification circuit and samples loaded into the caking device is shown in [Figure II-10](#).

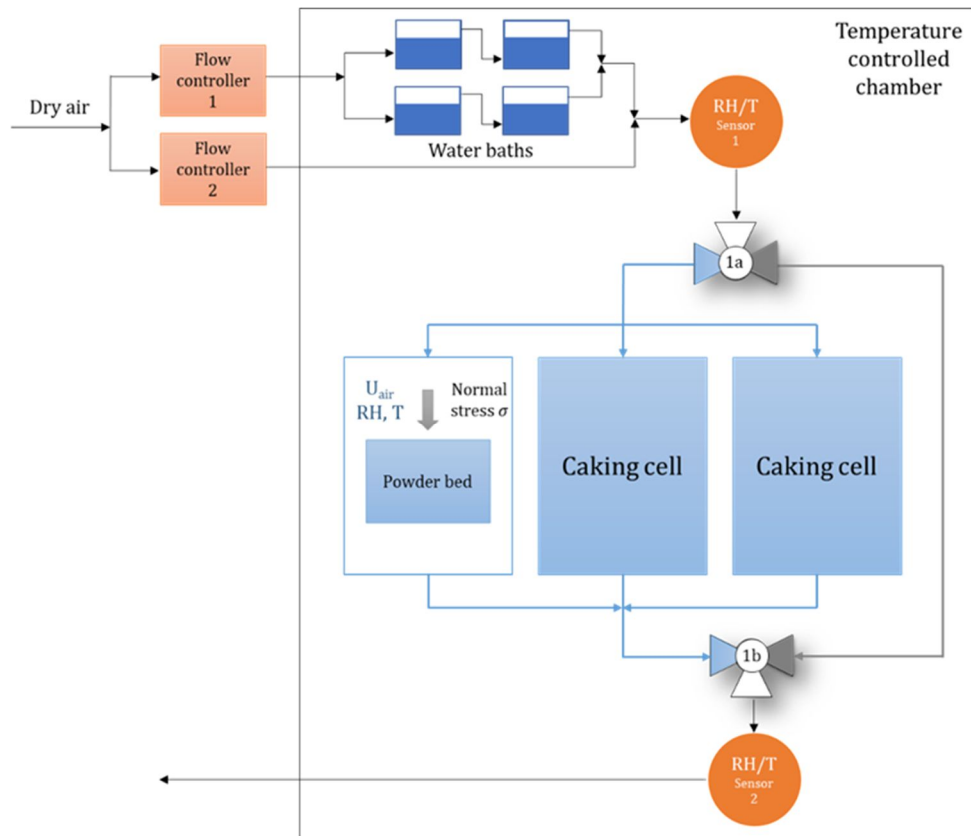


Figure II-10: Schematics of air circuit and humidification system (from [5])

3.3 Caking cells and preparation of samples

The sample preparation protocol is similar for both CLAIR and OLAF devices. Prior to any caking test, the powder samples were placed in a desiccator containing silica gel for at least 48 hours. The samples of lactose powder were prepared in plastic cells. Two types of sample cells were used: single cells and double cells the dimensions of which are given in [Figure II-11](#). The simple cells allow obtaining caked samples, which are demoulded then characterized by either uniaxial or radial compression tests. In order to facilitate demoulding for powders having a strong tendency to cake, a plastic tape was placed along the inner edge of the cell.

The double cell consists of two small plastic cells joined together by an adhesive tape. After preparing the cake, the adhesive tape is gently removed. The cell is then placed inside a two-part metal shell that allows for shear stress analysis to be carried out at a later stage provided that the sample has caked sufficiently. The samples could then be characterized by direct shearing across the cell. The first part of shell was fixed to the immobile lower plate

while the second one was fixed to the mobile top plate (Figure II-11). The top plate was then moved up at a 1 mm/min speed until the cake failed and the two cells were separated.

A porous disc (class 40) in stainless steel, 38.65 mm diameter and 3 mm thickness, was first placed at the bottom of the cells. The powder was then poured to the cell to obtain a bed of powder under identical initial conditions. The initial mass of lactose powder loaded was 18g for single cells and 36g for double-cells. Then the surface was cleanly trimmed. A second porous disc was gently deposited in the top of the powder bed. Each cell and its two accompanying porous discs were weighed with a microbalance ($\pm 10^{-4}$ g) prior to sample loading and then again after sample loading to determine the mass of powder present.

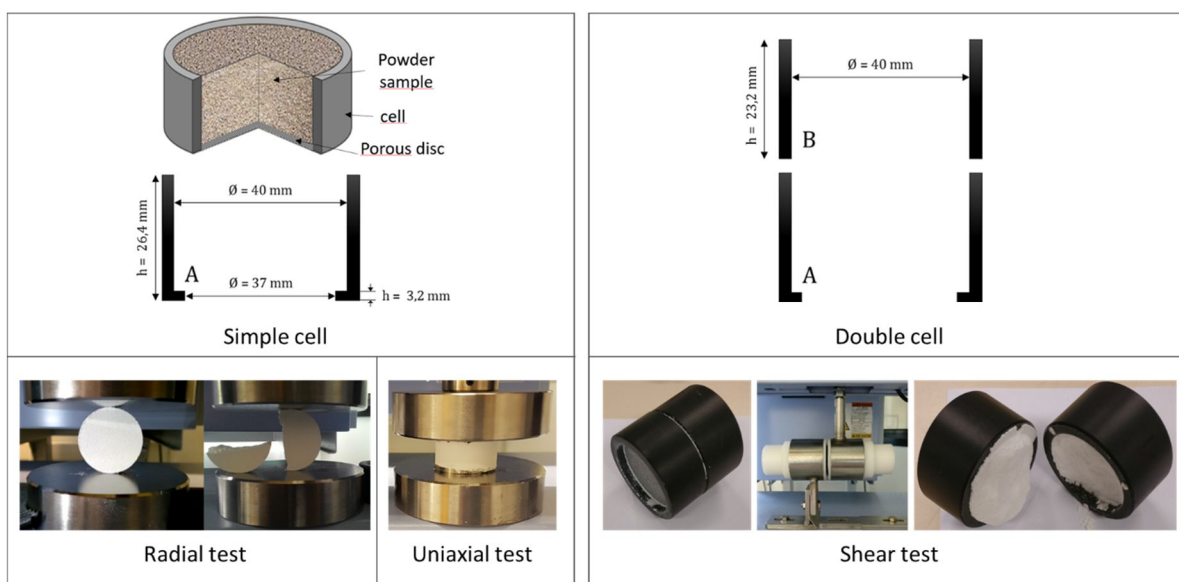


Figure II-11: Schematic of simple (left) and double cells (right) and associated failure tests

3.4 Post-caking analysis

3.4.1 Mechanical resistance tests

Following the caking experiment, the cells were first weighed once more to establish the amount of water absorbed by the samples.

The hardness of the lactose cakes was assessed with a Shimadzu tensile testing machine. The device is capable of measuring force and displacement using integrated software. Different attachments to the device enabled the determination of the radial and shear

stresses that the caked samples could withstand. The radial setting of the device was used for caked samples from the humidity chamber. Each sample was carefully removed from its cell and placed onto the Shimadzu base plate, then the device was calibrated. During testing the crosshead and attached compression plate were lowered at a constant rate onto the sample until the sample fractured. The shear stress testing function was used for samples from the caking device. In this case, the caked sample remained inside the cell and was loaded horizontally into the Shimadzu shearing test clamp. After calibration, the test was started and one half of the clamp is raised at a constant rate whilst the other half remained stationary. When the sample broke, the test was stopped. The arrangement for each Shimadzu setup is depicted in [Figure II-11](#). After testing, the samples were labelled, photographed and stored in a refrigerator until they were needed again. Both raw and caked samples were sent away for X-ray diffraction analysis (XRD), DSC analysis and scanning electron microscope imaging.

3.4.2 Sieving testing method

For weakly caking powders a sieving test was conducted on the caked samples to assess the extent of caking. It consists of a rotating sieve (1 mm aperture) placed horizontally on the top of a balance ([Figure II-12](#)). The caked sample is placed inside the pan and the pan rotates at a given rate. The mass of powder passing through the sieve is monitored to determine the rate of attrition.

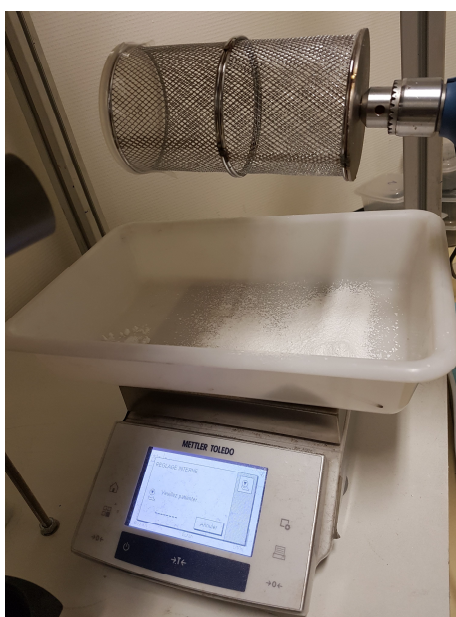


Figure II-12: Photograph of sieving test

4 Lactose samples

Several grades of lactose were used in this work. Samples were either produced on a pilot scale or obtained directly from commercial suppliers. In this section, we present only a brief view of batches used. The main characteristics of each batch and additional specific information for each product will be presented later in the relevant chapters.

4.1 Monohydrate lactose powders

Two types of lactose monohydrate were used in this work:

- FlowLac® 100 α - lactose monohydrate supplied by Meggler (Figure II-13). For more detail see the manufacturer brochure, Appendix B)
- Lactose monohydrated supplied by Sigma-Aldrich France (Figure II-13)

Both powders are white, crystalline, odorless powders that are freely but slowly soluble in water.

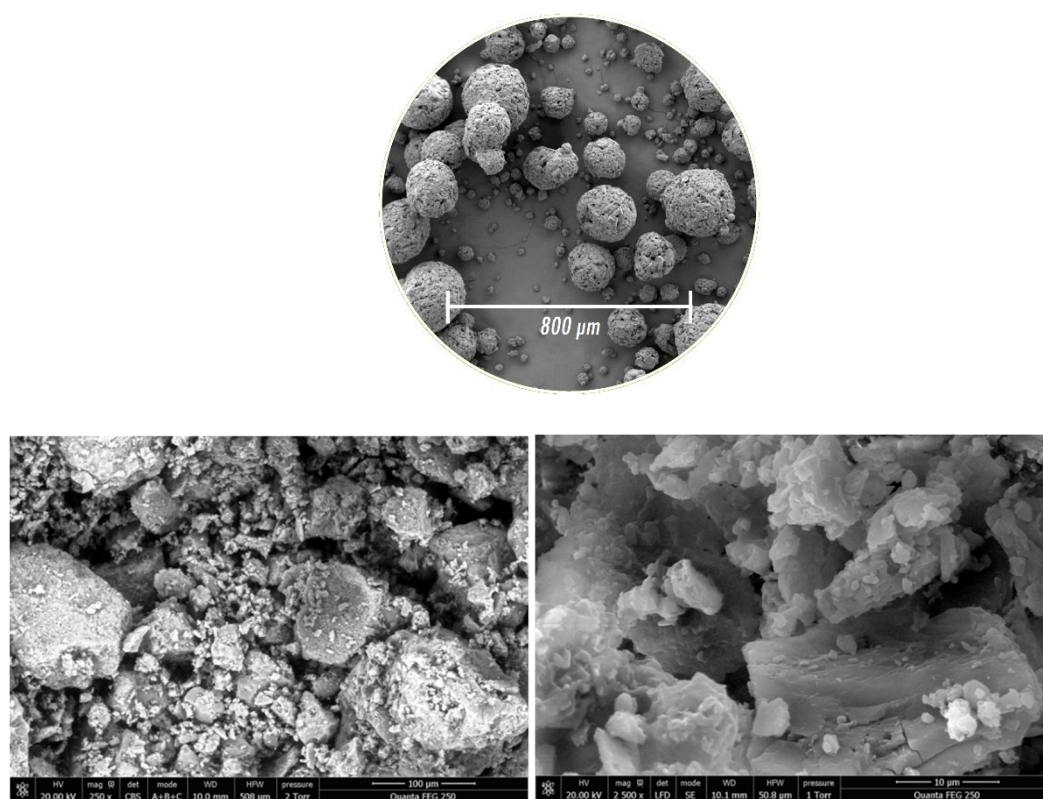


Figure II-13: ESEM images of α -lactose monohydrate from Meggler (top [6]) and Sigma-Aldrich (bottom)

4.2 Anhydrous lactose powder

Anhydrous lactose powder was DuraLac® H from Meggle. It is a white, crystalline, odorless powder and is freely but slowly soluble in water. According to the information provided by the manufacturer, the anhydrous powder is produced via roller-drying followed by milling and sieving to obtain the desired particle size distribution. Its primary application is as a tableting excipient, especially in direct compression processes. The manufacturer reports that the powder contained 16.3% anhydrous α -lactose and 83.7% anhydrous β -lactose (for more details see Appendix B).

The micrographs in [Figure II-14](#) gives an overview of particles at two different zooms.

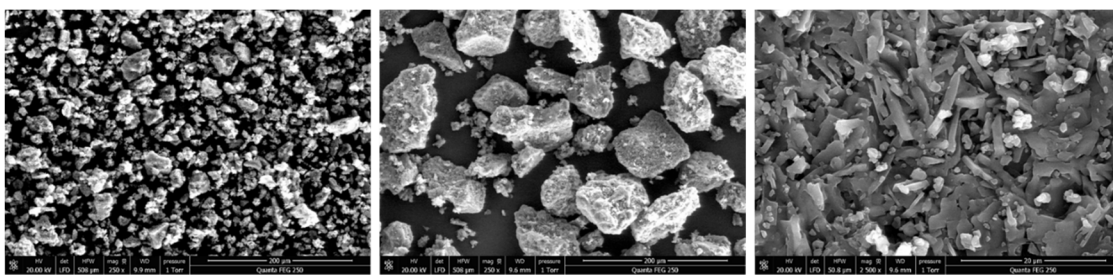


Figure II-14: ESEM images of DuraLac® H from Meggle

4.3 Amorphous lactose samples

The amorphous lactose samples used as model products were prepared by two separate techniques: freeze drying and spray drying. Both techniques are based on dehydration at conditions so that the lactose cannot crystallize [7, 8]. The former technique proceeds at very low temperatures at which crystallization is inhibited whereas the latter technique generates a rapid evaporation of water at kinetic rates much higher than the crystallization rate [9, 10]. Both methods have been shown to produce amorphous lactose but with very different properties ([Figure II-15](#)). The first batches of spray-dried lactose were prepared with the help of the team of Professor Tchoreloff at the "Laboratoire de Pharmacie Galénique et Biopharmacie" of the "UFR Sciences Pharmaceutiques de l'Université de Bordeaux". Further samples were prepared in UTC following the same experimental protocol.

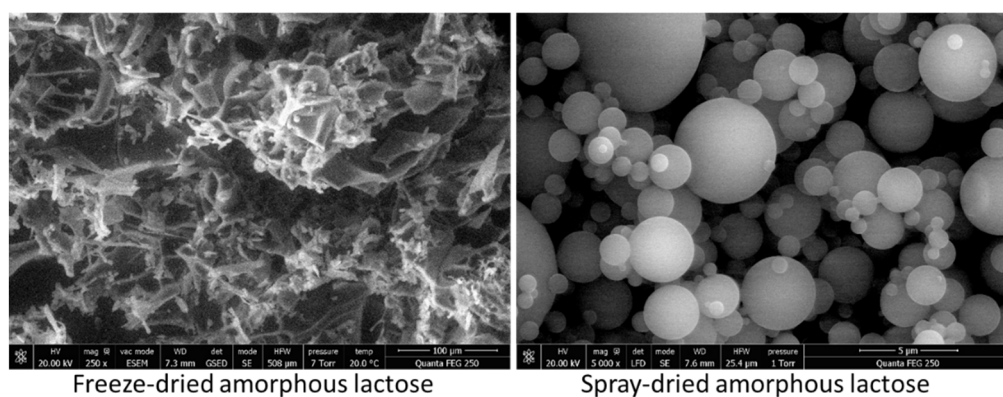


Figure II-15. ESEM images of the freeze-fried (left) and spray dried (right) samples

4.3.1 Freeze drying

In the freeze-drying process, the liquid product is first frozen and then the water is removed by sublimation. This is a low temperature process, and is considered to be superior than other drying methods in terms of product quality though being relatively expensive. Due to the frozen and immobilized matrix, lactose molecules lack the mobility to rearrange themselves into a crystalline lattice. While evaporating the moisture, the product becomes porous in nature and the solid network should be able to hold this porous structure.

The amorphous lactose samples in this case were prepared using the α -lactose monohydrate powder presented earlier. De-ionized water was used for all experiments. α -lactose monohydrate was dissolved in de-ionized water to obtain 20% (w/w) solution using continuous stirring for 24 h at room temperature (~ 25 °C). The solution thus prepared was poured, in equal parts, into the 6 glass ampoules (125mL) of the freeze-dryer. All samples in the glass vessels were frozen in a bath of liquid nitrogen and then subsequently tempered at -80 °C for 6 h prior to freeze-drying using a laboratory freeze-dryer (Lyovac GT2 Freeze Dryer, Amsco Finn-Aqua GmbH, Steris®, Hürth, Germany). After freeze-drying at 0.1 mbar during 84 hours, the samples were manually crushed and then screened with a 100 μ m sieve. Prior to subsequent analysis and caking tests, the samples were stored in a vacuum desiccators over P_2O_5 (Sigma-Aldrich).

4.3.2 Spray drying

Amorphous lactose was produced using a laboratory atomizer (Büchi B-191) the technical characteristics of which are given in the appendix C. The main parts of the installation are shown in Figure II-16.

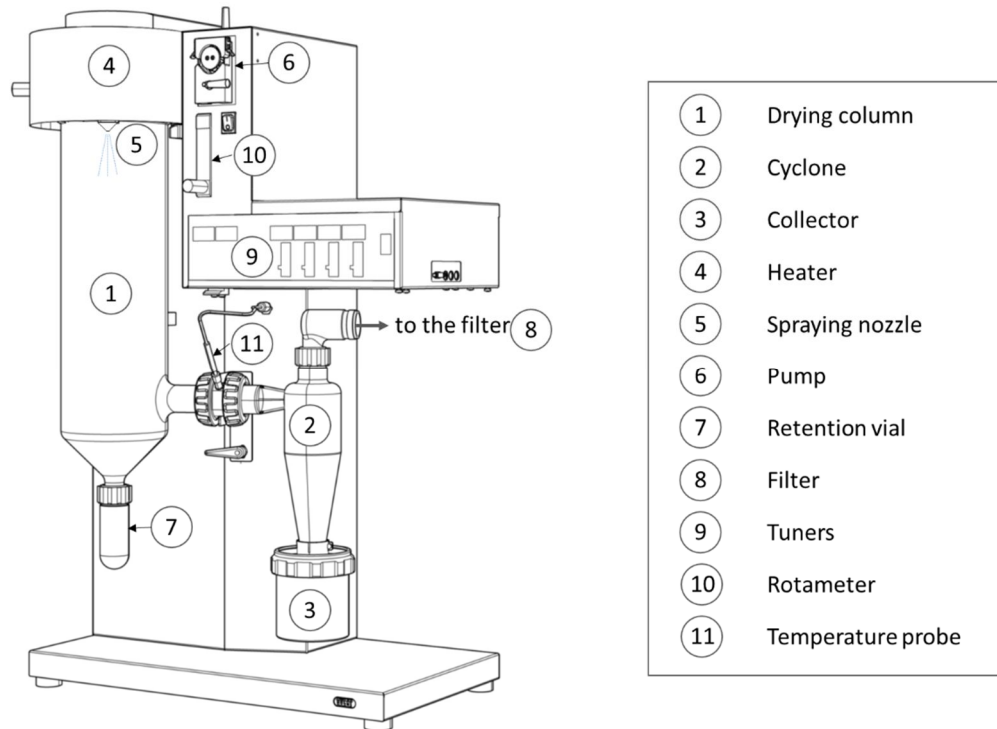


Figure II-16: Schematic of Büchi spray dryer

The spray-dryer consists of:

- a drying column ① of 100mm ID and 500 mm height,
- a cyclone ② allowing the recovery of the dried particles inside a collector ③
- an air preheating system ④ with a power of 2kW installed on the head of the column in the form of a ring with a central hole, which allows the passage, and fixing of the spray nozzle
- a pneumatic spray nozzle ⑤
- a peristaltic pump ⑥ to feed the solution to be dried with the desired flow rate
- a retention vial ⑦ placed at the bottom of the column to recover undried droplets

- a filter ⑧ making to capture the residual particles before the air is released into the atmosphere.

The dryer is also equipped with several tuning buttons (potentiometers) ⑨ to adjust the drying air flow rate and the air temperature at the entrance of the column. The spraying air flow rate is regulated by a rotameter ⑩. The dryer works in co-current mode. A temperature probe ⑪ placed between the drying column and the cyclone makes it possible to measure the temperature of the current at this point.

Both the column, the cyclone and the collector are made of glass, which allows a visualization of the phenomena during the operation.

The other technical characteristics of the equipment are given in the Appendix C.

The protocol for preparing lactose solutions was identical to that used for freeze-drying.

In order to carry out a drying test, the apparatus is first started by setting an air flow rate and a temperature at the inlet of the column without spraying the liquid. The temperatures at the inlet and at the outlet of the column are then expected to stabilize. Then the distilled water is sprayed with the same flow rate as that provided for the solution. This operation leads to a temporary drop in temperatures. Once the temperatures stabilize again around the desired values, the distilled water is replaced by the solution to be dried.

5 Conclusion

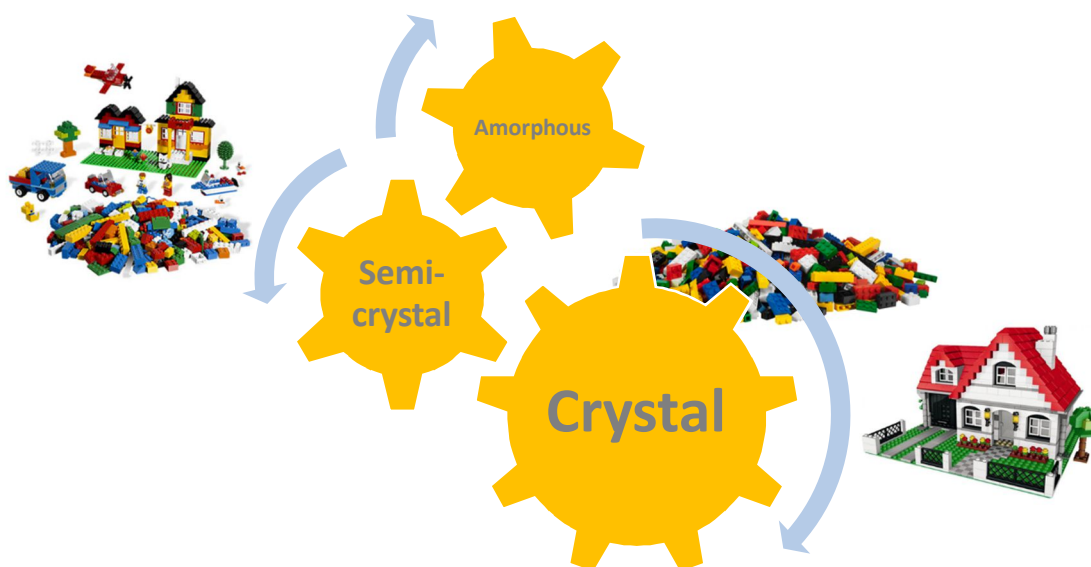
In this chapter we described the main analytical techniques used to characterize the properties of different types of lactose used in this work. The two pieces of homemade instruments used for cake formation were described. Then, the procedure of cake preparation and mechanical resistance measurements were detailed. Finally, the different lactose grades utilized as the support in the present work were introduced briefly. This presentation of the lots has been intentionally shortened and the main characteristics of the lots will be presented in the corresponding chapters.

References

1. Allen, T., *Powder Sampling and Particle Size Determination*, ed. T. Allen. 2003, Amsterdam: Elsevier. 660.
2. Viana, M., P. Jouannin, C. Pontier and D. Chulia, *About pycnometric density measurements*. *Talanta*, 2002. **57**(3): p. 583-593.
3. Saleh, K. and P. Guigon, *Caractérisation et analyse des poudres Propriétés physiques des solides divisés*. Techniques de l'ingénieur Principes de formulation, 2009. **base documentaire : TIB489DUO**(ref. article : j2251).
4. Brittain, H.G. and R.L. Blaine. *α -Monohydrate Phase in Lactose by DSC*. *TA Instruments*. [online]. [viewed 3rd June 2017]. Available at: <http://www.tainstruments.com/pdf/literature/TA293.pdf>. 2016.
5. Samain, S., M. Leturia, S. Mottelet, M. Benali and K. Saleh, *Characterization of caking for crystalline materials: comparison and statistical analysis of three mechanical tests*. Chemical Engineering Science, 2018.
6. *Brochure technique Flowlac*, M.E.a. Technology, Editor. 2016.
7. Roos, Y. and S. Drusch, *Phase Transitions in Foods: Second Edition*. 2015. 1-367.
8. Roos, Y. and M. Karel, *Phase Transitions of Mixtures of Amorphous Polysaccharides and Sugars*. *Biotechnology Progress*, 1991. **7**(1): p. 49-53.
9. Gomez, F. and K. Saleh, *Mise en œuvre des poudres Séchage par atomisation. Procédé*. Techniques de l'ingénieur Mise en forme des médicaments, 2012. **base documentaire : TIB611DUO**(ref. article : j2257).
10. Gomez, F. and K. Saleh, *Mise en forme des poudres Séchage par atomisation. Principes*. Techniques de l'ingénieur Opérations unitaires : évaporation et séchage, 2012. **base documentaire : TIB316DUO**(ref. article : j2256).

Chapter III

The role of amorphous amount in caking of Monohydrate Lactose



This chapter deals with caking behavior of lactose monohydrate powders containing small amounts of amorphous lactose. The objective was to elucidate the relation between the caking ability of powder mixtures and the crystallization behavior of amorphous lactose. Binary mixtures consisting of amorphous lactose and α -lactose monohydrate were prepared and tested using an accelerated caking test. Amorphous lactose samples were prepared using both freeze-drying and spray-drying techniques. Two caking devices were developed to characterize the caking ability of powders. The effect of amorphous content, relative humidity, temperature and pressure on the caking behavior of samples was investigated. The results showed that the presence of even small amounts of amorphous lactose (as low as 0.125%) could cause caking. The most influencing parameters were found to be the relative humidity and the temperature whereas the pressure had no significant effect. The caking behavior was shown to be closely linked with crystallization extent and kinetics. A dimensionless time based on Avrami model for crystallization rate was defined allowing unifying the experimental data.

1. Introduction

In this chapter, we present the results of an experimental study on the caking of lactose monohydrate powders containing small quantities of amorphous lactose. In fact, because the lactose monohydrate is the most stable polymorph of lactose, in the pure state it is not subject to caking. However, the presence of an amorphous phase, even if only in very small quantities, can tip this stability.

Most of the work reported in the literature has addressed the problem of caking of amorphous powders under an angle of their propensity to deform and creep above the glass transition [1-6]. However, it is now well established that amorphous powders including lactose or other sugars can undergo solid phase crystallization when exposed to the ambient humidity [7-23]. This crystallization whose kinetics increases with the difference of the temperature with respect to the glass transition temperature of the product ($T-T_g$) can lead to formation of solid bridges between particles and thus to caking [9, 24]. However, so far, the studies carried out on the solid-phase crystallization of lactose have focused more on the problems of Nucleation/crystallization and resulting polymorphs [13, 19, 25-28], kinetics (*e.g.* [7, 8, 11, 14, 19, 23, 29-31]) and stability of the product (*e.g.* [12]) than on the caking phenomenon itself.

The phenomena of water sorption and subsequent crystallization of amorphous lactose due to humidification are quite well documented and described in the literature. Several authors have studied the sorption of water by amorphous lactose produced by freeze drying or by spray drying [32-36]. All these works show that when exposed to ambient humidity, amorphous lactose is able to retain significant amounts of water (*i.e.* up to about 12% w/w). This increase in the water content of amorphous lactose with moisture is independent of the particle size and exceeds what can be expected from adsorption on the surface of the particles. This shows that the mechanism underlying the water uptake corresponds to the absorption phenomenon. Several investigators have established sorption isotherms of amorphous lactose for water activities varying from 0 to 0.5. Clark [11] provided a comparison of some data reported in the literature ([Figure III-1](#)). All these data show a progressive increase of the water uptake from 0 to about 0.09-0.10 (g of water/g of dry powder) when the water activity varies from 0 to 0.45.

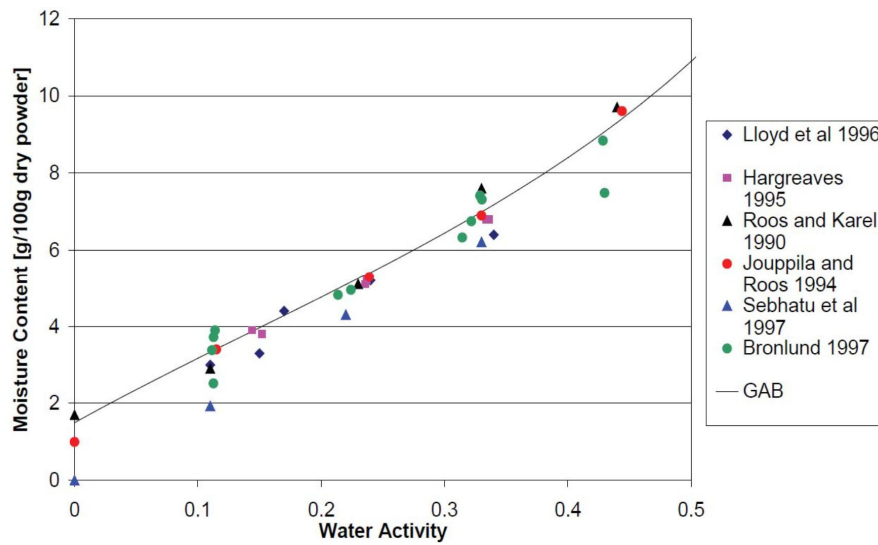


Figure III-1. Amorphous lactose moisture isotherm (From Clark [11]).

These studies also show a sharp decrease in the water content of amorphous lactose for water activities higher than 0.5. This drop is due to the crystallization of amorphous lactose and the subsequent water release. Indeed, it is well known that the presence of water within the solid matrix leads to a decrease in the glass transition temperature, T_g , which is known as the plasticizing effect of water. For a binary mixture, this decrease in T_g is properly represented by the Gordon and Taylor model [1, 12, 37]:

$$T_g = \frac{x_1 T_{g1} + k x_2 T_{g2}}{x_1 + k x_2} \quad (\text{III-1})$$

in which x_1 and x_2 are the mole fractions of species 1 and 2 and T_{g1} and T_{g2} their respective glass transition temperature. According to the literature, the T_g of pure water and lactose are $-130\text{ }^\circ\text{C}$ and $+110\text{ }^\circ\text{C}$, respectively. The value of k is generally assumed to be equal to 6.56.

Note that combining the water sorption isotherm and the T_g curve as a function of water content allows to establish the relationship between the glass transition temperature and water activity (hygro-sensitivity diagram). Figure III-2 gives an example of such a diagram reported in the literature. The dashed line in this figure suggested by Thomsen et al. [38] separate the stable zone from the unstable zone. Brooks [39] also proposed the following correlation for amorphous lactose $0 < a_w < 0.575$ (also plotted in Figure III-2):

$$T_g = -530.66 a_w^3 + 652.06 a_w^2 - 366.33 a_w + 99.458 \quad (\text{III-2})$$

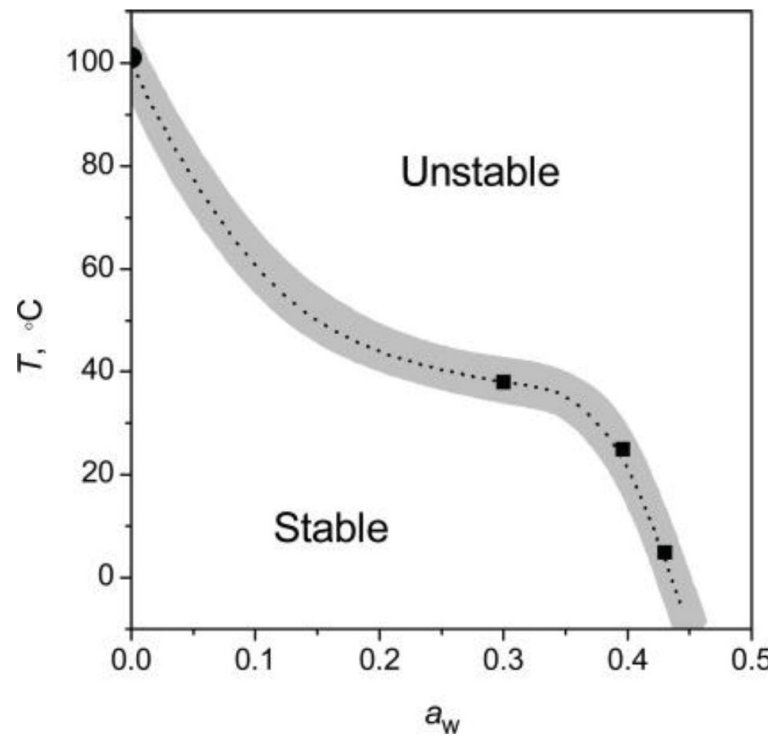


Figure III-2. Hygro-sensitivity diagram for amorphous lactose (Thomsen *et al.*, 2005 [38]).

Note that the data proposed in the literature could vary significantly from one investigation to another. If we choose as the reference, the data from [Figure III-1](#) and the GT model, the T_g of amorphous lactose containing 11% of water (corresponding to the equilibrium water uptake at $a_w=0.50$ and $T=25^\circ\text{C}$, *i.e.* just before the onset of crystallization) is expected to be about 3°C , in other words 22°C below the product storage temperature. At these conditions, the solid becomes soft and can be considered as a very viscous liquid whose viscosity decreases very rapidly with $(T - T_g)$. The dependence of the viscosity with temperature is generally represented by the William-Landel-Ferrey (WLF) model [40] described in chapter I:

$$\ln\left(\frac{\eta}{\eta_g}\right) = \frac{C_1(T - T_g)}{C_2 + (T - T_g)} \quad (\text{III-3})$$

where T , T_g , η , η_g refers to actual temperature, onset glass transition temperature, viscosity and viscosity at glass transition temperature, respectively. C_1 and C_2 are the constants of WLF model. These authors found that for most of the polymers $C_1 = -17.4$ and $C_2 = 51.6 K$. Generally, the viscosity of amorphous lactose in glass transition in the literature has been reported to be about $\approx 10^{12}$ Pa·s. However, Paterson et al. [41] measured the viscosity of an amorphous freeze-dried lactose at glass transition point using a creep experiment. The value of viscosity obtained by these authors was 1.1×10^{14} Pa s, which is two orders of magnitude higher than that assumed in the literature. Moreover, in the case of lactose, these authors recommend the use of the constants proposed by Peleg [42] (*i.e.* $C_1 = -10.5$ and $C_2 = 85.6 K$) rather than the original constants of the WLF model.

At a certain viscosity, a reorganization of the molecules into a crystalline structure becomes possible. Given that in case of amorphous lactose the crystallization appears at $T=25^\circ\text{C}$ and $a_w=0.50$ (*i.e.* $T - T_g=22^\circ\text{C}$), using WLF model and the constants recommended by Peleg and Paterson *et al.*, it can be estimated that this critical viscosity is about $1.0 \times 10^{13} - 1.4 \times 10^{13}$ Pa · s.

As mentioned before, according to the literature, at room temperature, the crystallization of amorphous lactose takes place beyond a relative humidity of 50%. However, the crystalline forms in which the reaction results are different dependent on the relative humidity. According to Bronlund [35], at low relative humidity ($\text{RH}<55\%$) β -lactose and α -lactose anhydride are obtained. When sufficient amount of water is available ($\text{RH}>55\%$), α -lactose monohydrate is preferentially formed. In general, low temperature and high RH favour the formation of α -lactose monohydrate whereas β -lactose appears preferentially at higher temperatures. In all cases, the crystallization results in a mixture of different crystalline forms. For example, Miao and Roos [19] findings showed that freeze-dried amorphous lactose stored at 54.5%, 65.6%, 76.1% RH crystallizes into a mixture of α -lactose monohydrate, anhydrous β -lactose and anhydrous α -lactose in 5:3 and 4:1 molar ratio. Schmitt *et al.* [21] also found that at 57.5% RH, amorphous lactose crystallizes in a mix of α -lactose monohydrate and anhydrous β -lactose. However, Nijdam et al. [43] found that at higher temperatures, ranging from 50°C to 110°C , only negligible amounts of α -lactose monohydrate forms and the mixture is composed of anhydrous forms of α and β lactose.

The kinetics of amorphous lactose crystallization have been the subject of several studies since the last two decades. The most common experimental methods are isothermal calorimetry [44-47], differential scanning calorimetry, (DSC) [13, 15, 19, 21, 26, 28, 48-52] and Dynamic Vapor Sorption (DVS) using gravimetric approach [14, 16, 19, 23, 27, 53, 54]. Several authors reported an exponential relationship between the crystallization rate and the temperature difference above T_g , well represented by WLF or by Avrami type models.

Figure III-3 provides a typical example of the variation of the kinetics of water sorption and desorption when an amorphous lactose is first dried and then exposed to a high relative humidity allowing crystallization to be initiated. This type of variation for amorphous lactose has been reported by several investigators [8, 14, 16, 27, 55] and could be generalized for many other amorphous materials (*e.g.* sucrose).

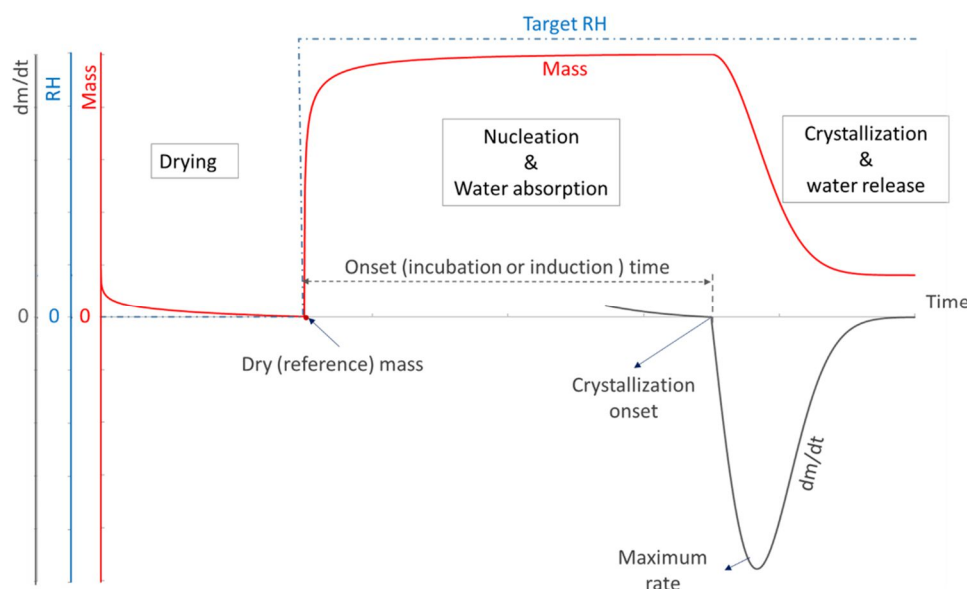


Figure III-3: Typical evolution of water sorption dynamic for amorphous powders

This curve indicates a first drying step where the mass of the sample exposed to dry air decreases. When RH is abruptly raised to a level that allows crystallization, the mass of the sample increases rapidly due to the absorption of water to reach a new plateau. After a period of latency, called *onset time*, the sample begins to lose a significant amount of water. Many investigators has reported this characteristic mass loss [8, 14, 16, 27, 55] and assigned it to the crystallization of amorphous lactose. Once crystallization is complete, further increase of

RH leads (not shown in Figure III-3) only to a small mass increase due to adsorption. The onset time can be determined from the first derivative of the mass versus time (shown by grey line in Figure III-3) by the point of interception with the x-axis. Moreover, the maximum point of this curve corresponds to the maximum rate of transformation. Assuming that the rate limiting step during the mass loss period is crystallization (*i.e.* diffusion and desorption are relatively fast), the data have been used by several authors to establish a rate law for crystallization. The two major families of models, most used to fit the data, are Avrami equation and Williams-Landel-Ferry (WLF) equation (both being empirical). Other models have also been proposed based on Hoffman and Arrhenius equations. Peleg et al. [31] established also non-Arrhenius and non-WLF kinetics for food systems. However, all these models remain equally empirical and do not bring further mechanistic understanding of the system. Therefore, in which follows, only Avrami and WLF models are considered.

The general form of Avrami equation is:

$$Y = 1 - \exp(-Kt^n) \quad (\text{III-4})$$

where Y is the crystallized fraction of amorphous lactose, K is the rate constant of the model and n is the Avrami exponent. Originally, this model was established to describe isothermal phase transformations (including crystallization) in solids. It applies more particularly to the description of the kinetics of crystallization, which is often characterized by low rates of evolution at the beginning and at the end of transformation, passing through a maximum in an intermediate period. Bronlund [35] suggested a modified form of Avrami model based on the differentiated form of this model and found n to be close to 3. He interpreted this observation as a sign of uniform crystalline growth in the three directions of space. Bronlund established the following expression for the rate constant involving T_g for the case where nucleation is not the limiting step:

$$K = C_3 \left[\exp\left(\frac{-C_1}{R(C_2 + T - T_g)}\right) \right]^n \quad (\text{III-5})$$

Note that Brooks [39] found these constants to be $C_1 = 3.54 \times 10^4$, $C_2 = 110.9$ and $C_3 = 2.66 \times 10^{27}$.

As for WLF model, it assumes that the crystallization rate is directly related to the viscosity of the medium and must, logically, follow the same evolution with the temperature deviation ($T - T_g$). The corresponding relation is similar to that presented previously (Eq.2) except that η and η_g are replaced by crystallization time, t_{cr} , and crystallization time at T_g , respectively.

Figure III-4 adopted from Clark [11] gives a comparison between the predictions of Avrami and WLF models for the characterization time (of 90% crystallization) and some data from the literature. As can be seen, significant deviations between data exists, especially at high $T - T_g$ values.

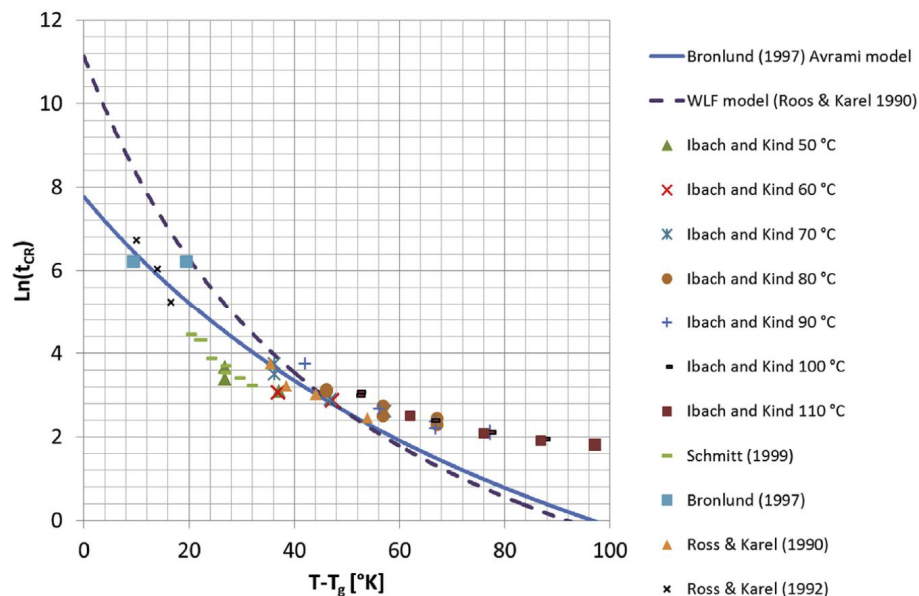


Figure III-4: Literature data on the solid-state crystallization time of amorphous lactose as a function of $T - T_g$ [11]

However, it should be kept in mind that, from a phenomenological point of view, the mass evolution shown in Figure III-3 is an overall process including several competitive and consecutive steps (diffusion from ambient air toward the particle's surface through the external boundary layer, adsorption, absorption or internal diffusion, nucleation, crystalline growth, water release and water evaporation through the inverse sequence of internal diffusion, desorption and external diffusion). The heat transfer is also important because the adsorption, desorption and crystallization phenomena are all associated with a heat change. However, the limiting phenomenon remains the mass transfer, which is one to two orders of

magnitude lower than heat transfer [56]. Also, several investigations, specially based on comparison of experimental data and phenomenological models, suggested that the diffusion is not the limiting step of the process [35, 56]. However, Clark et al. [23] investigated the kinetics of moisture induced crystallization of amorphous lactose at constant and high ($T - T_g$) ranging from 23°C to 38°C. They found that crystallization itself took place very rapidly so that it was an “all or nothing” event. This was attributed to an autocatalytic effect of released water that lowers the T_g and facilitates further crystallization of lactose. According to these authors, the moisture diffusion is not the rate limiting step of the process and the long incubation period, which precede the crystallization, is mainly due to nucleation. This statement was supported by the fact that when the crystallization was “seeded” by using samples of amorphous lactose (supertab™) originally containing a certain amount of crystalline form, the process occurred at a much lower $T - T_g$.

2. Materials and methods

In the majority of cases, the industrial powders, in particular, those obtained by spray drying (as is the case with certain grades of lactose), are an amalgam consisting of crystalline phase and amorphous phase. However, it is practically impossible to reproduce such mixtures with controlled compositions at the laboratory scale. We therefore opted to work with reconstituted mixtures of crystalline and amorphous particles. The latter were prepared in the laboratory by the two different techniques described in chapter II (*i.e.* freeze-drying and spray drying). Amorphous lactose samples were then incorporated into batches of crystalline particles to obtain the desired compositions of the mixture. The batches thus obtained were used to study the influence of the composition of the mixture as well as the operating conditions on the caking behavior of the products and the kinetics of the process.

Two series of experiments were carried out. First, a preliminary study using freeze-dried amorphous lactose and the closed-loop air caking (CLAIR) device was carried out. These experiments allowed to assess the caking tendency of the mixtures and to identify the range of operating conditions to obtain sufficiently resistant cakes and reliable results. In a second time, a parametric and kinetic study of the caking process were carried out in the open-loop air flow caking (OLAF) device by using spray-dried amorphous lactose.

3. Results and discussion

3.1. Sample characterization

Figure III-5 shows some ESEM images of α -Lactose monohydrate (Sigma-Aldrich) as well as the amorphous lactose samples obtained by spray drying and by freeze-drying. The main granulometric characteristics of these samples are also summarized in Table III-1. As we can see, the two amorphous products have very different structural properties. Spray-dried samples are spherical with a relatively narrow size distribution while freeze-dried particles have no characteristic shape and consist of a set of several smaller particles. This arises from the preparation process, which comprises a grinding step followed by a sieving step.

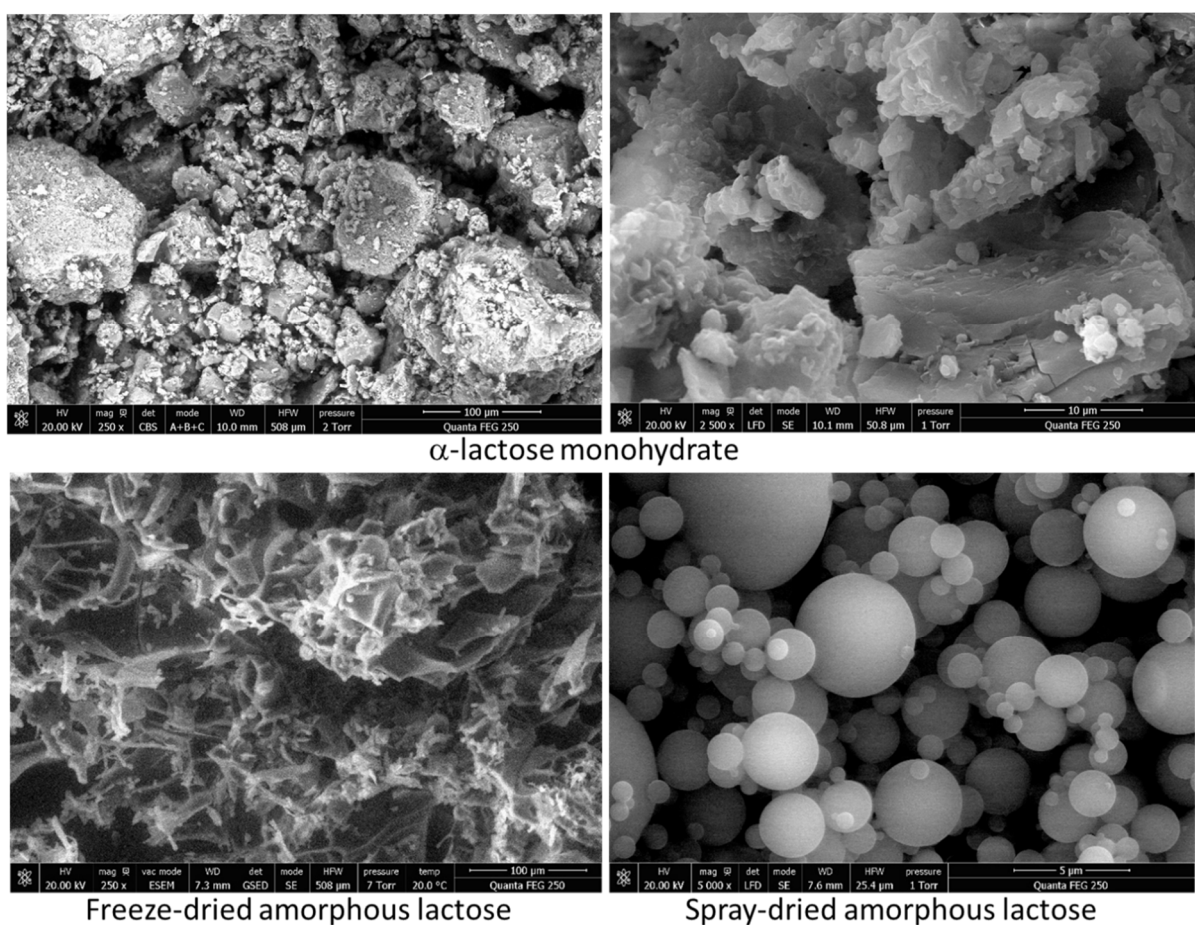


Figure III-5: ESEM images of α -lactose monohydrate (Sigma-Aldrich), freeze-dried and spray-dried amorphous lactose samples

Table III-1: Granulometric characteristics of material used

	d _{10%} (μm)	d _{50%} (μm)	d _{90%} (μm)	d ₃₂ (μm)
α-Lactose monohydrate	5.0	180.3	301.5	46.7
Freeze-dried amorphous lactose	1.0	3.7	9.0	1.2
Spray-dried amorphous lactose	3.0	55.0	91.0	35.0

In addition, we determined the T_g of these products by thermal analyses. The analyses were carried out following the experimental protocol recommended by Fan and Roos [12]. The heating rate was set at 10 °C.min⁻¹. The results of the second heating cycles for both spray-dried and freeze-dried samples are shown in Figure 8. These results show that the freeze-dried product has a T_g of 104 °C, which is very close to the value of 105 °C reported in the literature as the T_g of completely dry amorphous lactose [50, 57]. The small difference can be attributed to the presence of traces of residual water or impurities in the sample. As for the spray-dried lactose, its T_g at the exit of the dryer is 82°C which shows that the drying is not complete. However, as shown in Figure III-6, after desiccation in the presence of P₂O₅ during 48h, the T_g of spray-dried lactose increases significantly to reach a value very close to that of freeze-dried lactose.

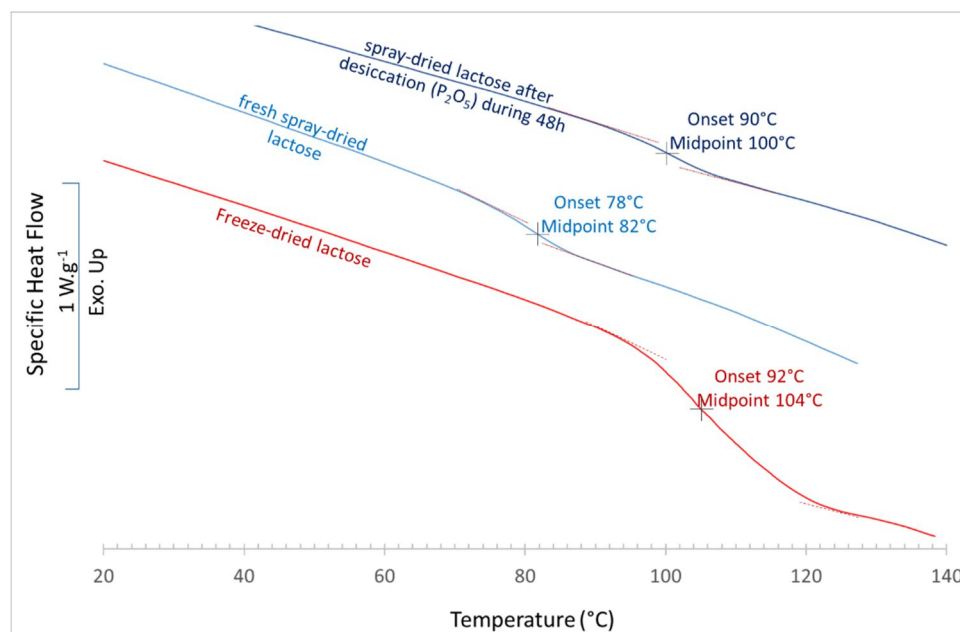


Figure III-6: DSC thermograms of the second heating cycles for both spray-dried and freeze-dried samples

Note that the decrease of the specific heat flow is more significant for freeze-dried sample. This indicates that the amount of amorphous material is higher for this sample. In fact, the spray-dried lactose might be composed of a mix of amorphous and crystalline phases. In order to verify this hypothesis, XRD analyses was carried out on both freeze-dried and spray-dried samples.

Figure III-7 shows the XRD spectra of the two samples after 48h of desiccation. The results are compared to the XRD spectrum of lactose monohydrate used to prepare the solutions. These results confirm that freeze-dried lactose does have an amorphous structure. On the other hand, the spray-dried lactose contains a small fraction of crystalline phase, which is evidenced by the presence of characteristic peaks at 12.5° , 16.5° and within the region between 18° and 22° .

This comparison remains however qualitative only and an accurate estimation of the amount of amorphous lactose cannot be made based on these analyses.

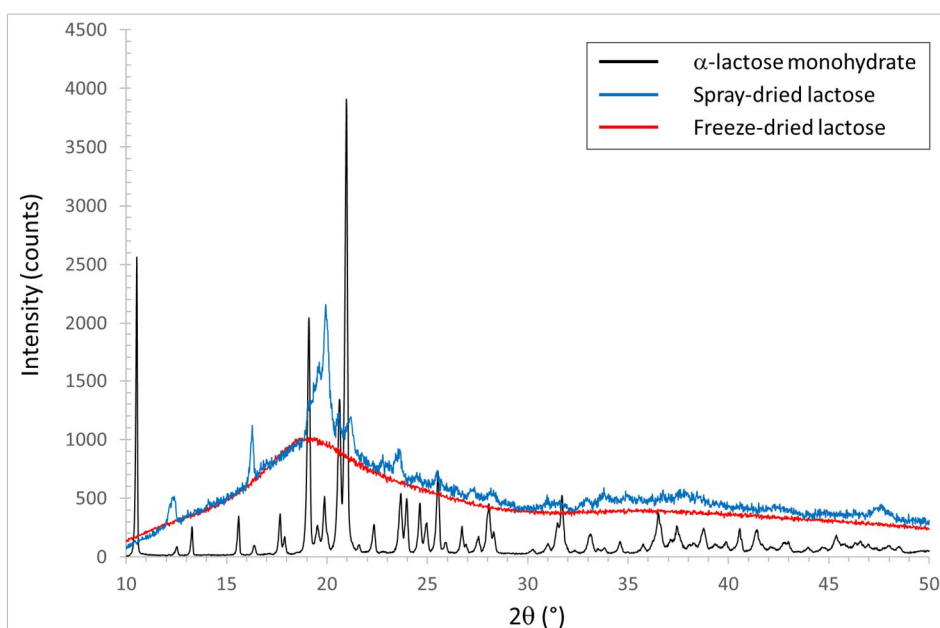


Figure III-7: XRD spectra of α -lactose monohydrate, freeze-dried amorphous lactose and spray-dried amorphous lactose samples

3.2. Water sorption and crystallization kinetics

In order to better quantify the amorphous phase, we opted then for dynamic vapor sorption analysis. According to literature [8, 45, 58, 59], this technique is able to determine

amorphous contents below 1%. Figure III-8-a shows the sorption isotherms (25°C) of the two amorphous lactose samples prepared by freeze-drying and spray-drying, respectively. These results are consistent with those reported in the literature for amorphous lactose. They highlight an evolution in three phases. In the first phase, a gradual increase in the water content of the samples with water activity is observed. This phase occurs at low water activities ranging from 0 to 0.48. During this period, water is absorbed within the solid matrix. The presence of water will then increase the mobility of lactose molecules (lubricating or plasticizing effect of water). Beyond a critical activity, this mobility becomes significant so that a crystallization in solid phase occurs. This crystallization process leads to a release of water that will take place as long as the crystallization continues. A substantial drop in the water content of the samples characterizes this second phase.

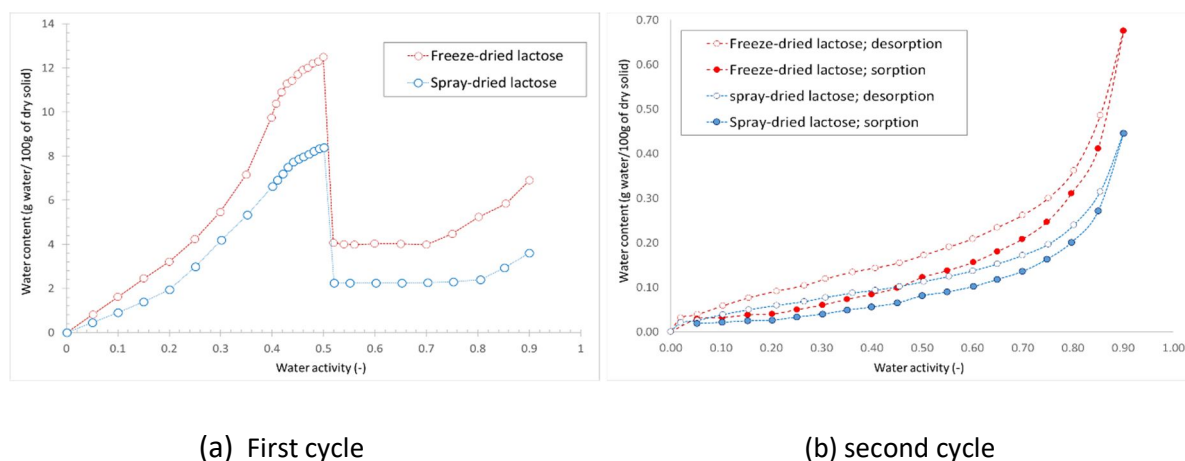


Figure III-8: Sorption isotherms of freeze-dried and spray-dried amorphous lactose samples

It can be noted that the critical activity of crystallization is sensibly identical for the two samples and close to 0.49-0.50. However, the respective water contents of the samples are different, which can be explained by the difference in structural properties of the two products. Indeed, the specific water uptake (*i.e.*; g of water per g of dry lactose) is lower for spray-dried lactose, which could be explained by the lower amorphous material content of this product. Finally, a third phase characterized by a low rise in water content is observed. This phase corresponds to the adsorption of water on the surface of the crystalline lactose formed during the second phase. If we consider that initially both samples are totally dried, the fact that the water content of the products after crystallization remains below 5%

(theoretical value for pure lactose monohydrate) shows that the final product is not composed of lactose monohydrate alone but of a mixture of different crystalline polymorphs of lactose. This is in agreement with several works of the literature [19, 47, 49] who showed that at low temperatures ($<25^{\circ}\text{C}$) and high RH (>0.55) crystallization preferentially led to the formation of α -lactose monohydrate with small amounts of other crystalline polymorphs.

Note that at ordinary conditions, the crystallization process is irreversible. [Figure III-8-b](#) shows the results of the subsequent cycles of humidification and drying of both samples after the first crystallization. Here we consider that the reference mass is the one recorded when the water activity after the crystallization cycle returns to zero. As can be seen, the water uptake is much lower than that occurred during the first humidification cycle. The process remains reversible with a slight hysteresis between sorption and desorption cycles. These results indicate that once the amorphous lactose has been transformed into the crystalline phase, the interactions with the water vapor become purely an interface phenomenon. A comparison between the specific surface area determined by BET theory from the results shown in [Figure III-8-b](#) and the external surface estimated by the mean particle size of particles confirmed this hypothesis.

It is also important to consider the rate at which the crystallization process takes place at different operating conditions. In order to understand the kinetics of crystallization, we performed a series of sorption measurements using the SPS instrument and an experimental procedure similar than that used by Burnet et al. [8]. For this series of measurements, we first exposed the samples at the desired temperature and 0% RH. Once the balance was established (reference mass), we proceeded to a step change of RH while keeping the temperature constant. The level of RH was chosen in the field where the crystallization can indeed take place (*e.g.* $T = 25^{\circ}\text{C}$ and $\text{RH} \geq 50\%$).

Four measurements were performed on the spray-dried sample at two temperature levels ($T = 20^{\circ}\text{C}$ and 25°C) and two levels of relative humidity ($\text{RH} = 50\%$ and 80%).

[Figure III-9](#) shows a typical example of dynamic vapor sorption data obtained at 25°C and 50% RH. This set of data is highly representative of all isotherms obtained under the different conditions. The circles indicate the time variation of the percentage of mass change (referenced from the dry mass, *i.e.* the mass of the sample just before RH jump) on the y-axis

on the left. The dashed line on the right y-axis gives the target RH (red). In this figure, are also superimposed the derivative of the amorphous fraction as a function of time, which corresponds to the instantaneous rate of the reaction. In order to mitigate the effect of local disturbances, for each point of the curve the derivative was calculated on the smoothed curve (10-point moving average).

In agreement with the literature, these results clearly show a phenomenon of crystallization after a period of latency. Indeed, during dehumidification at RH = 0%, the powder loses a small amount of water. When the new level of RH is imposed, the water content of the sample increases significantly (about 8.4%). After this first period of mass rise, considered as the *induction (or onset) time*, the crystallization of lactose occurs. The *onset point*, determined by the intersection of the derivative of the water content with time axis was about 670 minutes. The crystallization is characterized by a rapid decline in the water content of the sample (about 6%). Actually, the XRD spectra of samples after humidification confirmed that the amorphous lactose was indeed converted mainly (but not exclusively) into lactose monohydrate.

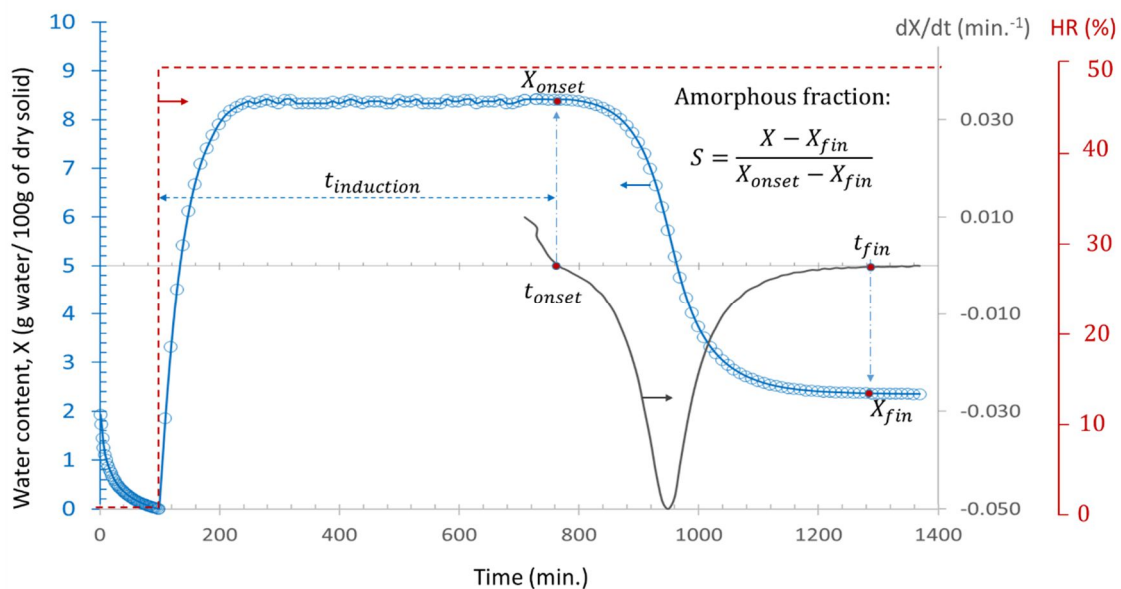


Figure III-9: Vapor sorption kinetics of spray-dried amorphous lactose at T=25°C (first sorption cycle)

Note also that the derivative (rate) curve represents a peak corresponding to the maximum speed of the reaction. This trend is characteristic of the evolution of an autocatalytic transformation: the reaction rate increases first and then decreases. Indeed, as we mentioned earlier, on the one hand, the presence of water is essential to start the crystallization process and, on the other hand, the crystallization leads in turn to the release of water. Thus, one may assume that at the beginning, the reaction is inhibited by the lack of water. Once the necessary conditions for nucleation and crystalline growth are brought together, water is released which explains the increase in reaction rate caused by the appearance of water in the medium. As the transformation progresses, the amorphous phase becomes less available and the reaction rate decreases to reach a value close to zero when all the amorphous lactose has been transformed into crystalline phase. The presence of a unique peak indicates that the crystallization occurs following a one-step mechanism. Note that these results are in slight disagreement with those of Burnett et al. [8] who reported the presence of 2 peaks for spray-dried lactose in the conditions close to those used here. In addition, the peak observed in the case of this work occurs between the 2 peaks reported by these authors (520 minutes against 400 for the first peak and 600 for the second). This shows that the results cannot be considered as an intrinsic property of the product. Indeed, the parameters of the drying process, the particle size distribution, the porosity, the presence of impurities, the history of the product and its storage conditions can significantly influence the induction time and kinetics (or even the mechanisms) of the transformation.

[Figure III-10](#) focuses on the crystallization step itself. It shows the variation of amorphous fraction (defined as suggested by Burnett et al. [8] and presented in [Figure III-9](#)) as a function of shifted time (with respect to the onset point). Also shown in this figure are the predictions of the Avrami model. The value of K and n was identified by the best fit between the experimental data and model predictions. Two different methods for regression were tested. First, we used the both constants K and n as the regression variables. In a second step, we set the value of n as suggested by Roos to 3 and we used the constant K as the only adjustable parameter. Both cases are shown in [Figure III-10](#).

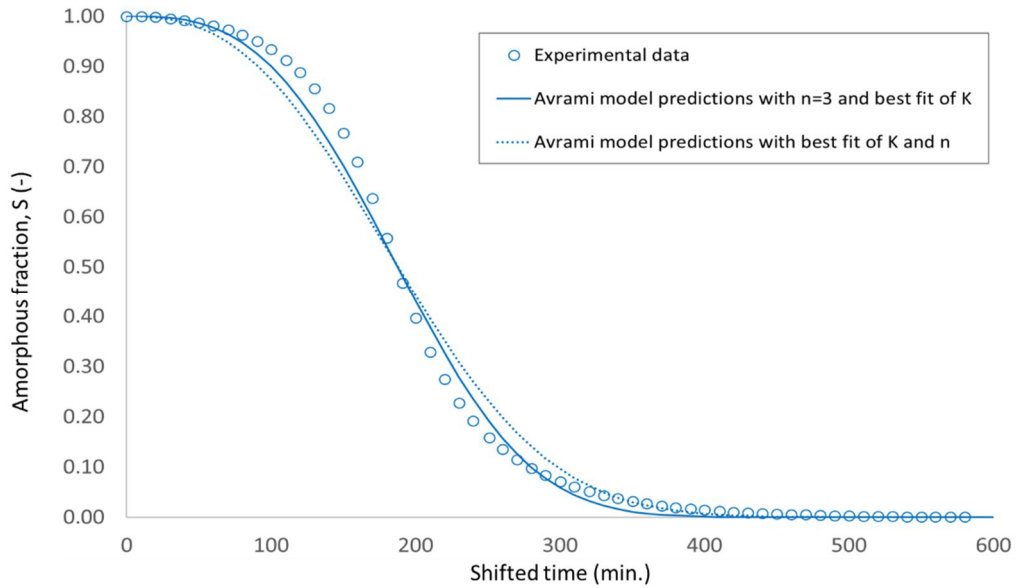


Figure III-10: Variation of amorphous fraction with shifted time (with respect to the onset time). Comparison of experimental data ($T=25^{\circ}\text{C}$ and $\text{RH}=50\%$) with Avrami model's prediction with the best fit of $\text{---} K$ and n ($n=2.56$ and $K=8.58 \times 10^{-7} \text{ min}^{-1}$) and $\text{---} K$ only ($n=3$ and $K=1.05 \times 10^{-7} \text{ min}^{-1}$)

As can be seen, the agreement between the model and experimental data are satisfactory. Since the differences between the experimental data and the model shown in this figure were very close in both cases the second method was preferred.

Figure III-11 shows the normalized variations of the amorphous fraction obtained for the 4 dynamic vapor sorption tests obtained at different conditions. The predictions of the Avrami model with $n=3$ and the value of K allowing the best fit between the experimental data and the model's predictions are also displayed in this figure. The corresponding values of induction time and K are gathered in Table III-2.

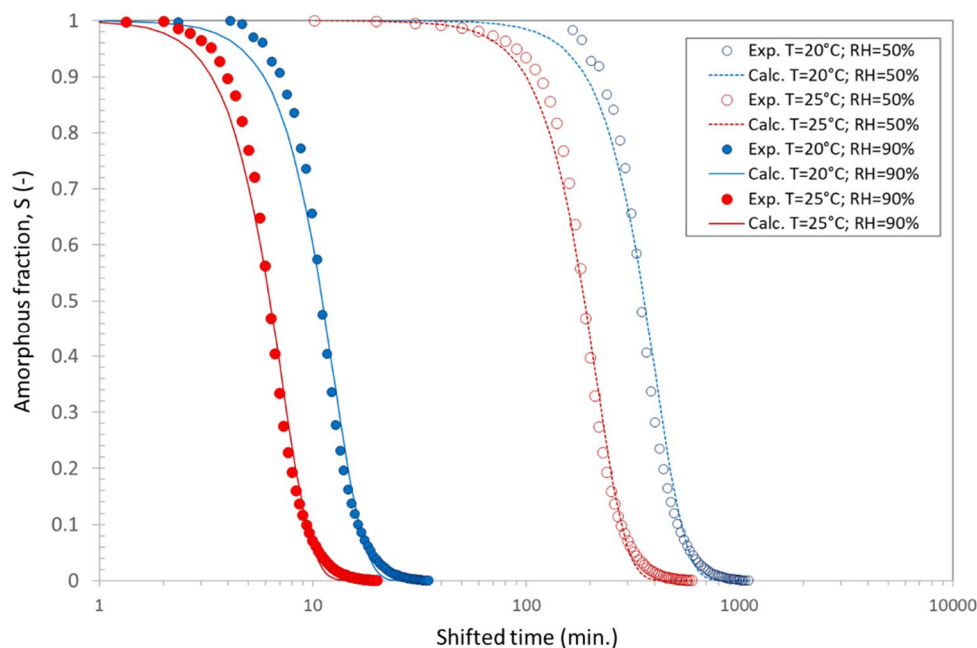


Figure III-11: Variation of amorphous fraction with shifted time (with respect to the onset time) for the four conditions

Table III-2: Induction times and Avrami rate constants of amorphous lactose obtained by Dynamic Vapor Sorption analysis

RH (%)	T (°C)	K (min ⁻³)	t _{induction} (min)
50	20	1.51×10^{-8}	1800
50	25	1.05×10^{-7}	600
80	20	5.12×10^{-4}	150
80	25	2.79×10^{-3}	90

These results confirm that the rate constant increases whereas the onset time shortens with the increase of T or RH. At this stage, it is premature to try to establish a general kinetic law, including the influence of temperature and RH with only 4 series of measurements. Indeed, a more in-depth study is necessary to include the effect of these parameters in the rate law. However, the fact of not having a detailed law is not a major problem in this study because the caking tests were carried out under the same conditions of T and RH as the dynamic vapor sorption measurements.

3.3. Caking experiments

In order to study the influence of the amorphous lactose fraction on the caking ability of powder mixtures composed of amorphous lactose and anhydrous lactose, different mixtures constituted of these two components were prepared.

The caking ability of a series of binary mixtures was investigated by varying the fraction of the amorphous product, the pressure, the relative humidity and the duration of the caking experiment. The work was conducted in two stages. First, a preliminary study was carried out using the CLAIR caking device. The objectives of these preliminary tests were :

- to identify the conditions at which caking become significant enough to be detected and characterized by our caking tests,
- to evaluate the relevance of mechanical strength tests and to choose a reliable method and procedure to characterize the caked samples

Following this preliminary phase, a parametric study of the caking of these mixtures was carried out at more controlled conditions using the OLAF caking device.




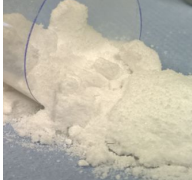


3.3.1. Preliminary experiments in CLAIR caking Device

Prior to a parametric study of caking, a series of experiments was carried out at varying RH, pressure and time for a qualitative assessment of the caking behavior of the samples.

Table III-3 gives an overview of experimental conditions and the main results obtained from these experiments.

The first information that can be drawn was that no caking phenomenon was observed below a relative humidity of 50%. Otherwise, the α -lactose monohydrate is very stable. In pure state, it does not cake even under significant pressures and for long test periods. However, the presence of amorphous lactose, even in very small amounts substantially modifies this stability. Indeed, we proceeded to a progressive decrease of the content of amorphous lactose until this caking tendency disappears. The results (presented in Table III-3) showed that under our experimental conditions, the mixture could cake for amounts of amorphous lactose as low as 0.125% (w/w). Note that XRD and DSC analyses did not reveal any evidence of the presence of amorphous lactose in caked samples. For example, Figure III-12 presents the XRD spectra of caked samples presented in Table III-3. It shows that the amorphous lactose crystallizes to a mix of α -Lactose Monohydrate and anhydrous β -Lactose.

Table III-3: summary of preliminary caking tests

Sample	Time	RH%	Pressure (kPa)	Caking?	Picture
100% Amorphous Lactose	24 h	80%	10 kPa	Yes	
20% Amorphous Lactose + 80% Monohydrate Lactose	14 h	50%	10 kPa	Yes	
10% Amorphous Lactose + 90% Monohydrate Lactose	7 h	80%	10 kPa	Yes	
10% Amorphous Lactose + 90% Monohydrate Lactose	14 h	50%	10 kPa	Yes	
10% Amorphous Lactose + 90% Monohydrate Lactose	24 h	50%	20 kPa	Yes	
5% Amorphous lactose + 95% Monohydrate Lactose	7 h	80%	10 kPa	Yes	
2,5% Amorphous lactose + 97,5% Monohydrate Lactose	7 h	80%	10 kPa	Yes	
1,25% Amorphous lactose + 98,75% Monohydrate Lactose	7 h	80%	10 kPa	weakly	
1,25% Amorphous lactose + 98,75% Monohydrate Lactose	14 h	80%	10 kPa	Yes	
0,625% Amorphous lactose + 99,375% Monohydrate Lactose	14h	80%	10 kPa	No	

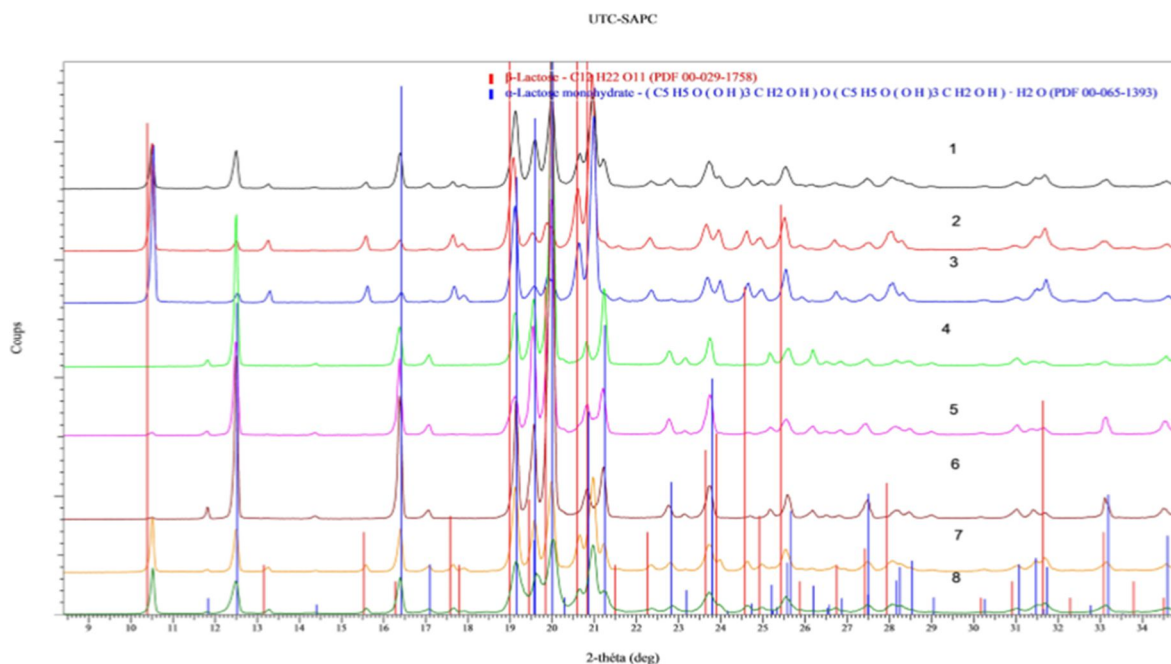


Figure III-12. XRD spectra of caked samples

3.3.2. Choice of a proper yield strength test

In order to examine the most appropriate method among the three methods presented for the characterization of the mechanical strength of cakes, a series of tests were conducted with binary mixtures containing different amounts of amorphous lactose and under the conditions where caking observed systematically. Table III-4 summarizes the experimental conditions used for these preliminary measurements. Three amorphous contents ($x=0.01$, 0.03 and 0.05) were studied and each test was repeated 3 times. The corresponding mean values and standard deviations for each condition are also given in this table. Values in parentheses correspond to the coefficient of variation of the data, CV, defined as the ratio of the standard deviation to the mean value.

Table III-4: Results of mechanical strength obtained by the three failure tests (time 720 min., pressure 20kPa, T=25°C, RH=80%)

Amorphous fraction (w/w)	Yield stress (kPa)		
	Radial	shear	uniaxial
0.01	$\sigma=3.1 \pm 2.8$ CV=0.93	$\sigma=8.5 \pm 2.6$ CV=0.31	12.9 ± 3.2 CV=0.25
0.03	$\sigma=6.2 \pm 5.2$ CV=0.84	$\sigma=22.2 \pm 3.3$ CV=0.15	38.1 ± 5.1 CV=0.13
0.05	$\sigma=13.1 \pm 7.1$ CV=0.54	$\sigma=30.2 \pm 3.2$ CV=0.11	53.5 ± 6.2 CV=0.12

Figure III-13 shows the evolutions of the yield stress of the samples as a function of the amorphous lactose fraction, measured by the three methods of breakage (*i.e.* uniaxial, radial and shearing), for different conditions and different durations of experience. Logically, as long as the amorphous lactose fraction remains relatively small, (*i.e.* the amorphous particles remain a minority and only fill the interstitial space between the crystalline particles), a linear evolution of the breaking strength with the fraction of the amorphous particles might be expected. In fact, in this case, the increase in the fraction of the minority constituent leads simply to a direct increase of the solid bridges between the particles. According to Rumpf's model [60, 61], the resulting yield strength is directly proportional to the number of bridges and, consequently, to the fraction of the amorphous particles.

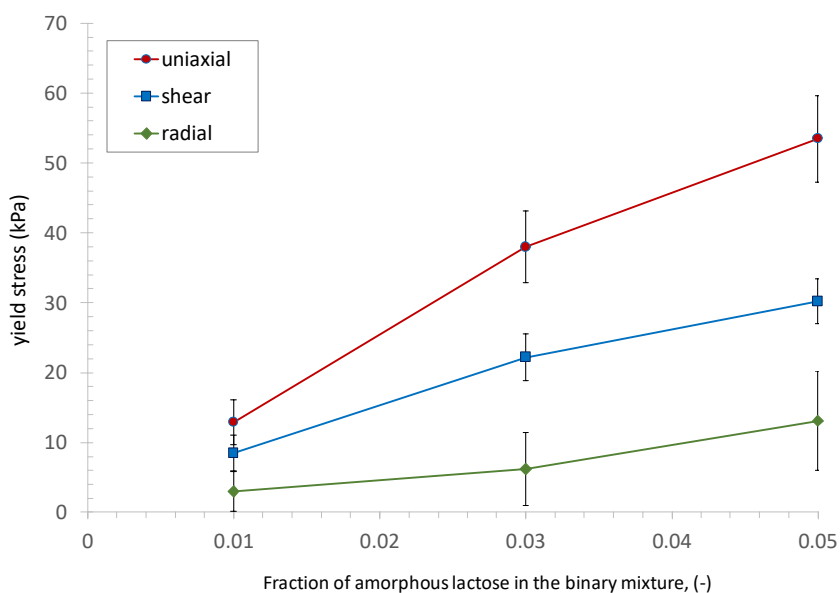


Figure III-13: Comparison of the three methods used for yield stress measurements (T=25°C, HR=80%, P=20kPa, t=720 min.)

The results obtained by the three methods generally confirm this trend. The linearity between the yield stress, σ , and the mass fraction of amorphous lactose, x , shows that in order to compare the results of the tests carried out with different amounts of amorphous product, it is more astute to use the ratio of σ/x than the yield stress itself. Furthermore, it can be seen that the results of the radial test are not discriminating enough. This test is not sensitive enough and the results are too scattered. This could be attributed to the small extent of the forces involved and by the random nature of the appearance of the cracks.

On the other hand, the axial compression test and the lateral shear test are more discriminating. It should be also noted that the results of the lateral shear test are less scattered. These observations confirm those reported by Samain et al. [62].

However, it should be noted that this test is more tedious to set up and is also more material and time consuming than the compression test. Moreover, the lateral shear test involves more manipulations, which may cause the samples to be damaged before the measurement. For all these reasons, we concluded that the uni-axial compression test was a good compromise, allowing to be discriminating enough while remaining relatively easy to achieve.

3.3.3. Influencing parameters

A new series of experiments were carried out at different operating conditions. The objective was to highlight the most influential parameters on the caking phenomenon. The experiments were done in triplicate. The caked samples were characterized using the uniaxial test. [Table III-5](#) summarizes the operating conditions used as well as the main results corresponding to these tests.

Table III-5: Yield stress of binary mixtures caked under different operating conditions

Mass fraction of amorphous lactose $x(-)$	Relative humidity RH(%)	Temperature T(°C)	Pressure (kPa)	Duration t(min)	Yield stress σ (kPa)
0.05	50	20	10	360	22.4 ± 15.7
0.05	50	20	10	720	48.1 ± 19.1
0.05	50	20	20	360	23.7 ± 15.0
0.05	50	20	20	720	48.2 ± 14.1
0.05	50	25	10	360	48.3 ± 17.2
0.05	50	25	10	720	49.2 ± 16.7
0.05	50	25	20	360	50.7 ± 17.9
0.05	50	25	20	720	53.5 ± 22.4
0.05	80	20	10	360	49.9 ± 16.1
0.05	80	20	10	720	51.0 ± 12.4
0.05	80	20	20	360	52.2 ± 14.1
0.05	80	20	20	720	53.1 ± 18.3
0.05	80	25	10	360	51.1 ± 11.8
0.05	80	25	10	720	52.1 ± 15.1
0.05	80	25	20	360	50.5 ± 17.2
0.05	80	25	20	720	51.7 ± 14.4
0.01	80	25	20	360	11.4 ± 4.4

From the results presented in this table, the following conclusions can be drawn:

- The fraction of amorphous lactose remains the most influential parameter on the caking tendency of the mixtures. As mentioned previously, this ability to caking is non-existent for pure lactose monohydrate and increases almost linearly with the fraction of amorphous particles.
- Another influencing parameter is the relative humidity of the air. Note that no caking phenomenon was observed below a relative humidity of 50%. On the other hand, beyond this RH, the caking of the products containing amorphous lactose, starting from an amorphous fraction was almost automatic. These results are consistent with those reported in the literature by Fan and Roos [12] that reported a quite good stability of amorphous lactose below a 48% RH. As mentioned before, the crystallization of amorphous lactose becomes significant for RH values higher than 50%. On the other hand, the results obtained at RH = 80% are very similar whatever

the other operating conditions. This most likely results from the fact that at this relative humidity, the crystallization rate is very fast (as shown in Figure III-9) and that consequently the crystallization time is much shorter than the duration of the experiment. It can therefore be considered that all samples prepared at RH = 50% have reached a similar state of evolution.

- The duration of the operation is also a key factor as to the caking ability of the mixtures. This is why we opted to investigate in more detail the influence of this parameter in the next section.
- Despite its small variation, temperature also seems to play a significant role. An increase in temperature leads to an acceleration of the caking phenomenon, which can be explained by an increase in $T - T_g$ and the consequent drop in the viscosity of the medium.
- On the other hand, the pressure has very little influence on the caking of the batches tested. This can be explained by the rigid and non-deformable nature of lactose monohydrate particles that resist significant deformation and consolidation of the bed. This behavior will be valid as long as amorphous lactose remains a minority. In the opposite case, it can be expected that the powder bed is pressed under the effect of pressure and therefore to an increase in the effect of the pressure.

It is also useful to interpret these results according to the theory of experimental design. However, before analyzing the results, it would be useful to reduce the number of variables. Given the linearity of the variation in compressive strength with the amorphous fraction, this parameter can be removed from the plan if the comparison is based on the ratio of σ/x . In addition, due to its weak influence, the effect of the pressure was not taken into account in the exploitation of the results. The analyses were performed on the results obtained at 20 kPa.

Applying this theory, the following model can be proposed to correlate the experimental results:

$$\frac{\sigma}{x} = a_0 + a_1 \cdot X_1 + a_2 \cdot X_2 + a_3 \cdot X_3 + a_{12} \cdot X_1 \cdot X_2 + a_{13} \cdot X_1 \cdot X_3 + a_{23} \cdot X_2 \cdot X_3 + a_{123} \cdot X_1 \cdot X_2 \cdot X_3 \quad (\text{III-6})$$

where X_1 , X_2 and X_3 correspond to temperature, T, experiment duration, t, and relative humidity, RH. The coefficients of the model, determined by matrix analysis are given in Table III-6.

Table III-6 : Coefficients of the experimental design model

a_0	a_1	a_2	a_3	a_{12}	a_{13}	a_{23}	a_{123}
959	73	73.5	78.5	-53.5	-88.5	-63	55

These results confirm the significant role of the three selected parameters (RH, T and time) on the caking behavior of lactose mixtures. Applying this approach, in addition to the previous remarks, we can draw additional conclusions about the interactions between the parameters. In particular, the predominant role of the pair (T, RH) is emphasized.

Figure III-14 shows the iso-response surfaces for different min and max values of influencing parameters. Again, it can be seen that the most influencing parameter is the relative humidity. At the minimum level of RH (50%), the role of time and temperature are important. However, for the highest level of RH (*i.e.* 80%), both temperature and time have small effects and the cake's strength seems to have reached its maximum value. Since the tests were carried out during long periods of time (*i.e.* sufficiently long compared to the crystallization time), a more pronounced influence of the duration of the experiment on caking can be expected at shorter times. Globally, the results are consistent with the hypothesis that the caking is mainly governed by the extent of crystallization, which increases with time and with T and RH and through their effect on the crystallization kinetics. A more in-depth study of the relation between the caking behavior and the crystallization extent is presented in the next section

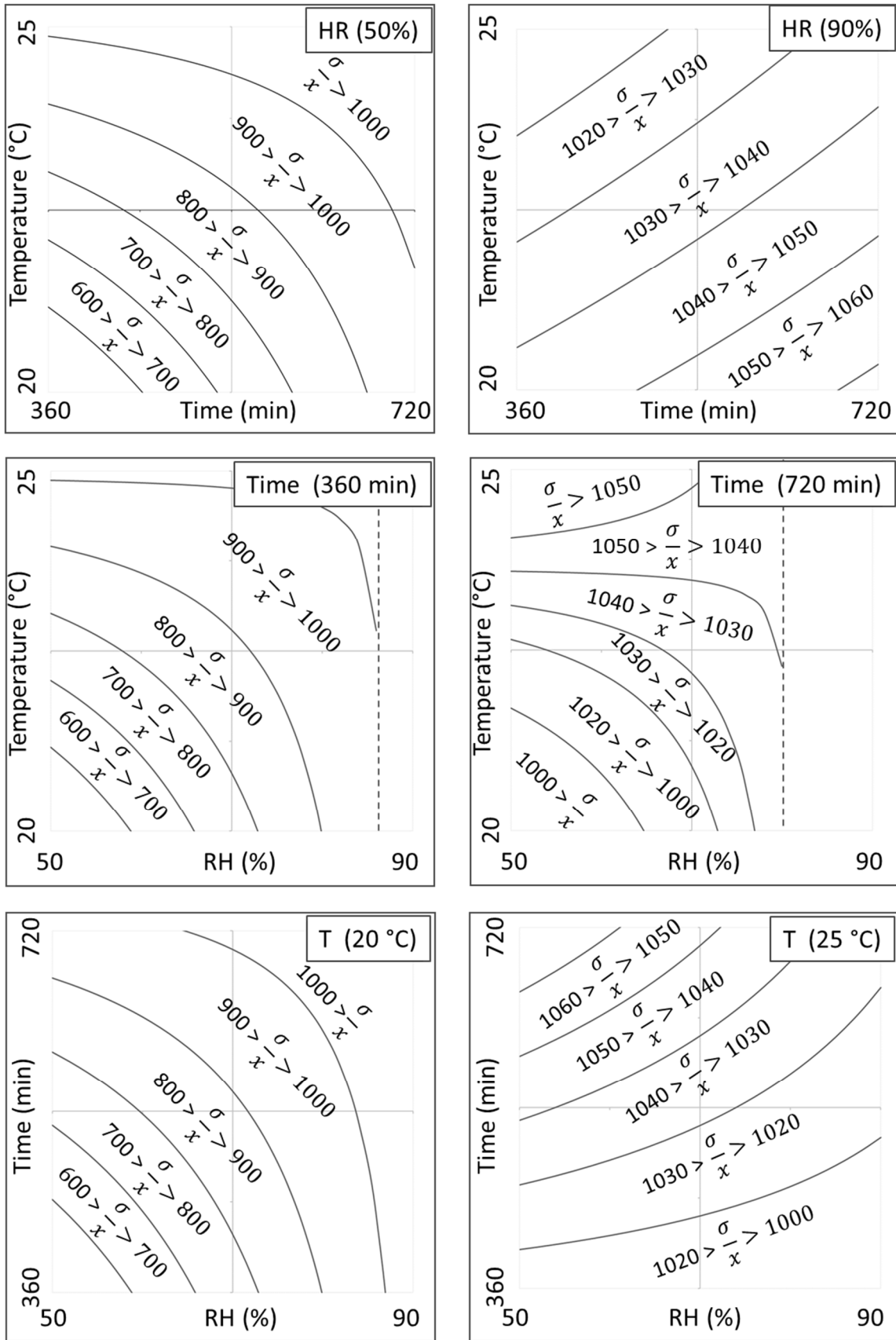


Figure III-14: iso-response surfaces for different min and max values of influencing parameters

3.3.4. Parametric study of caking using OLAF caking Device?

In light of the results obtained during the preliminary study presented in the previous section, a more complete and precise investigation of caking was carried out. These tests were performed using the OLAF device because it allows a better control of the operating parameters. Several RH and caking times were tested. In addition, due to lack of control over the freeze-dried particle size, we opted for the use of sprayed-dried lactose. Indeed, although this product is only partially amorphous, its production at the laboratory scale is much more reproducible due to the absence of grinding and sieving operations.

Several series of tests were carried out by varying the amorphous lactose content, the temperature and the relative humidity during the experiments. Given the insignificant role of the pressure demonstrated in the preliminary tests, all tests were performed at a constant pressure of 20kPa.

Figure III-15 presents the time evolution of the yield stress of the cakes obtained at two different RH, namely 50% and 80%, and two different temperatures of 20°C and 25°C, respectively. The amorphous lactose content for these 4 series of experiments was set at $x = 0.05$. Each point corresponds to the average value of 3 repetitions. The standard deviations of the measurements are also indicated.

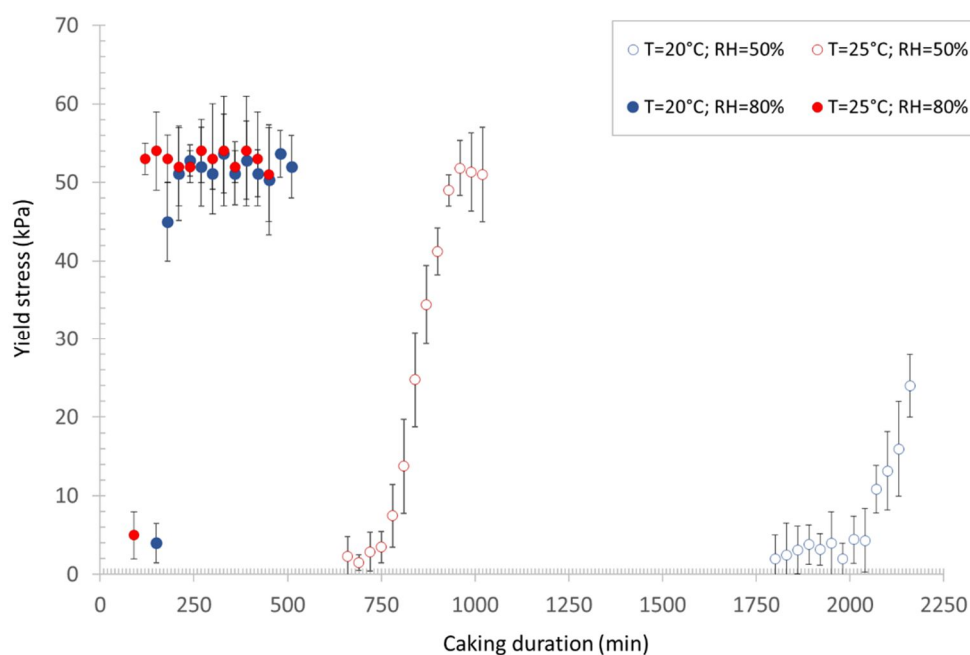


Figure III-15: Evolution of the yield stress as a function of time at different conditions (amorphous content $x=0.05$)

As can be seen, at the highest relative humidity (RH=80%), after a short period of latency during which only weak caking occurs, the yield stress, σ , increases very abruptly to achieve a threshold value of about 50-55 kPa. This value is already reached after only 120 minutes regardless of the temperature. However, at the lowest level of RH (50%), the profile of the yield stress varies much more slowly. The resistance of the cakes increases gradually to reach almost the same threshold value as at RH=80%. Note that the latency period is longer as the temperature is low. Furthermore, the latency times are in good correlation with the induction times for crystallization shown in Figure III-11. It can therefore be concluded that the sharp increase in the caking tendency for the tests carried out at RH = 80% is due to the faster kinetics and a shorter induction time. As can be seen from Figure III-11, the total crystallization time (including the induction and growth phases) at RH=80% and T=25°C is less than 30 minutes, which is the interval time of sampling. These results point out clearly the direct relation between the crystallization of the amorphous lactose and the caking phenomena of samples. The weak caking occurring within the induction period could be attributed to the sintering effect of amorphous lactose, which is in the rubbery state and can creep throughout this period. Once the crystallization takes place, the mechanical resistance of cakes is largely increased.

Moreover, Figure III-16-a gathers the results of 3 series of tests obtained for different mixture compositions at RH=50% and T=25°C.

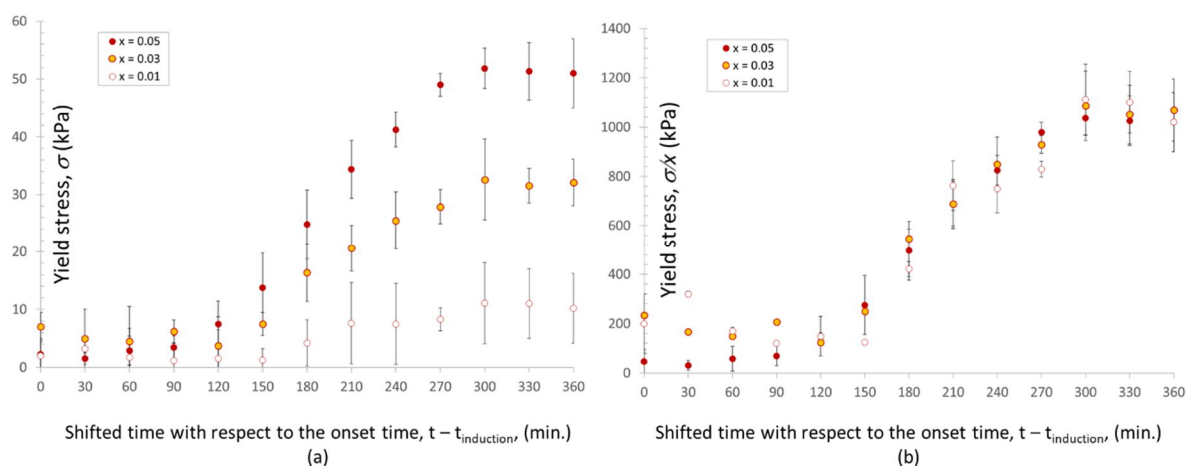


Figure III-16: Evolution of the yield stress as a function of shifted time for different amorphous contents (T=25°C, RH=50% and P=20 kPa)

As can be seen, the observed tendencies are very similar to those previously described. After a first period of latency, the yield stress of caked samples progressively increases with time to tend towards a limit value when the crystallization is completed. At identical conditions, the compressive strength increases as the proportion of amorphous lactose in the mixture increases. In agreement with the preliminary tests (Figure III-12) this increase is directly proportional to the amorphous content, which determines the number of contact points (bridges) between the particles. This hypothesis is corroborated by Figure III-16-b indicating that a normalization of the results with respect to the fraction of the amorphous particles allows unifying the overall tendency of the caking process.

Given these results, there is every reason to believe that the mechanism underlying the caking process of mixtures containing amorphous lactose is the crystallization of this latter in the presence of air humidity. If this were the case, logically, the tendency to agglomeration and thus the compressive strength of the samples obtained under different conditions should be directly related to the kinetics of crystallization of the samples. In this case, rather than the real time, it would be the characteristic crystallization times (induction and growth) that must be considered to compare the caking tendency of samples obtained under different conditions. This characteristic time results from the kinetics of the crystallization, itself a function of the operating parameters such as temperature, relative humidity and, above all, the temperature difference with respect to the glass transition temperature of the product. To verify this hypothesis, a dimensionless crystallization time based on the induction time and the kinetics of crystallization given by Avrami model can be defined as:

$$\begin{aligned}
 t^* &= \frac{t - t_{\text{induction}}}{t_{\text{induction}}} & \text{for } t < t_{\text{induction}} \\
 t^* &= K(t - t_{\text{induction}})^n & \text{for } t \geq t_{\text{induction}}
 \end{aligned}
 \tag{III-7}$$

Figure III-17 shows the variation of the $\frac{\sigma}{x}$ ratio as a function of the dimensionless crystallization time, t^* . As can be seen, such a presentation permits to reconcile all the results obtained. Indeed, all the experimental points are, within the uncertainty of the measurements, on the same curve. Of course, this conclusion is valid only if the intrinsic kinetics of crystallization is low compared to the kinetics of material transfer (water) between air and solid. In our case, this condition is guaranteed thanks to the high flow of moist air that

passes through the bed of powder. In the opposite case, for the definition of the characteristic crystallization time, account should also be taken of the external and inertial transfers to the grains, which could have slowing down effect on the phenomenon.

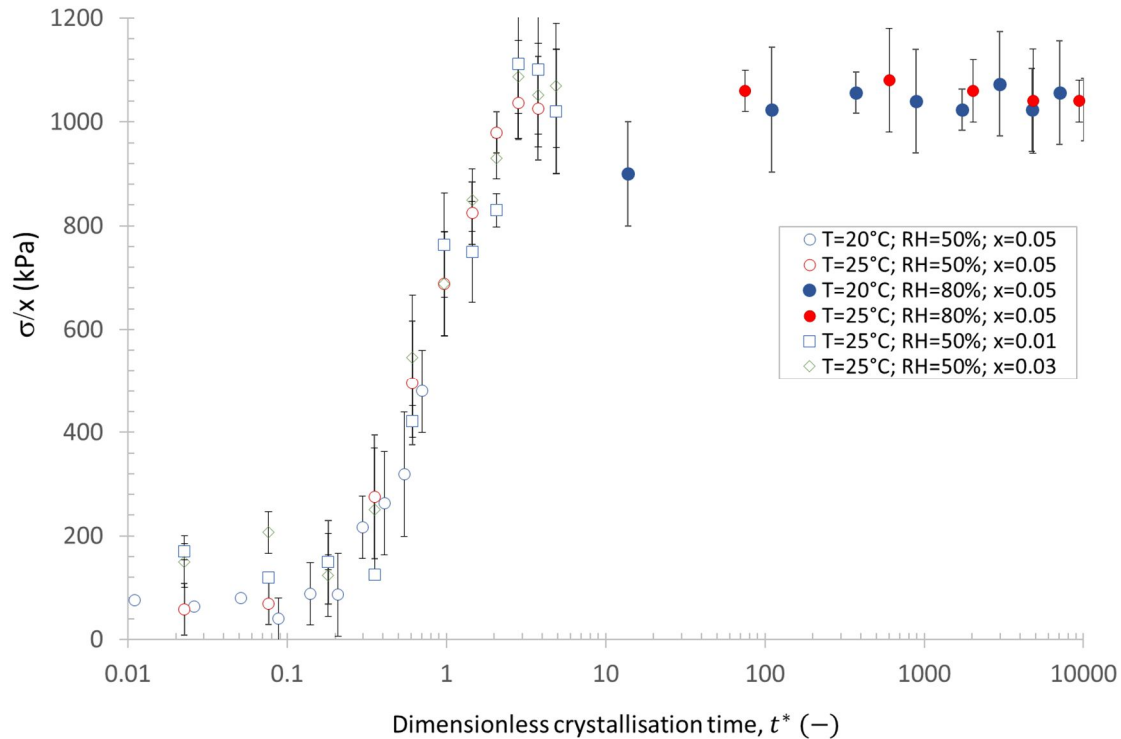


Figure III-17: Evolution of the σ/x ratio as a function of the dimensionless crystallization time, t^* , for all series of experiments

4. Conclusion

The caking behavior of binary mixtures of α -lactose monohydrate and amorphous lactose was studied using two specially designed accelerating tests. The results show the macroscopic (bulk) behavior of mixtures are closely related to the crystallization phenomenon, which occurs at meso (particle) state. The most influencing parameters revealed to be the air relative humidity and the temperature the increase of which increases the crystallization kinetics. This is consistent with the data from literature that indicates that the driving force of solid phase crystallization is the difference between the ambient temperature and the glass transition temperature. The crystallization kinetics is well represented by the Avrami type model. A dimensionless time based on the ratio between the storage time and the characteristic crystallization time ($t_{cr} = K^{-n}$) allows reconciliation of all

data. Further investigations focusing on the relationship between climatic conditions, T and RH, and the kinetic constants of the Avrami model is currently undertaken.

References

1. Descamps, N., S. Palzer, Y.H. Roos and J.J. Fitzpatrick, *Glass transition and flowability/caking behavior of maltodextrin DE 21*. Journal of Food Engineering, 2013. **119**(4): p. 809-813.
2. Descamps, N., S. Palzer and U. Zuercher, *The amorphous state of spray-dried maltodextrin: sub-sub-Tg enthalpy relaxation and impact of temperature and water annealing*. Carbohydr Res, 2009. **344**(1): p. 85-90.
3. Descamps, N., E. Schreyer and S. Palzer, *Modeling the sintering of water soluble amorphous particles*, in *PARTEC*. 2007.
4. Hartmann, M. and S. Palzer, *Caking of amorphous powders — Material aspects, modelling and applications*. Powder Technology, 2011. **206**(1–2): p. 112-121.
5. Palzer, S., *The effect of glass transition on the desired and undesired agglomeration of amorphous food powders*. Chemical Engineering Science, 2005. **60**(14): p. 3959-3968.
6. Fitzpatrick, J.J., M. Hodnett, M. Twomey, P.S.M. Cerqueira, J. O'Flynn and Y.H. Roos, *Glass transition and the flowability and caking of powders containing amorphous lactose*. Powder Technology, 2007. **178**(2): p. 119-128.
7. Baghel, S., H. Cathcart, W. Redington and N.J. O'Reilly, *An investigation into the crystallization tendency/kinetics of amorphous active pharmaceutical ingredients: A case study with dipyrindamole and cinnarizine*. European Journal of Pharmaceutics and Biopharmaceutics, 2016. **104**: p. 59-71.
8. Burnett, D.J., F. Thielmann, T. Sokoloski and J. Brum, *Investigating the moisture-induced crystallization kinetics of spray-dried lactose*. International Journal of Pharmaceutics, 2006. **313**(1): p. 23-28.
9. Carpin, M., H. Bertelsen, J.K. Bech, R. Jeantet, J. Risbo and P. Schuck, *Caking of lactose: A critical review*. Trends in Food Science & Technology, 2016. **53**: p. 1-12.
10. Chandrapala, J. and T. Vasiljevic, *Properties of spray dried lactose powders influenced by presence of lactic acid and calcium*. Journal of Food Engineering, 2017. **198**: p. 63-71.
11. Clark, Z., *Amorphous Lactose Crystallization Kinetics*. 2012, Massey University: Manawatu, New Zealand.
12. Fan, F. and Y.H. Roos, *Structural strength and crystallization of amorphous lactose in food model solids at various water activities*. Innovative Food Science & Emerging Technologies, 2017. **40**: p. 27-34.
13. Haque, M.K. and Y.H. Roos, *Crystallization and X-ray diffraction of spray-dried and freeze-dried amorphous lactose*. Carbohydrate Research, 2005. **340**(2): p. 293-301.
14. Ibach, A. and M. Kind, *Crystallization kinetics of amorphous lactose, whey-permeate and whey powders*. Carbohydrate Research, 2007. **342**(10): p. 1357-1365.
15. Kedward, C.J., W. MacNaughtan and J.R. Mitchell, *Isothermal and non-isothermal crystallization in amorphous sucrose and lactose at low moisture contents*. Carbohydrate Research, 2000. **329**(2): p. 423-430.
16. Langrish, T.A.G., *Assessing the rate of solid-phase crystallization for lactose: The effect of the difference between material and glass-transition temperatures*. Food Research International, 2008. **41**(6): p. 630-636.
17. Listiohadi, Y., J.A. Hourigan, R.W. Sleight and R.J. Steele, *Moisture sorption, compressibility and caking of lactose polymorphs*. International Journal of Pharmaceutics, 2008. **359**(1–2): p. 123-134.
18. McIntosh, A.I., B. Yang, S.M. Goldup, M. Watkinson and R.S. Donnan, *Crystallization of amorphous lactose at high humidity studied by terahertz time domain spectroscopy*. Chemical Physics Letters, 2013. **558**: p. 104-108.
19. Miao, S. and Y.H. Roos, *Crystallization Kinetics and X-ray Diffraction of Crystals Formed in Amorphous Lactose, Trehalose, and Lactose/Trehalose Mixtures*. Journal of Food Science, 2005. **70**(5): p. E350-E358.

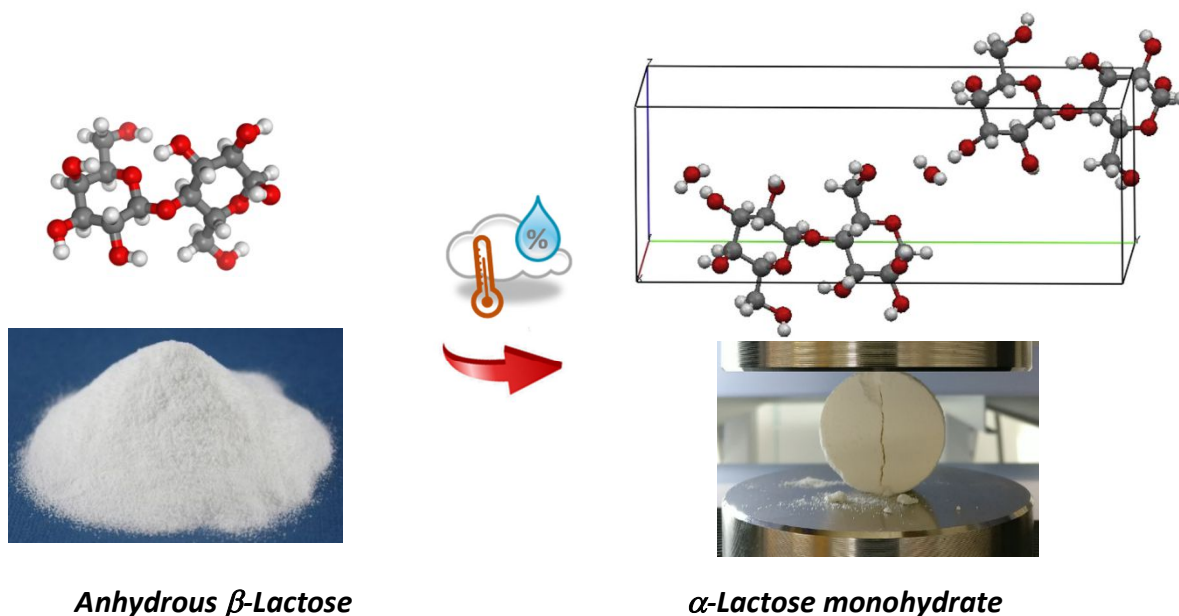
20. Roos, Y.H. and S. Drusch, *Phase Transitions in Foods.*, ed. S. Edition. 2016.
21. Schmitt, E.A., D. Law and G.G.Z. Zhang, *Nucleation and Crystallization Kinetics of Hydrated Amorphous Lactose Above the Glass Transition Temperature.* Journal of Pharmaceutical Sciences, 1999. **88**(3): p. 291-296.
22. Seliger, J. and V. Žagar, *Crystallization of an amorphous solid studied by nuclear quadrupole double resonance.* Chemical Physics, 2013. **421**: p. 44-48.
23. Clark, Z., A.H.J. Paterson, R. Joe and J.S. McLeod, *Amorphous lactose crystallization kinetics.* International Dairy Journal, 2016. **56**: p. 22-28.
24. Carpin, M., *Lactose caking: Understanding the mechanisms as a route to prevention*, in *INRA-Agrocampus Ouest, Science and Technology of Milk and Eggs (STLO)*, Rennes, France. 2018, European University of Brittany.
25. Chen, J., J. Wang, R. Li, A. Lu and Y. Li, *Thermal and X-ray Diffraction Analysis of Lactose Polymorph.* Procedia Engineering, 2015. **102**: p. 372-378.
26. Haque, M.K. and Y.H. Roos, *Differences in the physical state and thermal behavior of spray-dried and freeze-dried lactose and lactose/protein mixtures.* Innovative Food Science & Emerging Technologies, 2006. **7**(1): p. 62-73.
27. Jouppila, K., J. Kansikas and Y.H. Roos, *Glass Transition, Water Plasticization, and Lactose Crystallization in Skim Milk Powder.* Journal of Dairy Science, 1997. **80**(12): p. 3152-3160.
28. Potes, N. and Y. Roos, *Crystallization in Amorphous Lactose-Maltodextrin Mixtures.* 2011.
29. Das, D. and T.A.G. Langrish, *An activated-state model for the prediction of solid-phase crystallization growth kinetics in dried lactose particles.* Journal of Food Engineering, 2012. **109**(4): p. 691-700.
30. Lifran, E.V., T.T.L. Vu, R.J. Durham, J.A. Hourigan and R.W. Sleight, *Crystallization kinetics of lactose in the presence of lactose phosphate.* Powder Technology, 2007. **179**(1): p. 43-54.
31. Peleg, M., R. Engel, C. Gonzalez-Martinez and M.G. Corradini, *Non-Arrhenius and non-WLF kinetics in food systems.* Journal of the Science of Food and Agriculture, 2002. **82**(12): p. 1346-1355.
32. Jouppila, K. and Y.H. Roos, *Water Sorption and Time-Dependent Phenomena of Milk Powders.* Journal of Dairy Science, 1994. **77**(7): p. 1798-1808.
33. Lloyd, R.J., X.D. Chen and J.B. Hargreaves, *Glass transition and caking of spray-dried lactose.* International Journal of Food Science and Technology. 1996. **31**(4): p. 305-311.
34. Sebhatu, T., C. Ahlneck and G. Alderborn, *The effect of moisture content on the compression and bond-formation properties of amorphous lactose particles.* International Journal of Pharmaceutics, 1997. **146**(1): p. 101-114.
35. Bronlund, J. and T. Paterson, *Moisture sorption isotherms for crystalline, amorphous and predominantly crystalline lactose powders.* International Dairy Journal, 2004. **14**(3): p. 247-254.
36. Foster, K.D., J.E. Bronlund and A.H.J. Paterson, *The prediction of moisture sorption isotherms for dairy powders.* International Dairy Journal, 2005. **15**(4): p. 411-418.
37. Vuataz, G., *The phase diagram of milk: a new tool for optimising the drying process.* Lait, 2002. **82**(4): p. 485-500.
38. Thomsen, M.K., L. Jespersen, K. Sjostrom, J.R. Risbo and L.H. Skibsted, *Water activity-temperature state diagram of amorphous lactose.* Journal of Agriculture and Food Chemistry, 2005. **53**: p. 9182-9185.
39. Brooks, G.F., *The sticking and crystallization of amorphous lactose : a thesis presented in partial fulfilment of the requirements for the degree of Master of Technology in Chemical Technology at Massey University.* 2000, Massey University.
40. Williams, M.L., R.F. Landel and J.D. Ferry, *The Temperature Dependence of Relaxation Mechanisms in Amorphous Polymers and Other Glass-forming Liquids.* Journal of the American Chemical Society, 1955. **77**(14): p. 3701-3707.

41. Paterson, A.H.J., G.D. Ripberger and R.P. Bridges, *Measurement of the viscosity of freeze dried amorphous lactose near the glass transition temperature*. International Dairy Journal, 2015. **43**: p. 27-32.
42. Peleg, M., *On the use of the WLF model in polymers and foods*. Critical Reviews in Food Science and Nutrition, 1992. **32**(1): p. 59-66.
43. Nijdam, J., A. Ibach, K. Eichhorn and M. Kind, *An X-ray diffraction analysis of crystallised whey and whey-permeate powders*. Carbohydrate Research, 2007. **342**(16): p. 2354-2364.
44. Buckton, G., P. Darcy, D. Greenleaf and P. Holbrook, *The use of isothermal microcalorimetry in the study of changes in crystallinity of spray-dried salbutamol sulphate*. International Journal of Pharmaceutics, 1995. **116**(1): p. 113-118.
45. Buckton, G. and P. Darcy, *Water mobility in amorphous lactose below and close to the glass transition temperature*. International Journal of Pharmaceutics, 1996. **136**(1): p. 141-146.
46. Darcy, P. and G. Buckton, *The influence of heating/drying on the crystallization of amorphous lactose after structural collapse*. International Journal of Pharmaceutics, 1997. **158**(2): p. 157-164.
47. Dilworth, S.E., G. Buckton, S. Gaisford and R. Ramos, *Approaches to determine the enthalpy of crystallization, and amorphous content, of lactose from isothermal calorimetric data*. International Journal of Pharmaceutics, 2004. **284**(1): p. 83-94.
48. Elmonsef Omar, A.M. and Y.H. Roos, *Glass transition and crystallization behavior of freeze-dried lactose-salt mixtures*. LWT - Food Science and Technology, 2007. **40**(3): p. 536-543.
49. Omar, A.M.E. and Y.H. Roos, *Water sorption and time-dependent crystallization behavior of freeze-dried lactose-salt mixtures*. LWT - Food Science and Technology, 2007. **40**(3): p. 520-528.
50. Haque, M.K. and Y.H. Roos, *Water Plasticization and Crystallization of Lactose in Spray-dried Lactose/Protein Mixtures*. Journal of Food Science, 2008. **69**(1): p. FEP23-FEP29.
51. Knudsen, J.C., H.S. Antanuse, J. Risbo and L.H. Skibsted, *Induction time and kinetics of crystallization of amorphous lactose, infant formula and whole milk powder as studied by isothermal differential scanning calorimetry*. Milchwissenschaft, 2002. **57**(9-10): p. 543-546.
52. Roos, Y. and M. Karel, *Phase Transitions of Mixtures of Amorphous Polysaccharides and Sugars*. Biotechnology Progress, 1991. **7**(1): p. 49-53.
53. Wang, S. and T.A.G. Langrish, *Measurements of the crystallization rates of amorphous sucrose and lactose powders from spray drying*. International Journal of Food Engineering, 2007. **3**: p. 1-17.
54. Stubberud, L. and R.T. Forbes, *The use of gravimetry for the study of the effect of additives on the moisture-induced recrystallization of amorphous lactose*. International Journal of Pharmaceutics, 1998. **163**(1): p. 145-156.
55. Vollenbroek, J., G.A. Hebbink, S. Ziffels and H. Steckel, *Determination of low levels of amorphous content in inhalation grade lactose by moisture sorption isotherms*. International Journal of Pharmaceutics, 2010. **395**(1-2): p. 62-70.
56. Ripberger, G., *Mechanism of viscous droplet/solid stickiness during impact investigation of the diffusivity and viscosity of amorphous lactose*. 2010, Massey University, : Palmerston North.
57. Roos, Y.H., *Solid and Liquid States of Lactose*, in *Advanced Dairy Chemistry: Volume 3: Lactose, Water, Salts and Minor Constituents*, P. McSweeney and P.F. Fox, Editors. 2009, Springer New York: New York, NY. p. 17-33.
58. Saleki-Gerhardt, A., C. Ahlneck and G. Zograf, *Assessment of disorder in crystalline solids*. International Journal of Pharmaceutics, 1994. **101**(3): p. 237-247.
59. Mackin, L., R. Zanon, J.M. Park, K. Foster, H. Opalenik and M. Demonte, *Quantification of low levels (<10%) of amorphous content in micronised active batches using dynamic vapor sorption and isothermal microcalorimetry*. International Journal of Pharmaceutics, 2002. **231**(2): p. 227-236.
60. Rumpf, H., *Particle Technology*. 1990: Chapman and Hall.

61. Afrassiabian, Z., M. Leturia, M. Benali, M. Guessasma and K. Saleh, *An overview of the role of capillary condensation in wet caking of powders*. Chemical Engineering Research and Design, 2016. **110**: p. 245-254.
62. Samain, S., M. Leturia, S. Mottelet, M. Benali and K. Saleh, *Characterization of caking for crystalline materials: comparison and statistical analysis of three mechanical tests*. Chemical Engineering Science, 2018.

Chapter IV

Caking of anhydrous Lactose powder under humid conditions



This chapter deals with the phase transition of anhydrous Lactose in solid-state due to humidification. Experimental evidence is provided that anhydrous lactose is converted to lactose monohydrate when exposed to ambient moisture. The conversion rate and the kinetics of the lactose transformation from anhydrous to monohydrate state was then investigated at various temperatures and RH. A kinetics model to describe the rate of transformation was also developed and a simple kinetic law based on the comparison between the experimental data and the model was established. The limiting step of the transformation process was found to be the crystallization reaction of anhydrous β -lactose.

In the second part of this chapter, the effect of storage conditions on the caking behavior and kinetics of amorphous lactose due to its solid-phase crystallization was investigated.

1 Introduction

Lactose powders have important applications in food and pharmaceutical industries (*e.g.*, as a filler-binder in the manufacture of pharmaceutical tablets by direct compression). In solid state, lactose is a polymorphic material with five well-accepted forms [1-4]. Among these different forms, anhydrous lactose is especially suitable for the production of tablets by the direct compression because of its good compactability. In industry, anhydrous lactose is usually produced by roller drying of highly-concentrated solutions of lactose at temperatures in excess of 93.5°C [5]. The product thus obtained is essentially composed of the β anomer of lactose, which has a high solubility and then is suitable for applications where large-scale dissolution is required. Generally, β -lactose is less hygroscopic and then more stable than the α anomer [1, 3, 4]. Anhydrous lactose is a deliquescent component with a critical relative humidity of DRH=95% at 25°C. Consequently, this form of lactose is generally assumed to be relatively stable below 95% RH [6]. However, during long periods of storage under relative humidity less than DRH, anhydrous lactose could undergo a transformation to the monohydrate form losing its good compressibility and solubility. In addition, like most powders, lactose is subject to caking when stored in humid conditions, which can alter its desired end-use properties.

The present work deals with the study of the phase transformation of anhydrous lactose following its hydration in solid state under humid conditions. The main aims of the study is to:

- Establish an appropriate rate equation and a reliable physical model for the kinetics of the hydration process taking into account the effect of the ambient temperature and relative humidity.
- Investigate the relation between solid-phase crystallization of anhydrous lactose and its caking behavior and kinetics

2 Materials and methods

2.1 Raw materials and physical properties

Experiments were mainly conducted on Meggle DuraLac® H anhydrous lactose powder. FlowLac α -lactose monohydrate was also used as a reference in differential scanning calorimetric analysis. According to the manufacturer, the anhydrous powder is produced via roller-drying followed by milling and sieving to obtain the desired particle size distribution. Its primary application is as a tableting excipient, especially in direct compression processes. The manufacturer reports that the powder contained 16.3% anhydrous α -lactose and 83.7% anhydrous β -lactose. However, preliminary experiments in laboratory did not confirm this information and showed an anhydrous α -lactose content about 10-11%. The anhydrous sample is a white, crystalline, odorless powder and is freely but slowly soluble in water. Note that any proof of the presence of amorphous lactose (characterized by the existence of a glass transition temperature and its corresponding peak) was detected by DSC or TGA analyses. This was confirmed by XRD analyses, which confirmed that the samples were essentially composed of crystalline α - and β -anhydrous lactose with some traces of α -lactose monohydrate.

The true density of samples were measured by Helium pycnometry (Accupyc 1330, Micromeritics). The measurements were carried out on three samples (1 g) of each batch and repeated fivefold for each sample. The mean density was calculated by averaging the fifteen measurements. The true density of the product was $1530 \pm 7 \text{ kg}\cdot\text{m}^{-3}$.

The particle size distribution was verified by both laser diffraction and image analysis methods. The laser diffraction measurements were performed using a Malvern 2000 analyzer equipped with a dry dispersion unit. For each measurement, the Particle size distribution was calculated from an average of 10000 instant measurements (10 s; 1000s^{-1}). Five samples of each product were analyzed to determine the mean particle size distribution. In addition, the morphology and number density of the particle size distribution was measured by a MorphoG3® from Malvern Co.

In order to investigate the effect of the particle size, the raw material was divided in three sub-populations by sieving using 100 μm and 200 μm sieves. The resulting batches are referred to as Fine ($d < 100\mu\text{m}$), Medium ($100\mu\text{m} < d < 200\mu\text{m}$) and Large ($200\mu\text{m} < d$) fractions, respectively. [Figure IV-1](#) shows the mean particle size distribution of the raw material and the

three sub-populations. Table IV-1 summarizes the main granulometric characteristics of all batches.

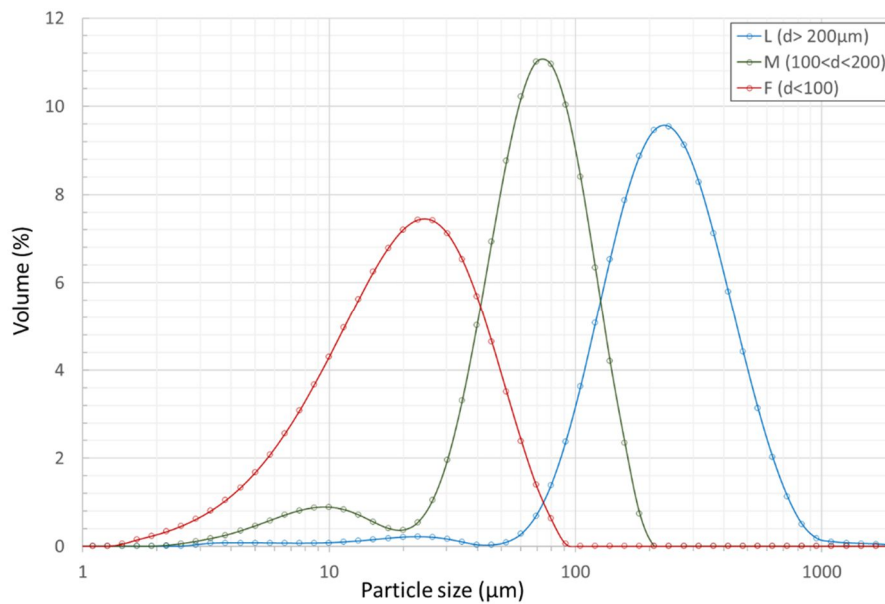


Figure IV-1: Mean Particle Size Distribution of Fine, Medium and large fractions

Table IV-1: Characteristic sizes of samples used

	Sample		
	Fine	Medium	Large
$d_{10\%}$ (μm)	6	27	103
$d_{50\%}$ (μm)	19	63	214
$d_{90\%}$ (μm)	43	113	248
d_{32} (μm)	13	37	135

ESEM images of samples, taken by a Philips XL30-ESEM FEG allowing observation of samples without the need for metallization, are also presented in Figure IV-2. As can be seen, Medium and Large fractions contain still small amounts of fine particles, which cannot be fully ousted because of high attractive interactions due to van der Waals forces.

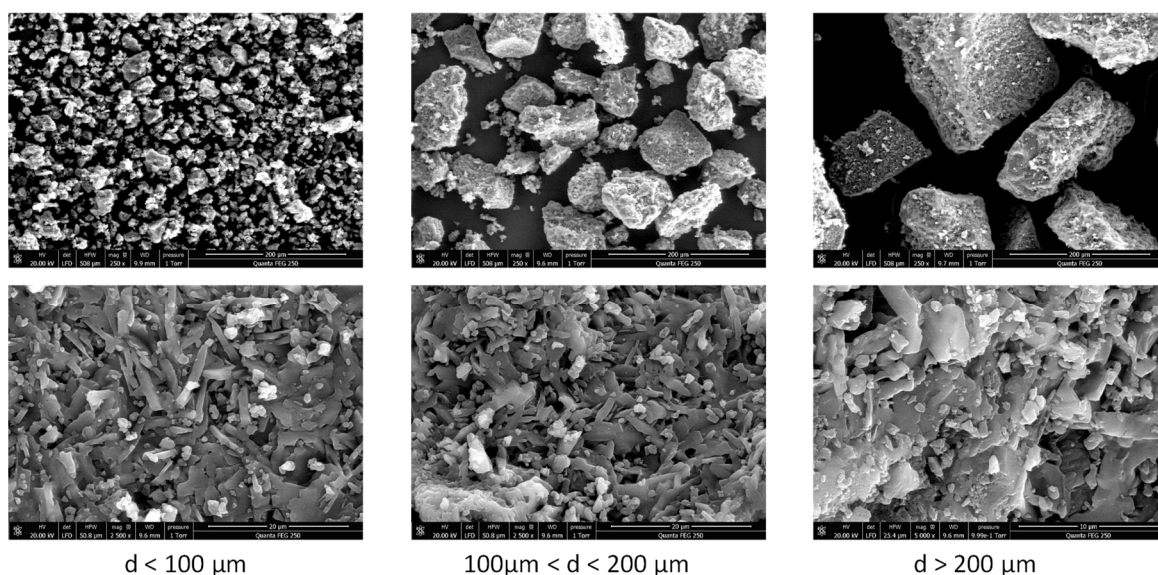


Figure IV-2: ESEM images of Fine (left), Medium (middle) and Large (right) fractions

2.2 Thermal Analyses: Differential Scanning Calorimetry

Differential scanning calorimetry (DSC Q100-TA Instruments) was carried out on the raw anhydrous lactose and on samples after hydration. Between 8 and 12mg of powder from each sample was loaded into 40 μL aluminum pans. The pans were then sealed with an aluminum lid and placed into the autosampler of the calorimeter. Samples were analyzed over a temperature range of -40°C to 250°C , using a heating rate of $5^{\circ}\text{C}/\text{min}$.

The DSC curves for raw anhydrous lactose (Meggle DuraLac[®] H) and raw α -lactose monohydrate (FlowLac[®]) are shown in Figure IV-3. The endotherms between 100°C and 150°C correspond to the enthalpy change that occurs due to the dehydration of water from the lactose monohydrate present in the samples. This dehydration has been shown to occur at approximately 145°C [7] and is confirmed experimentally by the DSC curve for pure lactose monohydrate shown in Figure IV-3. A strong dehydration endotherm was recorded at 142°C . The surface area of the endotherms peak in Figure IV-3 corresponds to the heat of dehydration and is proportional to the amount of lactose monohydrate present in each sample. These results show that the curve for raw anhydrous lactose also exhibits a slight dehydration isotherm, which confirms that a small amount of lactose monohydrate is present in the raw anhydrous lactose. This was also confirmed by the XRD analysis presented in the next section.

Taking into account the heat of dehydration of lactose monohydrate, its amount in raw anhydrous lactose could be estimated to 4.2%.

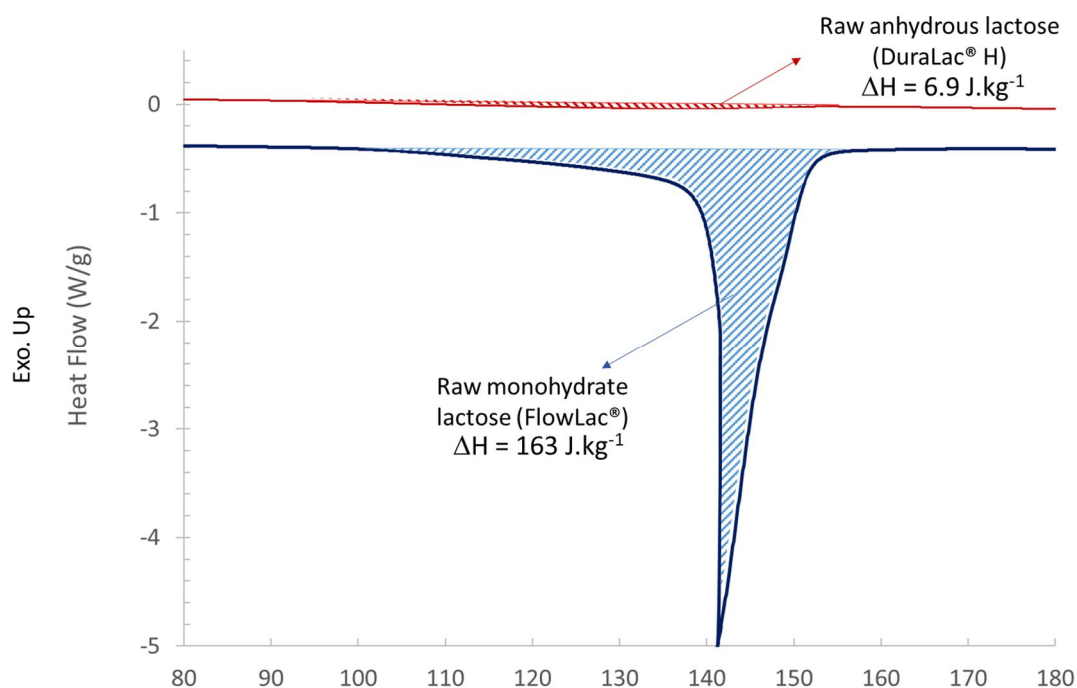


Figure IV-3: DSC thermograms of Anhydrous Lactose (DuraLac® H) and Lactose monohydrate (FlowLac®)

2.3 X-ray Diffraction

About 50 mg of each sample (lactose1 and 2) was analyzed in a Bruker D8 Advance diffractometer equipped with a Lynxeye-XE detector using the $\text{CuK}\alpha$ radiation (Ni filter, $\lambda = 1.5418\text{\AA}$). The X-ray powder diffraction (XRD) pattern was recorded from 10° to 50° (2θ) with a step size of 0.02° and counting time of 5 sec/step. The position of peaks in the diffractograms (2θ) were used to determine the interplanar distances (d_{hkl}) following Bragg's law. The d_{hkl} values were compared to standard powder diffraction data in the literature (ICDD PDF4+ database).

Figure IV-4 shows the XRD patterns for lactose samples used in this study. The results are compared to the theoretical XRD spectrum of α -lactose monohydrate and anhydrous β -lactose imported from the library database. These results confirm the presence of some anhydrous α -lactose (characteristic peaks 27° and 28°) as well as traces of α -lactose monohydrate in the anhydrous sample.

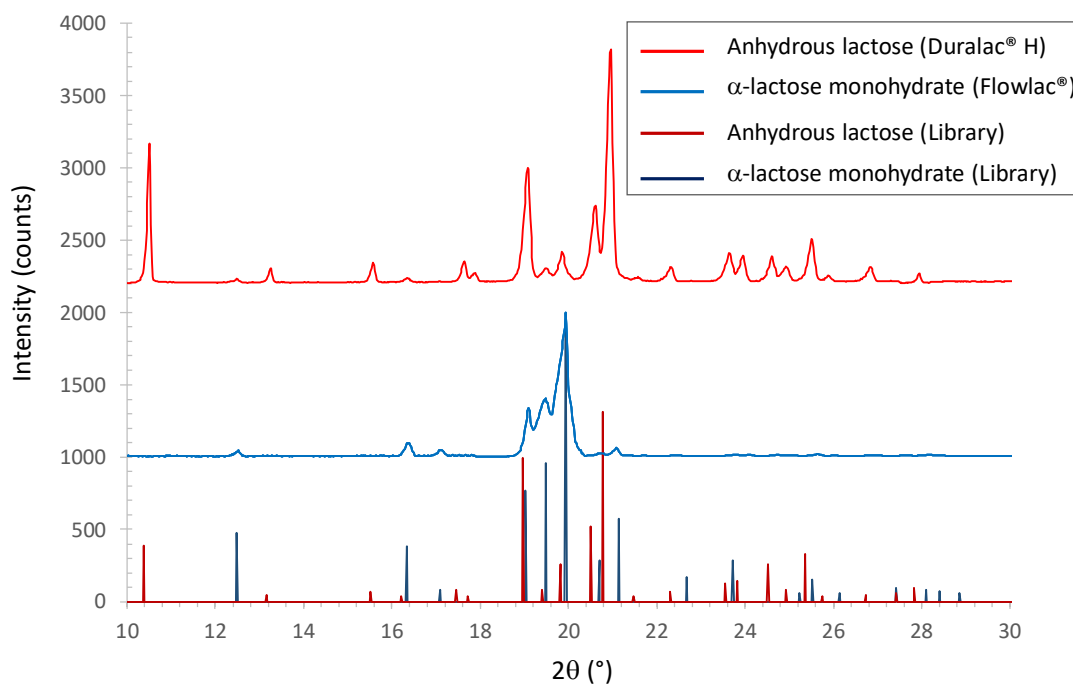


Figure IV-4: XRD spectra of α -lactose monohydrate and anhydrous β -lactose samples

2.4 Specific surface analysis by gas adsorption (BET)

The specific surface area measurements were carried out using N_2 adsorption method (ASAP 2010, micromeritics). The BET theory was applied to the data from the sorption-desorption isotherm. The analyses showed no presence of microporosity. The specific surface area calculated from BET model was found to be $1.2 \text{ m}^2 \cdot \text{g}^{-1}$ for the anhydrous sample and $0.9 \text{ m}^2 \cdot \text{g}^{-1}$ for Lactose monohydrate. These results are consistent with the particle size analysis and indicate that the specific surface area is mainly due to the external surface of particles. The higher value of the specific surface area measured by BET with respect to the particle size analysis is very likely due to the presence of roughness and fine particles in the sample.

2.5 Dynamic Vapor Sorption

The sorption isotherms and sorption kinetics of samples were determined using a gravimetric dynamic sorption analyzer (SPS23 ProUmid). This is a multisampling instrument capable of simultaneous measurement of water vapor sorption isotherms on up to 23

samples. All samples are maintained in a temperature and humidity controlled chamber ($\pm 0.6\%$) and are sequentially weighed using a high precision microbalance ($\pm 10 \mu\text{g}$).

Prior to experiments samples were kept at refrigerator ($3-4^\circ\text{C}$) and put in a desiccator for 48h before experiments. About 0.5 g of each sample was poured in an aluminum pan (50mm diam. and 10 mm height) so that a very thin layer of powder was formed. Preliminary measurements showed that for powder quantities less than 1 g the sorption kinetics were not affected by the external diffusion and thus were independent of the amount of samples. After filling, the pans were placed on a special tray, which was then introduced to the SPS analyzer. The samples were first dried at 0% RH and the set temperature. The mass of each sample at the end of this step was considered as its reference mass. Then the samples were exposed to successive jumps of relative humidity (step function) at constant temperature until the equilibrium was reached. Then, the desorption cycle was conducted by a step-by-step decrease of the RH up to zero. The value of the water uptake was recorded every 10 minutes. The criterion for equilibrium was set as $\frac{dm/m_0}{dt} < 1 \times 10^{-5} \% \cdot \text{min}^{-1}$ and the minimum and maximum time per step were set as 1h and 6h, respectively.

Figure IV-5 presents the sorption-desorption isotherms of anhydrous (Duralac[®] H) and monohydrate (Flowlac[®]) lactose, respectively.

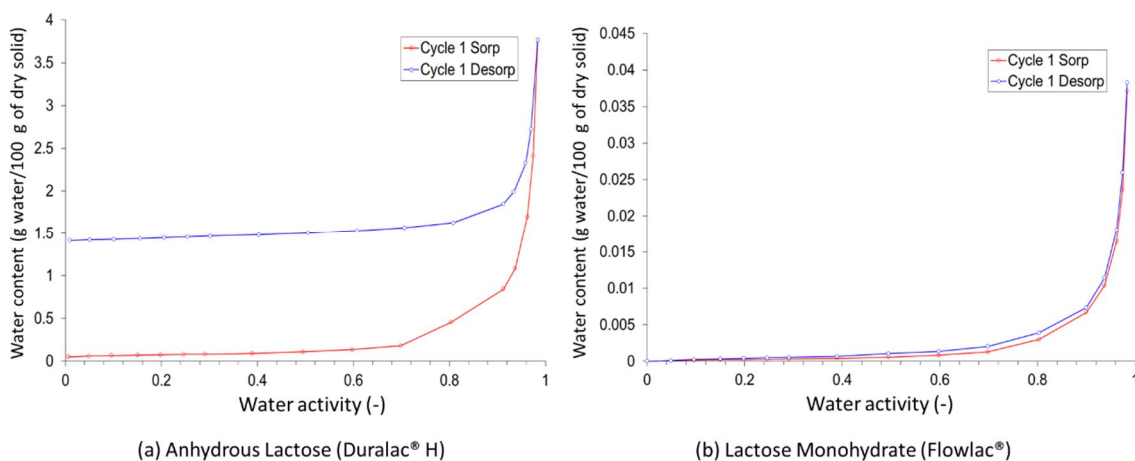


Figure IV-5: Sorption-desorption isotherms of anhydrous and monohydrate lactose samples

The monohydrate sample presents a type IV isotherm with a small hysteresis corresponding to the existence of some mesoporosity. The isotherm can be well represented

by conventional GAB model within the activity range between 0 and 0.8. However, the anhydrous sample shows a more complex behavior. In fact, the water sorption of anhydrous lactose is much higher than the monohydrate lactose. The high extent of water sorption cannot be attributed to the adsorption phenomenon only, otherwise the water content of anhydrous and monohydrate powders should be of the same order of magnitude. In fact, the high water sorption is due to the hydration reaction of anhydrous lactose giving rise to the formation of lactose monohydrate. This hypothesis is corroborated by the large difference observed between the sorption and desorption curves, which corresponds to the quantity of water that took part in the hydration reaction. In reality, it is not possible to measure the sorption or desorption isotherm of anhydrous lactose because the product evolves with hydration and the results depend on the duration of each step and the criterion set for equilibrium. Therefore, the data presented in the [Figure IV-5](#) are valid only for the specific criteria of our measurements.

3 Kinetic study of hydration, crystallization and dehydration of anhydrous lactose

3.1 Dynamic water vapor sorption experiments

Hydration kinetics of anhydrous lactose powder was investigated by dynamic water vapor sorption analysis using the SPS device. To establish isothermal sorption-desorption kinetics, the samples were first dried at 0% RH and the set temperature. Then, the samples were exposed to a constant relative humidity and temperature for known periods of time. Once the humidification step was complete, the samples were dried again at 0% RH and the set temperature until equilibrium is reached. The difference between the final mass of the sample and the reference mass was then calculated and considered as the mass of water that took part in the hydration reaction. The experiments were carried out for different hydration times and for all combinations between temperature (ranging from 15°C to 40 °C by 5°C step change) and Relative Humidity (ranging from 70% to 95% by 5% step change) by changing one parameter at a time. Using the 11-sample holder tray, it was possible to analyze 9 samples (*i.e.*, 3 samples of each batch S, M and L, in triplicate) at a time during each experiment.

3.2 Typical example of hydration kinetics

Figure IV-6 presents a typical set of data related to the time evolution of the total amount of water uptake for Medium size particles. Experiments were carried out in threefold at $T=25^{\circ}\text{C}$ and $\text{RH}=80\%$. All the experimental results obtained at other operating conditions closely followed the kinetic trends shown in this figure. The reproducibility of tests was very good (e.g., standard deviations does not exceed 1% of the average). In addition, the actual T and RH quickly reach the set point and then the conditions can be considered as constant throughout the experiments.

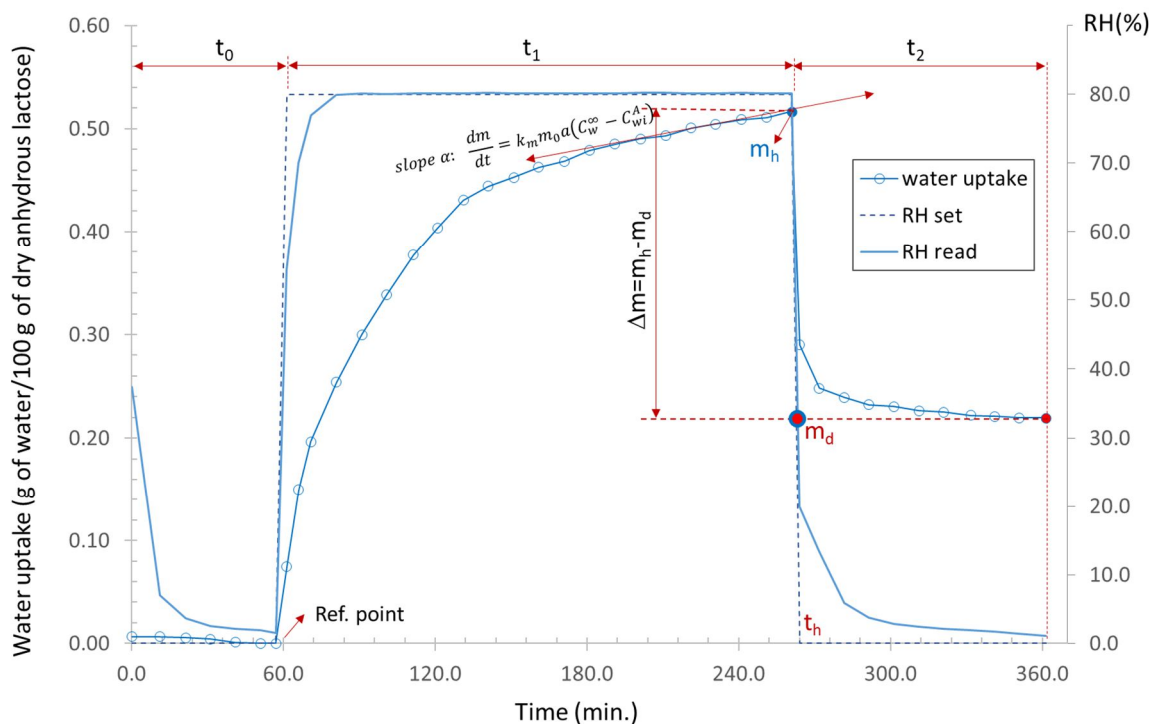


Figure IV-6: Typical example of a dynamic water vapor sorption experiment ($T=25^{\circ}\text{C}$ and $\text{RH}=80\%$)

Figure IV-6 indicates that the water uptake undergoes a rapid increase as soon as the hydration begins. Beyond this initial period, the water uptake continues to increase but at a less pronounced rate. In order to understand this trend, we must take into account several phenomena that take place simultaneously at the surface and within the particles: water vapor condensation at air-solid interface (adsorption), diffusion of water molecules from the surface towards the center of solid particles (absorption), hydration reaction of anhydrous lactose and, probably, capillary condensation. Among these mechanisms, the adsorption

possesses the fastest dynamic. The sharp increase in water uptake at the beginning can then be attributed to adsorption, although the contribution of the other two mechanisms should not be neglected completely. This explains why the end part of the sorption curve increases less quickly indicating that adsorption has reached its maximum level. It should be noticed that in this interval, the water uptake increases almost linearly with time. This can be explained by conversion of anhydrous lactose to lactose monohydrate, which occurs at a lower rate than adsorption. Indeed, for a complete conversion, the theoretical mass gain must be 5% w/w. However, in large majority of tests carried out in this work, in spite of relatively long periods of hydration, the water content of samples remained less than 1% (*i.e.* the conversion < 20%). In this case, it can be assumed that anhydrous lactose is available in large quantity and is in excess with respect to water. For higher conversions, it can be expected that the concentration of anhydrous lactose becomes the limiting factor thus leading to a lowering of the sorption kinetics. Therefore, within the range of operating conditions used in this work, the slope, α , of the linear part at quasi-steady-state regime provides information about the overall mass transfer rate between the particles and the surrounding humid air:

$$\text{slope } \alpha: \frac{dm}{m_0 dt} = k_m a (C_w^\infty - C_{wi}^A)$$

where C_w^∞ is the mean molar concentration of water vapor in main body of air and C_{wi}^A is the interfacial concentration of water vapor in air phase, which is assumed to be in equilibrium with the solid phase (Figure IV-7).

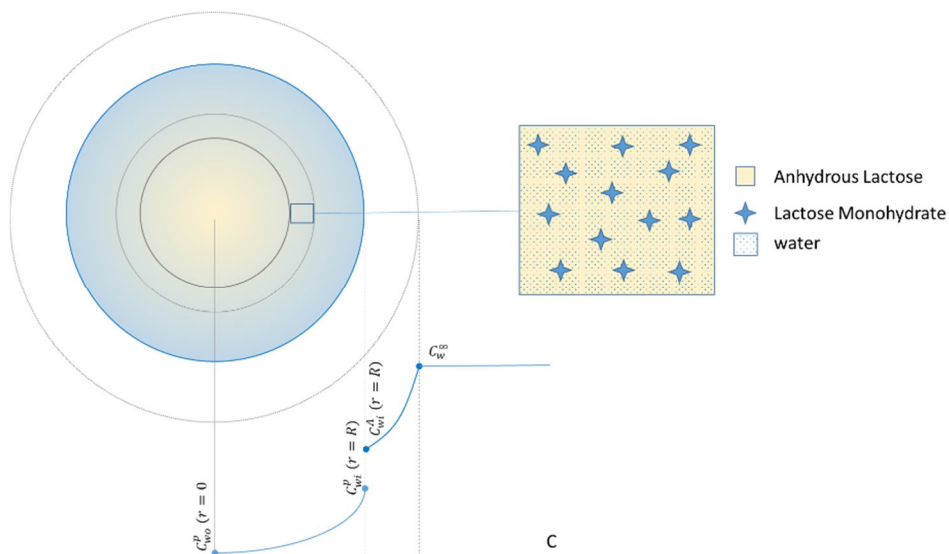


Figure IV-7: gradient of water concentration around particles

The fact that the slope of this segment is almost constant indicates that the driving force of transfer and then C_{wi}^A does not change significantly during the experiment. If we assume that this latter is in equilibrium with the water content of particles at their surface, C_{wi}^p , it means that the concentration of water in solid phase C_w^p remains almost constant (otherwise C_{wi}^A must decrease and the mass transfer must slow down). The hydration process proceeds then in a quasi-steady-state regime and the flow rate of incoming water by adsorption is equal to the rate of water consumed by the hydration (crystallization) reaction:

$$\frac{dm}{dt} = k_m a (C_w^\infty - C_{wi}^A) = k_r V_p \bar{C}_A \bar{C}_w$$

Here, k_r is the rate constant of the hydration reaction and V_p is the total volume of particles. \bar{C}_A and \bar{C}_w are the average concentration of anhydrous lactose and water within solid phase, respectively. Both could be considered as constant at early stages of hydration.

As for the desorption step, the corresponding curve is characterized by a sharp decrease in water content at the beginning, followed by a significant attenuation of drying kinetics thereafter. Again, the sharp decrease at the beginning of dehydration step can be attributed to water desorption from the external surface of particles. Furthermore, the water uptake does not fall back to zero but achieves an asymptotic threshold after almost 360 minutes (*i.e.* 96 minutes drying). This observation confirms that within the range of temperatures involved in this work, the transformation of anhydrous lactose is an irreversible process. Hence, the terminal point of the desorption curve (point m_d in [Figure IV-6](#)) corresponds to the net amount of water consumed by the reaction. Since the reaction substantially slows down during desorption, we conventionally assign the point m_d to time, t_h , that is, the point of transition from hydration to dehydration step. Note that the difference between the ordinates of the two terminal points, m_h and m_d (designated by Δm), corresponds to the total amount of water involved in non-reactive mechanisms (*i.e.* absorption and adsorption). In order to better understand the relative importance of these mechanisms, the previous experiment was repeated for longer durations of experiment. The results are presented in [Figure IV-8](#). Expectedly, the highest variation takes place during the first cycle for which both adsorption and conversion increases rapidly. The conversion continues to grow in subsequent cycles but at a slower pace. This initial higher conversion rate is most likely due to the presence of anhydrous α -lactose in samples, as it was verified by XRD experiments. The presence of sub-

micron particles at the surface of particles (see ESEM images in Figure IV-2) enhance certainly this step.

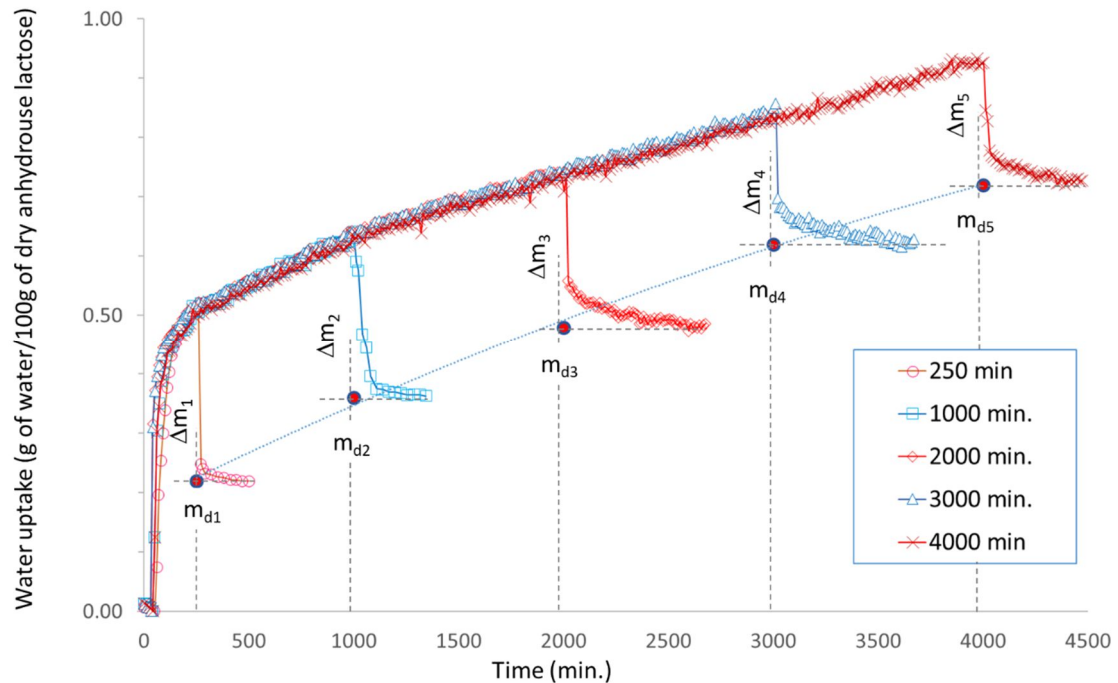


Figure IV-8: Dynamic water vapor sorption experiments at different durations ($T=25^{\circ}\text{C}$ and $\text{RH}=80\%$)

We can assume that after this first period, the reaction can only occur with more stable β polymorph of anhydrous lactose, which constitutes the major component of the powder. A further analysis of the data shows that the difference between the sorption and the desorption endpoints for successive cycles (i.e. Δm_i), decreases progressively. Remind that this difference corresponds to the mass gain due to both adsorption and absorption. If we make the assumption that, the humidification does not change the fine structure of particles (size, shape, specific surface area, porosity, roughness) the mass gain due to adsorption must be the same from one cycle to another. Hence, the decrease in Δm_i might arise from a decrease of the amount of absorbed water, which seems normal taking into account that less place is available for water in solid matrix as the reaction progresses. With these hypotheses, the limit value of Δm_i when the conversion tends hypothetically to 100% (i.e., m_{di} tends to 0.05) might correspond to the net contribution of adsorption. This (together with the assumption that the second part of the dehydration, characterized by a low rate, corresponds

to the internal diffusion of water) means also that for initial stages of hydration, at the sorption endpoint, unreacted water is still available inside the solid, which indicates that the reaction might constitute the limiting step of the process. This will be even more the case at the end of the process when anhydrous lactose runs out inside the system.

Furthermore, Figure IV-9 presents the behavior of samples submitted to successive hydration-dehydration cycles. As we will see later, this method provides valuable data for modelling and parameter identification.

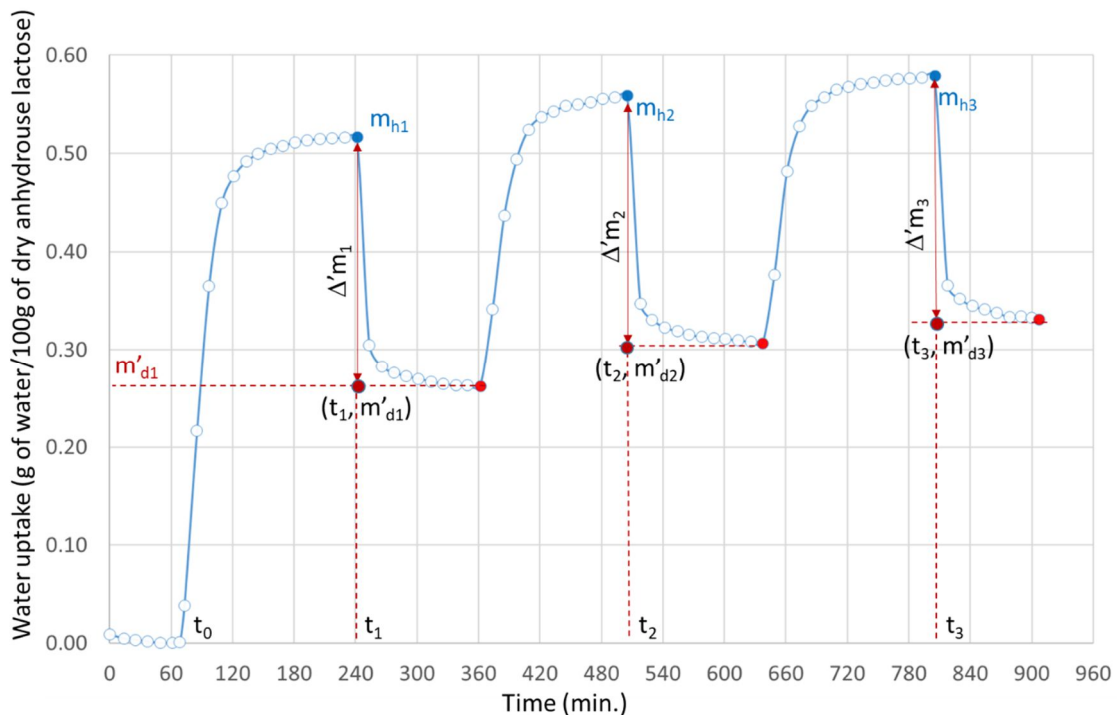


Figure IV-9: Dynamic vapor sorption results obtained for successive hydration-dehydration cycles ($T=25^{\circ}\text{C}$ and $\text{RH}=80\%$)

In agreement with the previous results, these data highlight a progressive increase of the conversion with the number of cycles. It should however be noted that despite its resemblance to the behavior of some sugars, the gradual gain in m_{di} values with successive cycles of sorption-desorption in the present work does not arise from the same mechanisms than for those sugars. Indeed, the recent works carried out in our research group [8, 9] has demonstrated the presence of residual water during successive cycles of sucrose hydration beyond its critical humidity of deliquescence ($\text{DRH}=86\%$). This was attributed to the partial

dissolution of the sugar in the water during the condensation then to the appearance of a very concentrated solution during the drying. The very high viscosity of this supersaturated solution leads to a low mobility of sucrose molecules, which do not have the possibility of reorganizing themselves into a crystalline structure. Moreover, the drying leads to the appearance of a crust on the surface, which traps a part of the water present in the solution. This must result in formation of an amorphous phase and presence of residual water after drying. However, in the present case, the hydration is conducted below the critical relative humidity of deliquescence of anhydrous lactose (DRH=95%). The presence of free water on the surface can then be excluded. In the same manner, it is unlikely that water appears by capillary condensation in the internal pores of agglomerates because for particle sizes and climate conditions ($RH < 95\%$) involved in this study this phenomenon remains irrelevant [10]. Accordingly, XRD and DSC analyses showed no evidence of the existence of amorphous lactose. Furthermore, this conclusion is supported by DVS analyses. In fact, if amorphous lactose is formed during the first hydration-drying cycle, a significant drop in the water content during the second cycle of hydration should happen. This is due to recrystallization of the amorphous phase and consequent release of entrapped water which takes place for $RH > 48\%$ [1-3, 11-18]. As it can be seen from [Figure IV-9](#), no discontinuity corresponding to this phenomenon is observed during the second cycle.

In what follows, a parametric study of the effect of particle size, temperature, T , and relative humidity, RH , is presented on the basis of principal characteristics of the sorption-desorption kinetics and the characteristic information presented in [Figures IV-8](#) and [IV-9](#), namely hydration curve, consumption curve (locus of dehydration endpoints, m_{di}) and the quasi-steady-state conversion rate (slope of hydration curve).

3.3 Effect of the particle size

[Figure IV-10](#) presents a comparison between the sorption-desorption isotherms obtained for three different population of particles, namely Fine ($d < 100 \mu\text{m}$), Medium ($100 < d < 200$) and Large ($d > 200 \mu\text{m}$). Several successive cycles of hydration-dehydration were performed. Unexpectedly, no significant effect of particle size on sorption-desorption isotherms of these different samples is observed. All samples show very similar kinetics. This behavior could be explained by two hypotheses. First of all, as can be seen from ESEM images

presented in Figure IV-2, whatever the population used (Fine, Medium or Large), the particles appear to be composed of smaller size crystals. In this case, rather than the size of the parent particles, it is the size of the elementary crystals that is important.

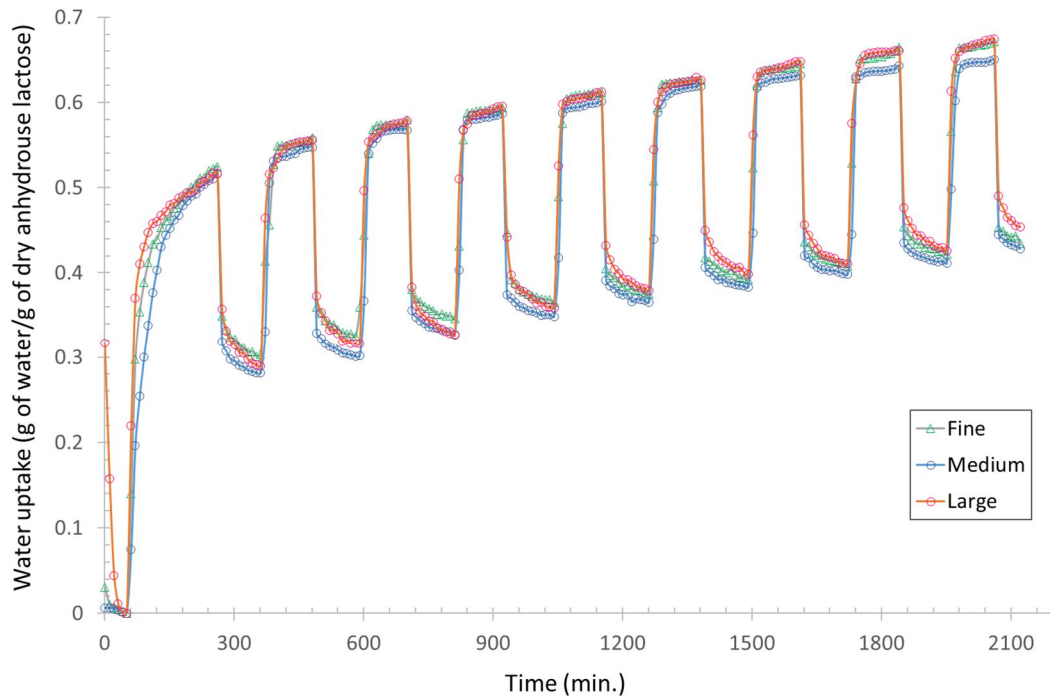


Figure IV-10: DVS results obtained for successive hydration-dehydration cycles

The results then indicate that the size of these crystals is identical in the three populations used. Another plausible hypothesis is that the limiting step of the mass transfer process is the crystallization reaction. In other words, the rate of the reaction would be very low with respect to adsorption and intragranular diffusion. As a result, the size of the particles does not play an important role because it only intervenes in the adsorption and diffusion steps. This hypothesis would indicate that after the initial rapid rise phase of water content, the particles become (and remain) saturated and that further transfer of water is governed by the reaction rate.

3.4 Effect of the relative humidity

Figure IV-11 shows sorption-desorption kinetics obtained at different RH for several durations. For a better readability of the data, instead of the complete curves, only the

hydration and conversion curves (*i.e.* loci of hydration and dehydration endpoints, respectively) are plotted.

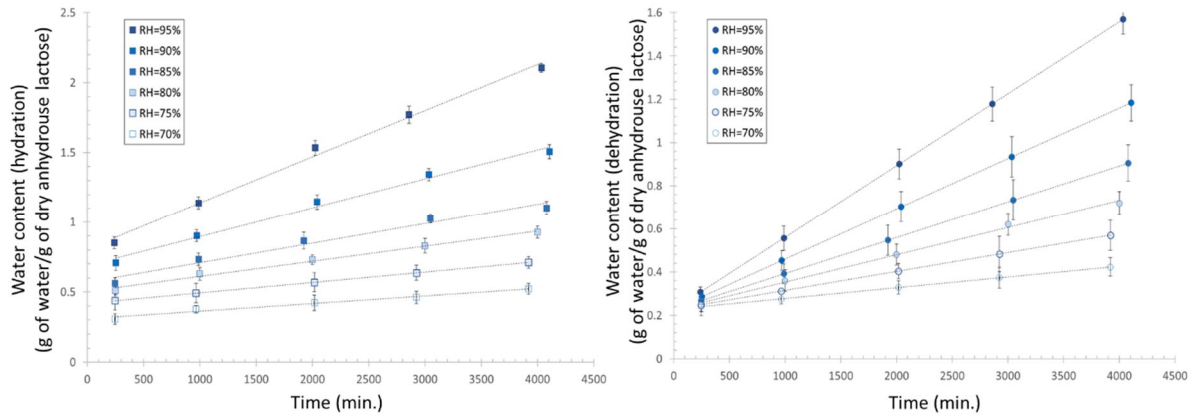


Figure IV-11: Kinetics of water sorption (left) and water consumption (right) obtained at 25°C and various RH

The results show a progressive increase of both hydration and conversion curves with relative humidity. This trend can be explained by one or other of the following assumptions:

- An increase in the internal diffusion coefficient with the increase in RH. Indeed, some authors consider that the coefficient of diffusion is a function of both the temperature and the moisture content of particles. For example, Chu and Hustrulid [19] proposed the following relation:

$$\mathcal{D} = A_{\mathcal{D}} e^{BX}$$

where X is the water content of particles and B and $A_{\mathcal{D}}$ are temperature dependent constants. Although the physical phenomena underlying this variation of the diffusion coefficient with the water content are not well explained, this trend has been experimentally reported by some investigators [19-22].

- The second explanation could be the increase of the driving force of internal mass transfer with increasing the relative humidity. Indeed, according to the theory of boundary layers (Figure IV-7), by making the assumption that at the solid-gas interface the two phases are in equilibrium, the conditions at the interface (particle's surface) could be described by the water vapor sorption

isotherm of solids. If we consider that the transfer resistance lies inside the particle, the margin of increase for water content (concentration) on the surface of the solid (which corresponds to the equilibrium conditions and is given by the sorption isotherm) is higher at higher RH. This increase is generally well represented by conventional sorption models of the BET or GAB type. This then leads to a subsequent increase in the driving force of the internal diffusion.

At this point, it is difficult to definitively confirm the relevance of either of these two hypotheses. However, the first hypothesis assumes an exponential acceleration of diffusion over time (*i.e.*, as the absorption progresses), which is not confirmed in this study (Figures IV-8 to IV-10). Moreover, the link between RH and the moisture content does not appear directly in this model. Finally, if the chemical reaction is the limiting step (as seems to be the case here), the increase of the diffusion coefficient should not affect significantly the conversion rate.

Regarding the second explanation, to verify its relevance, it is necessary to know the equilibrium conditions at the solid-gas interface. Assuming that the driving force of the transfer is proportional to the water concentration at the surface of the particles, C_{wi}^p , it can be expected that the hydration curve will follow the same trend as the product sorption isotherm (C_{wi}^p vs. C_{wi}^A). Unfortunately, because the absorption phenomenon and the crystallization reaction occurs in parallel with adsorption, the sorption isotherm of anhydrous lactose cannot be established precisely experimentally. Normally, the isotherm must vary between the two isotherms presented in Figure IV-5-a and -b for anhydrous and monohydrate lactose, respectively. Although it is not possible to know exactly this information, the sorption isotherms presented in this figure show, both, a regular variation of the water content of the solids between 70% and 95% RH. This can explain qualitatively the trend observed for the hydration kinetics.

As for the conversion, Figure IV-11 shows a regular increase of this parameter with relative humidity. This increase can be attributed to the subsequent increase in the water content (concentration) of particles, which accelerates the reaction kinetics. As can be seen, the increase is almost linear with RH, *i.e.*, an increase of RH of a given ratio leads to an increase of the conversion rate by almost the same ratio. Note that the amount of free water available

in the particles corresponds to the difference between the hydration and dehydration (conversion) endpoints, denoted by Δm . If we take the values obtained at RH=70% as a base of comparison, we can see in Figure IV-12 that for a given time, the rate of increase of water consumption (conversion rate) at different RH ($\frac{m_{d,x\%} - m_{d,70\%}}{m_{d,70\%}}$) varies almost linearly with the rate of excess of the amount (concentration) of free water, ($\frac{\Delta m_{x\%} - \Delta m_{70\%}}{\Delta m_{70\%}}$). This linearity indicates that the crystallization reaction is of the first order with respect to water concentration.

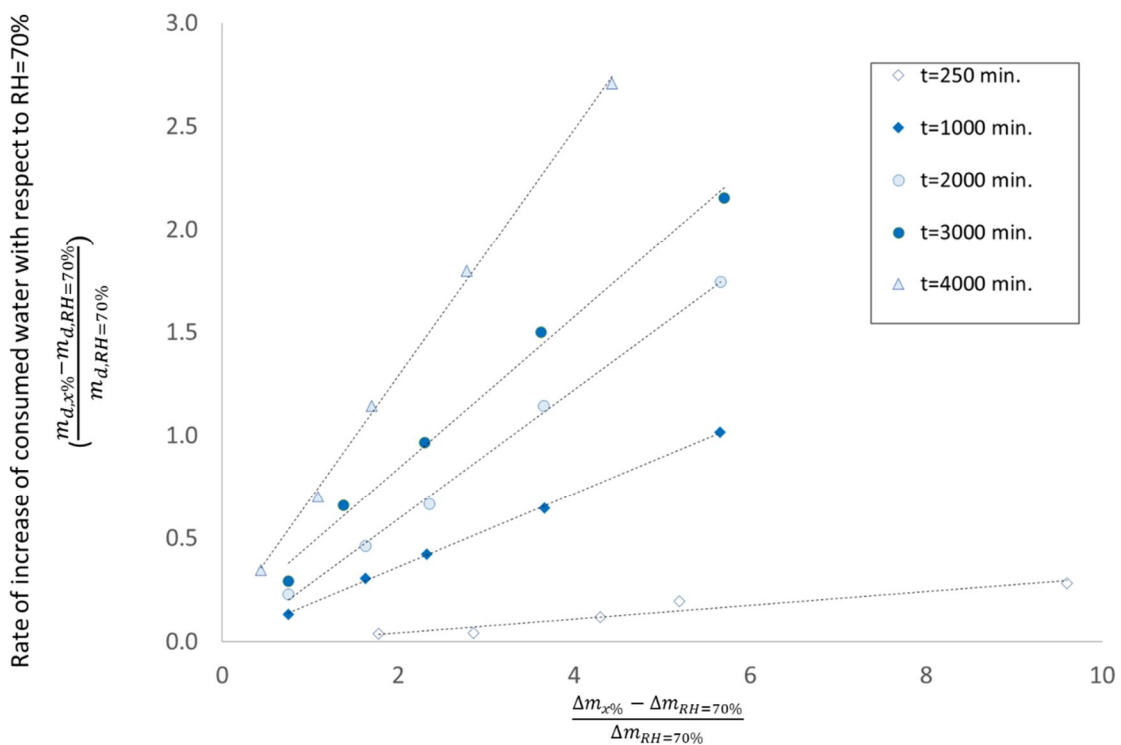


Figure IV-12: Rate of increase of the amount of free water with respect to RH=70%

$$\left(\frac{\Delta m_{x\%} - \Delta m_{RH=70\%}}{\Delta m_{RH=70\%}} \right)$$

3.5 Effect of temperature

Figure IV-13 shows the time variation of conversion data at different temperatures. It appears from the results that the increase of temperature leads to an increase of the conversion rate. This behavior can be easily explained by the increase the kinetic constant with temperature as stated by a classical Arrhenius law.

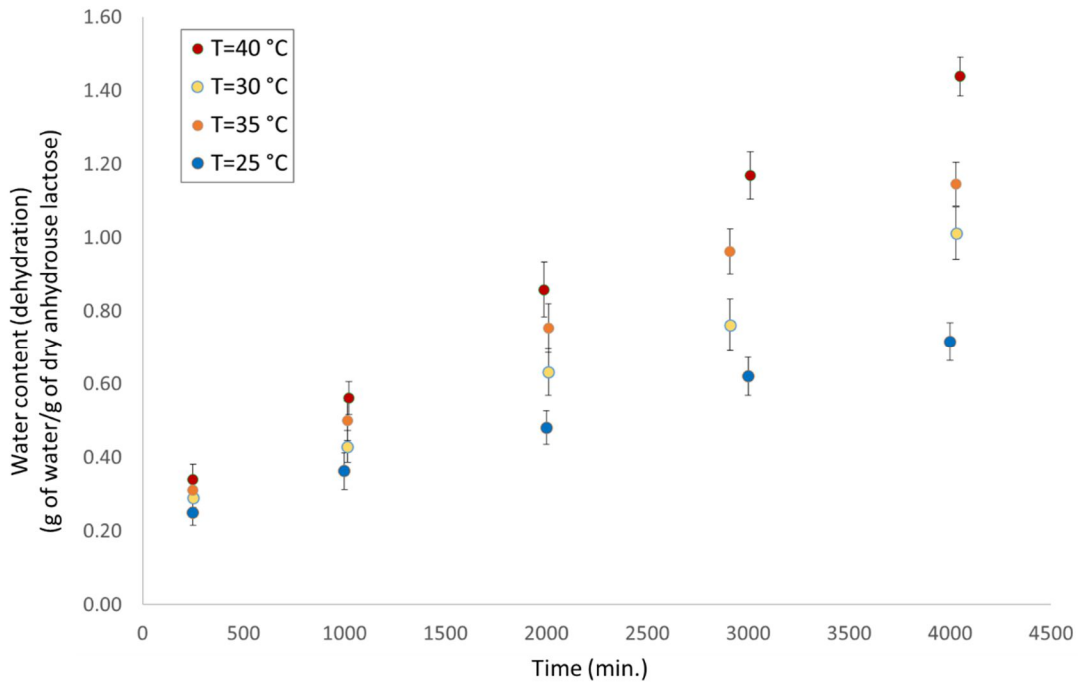


Figure IV-13: Kinetics of water consumption at RH=80% and various Temperature

It is possible to establish, from the data presented here, a kinetic law for the apparent kinetics of the crystallization process. Assuming that for low conversions the concentration of anhydrous lactose is in large excess so that it can be considered as constant and that the reaction is of first order with respect to the water, the apparent rate constant of the reaction is given by:

$$r_M = k_r V_p \bar{C}_A \bar{C}_w = \mathcal{K} \bar{C}_w$$

or

$$\frac{dX_A}{dt} = -\mathcal{K}(1 - X_A)$$

where r_M is the rate of lactose monohydrate formation (or anhydrous lactose disappearance), \mathcal{K} , is the apparent rate constant of reaction, \bar{C}_w is the concentration of water and X_A is the fractional conversion of anhydrous lactose. Note that the conversion can be obtained by the following relation:

$$X_A = \frac{m_d}{m_d^f}$$

where m_d^f corresponds to the final amount of water once all the anhydrous phase has been converted. The theoretical value of m_d^f calculated from a stoichiometric balance is 5%. Hence, excluding the first part of rapid conversion at the beginning of sorption (which means that the origin is considered to be $t=250$ min.), the reaction rate can be deduced from the derivative $\frac{dm_d}{dt}$ (i.e., the slope of the conversion curve at quasi-steady-state regime).

The apparent rate constant \mathcal{K} can be estimated using the conventional integral method of kinetics data analysis. According to this method, if the hypothesis of a first order kinetic law is relevant, the variation of $[-\ln(1 - X_A)]$ as a function of time, t , must be a straight line passing through the origin whose slope is equal to the constant \mathcal{K} . Figure IV-14 shows that a first order law fits quite well all the data.

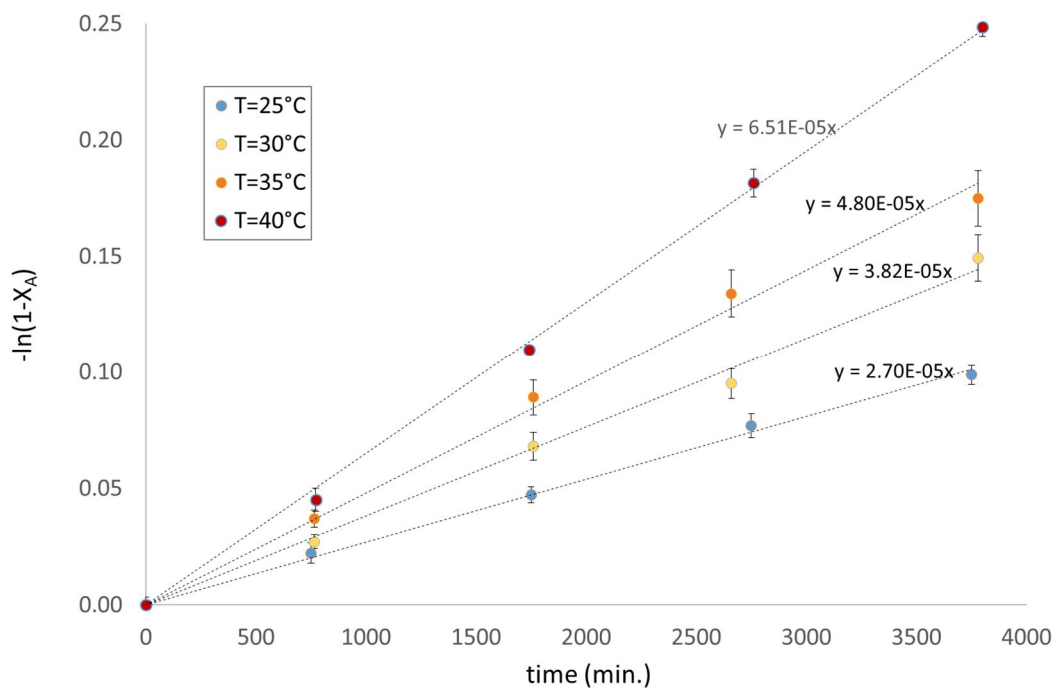


Figure IV-14: Linearization of conversion data according to a first order rate law (RH=80%)

Calculated values of \mathcal{K} are summarized in Table IV-2.

Table IV-2: Calculated values of the apparent rate constant, \mathcal{K}

T (K)	298	303	308	313
\mathcal{K} (min ⁻¹)	2.70×10^{-5}	3.82×10^{-5}	4.80×10^{-5}	6.51×10^{-5}

The pre-exponential factor and the activation energy calculated using an Arrhenius-type relationship for \mathcal{K} (Figure IV-15) were 44504 J.mol⁻¹ and 1736 min.⁻¹, respectively. They can therefore vary according to the size of the particles and operating conditions. A further analysis of the results, based on a phenomenological modelling of the process, is necessary to better elucidate the effect of parameters. However, for the experimental study of caking presented in the following section, this is not an obstacle because the tests were carried out with the same products as those studied so far.

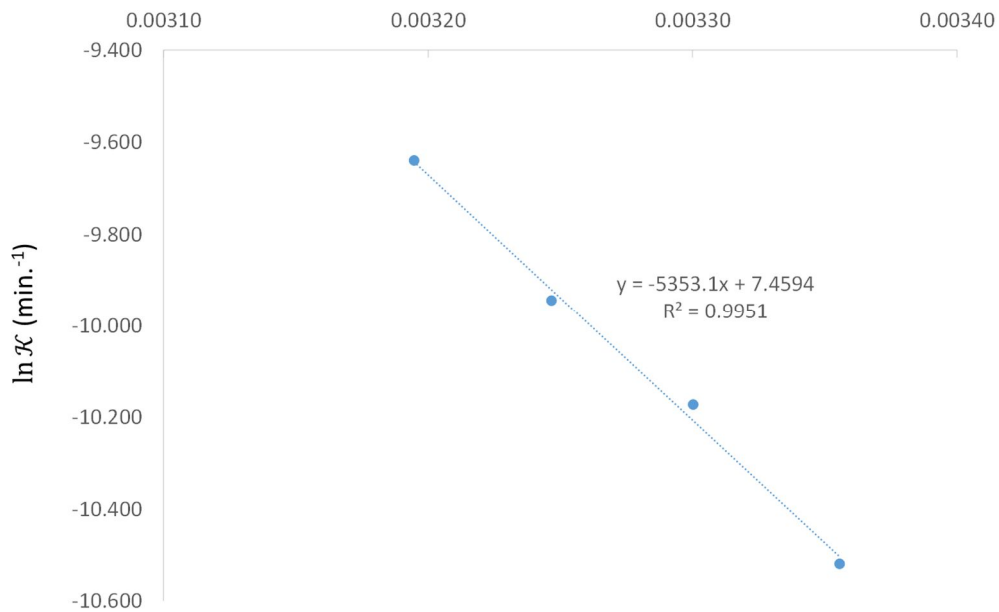


Figure IV-15: Linearization of kinetics data according to Arrhenius law

4 Caking experiments

Two series of experiments were carried out to assess the caking ability of anhydrous lactose powder owing to its crystallization. The caking procedure included the sample preparation, the caking test itself, and the characterization of resulted cakes. First, a preliminary study using a closed-loop air flow caking device was carried out. These experiments allowed to assess the caking tendency of the mixtures and to identify the range of operating conditions to obtain sufficiently resistant cakes and reliable results. In a second time, a parametric and kinetic study of the caking process were carried out.

The caking experiments were conducted using the two principal items of equipment detailed in chapter II, *i.e.* CLAIR and OLAF caking devices. For both instruments, tests were carried out at different RH (70% to 90%), different temperatures (25°C and 35°C), different pressures (10 and 20 kPa) and over different periods of time. The sample preparation protocol was the same for both CLAIR and OLAF devices. Prior to any caking test, the powder samples were placed in a desiccator containing silica gel for at least 48 hours. The samples of lactose powder (18 g) were prepared in single plastic cells (40 mm ID, 23mm height). The cells allow obtaining caked samples, which are demoulded then characterized by uniaxial compression tests using a Shimadzu tensile testing machine (AGS-X). For uniaxial tests, each sample was carefully removed from its cell and were then placed on the base of the device. The compression plate were lowered at a constant rate ($1 \text{ mm}\cdot\text{s}^{-1}$) onto the sample until the sample fractured. After testing, the samples were labelled, photographed and stored in a refrigerator. Both raw and caked samples were analyzed by X-ray diffraction analysis (XRD), DSC analysis and scanning electron microscope imaging. For weakly caking powders the sieving test described in chapter II was used.

4.1 Experimental results and discussion

4.1.1 Preliminary experiments in CLAIR caking Device

A series of preliminary experiments was carried out at 25°C and different RH (from 50% to 90%), different pressures (5 and 15 kPa) and different durations (24, 48, 72 and 96h). The experiments were carried out using the CLAIR device. The objective of this study was:

- qualitative assessment of the caking behavior of the samples

- quantitative measurement of the mechanical strength of samples when caking occurred.

The qualitative observations allowed distinguishing four categories of behavior with respect to caking:

- Cat I. Not caked/very soft cake, disintegrated to powder or small crumbles when demolded
- Cat II. Very soft cake, disintegrated and crumbled when handled
- Cat III. Soft cake, splitting into large pieces when handled. Each piece remained intact but uniaxial compression test could not be applied
- Cat IV. Hard, well-defined cake, remaining in one piece when handled so that uniaxial compression test could be carried out.

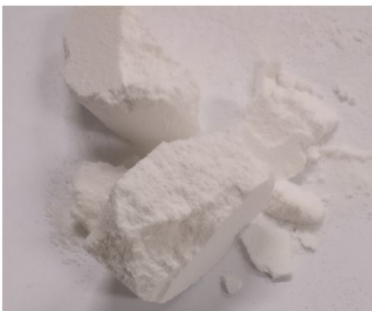
Representative examples of cakes belonging to each category are illustrated in [Figure IV-16](#).



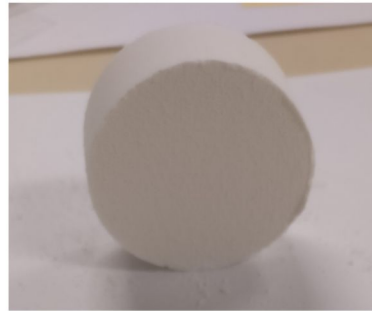
Cat. I: Not caked/very soft cake disintegrated to powder or small brittle crumbles when demolded



Cat. II: very soft cake disintegrated and crumbled when handled



Cat. III: Soft cake, splitting into large pieces when handled. Uniaxial compression test could not be applied



Cat. IV: Hard, well-defined cake, remaining in one piece when handled- uniaxial compression test could be carried out

Figure IV-16: Representative examples of different categories of cake obtained at different operating conditions

Only the mechanical properties of the last two categories could be characterized. The yield stress properties of the samples of the fourth categories was assessed by uni-axial strength test whereas for the third category sieving (rotating pan) test was used.

For the preliminary study, 48 tests were conducted in triplicate (*i.e.* 144 samples and 48 conditions tested). No sample caked at a relative humidity of less than 50% regardless of pressure and duration. At 50% relative humidity in a 24 hour test, very soft cakes (cat. II) were produced for all samples (5kPa and 15kPa). At 60% relative humidity and after 24 hours, some partial caking was observed but once again, the resulting cakes were soft and broke apart when handled (cat. II). Even for samples stored for 24 hours at 70% relative humidity, the samples were not sufficiently caked for uniaxial compression test (cat. III). Hard cakes were formed in samples stored for 24 hours when the relative humidity was increased to 80%. In all three samples stored in these conditions, the resulting cakes were hard enough to be handled without any breakage. This enabled uniaxial compression testing to be carried out using the Shimadzu device, where the maximum value of yield stress was 1.1 kPa. Samples were also tested at a relative humidity of 85%. The resulting cakes exhibited similar visible characteristics to the samples caked at 80% relative humidity. The maximum measured radial resistance was 11.0 kPa.

Figure IV-17 gives a qualitative presentation of the preliminary results indicating the category of caking encountered at each condition. Note that no significant effect of pressure on the caking category was observed. These results show that the most influential parameters were the relative humidity and the duration of the experiment. On the other hand, the pressure has little (not to say none) influence on the caking ability of the samples. This is probably due to the undeformable and fairly rigid nature of anhydrous lactose particles.

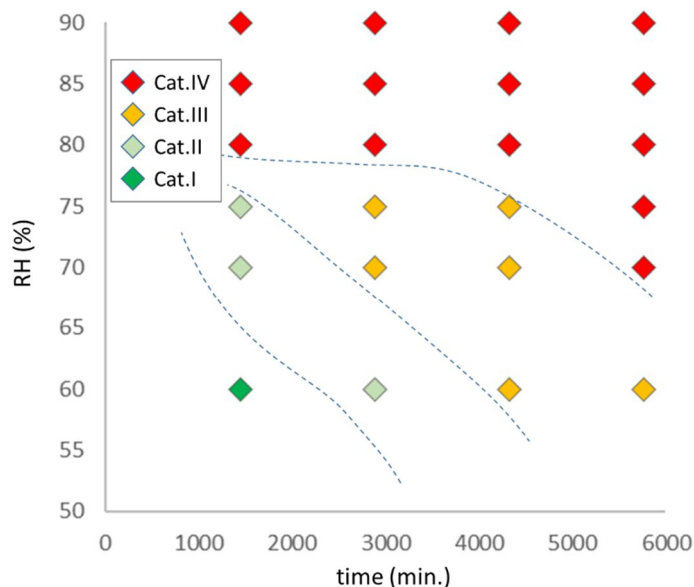


Figure IV-17: Qualitative presentation of caking categories encountered during preliminary experiments at P=5 and 15kPa

4.1.2 Kinetic study of caking

4.1.2.1 Hard caking

A series of experiments was conducted using OLAF caking device and under operating conditions for which hard caking was observed during the preliminary experiments. Taking into account the significant role of the RH and the caking duration, pointed out during the preliminary study, a kinetic study of caking was undertaken at different RH. Several series of tests were carried out by varying relative humidity and test duration. All tests were performed at two different temperatures, namely 25°C and 35 °C. Given the insignificant role of the pressure, all tests were performed at a constant pressure of 15kPa. Furthermore, a series of tests carried out at three different air flowrates (5, 10 and 15 NL.min⁻¹) revealed no significant effect of this parameter, which is not surprising taking into account that the rate limiting step of process is the crystallization reaction and not external mass transfer. Hence, the air flowrate was set to 15 NL.min⁻¹ (*i.e.* the most favorable conditions for caking). All experiments were conducted in triplicate.

Figure IV-18 shows the time evolution of the yield strength of category IV cakes obtained at different RH and T conditions. It can be seen that after a first period of increase, the yield strength becomes constant and undergoes no further significant variation over time. Furthermore, the threshold value seems to be temperature independent. Indeed, increasing

the temperature has two main effects. First, it accelerates the caking rate and shortens the time after which the threshold value is achieved. In addition, this allows caking at a lower relative humidity for which no category IV cake was obtained at the lower temperature limit.

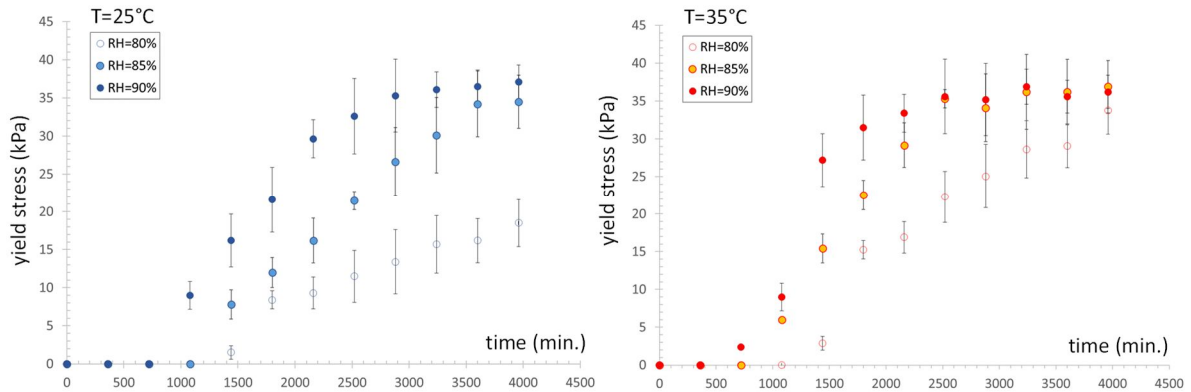


Figure IV-18: Time evolution of yield stress of caked samples

Differential scanning calorimetry was used to provide a more quantitative assessment of the compositions of both the raw material and the caked samples. The DSC curves for raw anhydrous lactose and a selection of caked samples obtained at 25°C after 24 hours of humidification at different RH are shown in Figure IV-19.

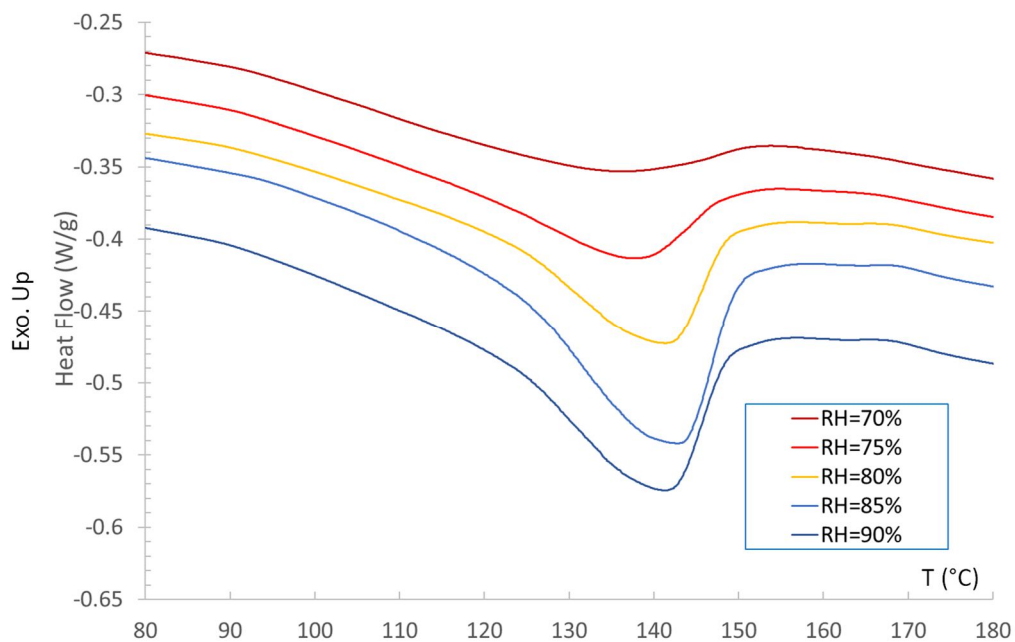


Figure IV-19: DSC thermograms of hydrated samples of Anhydrous Lactose (DuraLac® H) (t=24h, p=15 kPa)

The DSC curves show a progressive increase of the characteristic endothermic peak (between 100°C and 150°C) relative to dehydration of water from the lactose monohydrate. The amount of lactose monohydrate present in samples was calculated by comparing the dehydration enthalpies measured in DSC analysis with the dehydration enthalpy for pure lactose monohydrate. The corresponding values of the amount of monohydrate lactose deduced from DSC data are gathered in Table IV-3. It is worth mentioning that calculated amount of monohydrate lactose obtained by this technique is in very good agreement with the results obtained by DVS measurements (Figure IV-11, right). This result confirms that a partial phase transition from anhydrous lactose to lactose monohydrate occurs during. The DSC curves for cakes stored in higher relative humidity exhibited larger dehydration endotherms that implies that more conversion to lactose monohydrate occurred under these conditions. This indicated that the driving force of crystallization is indeed the relative humidity. As we will see later, it was also found that the strongest cakes were formed under conditions of high humidity so this finding confirms that the formation of lactose monohydrate is the main caking mechanism.

Table IV-3. Calculated amount (mass fraction) of monohydrate Lactose obtained after 24h humidification under 15kPa normal stress and at different RH

RH %	70%	75%	80%	85%	90%
Monohydrate content	0.036	0.056	0.076	0.109	0.120

Figure IV-20 presents the results of the yield strength versus the fractional conversion of anhydrous lactose. Two essential information can be drawn from these results. First, category IV caking appears when a minimum conversion rate of 8% is reached. In addition, whatever the operating conditions, the maximum cake resistance is reached for a conversion of the order of 15-17%. No further intensification of the caking beyond this conversion is noticed. These results can be explained by the fact that caking arises from the creation of solid bridges due to crystallization at the surface and contact points between particles. This transformation happens at first stages of the process. Thus, further progression of the crystallization within the grains does not affect the mechanical strength of the cakes.

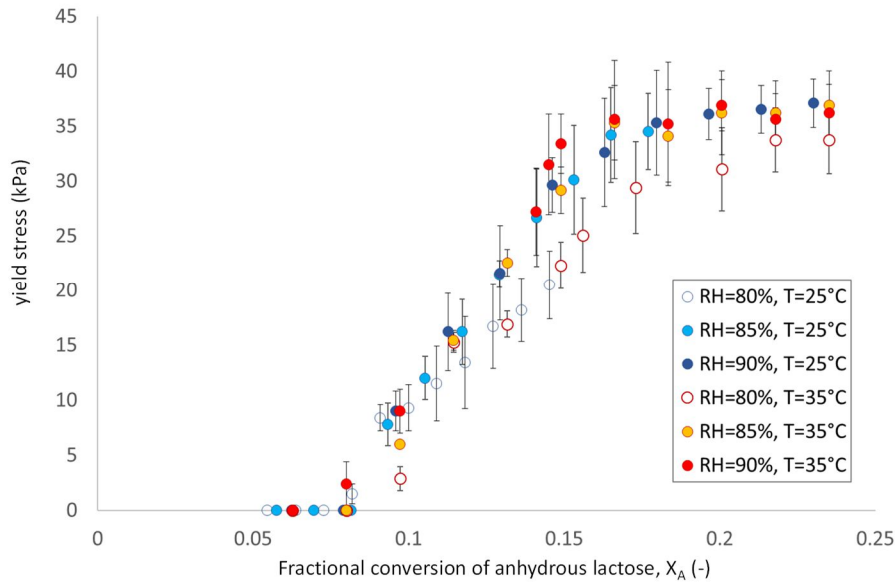


Figure IV-20: Evolution of yield stress as a function of fractional conversion of anhydrous lactose

4.1.2.2 Soft caking

Cakes belonging to category III were produced at lower RH (60%, 70% and 75%) compared to the previous series of experiments. The air flowrate and the normal stress were the same as previously, namely $15 \text{ NL}\cdot\text{min}^{-1}$ and 15 kPa. All cakes were characterized using the rotary sieve test. A typical example of results obtained for a series of experiments conducted during different times at $T=25^\circ\text{C}$ and $\text{RH}=70\%$ are presented in Figure IV-21-(a). All curves show a progression of the cumulative mass having passed through the rotating sieve that follows a deceleration exponential function characterized with an apparent kinetic constant of k , tending to an asymptotic value equal to the initial mass of the sample:

$$M = M_0(1 - e^{-kt}) \quad \text{or} \quad t = -\frac{1}{k} \ln\left(1 - \frac{M}{M_0}\right)$$

The solid lines in Figure IV-21-(b) represent the corresponding evolution according to a deceleration exponential function allowing the best fit between the experimental results and the model found by linearization of the previous equation (*i.e.*, the inverse of the slope of the line $-\ln\left(1 - \frac{M}{M_0}\right)$ versus t).

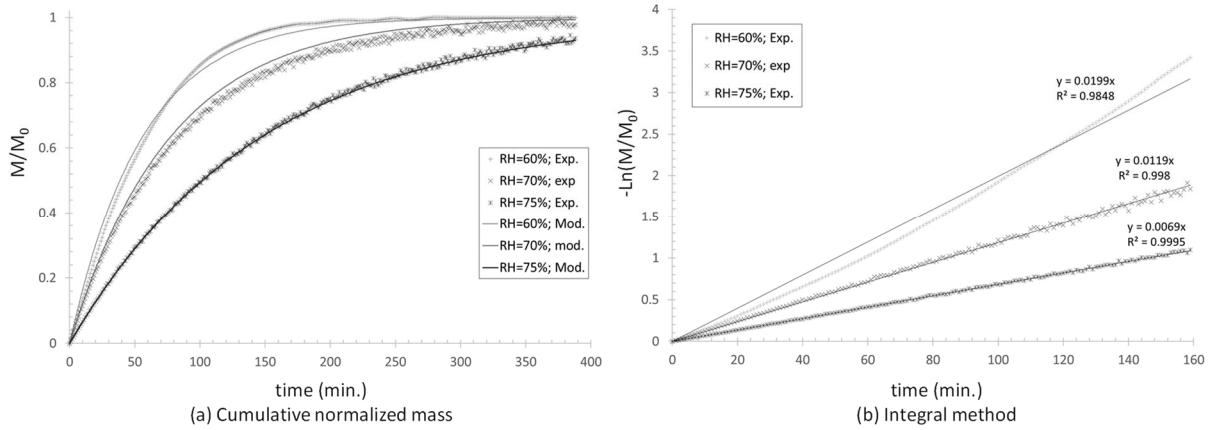


Figure IV-21: Results of sieving test for weak cakes obtained at 60%, 70% and 75% after 66h humidification (P=15 kPa)

Figure IV-22 shows the variation of the characteristic time of attrition, defined as $(1/k)$, obtained for all weakly caked samples as a function of the fractional conversion of anhydrous lactose. As can be seen, this category of caking appears from almost 4% conversion. Despite a more scattering of results with respect to yield strength tests, a global trend can be distinguished showing a progressive increase (decrease) of the characteristic time (attrition rate) constant with the fractional conversion of anhydrous lactose.

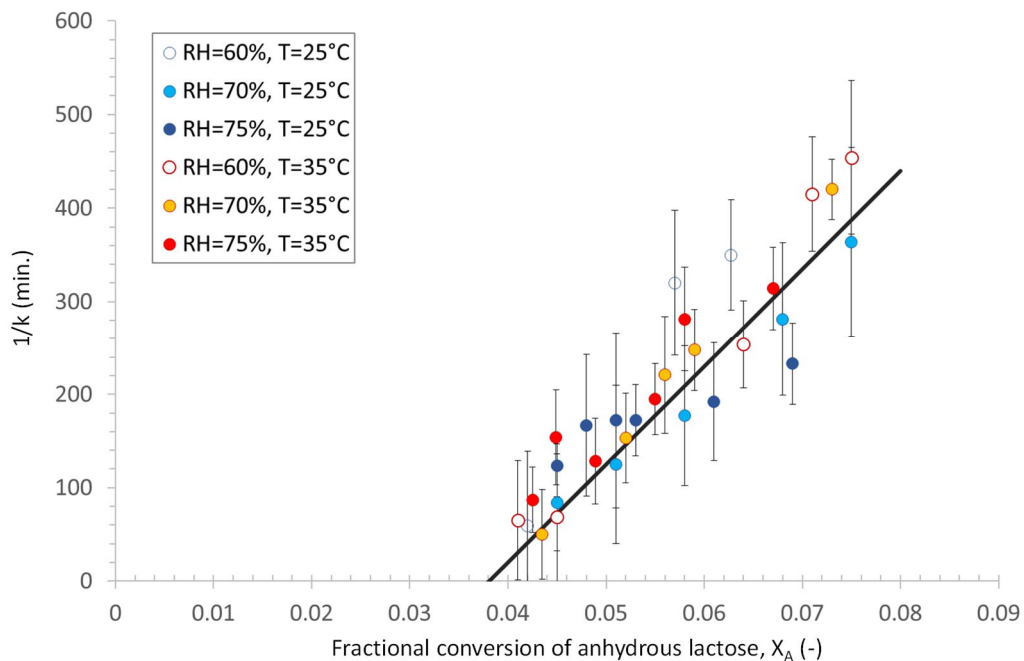


Figure IV-22: Characteristic times of attrition as a function of fractional conversion

5 Conclusion

In this work we presented a parametric and kinetics study of solid-state crystallization of anhydrous lactose in relation with its caking ability. The results showed that at under humid conditions, anhydrous lactose crystallizes to its monohydrate polymorph. The limiting step of crystallization process was the chemical reaction. The most influential parameters were found to be the temperature and the relative humidity whereas the size of particles did not affect the kinetics of transformation. The crystallization rate was of first order with respect to the free water concentration. Furthermore, the rate constants at different temperatures were calculated allowing the estimation of the activation energy of reaction.

Then, a parametric study of caking behavior of anhydrous lactose powder was carried out. The results showed that crystallization does indeed lead to the caking of anhydrous lactose powders. Four major categories of caking were distinguished, namely, non-caking, very soft caking, soft caking and hard caking. The key parameter regarding the extent of caking was found to be the fractional conversion of anhydrous lactose. Hard cakes were obtained at fractional conversion higher than almost 8%. Their yield strength increased steadily until it reached a conversion of about 15-17%, then stagnated beyond that limit. As for soft cakes, they appear from around 4% conversion.

It should be noted that the results obtained during the caking study are in perfect adequacy with the kinetic study carried out using DVS experiments. Indeed, the conversion rates calculated from DSC analysis on caked samples correspond quite well to conversion rates obtained by DVS analysis. Furthermore, the IIIth and IVth categories of caking could be conveniently superimposed on hydration and conversion kinetics such as that presented in [Figure IV-11](#). This is very important information because it shows that the kinetic laws deduced for the crystallization of anhydrous lactose can be used to predict its caking ability under conditions other than those experimentally tested in the present work. Taking into account the importance of such a kinetic law, future works will focus on further analysis of the results based on phenomenological modelling of the process.

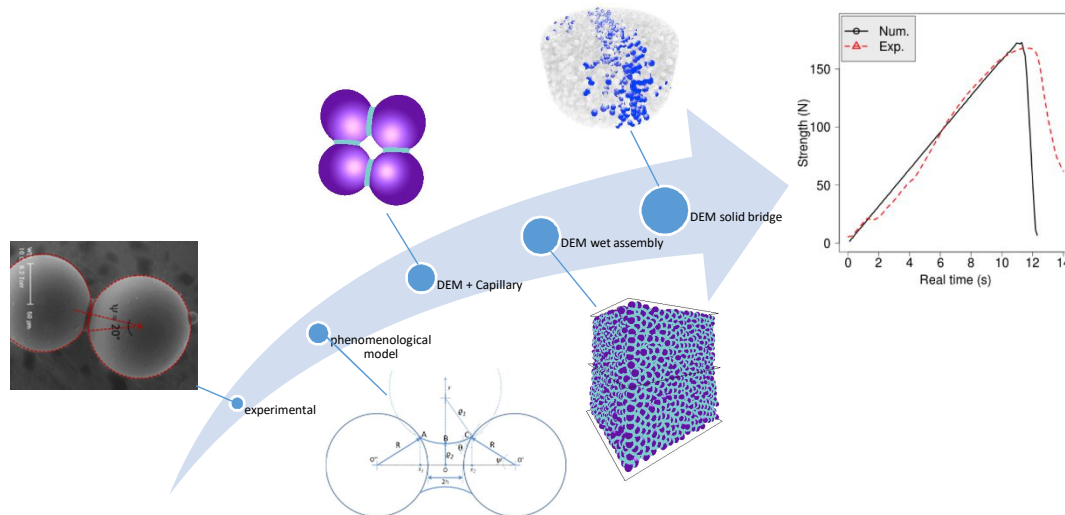
References

1. Carpin, M., H. Bertelsen, J.K. Bech, R. Jeantet, J. Risbo and P. Schuck, *Caking of lactose: A critical review*. Trends in Food Science & Technology, 2016. **53**: p. 1-12.
2. Langrish, T.A.G., *Assessing the rate of solid-phase crystallization for lactose: The effect of the difference between material and glass-transition temperatures*. Food Research International, 2008. **41**(6): p. 630-636.
3. Roos, Y.H., *Solid and Liquid States of Lactose*, in *Advanced Dairy Chemistry: Volume 3: Lactose, Water, Salts and Minor Constituents*, P. McSweeney and P.F. Fox, Editors. 2009, Springer New York: New York, NY. p. 17-33.
4. Roos, Y.H. and S. Drusch, *Phase Transitions in Foods.*, ed. S. Edition. 2016.
5. <http://www.drug-dev.com/Main/Back-Issues/Lactose-in-Pharmaceutical-Applications-466.aspx>.
6. Salameh, A.K., L.J. Mauer and L.S. Taylor, *Deliquescence Lowering in Food Ingredient Mixtures*. Journal of Food Science, 2006. **71**(1): p. E10-E16.
7. Brittain, H.G. and R.L. Blaine. *α -Monohydrate Phase in Lactose by DSC. TA Instruments*. [online]. [viewed 3rd June 2017]. Available at: <http://www.tainstruments.com/pdf/literature/TA293.pdf>. 2016.
8. Samain, S., *Caractérisation multi-échelle de l'efflorescence et du mottage du saccharose*, in *Génie des Procédés Industriels*. 2018, Université de Technologie de Compiègne: Compiègne, France.
9. Dupas-Langlet, M., M. Benali, I. Pezron, K. Saleh and L. Metlas-Komunjer, *The impact of deliquescence lowering on the caking of powder mixtures*. Powder Technology, 2015. **270**, Part B: p. 502-509.
10. Afrassiabian, Z., M. Leturia, M. Benali, M. Guessasma and K. Saleh, *An overview of the role of capillary condensation in wet caking of powders*. Chemical Engineering Research and Design, 2016. **110**: p. 245-254.
11. Baghel, S., H. Cathcart, W. Redington and N.J. O'Reilly, *An investigation into the crystallization tendency/kinetics of amorphous active pharmaceutical ingredients: A case study with dipyrindamole and cinnarizine*. European Journal of Pharmaceutics and Biopharmaceutics, 2016. **104**: p. 59-71.
12. Burnett, D.J., F. Thielmann, T. Sokoloski and J. Brum, *Investigating the moisture-induced crystallization kinetics of spray-dried lactose*. International Journal of Pharmaceutics, 2006. **313**(1): p. 23-28.
13. Clark, Z., A.H.J. Paterson, R. Joe and J.S. McLeod, *Amorphous lactose crystallization kinetics*. International Dairy Journal, 2016. **56**: p. 22-28.
14. Fan, F. and Y.H. Roos, *Structural strength and crystallization of amorphous lactose in food model solids at various water activities*. Innovative Food Science & Emerging Technologies, 2017. **40**: p. 27-34.
15. Haque, M.K. and Y.H. Roos, *Crystallization and X-ray diffraction of spray-dried and freeze-dried amorphous lactose*. Carbohydrate Research, 2005. **340**(2): p. 293-301.
16. Ibach, A. and M. Kind, *Crystallization kinetics of amorphous lactose, whey-permeate and whey powders*. Carbohydrate Research, 2007. **342**(10): p. 1357-1365.
17. Listiohadi, Y., J.A. Hourigan, R.W. Sleigh and R.J. Steele, *Properties of lactose and its caking behavior*. Australian Journal of Dairy Technology, 2005. **60**: p. 33-52.
18. Miao, S. and Y.H. Roos, *Crystallization Kinetics and X-ray Diffraction of Crystals Formed in Amorphous Lactose, Trehalose, and Lactose/Trehalose Mixtures*. Journal of Food Science, 2005. **70**(5): p. E350-E358.
19. S-T, C. and H. A, *Numerical solution of diffusion equations*. Transactions of the ASAE, 1968. **11**(5): p. 705-708.

20. Mourad, M., M. Hemati and C. Laguerie, *Séchage intermittent de maïs en lit fluidisé à flottation : étude expérimentale et modélisation*. International Journal of Heat and Mass Transfer, 1997. **40**(5): p. 1109-1119.
21. Mourad, M., M. Hemati and C. Laguérie, *Séchage de maïs en lit fluidisé à flottation. I: étude expérimentale de la cinétique de séchage*. The Chemical Engineering Journal and the Biochemical Engineering Journal, 1995. **59**(3): p. 221-228.
22. Mourad, M., M. Hémati and C. Laguérie, *Séchage de maïs en lit fluidisé à flottation II: modélisation de la cinétique de séchage*. The Chemical Engineering Journal and the Biochemical Engineering Journal, 1995. **60**(1): p. 39-47.

Chapter V:

Phenomenological modelling and Numerical simulation of mechanical resistance of caked powders



This chapter presents the results of a study on modelling and numerical simulation of mechanical resistance of caked samples. The numerical simulations were carried out based on Discrete Element Method (DEM). The overall objective of the study was to simulate the behavior of the caked samples subjected to a mechanical, compressive or tractive, stress.

First, simulations were performed on an assembly of particles subjected to capillary forces. Indeed, the capillary forces being amenable to a theoretical description, the tensile strength of wet cakes can be calculated theoretically and be used as a reference to validate the numerical simulation results. Thus, the simulation results were validated by comparing them with those obtained by Rumpf's model for a wet cake subjected to a tensile stress. Once validated, numerical simulations were used to study the mechanical behavior of wet or dry cakes subjected to compression. The stress-strain curves were then simulated and compared to the experimental results. The results showed a good qualitative agreement between simulation and experimental data.

1 Introduction

Modelling of dispersed media in order to link microscopic phenomena occurring at the particle scale to their overall macroscopic behavior remains still a major challenge in powder science and technology. In the case of caking, for example, given the complexity of phenomena occurring simultaneously at particle's scale (*i.e.*, adsorption, absorption, capillary condensation, crystallization, diffusion, desorption, liquid or solid bridging, etc.) on the one hand, and the heterogeneity of the system (shape, size, composition, etc.), on the other hand, a detailed description of the media, even on a small scale, remains almost inaccessible. To this must be added the problem of the excessive number of particles present in real systems, which makes a complete description of the system almost impossible until now.

The main modelling methods in this field can be classified into four major categories:

- Methods based on a continuum approach of granular media. The models belonging to this category consider the granular medium as a continuous, solid or pseudo-fluid, medium and describe the overall behavior of the system using macroscopic laws (plasticity, pseudo-viscosity, yield loci, etc.) without taking account of the heterogeneity and the local distribution of physical phenomena. Among these methods, those considering the granular medium as a deformable solid phase are based on solids mechanics, and more specifically on mechanics of soils. On the other hand, fluid-like methods have been reported also, based on fluid mechanics and resolution of Navier-Stokes equations, which necessitates the use of adequate (usually artificial) rheological laws. These methods have the advantage of treating the system as a whole. From the computational point of view, they are not time consuming. On the other hand, they do not give information at interparticle scale and then even less at intraparticle scale.
- Stochastic methods that are based on statistical and probabilistic description of particles populations. These methods consider that the variables (properties) of the system evolve randomly within a specified range with certain probabilities. Generally, the particles population and/or their related properties are ranked in "classes" (*i.e.* size, conversion, residence time, etc.) and the evolution of classes are traced with time. The global behavior of the system is obtained by integration.

Among the methods of this category are Population Balance Equations (PBE), Monte-Carlo simulation and Markov chains.

- Hybrid methods combining phenomenological, mechanistic and statistic approaches. Among these methods, we can mention for example, the so-called “grain-bulk” approach, which is adequate when the particles can be assumed as independent bodies evolving individually with time. The overall properties of the system can then be calculated by integration of contributions of individual particles. These methods constitute a good promise between the complexity of model’s equation to be solved, the computational time and have the advantage of leading sometimes to analytical solutions.
- Methods based on a discrete description of granular media. These methods take into account the evolution of discrete bodies using the Lagrangian approach. Every particle in the system is tracked and all particle contacts and interactions are taken into account. As a result, DEM generally provides more accurate results and local information compared to continuum approach. In return, the calculation requirements are also exorbitant and prevents the entire system from being processed. It is generally usual to treat only a Representative Elemental Volume (REV), *i.e.* the minimum number of particles whose overall behavior is assumed to be representative of that of the entire system. The advent of powerful numerical tools in recent years has strongly contributed to the characterization of the mechanical behavior of powders under mechanical stresses close to those applied in real experimental conditions.

In the present work, two models belonging to each of the last two categories have been developed to describe the mechanical resistance of cakes. The first model, based on the “grain-bulk” approach, was established to study the tensile strength of wet cakes. The focus was on two physical phenomena, (*i.e.* capillary condensation and capillary forces) that are described by the two fundamental relationships of surface chemistry (*i.e.* Kelvin and Laplace equations, respectively). The basic idea of the model consists in calculating the quantity and the geometry of the capillary bridges that can appear between two (separated or touching)

particles, of known shape, size and wettability exposed to ambient humidity. Indeed, if the geometry of the capillary bridges is fixed, it is possible to calculate (§2):

- on the one hand, the activity of the water to which the bridges are formed according to Kelvin's law
- on the other hand, the capillary (attractive) forces using Laplace's law.

The integration of binary interactions within a particle assembly, using the Rumpf's model, allows then calculating the tensile strength of the wet cake. This calculation is based on a random distribution of both particles and liquid bridges.

In the second time, Discrete Element Method (DEM) was used for numerical simulation of the mechanical strength of caked samples. Firstly, the simulations were carried out on the tensile strength of wet cakes due to the presence of liquid bridges. The results for tensile strength of wet cakes calculated the first model were used as a reference case to validate the consistency of simulation results. After validation, DEM simulations were used to describe the yield strength of cakes resulting from different attractive forces (liquid bridge, solid bridge, etc.).

The purpose of simulations is twofold:

- on the one hand, to provide a better understanding and interpretation of the experimental results taking into account the phenomena related to the heterogeneity of the medium as well as to have a reliable numerical tool for the prediction of the behavior of cakes in the conditions other than those experimentally tested.
- on the other hand, to use the results of the simulation to optimize the experimental methods of the characterization of cakes by recommending improvements on the geometry of the samples, their quantity, the mode of stress (compression, traction, shear), etc.

2 "Grain-bulk" model of capillary condensation within a granular medium

In granular media, liquid water appears as a consequence of water vapor condensation or liquid water migration to the surface of particles. Besides the particles themselves, the main

source of humidity is the surrounding atmosphere. Indeed, the water vapor from the surrounding air could be fixed on the surface of particles by adsorption (or absorption) due to intermolecular interactions. The amount of adsorbed water in equilibrium with the relative humidity of air at a given temperature is given by the sorption isotherm, which gives the water content of solids as a function of the water activity, a_w (*i.e.* Relative Humidity at equilibrium).

At low water activities (*i.e.* early stages of adsorption - typically between 5%-35%) the solids surface is covered by a few layers of water molecules. This zone is characterized by a linear and slight increase in water sorption isotherm and can be modeled by classical multilayer adsorption models (*e.g.* BET or GAB models). In fact, the amount of adsorbed water in this zone is low but even this small amount could affect the van der Waals forces because of strong interactions between water molecules. However, this effect remains much less significant than that of surface tension forces due to the appearance of liquid bridges subsequent to capillary condensation.

At higher water activities, water molecules become mobile enough to form liquid bridges [1, 2]. Further, a capillary condensation phenomenon occurs leading to the filling of small gaps at the contact points between particles. In this zone, all spaces that could be assimilated to meso-pores (mean pore size between 2 and 50 nm) are filled. Indeed, in those confined spaces, when the thickness of the adsorbed layer reaches a few nanometers (*i.e.* ≈ 3 nm) [1, 2] the adsorbed molecules become mobile and form a liquid-like meniscus. Kelvin model is usually used to describe the capillary condensation phenomenon occurring at high a_w . In the case of wetting systems (contact angles less than 90°), the liquid interface is concave. It is well established that for such a curved fluid/fluid interface, a difference of pressure exists between the two phases. In the general case of an interface with two given principal radii, ρ_1 and ρ_2 , the mean radius of curvature (called also capillary radius, r_c) is defined by:

$$\frac{1}{r_c} = \frac{1}{2} \left(\frac{1}{\rho_1} + \frac{1}{\rho_2} \right) \quad (V-1)$$

and the condition of mechanical equilibrium at the interface is given by the Kelvin equation:

$$\ln a_w = \frac{-2 V_l \cdot \gamma}{r_c \cdot \mathcal{R} \cdot T} \quad (V-2)$$

where γ is the vapor-liquid surface tension, \mathcal{R} the universal gas constant, T the temperature, and V_l the molar volume of liquid. Note that by convention, the radius of curvature is taken as positive on the concave side and as negative on the convex side. Eq. (V-2) indicates that in case of a positive capillary radius, the activity of water is less than unity, which means that at a given temperature, water molecules will condense at a partial pressure less than their normal saturated vapor pressure.

Hence, provided that the geometry of liquid bonds is known, the two principal radii of curvature, ϱ_1 and ϱ_2 , can be determined. Then, using the Kelvin equation, it is possible to calculate both the equivalent capillary radius, r_c , (Eq. V-1) and the volume of the liquid bridge for a given water activity, a_w (Eq. V-2).

2.1 Binary contact

Let us consider the case of two equal-sized spherical particles distant of $2h$ joined by a liquid bridge (Figure V-1). This configuration corresponds to a specific case ($R_1=R_2$) of the general configuration described by Tselishchev and Val'tsifer [3].

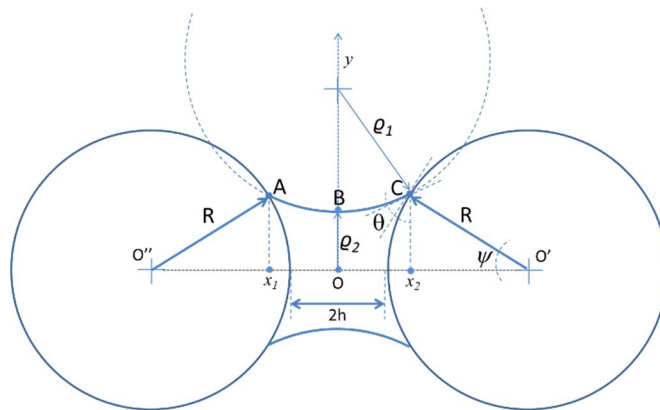


Figure V-1: Schematic representation of a pendular liquid bridge between two equal-sized particles

Assuming a circular liquid profile, the first principal radius of curvature is obtained by the following equation [3, 4]:

$$\varrho_1 = -\frac{R(1 - \cos \psi) + h}{\cos(\psi + \theta)} \quad (\text{V-3})$$

where ψ is the filling angle and θ is the average liquid-solid contact angle as shown in Figure V-2.

As for the second principal radius of curvature, according to the same references, we have:

$$\varrho_2 = R \sin \psi - \varrho_1 [1 - \sin(\psi + \theta)] \quad (\text{V-4})$$

The algebraic equation of the arc \widehat{ABC} formed by the upper interface of the liquid bridge is then:

$$y = \varrho_1 + \varrho_2 - \sqrt{\varrho_1^2 - x^2} \quad (\text{V-5})$$

and the volume of liquid is given by [3, 4]:

$$V_L = \int_{x_1}^{x_2} \pi y^2 dx - V_s \quad (\text{V-6})$$

where V_s is the volume of wetted segments of the two spheres given by [4]:

$$V_s = \frac{2\pi R^3}{3} (2 - 3 \cos \psi - \cos^3 \psi) \quad (\text{V-7})$$

Integrating Eq. (V-6) between $x_1 = -\varrho_1 \cdot \cos(\psi + \theta)$ and $x_2 = \varrho_1 \cdot \cos(\psi + \theta)$ leads to the following expression for the dimensionless volume of liquid (*i.e.*, volume of liquid per unit volume of solid):

$$\begin{aligned} V^* = \frac{3V_L}{4\pi R^3} = \frac{3}{4R^3} \left\{ -\frac{2}{3} \varrho_1^3 \cos^3(\psi + \theta) + 2\varrho_1^3 \cos(\psi + \theta) - R\varrho_1^2(\pi - 2(\psi + \theta)) \sin \psi \right. \\ \left. - \varrho_1^3(\pi - 2(\psi + \theta)) \sin(\psi + \theta) + 2R\varrho_1^2 \sin \psi \sin(\psi + \theta) \cos(\psi + \theta) \right. \\ \left. + 2 \sin^2 \psi R^2 \varrho_1 \cos(\psi + \theta) - \frac{2}{3} R^3 (2 - 3 \cos \psi + \cos^3 \psi) \right\} \quad (\text{V-8}) \end{aligned}$$

The set of equations (V-1 to V4 and V-8) allows the determination of the liquid uptake between two particles for different water activities at a given temperature.

Furthermore, according to Laplace theory for capillary forces, the total attractive force between the two particles including both the capillary and the surface tension components is given by [5]:

$$F = 4\pi R\gamma \sin(\psi) \left[\sin(\psi + \theta) + \frac{R}{2} \sin \psi \left(\frac{1}{\rho_1} + \frac{1}{\rho_2} \right) \right] \quad (\text{V-9})$$

Knowing the force of individual binary bonds, it is possible to estimate the agglomerate strength. However, this requires the knowledge of real stresses acting on each particle. Because this information is not generally available, this characteristic is usually represented by the tensile strength of agglomerates, *i.e.*, the tensile force at failure divided by the cross-section of the failure plane of the agglomerate.

The relationship between the amount of liquid and the resulting tensile strength of agglomerates or cakes have long been studied and are now well established (*e.g.*, [6-8]). For a bed of particles, the total tensile strength of the packing is a function of the liquid saturation, S , (*i.e.* the fraction of interstitial void occupied by the liquid). According to the degree of saturation, three states of moist cakes are distinguished namely: pendular, funicular and capillary states. In pendular state ($S < 0.25-0.3$), for which binary bridges are still discernible, it is generally admitted that each bond contributes individually to the overall strength [5]. Consequently, the tensile strength in pendular state is equal to the sum of individual bonding forces within the cross-sectional area of the failure plane. According to Rumpf's model [5], for a random packing of monosized spherical particles and an even distribution of liquid, the tensile strength is given by the average number of bonds per unit area, n_b , multiplied by the mean adhesive force of a single binary bond, F (Eq. V-9):

$$\sigma_T = n_b \cdot F \quad (\text{V-10-a})$$

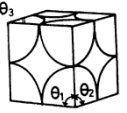
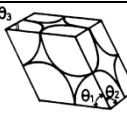
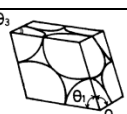
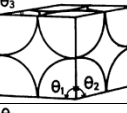
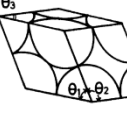
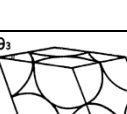
Furthermore, based on statistical considerations, Rumpf established the following expression for the average number of bonds per cross-sectional unit area:

$$n_b = \frac{1 - \varepsilon k}{\pi d_p^2} \quad (\text{V-10-b})$$

where ε is the mean void fraction of the bed and k is the characteristic coordination number of the packing (*i.e.* the average number of contacts a given particle has with its neighbors).

Factually, both tensile strength and liquid saturation degree depend on the arrangement of particles and, in particular, on the coordination number. For some well-established arrangements of particles, the coordination number can be obtained theoretically. [Table V-1](#), summarizes the specific cases [9] that are dealt with in the following sections.

Table V-1: Regular packing of equal-sized spheres and their properties (Shinohara K., 1997 [9])

Primary Layer	Arrangement	Structure/Geometry	Porosity, ε	Coordination number, k
Square	1) cubic	 $\theta_1 = 90^\circ$ $\theta_2 = 90^\circ$ $\theta_3 = 90^\circ$	0.4764	6
	2) orthorhombic	 $\theta_1 = 60^\circ$ $\theta_2 = 90^\circ$ $\theta_3 = 90^\circ$	0.3954	8
	3) rhombohedral	 $\theta_1 = 60^\circ$ $\theta_2 = 60^\circ$ $\theta_3 = 90^\circ$	0.2594	12
Simple rhombic	4) orthorhombic	 $\theta_1 = 90^\circ$ $\theta_2 = 90^\circ$ $\theta_3 = 60^\circ$	0.3954	8
	5) tetragonal-sphenoidal	 $\theta_1 = 60^\circ$ $\theta_2 = 104.29^\circ$ $\theta_3 = 60^\circ$	0.3019	10
	6) rhombohedral	 $\theta_1 = 60^\circ$ $\theta_2 = 90^\circ$ $\theta_3 = 60^\circ$	0.2595	12

Furthermore, for randomly packed beds of particles, several correlations have been proposed in literature relating the coordination number to the average bed porosity [10, 11]. Note that for usual porosities ($0.25 < \varepsilon < 0.65$), the difference between these correlations does not exceed $\pm 10\%$ and the relationship proposed by [Meissner et al.](#) [10] could be used as a suitable average:

$$k = 2 \exp[2.4(1 - \varepsilon)] \quad (\text{for } 0.26 < \varepsilon < 1) \quad (\text{V-11})$$

Knowing the coordination number of the packing, the saturation degree of the bed could be calculated:

$$S = \frac{3kV_L}{(6 - \pi)d_p^3} \quad (\text{V-12})$$

2.2 Influencing parameters

This section aims to point out the effect of key parameters on appearance of the capillary condensation with humidity using the aforementioned relationships, consolidated by some experimental observations.

The resolution of the set of equations (V-1 to V-4; and V-8 to V-12) allows determining the saturation degree and the tensile strength of agglomerates. The procedure is straightforward and needs no special numerical method. Note that for some cases, it is suitable to make use of the following dimensionless parameters:

- dimensionless interparticle gap, $h^* = \frac{h}{R}$
- dimensionless radius of curvature, $\varrho_i^* = \frac{\varrho_i}{R} \quad (i=1;2)$
- dimensionless capillary radius, $\frac{2}{r_c^*} = \frac{1}{\varrho_1^*} + \frac{1}{\varrho_2^*}$
- dimensionless volume of liquid, $V^* = \frac{3V_L}{4\pi R^3}$
- dimensionless interparticle force, $F^* = \frac{F}{4\pi\gamma R}$

2.2.1 Binary agglomerate

Before dealing with the behavior of an assembly of particles, it is useful to emphasize some characteristics of a binary agglomerate subjected to humidification and capillary condensation. As far as capillary condensation is concerned, note that this phenomenon appears between two limiting values of the filling angle, ψ . In order to illustrate this purpose, [Figure V-2](#) shows the variation of the first and the second principal radii of curvature as a function of the filling angle for a perfectly wetting system ($\theta = 0$).

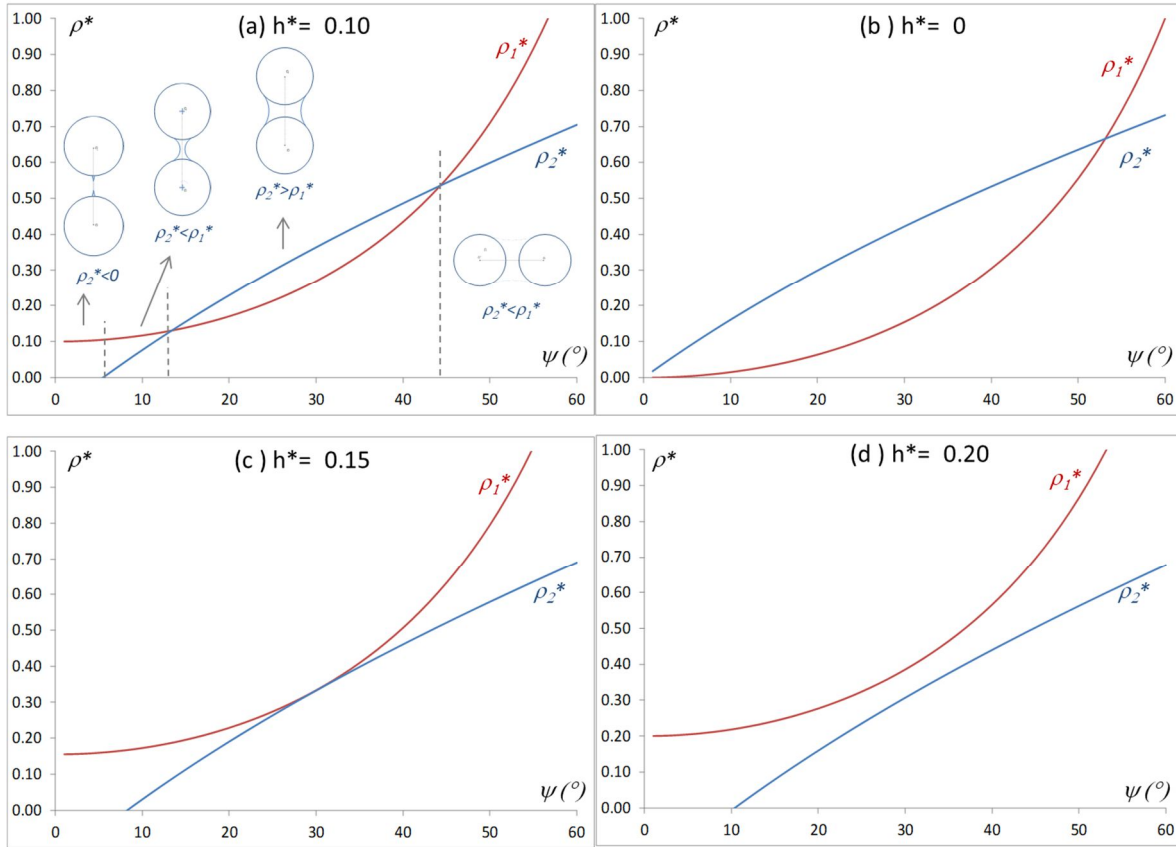


Figure V-2 : The effect of interparticle gap on principal radii of curvature (perfect wetting, $\theta=0$)

Four different representative values of separating gap have been considered. In all cases, both curvature radii are increasing functions of the filling angle. However, the second radius is a positive unipolar concave curve whereas the first radius has a unipolar positive convex shape (*i.e.* the rate of increase for the first radius accelerates with the filling angle whereas it slows down for the second radius). In the most general case (represented by [Figure V-3-a](#)), for a given set of contact angle and separating gap, according to the relative importance of the first and the second radii of curvature, different zones could be distinguished. At very small filling angles, the second radius would be negative which is physically impossible. In fact, in this zone, the neck of the hypothetical bridge which would be formed due to condensation must fall under OO' axis in [Figure V-2](#). This signifies that for the condensation process, a continuous bridge cannot be created and for evaporation process (water withdrawal) this is equivalent to a rupture in the bridge. For higher filling angles, the second radius becomes positive but remains smaller than the first radius. The overall curvature (r_c) is then negative which signifies that from a thermodynamic point of view, the

capillary condensation could not occur spontaneously. The presence of a minimum amount of liquid is thus necessary for the condensation to be initiated.

A first intersection between the two curves is observed at a minimum filling angle (when $\varrho_1 = \varrho_2$) beyond which the first principal radius becomes inferior to the second one. The capillary condensation could therefore happen until a second intersection between the two curves is reached at a maximum limiting filling angle. Beyond this value, the balance is inverted and the equivalent capillary radius becomes negative again, which means that the capillary condensation is brought to an end.

Figure V-3 also indicates that as the interparticle gap increases, the minimum limiting filling angle increases whereas the maximum one decreases. Consequently, if the separating distance is too long, the curve corresponding to the first radius of curvature lies wholly under that of the second radius. No intersection between the two curves exists anymore and the capillary condensation cannot take place (Figure V-3-d).

Furthermore, it should be noted that according to equations (V-3) and (V-4), the maximum separation gap at which the capillary condensation phenomenon stops diminishes with increasing the wetting angle. It can be then concluded that the largest domain for the feasibility of the capillary condensation corresponds to perfect wetting of particles in contact for which the minimum and the maximum limiting filling angles are equal to 0° and 53° , respectively.

For the special case of partially wetting particles ($\theta \neq 0$) in contact ($h^* = 0$), it can be shown that the maximum filling angle is given by:

$$\psi_{max} = \cos^{-1} \left(\frac{3 + 4 \sin \theta + 2 \sin^2 \theta}{5 + 4 \sin \theta} \right) \quad (V-13)$$

Finally, in the general case, for a given set of geometrical and wetting parameters, the limiting values of the filling angle and the separation gap can be obtained by equalizing equations (V-3) and (V-4). Consequently, the maximum volume of liquid and the corresponding capillary force can be obtained by replacing ψ by ψ_{max} in equation (V-8) and (V-9).

Figure V-4 depicts the variation of these parameters with the wetting angle and the interparticle gap, respectively. As can be seen from Figure V-4-a, the limiting filling angle is maximum for a perfect wetting system and reduces progressively when the wetting angle increases. In a similar manner, the normalized limiting volume of liquid (Figure V-4-b) and the resulting capillary force (Figure V-4-c) decrease regularly from their maximum value (at $\theta = 0$) to a minimum when the contact angle attains 90° .

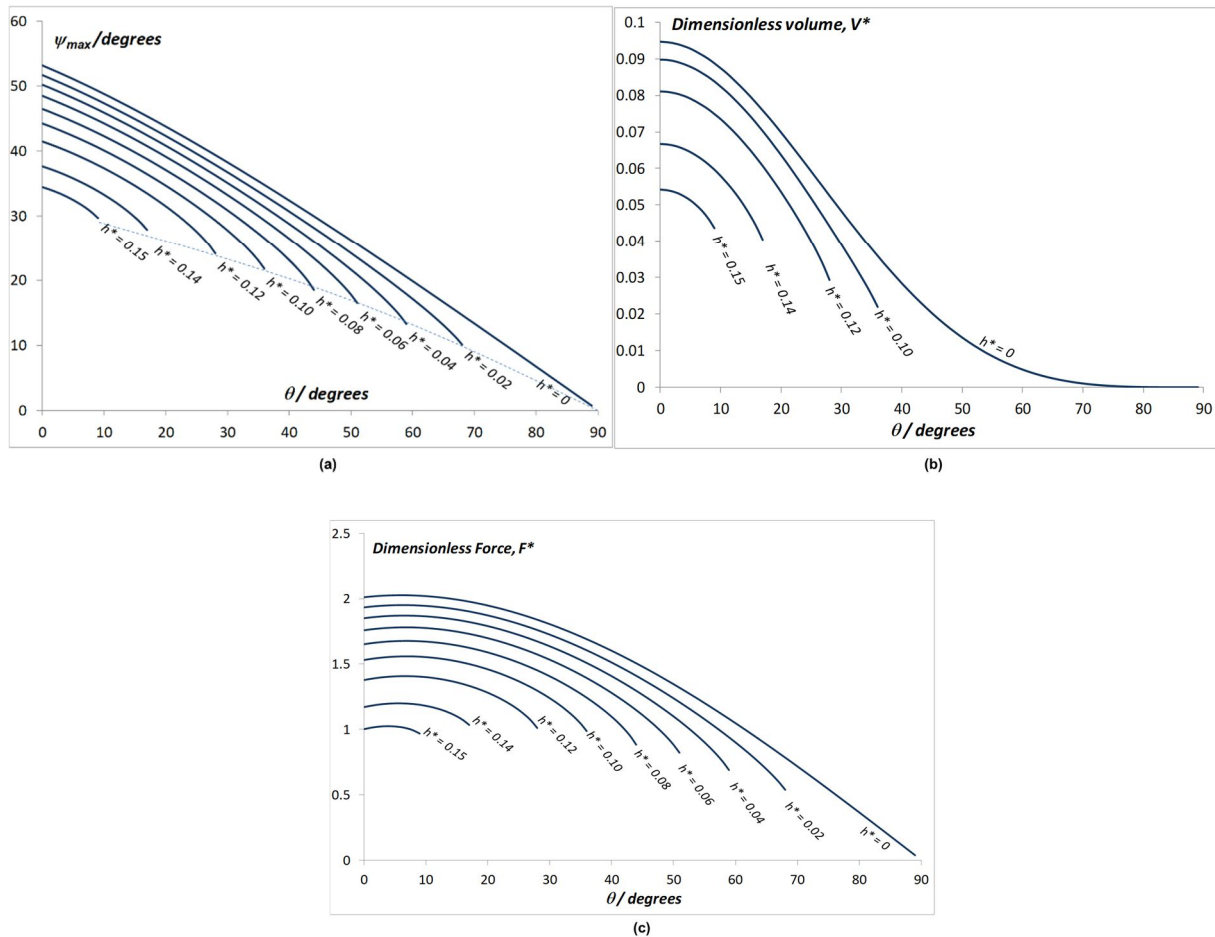


Figure V-3: The effect of contact angle on the maximum filling angle (a), dimensionless volume (b) and dimensionless force (c)

Regarding the effect of the interparticle gap, Figure V-4(a) indicates that whatever the contact angle is, increasing the gap between particles leads to a decrease in the maximum filling angle. The total volume decreases significantly with the contact angle and the interparticle gap until its limit value is achieved. Finally, the dimensionless force of the binary agglomerate decreases constantly with the particle gap.

The sequence of ESEM images presented in Figure V-5 clearly shows the existence of a maximum filling angle during the capillary condensation phenomenon. These images were taken using an Environmental Scanning Electron Microscopy (ESEM) instrument [12], which allows the direct observation of samples under controlled temperature, pressure and humidity with no need for any special preparation or metal coating. The solid particles are 125-150 μm glass beads prepared by sieving. The solid-liquid contact angle measured by capillary rise test [12] was $16^\circ \pm 1^\circ$. During this experiment, the relative humidity within the observation chamber varied from zero to total saturation.

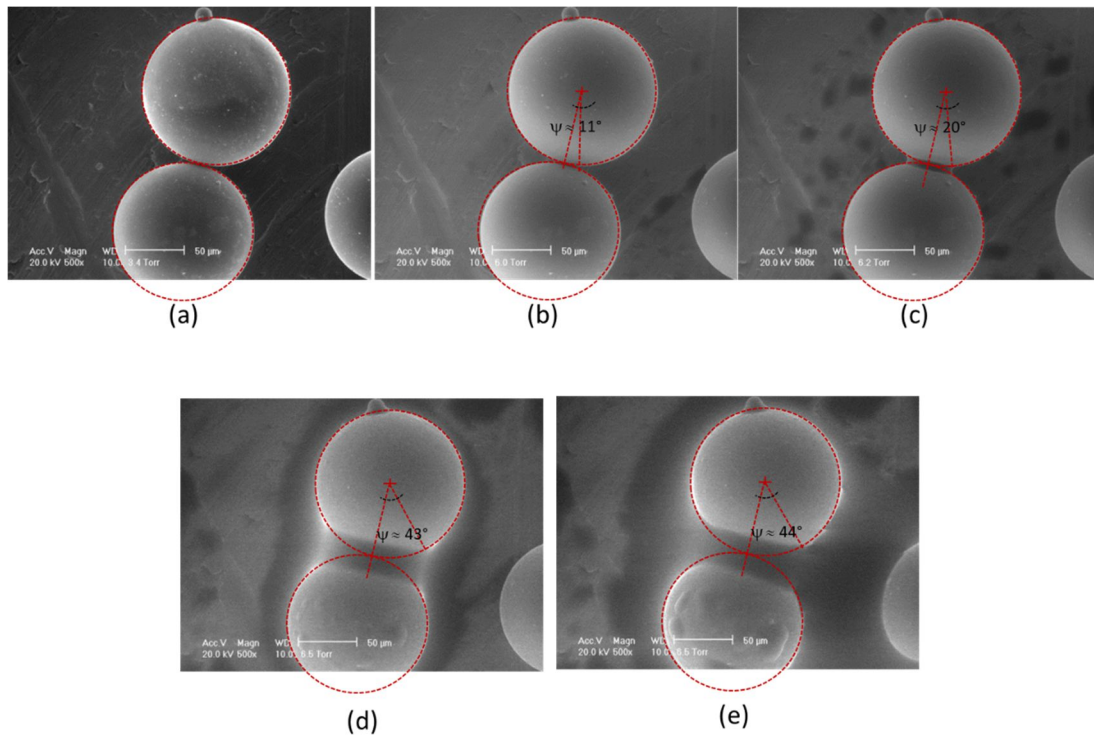


Figure V-4: Capillary condensation in a binary agglomerate during a step variation of RH from 0 (a) to 99% RH (b to e)

Images (a) to (e) correspond to the transient response for a step variation of the relative humidity from RH=0% (Figure V-5-a) to RH=99%. The last image (Figure V-5-e) corresponds to the equilibrium state. Obviously, increasing the water activity leads to the formation of a capillary bridge between the two touching particles situated in the middle of the frame whereas this is not the case for the third particle (at the right) which is separated ($h^* \approx 0.5$). As expected, the filling angle increases with the increase of water activity. Moreover, a maximum filling angle of about 44° is reached when a_w approaches the unity. This value is in good agreement with the theoretical value of 46° predicted by the model (Figure V-4-a). The slight

deviation from the theory could be explained by the heterogeneity of the surface and the fact that, in practice, the actual gap between particles could not be absolutely equal to zero.

However, it should be noted that in case of an assembly of particles, before the aforementioned filling angles are reached, liquid bridges on neighboring particles will gather together changing the geometry of condensing pores (Figure V-6).

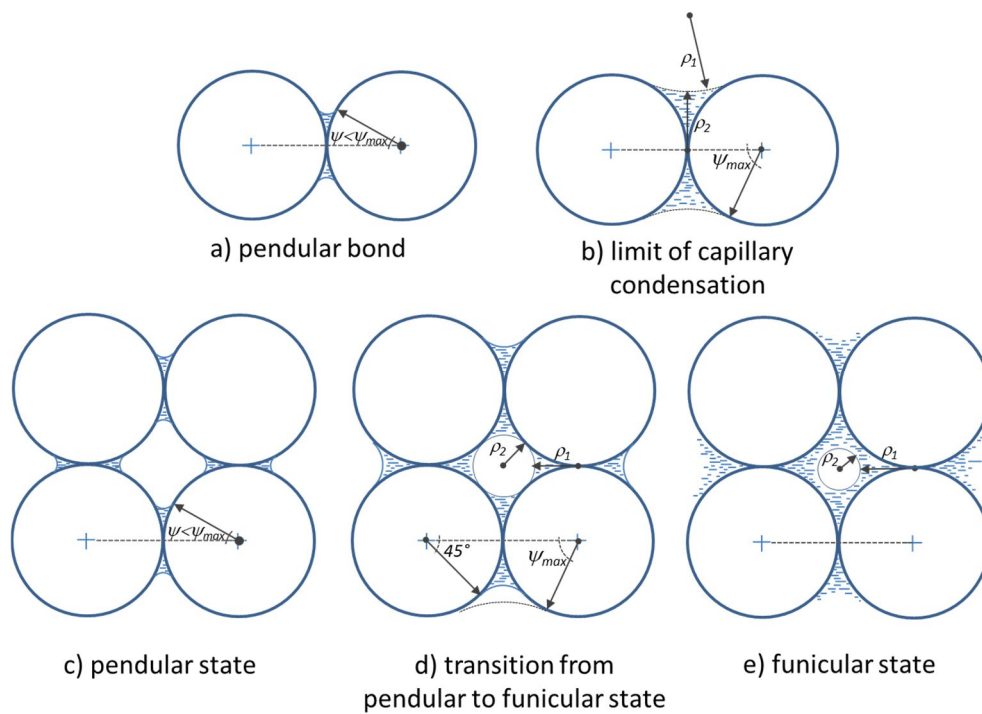


Figure V-5: Capillary condensation in a binary agglomerate (a) and (b) and in a square cubic packing of equal-sized spheres (c) to (e).

For example, for a regular packing of equal-sized particles, this phenomenon happens at a filling angle of 45° for a square and 30° for a triangular packing of particles. After this limit value, the liquid phase becomes continuous and this limit can be considered as the starting point of the funicular state with no more increase in the filling angle. The condensation continues however with the equivalent capillary size becoming the characteristic capillary size of funiculars. These statements are clearly confirmed by the ESEM images of Figure V-6 captured during the humidification of a 2D triangular arrangement of glass beads.

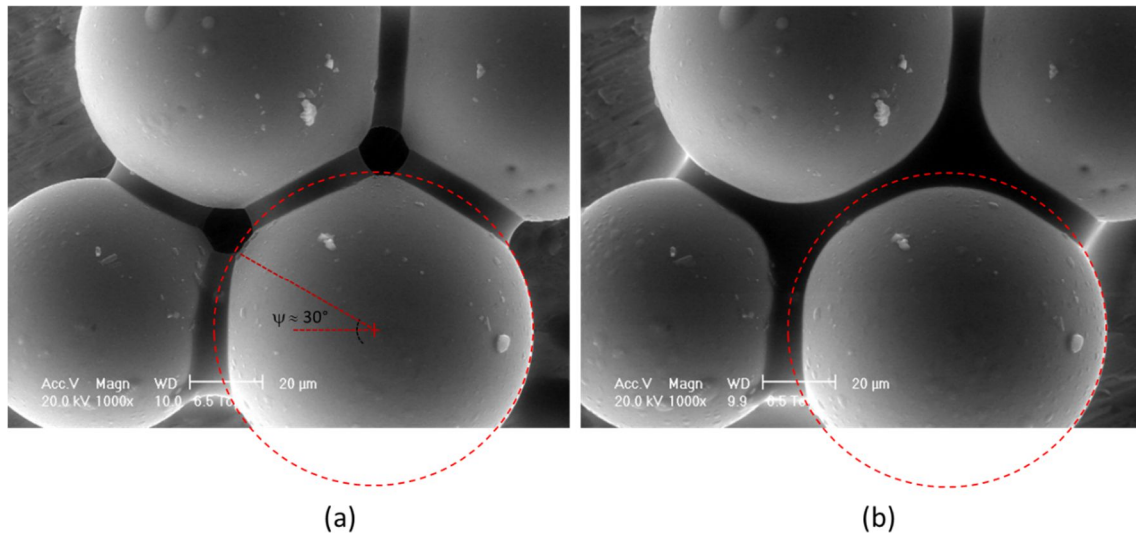


Figure V-6: Capillary condensation a 2D triangular assembly of glass beads

As can be seen from [Figure V-6-b](#), once a filling angle of about 30° is attained, the neighboring liquid bonds come in touch and gather together. Further humidification leads to complete filling of the interstitial void spaces by the conjugated effect of the capillary condensation and the fact that the liquid phase becomes continuous and mobile. Note that for randomly packed beds, the transition from pendular to funicular state is highly dependent on the packing geometry and remains difficult to make out accurately.

2.2.2 Assembly of particles

In this section, we consider the case of an assembly of particles. [Table V-2](#) summarizes the reference conditions used for calculations. The discussion is limited to a water activity range between 0.4 and 1, which more likely corresponds to the domain of validity of Kelvin's equation. In order to better emphasize the trends and the differences between results, semi-log coordinates are used.

Table V-2: Reference conditions for model calculation

Contact angle, θ	0°
Particle diameter	$1\mu\text{m}$
Interparticle gap, h^*	0
Arrangement	Square cubic
Coordination number, k	6
Porosity, ε	0.4764
Molar volume of liquid, V_l	$1.8 \times 10^{-5} \text{ m}^3 \cdot \text{mole}^{-1}$
Liquid surface tension, γ	$72 \text{ mN} \cdot \text{m}^{-1}$
Temperature, T	273 K

2.2.2.1 Effect of particle size

Figure V-7 depicts the evolution of the saturation degree, S , and the tensile strength σ_T (at equilibrium) with the water activity for different particle mean sizes.

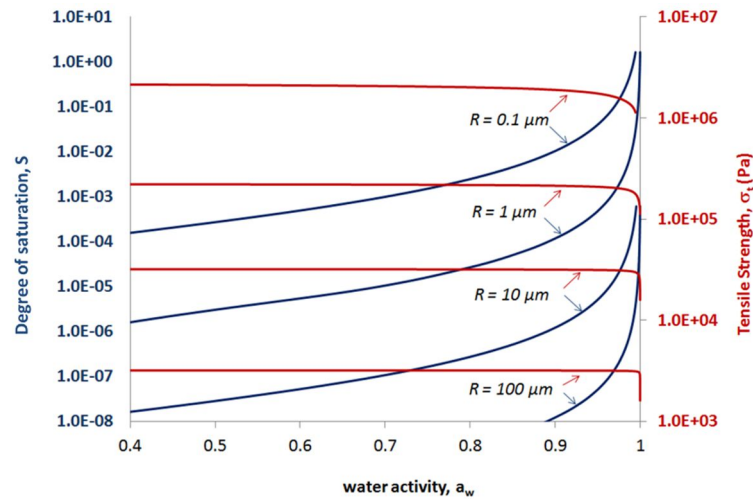


Figure V-7: Evolution of the degree of saturation and the tensile strength with water activity – the effect of particle mean size

As it can be seen, the degree of saturation increases continuously with the water activity. The trend accelerates as a_w approaches unity. This behavior is explained by the exponential dependence of the capillary size at which condensation occurs with the water activity (Kelvin's equation). At the same time, the tensile strength remains almost constant first but drops sharply off at the end of condensation. This trend is directly related to the evolution of attractive force of a binary agglomerate which undergoes a significant decrease as the filling angle approaches 53° (*i.e.* capillary curvature, $1/r_c$, close to zero). At this condition, the capillary component of adhesive force cancels and only the surface tension component counts.

Figure V-7 shows also the major role of the particle size. Regarding the degree of saturation, this parameter increases smoothly first and increases sharply at the end of operation. Figure V-7 shows that the particle size influences both the degree of saturation and the transition point at which the saturation degree takes off. As can be seen from this figure, in the first period of operation, for a given water activity the degree of saturation increases by 2 or 3 orders of magnitude when the particles size is raised by one order of magnitude. As for

the tensile strength, the onset of the capillary condensation is pushed away as the particle size increases. For a given average size of particles, this parameter remains constant first and undergoes a sharp decrease at high saturation degrees. This trend is directly dictated by the evolution of the capillary force of binary agglomerates and the direct relationship between σ_T and F according to Rumpf's model (Eq. V-10). Furthermore, according to this equation, it can be seen from Figure V-7 that for a given water activity, the tensile strength varies by the same factor as the particle size.

These results show also that for smooth and non soluble particles, capillary condensation plays a significant role only for sub-micronic powders for which the presence of water in liquid state (then liquid bridges) is expected at low water activities, sensibly less than the saturation activity ($a_w=1$). For comparison, for micronic particles, the degree of saturation remains lower than 1% until a very high water activity (> 98%) is reached whereas for 0.1 μm particles this level of saturation is reached at $a_w \approx 0.9$. The order of magnitude of the tensile strength is meaningfully high for submicronic packings (*e.g.* $> 10^6$ Pa, which means that a small cylindrical bloc of powder of 1 cm^2 cross-sectional area could resist to the tensile action of a mass of 10 kg). This resistance decreases proportionally to the particle size so that for 1000 μm particles, it approaches 10^2 Pa only which signifies that the bloc of powder could break up under its own weight.

2.2.2.2 Effect of the contact (wetting) angle

Figure V-8 illustrates the effect of the wetting angle on the saturation degree and on the tensile strength, respectively. As expected, higher contact angles (*i.e.* poor wetting) lower both the degree of saturation and the tensile strength of the bed. Both these parameters decrease regularly to attain a zero level when the contact angle approaches 90° . This is because on the one hand, for a given water activity, the corresponding capillary radius decreases with the contact angle (*i.e.* the volume of liquid is lower compared to a perfectly wetting surface). On the other hand, the capillary force of a binary agglomerate decreases with increasing the contact angle (Figure V-4) giving rise to a lower tensile strength. Note that the variation of S and σ_T are not proportional to θ but to $\cos \theta$.

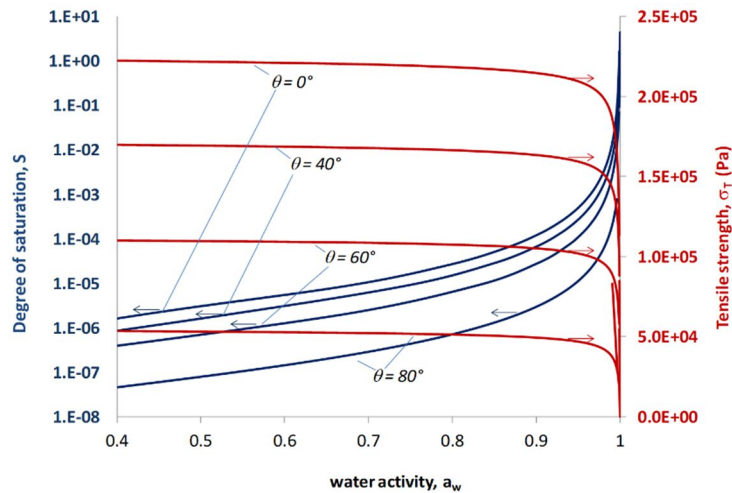


Figure V-8: Evolution of the degree of saturation and the tensile strength with water activity – the effect of contact angle

2.2.2.3 Effect of the coordination number

The effect of the coordination number for some well-established arrangements presented in Table V-1 is depicted in Figure V-9-a. In addition, Figure V-9-b presents the effect of this parameter for looser packed beds ($k < 6$). Note that the effect of the coordination number on the degree of saturation can be directly predicted from Eq. (V-12) by referring to the reference case and is not detailed. As can be seen from Figure 9-a, the coordination number has a large influence on the tensile strength. Indeed, increasing k leads to a higher tensile strength due to conjugated effect of the contact points and the voidage which decreases with increasing k (*i.e.* increasing $k(1 - \varepsilon)$ in Eq. V-10).

For more loosed packed beds we can use the correlation of Meissner *et al.* [10] (Eq. V-11) for the relation between the coordination number, k , and the bed porosity, ε . Figure V-9-b shows the same effect of the coordination number on the tensile strength for more loosed packed beds.

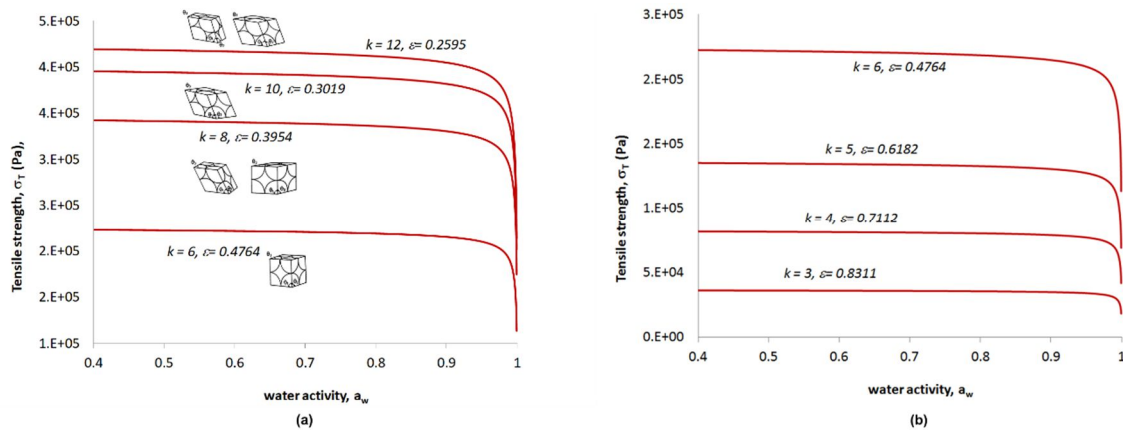


Figure V-9: Evolution of the tensile strength with water activity - the effect of coordination number for regular (a) and random packed beds (b)

2.3 Partial conclusions on "grain-bulk" model

In this first section, we presented the basic concepts that describe the behavior of a homogeneous population of particles subjected to humidification in relation with caking phenomena. The focus has been on two physical phenomena, (*i.e.* capillary condensation and capillary forces) that are described by the two fundamental relationships of surface chemistry (*i.e.* Kelvin and Laplace equations, respectively). The predominant role of the particle size, the contact angle and the particle arrangement on the extent of capillary condensation and resulting adhesive forces has been pointed out. The results show that for smooth and spherical particles considered in this work, the capillary condensation phenomenon comes into play only in the case of sub-micronic particles. It appears that the capillary condensation and more specifically the degree of saturation are limited by the thermodynamic consideration. Furthermore, increasing the contact angle or the interparticle gap as well as decreasing the coordination number tends to reduce both the onset and the extent of the capillary condensation phenomenon.

Finally, we should note that although the caking does not result always from the creation of moving bridges, the results presented in this section remain important in several ways:

- First, whatever the caking mechanism, it is always necessary to separate the role of the capillary condensation from that of the other mechanism. The models that we

have presented in this part allow to better evaluate the relative role of the elementary mechanisms

- In the case of phase transition caking, for example for amorphous products, the Rumpf model for resistance as well as the packing laws remain valid but the binding force will be that of a solid bridge instead of a liquid bridge.

In the second part of this chapter, a study on the mechanical strength of wet or dry cakes is carried out using Discrete Element Method (DEM). The results presented in this section were used to verify the reliability of simulation results and then to validate the numerical method. After validation, the DEM method was used to simulate the behavior of two cases that could not be treated by the current model, *i.e.* wet cakes subjected to a compressive stress and dry cakes (solid bridges) subjected to compressive or tractive stresses.

3 Discrete Element Method (DEM)

As it was mentioned in introduction, with increasing capacity of computational tools in recent decades, a large number of researchers have used DEM to simulate granular flows. Consequently, the contribution of DEM in simulation of granular materials has significantly increased.

DEM can be divided into two main groups of models based on the approach of the simulation: hard sphere model and soft sphere model. Hard sphere model is an event-driven method (EDM) that is suitable for dilute systems in which the number of contacts is small [13-15]. On the other hand, soft sphere method is a time-driven method and efficient in dense systems [16-18]. As a result, as in most studies in the field of dense granular material simulation, in this study we used the soft sphere method. This method is based on the "*spring-dashpot*" model to describe the contact of particles. A viscoelastic model including an elastic component and a dissipative component is used to represent the rheological behavior of the assembly. A spring and a dashpot, respectively represent the elastic and viscous components. There are two types of combinations to represent the normal and tangential interactions (Figure V-10): Kelvin model, which connects a spring and a dashpot in parallel, and Maxwell model, which connects a spring and a dashpot in series. Different combinations of Maxwell and Kelvin models can be assembled to simulate various viscoelastic contact models. An example of a four-parameter model is given in Figure V-10.

Krugger-Emben *et al.* [19] categorized the viscoelastic models into linear and nonlinear types. The linear viscoelastic models make use of spring-dashpot contacts according to Kelvin or Maxwell scheme (or a combination of these), whereas for nonlinear viscoelastic models, generally the Hertz model is used for the elastic part. Non-linear models require more computational time. However, with increasing computational powers, non-linear (Hertzian) contact models instead of linear Hooke's contact theory become more and more popular in DEM simulations.

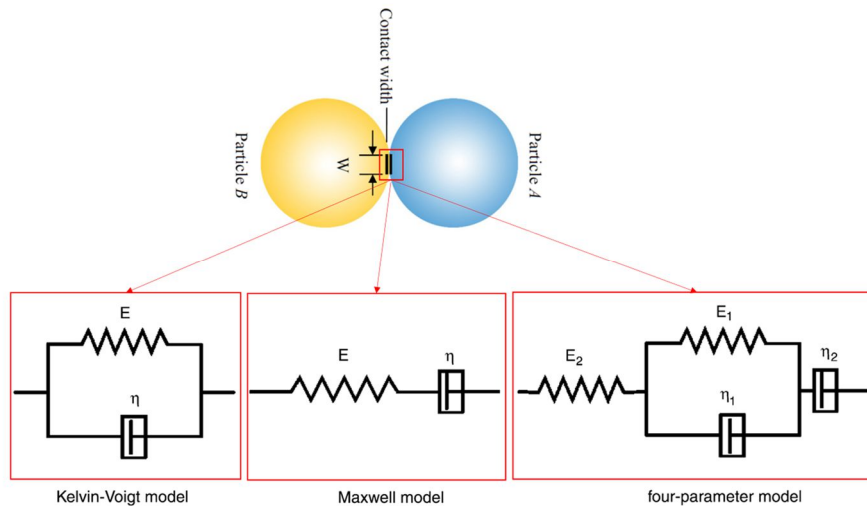


Figure V-10: Components of the spring-dashpot contact schemes for viscoelastic models

It should be mentioned that alongside the soft sphere method that utilizes the spring-dashpot method to model the contact of particles, collisional flow mechanics have also been studied in details and several methods have been provided for the modelling of collisions. For instance, we can mention:

- Collisional flow mechanics in dense granular flows that were comprehensively investigated by Thornton *et al.* [20, 21].
- Adhesive and sliding friction components for slip-stick behavior observed in rigid plastic and elastic plastic contacts, detailed by Walton [22].
- Sliding (enduring) contacts of particles using load-dependent friction models [14, 23].
- Effective frictional contacts using the attractive-repulsive molecular potentials introduced in molecular rheology simulations of complex fluids [24].
- Several investigations have also been performed to include the individual particle motion physics in contacting assemblies, focusing on jamming, stress-induced anisotropy and complex force chains [25, 26].

From a geometrical point of view, DEM simulations of granular flow can be divided into two-dimensional and three-dimensional simulations. Two-dimensional simulations require less computations [27-32]. However with increasing the computational equipment in recent decade, the number of three-dimensional DEM simulations is increasing rapidly [19, 29-36].

The most time-consuming part of DEM is the detection of contacts between particles. Several methods have been proposed for the contact detection in DEM. Majority of these methods can be categorized into three main groups of cell-based, sort-based and tree-based algorithms [37]. Extensive details on the contact detection algorithms used in the framework of DEM can be found elsewhere [37, 38].

Finally, the integration algorithms for velocity and acceleration calculations can be divided into three groups of single-step (including forward Euler, modified Euler, Taylor second, third and fourth order, central difference, position Verlet and Runge-Kutta algorithms), multi-step (including velocity Verlet, Adams-Bashforth second, third and fourth order) and predictor corrector (including Adams-Moulton third, Fourth and fifth order and Gear methods) algorithms. The accuracy and required computational time of these algorithms have been compared and reported elsewhere [37]. It was found that the predictor-corrector algorithms gives the highest accuracy but require the longest computational times [37]. The multi-step algorithms provide adequate accuracy of the simulation while keeping the computational time low.

3.1 DEM simulation of mechanical strength of cakes due to capillary (liquid) and solid bridges

In this work, discrete numerical modeling was first used to study the effect of capillary condensation in granular media at a Representative Element of Volume (REV). This amounts to solving the classical equations of dynamics for a particle assembly. This method has already been used to model the behavior of granular materials in the presence of capillary forces [39, 40]. The advantage of a discrete approach lies particularly in its ability to integrate physical quantities by being closer to the microstructure of the granular medium (at contact scale). Expressed in the global coordinate system, the set of equations originally developed by Cundall and Strack [16] is the following:

$$\begin{cases} m_i \ddot{u} = F_i^{ext} + \sum_j F^{j \rightarrow i} \\ I_i \ddot{\theta} = M_i^{ext} + \sum_j M^{j \rightarrow i} \end{cases} \quad (V-14)$$

where \ddot{u} and $\ddot{\theta}$ are linear and angular acceleration matrix, respectively, m_i and I_i are respectively the mass and the moment of inertia matrix of the particle i , $F^{j \rightarrow i}$ and $M^{j \rightarrow i}$ the force and moment vectors due to the action of the particle j on the particle i , and F_i^{ext} and M_i^{ext} the external force and moment vectors.

Mechanical contact interactions are calculated with an explicit contact law [16]. The particles were assimilated to rigid spheres. The contact forces in the absence of capillary effect, were presented with a linear contact model depending on elastic force displacement law, Coulomb friction and viscous damping coefficient. For a pair of particles in contact ($i; j$) the normal and tangential forces, $F_{n,t}$, expressed in the coordinate system related to the contact plane were provided by the Kelvin-Voigt model:

$$\begin{cases} F_{n,t} = -k_{n,t} \delta_{n,t} - c_{n,t} v_{n,t} \\ \text{with : } F_t = -\min(F_t, \mu F_n) \times \text{sgn}(v_t) \\ \frac{k_t}{k_n} \in \left[\frac{2}{3}, 1 \right] \\ c_{n,t} = 2\sqrt{k_{n,t} m^*} \end{cases} \quad (V-15)$$

where $k_{n,t}$ and $c_{n,t}$ are the normal and tangential stiffness of contact and damping coefficients, respectively, and μ is the dry friction coefficient of Coulomb. $\delta_{n,t}$ and $v_{n,t}$ are the relative displacements et velocities, respectively, according to the normal and tangential directions. In the presence of capillary condensation, the normal component of the contact force F_n is the resultant of repulsion and attraction interactions: $F_n = -k_n \delta_n - c_n v_n - F_{cap}$. In this study, it is assumed that the tangential effect of the capillary bridge is negligible and that, in addition, the wettability is perfect (contact angle $\theta = 0$). The viscous effect of liquid is neglected in the modelling.

The mechanical system requires an explicit time integration based on the velocity-Verlet scheme.

$$\begin{cases} u(t + \Delta t) = u(t) + \Delta t \dot{u}(t) + \frac{\Delta t^2}{2} \ddot{u}(t) \\ \dot{u}(t + \Delta t) = \dot{u}(t) + \frac{\Delta t}{2} (\ddot{u}(t) + \ddot{u}(t + \Delta t)) \end{cases} \quad (\text{V-16})$$

Using a Representative Elemental Volume (REV), the DEM was used to study the influence of the presence of liquid and solid bridges on the macroscopic behavior of an assembly composed of several thousands of micrometric particles. All numerical simulations were performed with the MULTICOR-3D and MULTICOR3D ++ discrete element codes [41, 42]. The method allows describing both the case of liquid capillary and solid bridges (crystallization of liquid bridges).

3.2 Discrete simulations of capillary effects at a REV scale

First, we focus on the role of capillary condensation and subsequent liquid bridge formation within a granular medium exposed to fluctuations of ambient relative humidity. As we saw in the previous section, such bridges cause an attractive force between particles, leading to the formation of a cake with intrinsic physicochemical and mechanical properties. By considering a Representative Elementary Volume (REV) of 10.000 particles, the DEM was then performed by means of MULTICOR3D software taking into account the properties of the cake (degree of saturation) in order to establish relationships between the microscopic parameters and the macroscopic behavior (tensile strength) of cakes. The software uses the explicit (also called smoothed) formulation [43].

DEM simulations were based on the combination of conventional DEM method and the phenomenological model of capillary condensation, presented in the previous section. At each step of time, capillary forces at each binary contact were calculated by assuming that the system is in thermodynamic equilibrium ($a_w = RH$). The volume of liquid bridges and the extent of capillary forces within a known arrangement of particles at a desired water activity was calculated by the combination of the Kelvin law of capillary condensation and the Laplace law for capillary forces, as explained earlier:

- Initially, the degree of saturation in water was set at a given value, the corresponding volume of liquid was distributed equitably over the potential contacts ($0 < 2h^* < 0.3$).

- At each time step, the geometric parameters of each capillary bridge ($\psi, \varrho_1, \varrho_2$) were obtained by an iterative calculation.
- Finally, the redistribution of the liquid volume for the following time step was calculated based on the evolution of the contacts.

Figure V-11 presents a snapshot from MULTICOR3D software, showing four binary contacts for different separating distances $2h^*$ (0.02; 0.08; 0.20; 0.30). At each contact, the capillary bridge shape is drawn with respect to their respective geometric parameters, namely the principal radii, ϱ_1, ϱ_2 , and the filling angle, ψ .

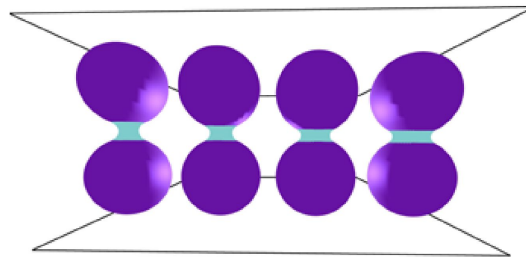


Figure V-11: Presentation of four binary contacts for different separating distances (from left to right: $2h^* = 0.02; 0.08; 0.20$ and 0.30 , respectively)

3.3 Modeling of densification of regular packings under the effect of capillary bridges

Initially, the implementation of DEM allowed to model the effect of capillary condensation on regular packing of particles (CS, CC and CFC), with a particle radius of $R=1.5 \mu\text{m}$. The objective was to simulate the densification of stacks initially generated with non-contact particles ($0 < 2h^* \leq 0.3$). After having fixed the degree of saturation, the creation of capillary bridges between particles mechanically leads to a densification of the stack. At the end of this step, the theoretical values of compactness are verified respectively for the different studied cases, namely 52% for the CS, 68% for the CC and 74% for the CFC packing (Figure V-12(a)). The results of Figure V-12(b) show a homogeneous densification of the stack. The kinetics of densification of all the particles was similar to the behavior of two isolated particles. These test cases are, of course, not representative of the actual packings, but they allow to be placed in an ideal case without rearrangement and thus validate the results provided by the discrete model.

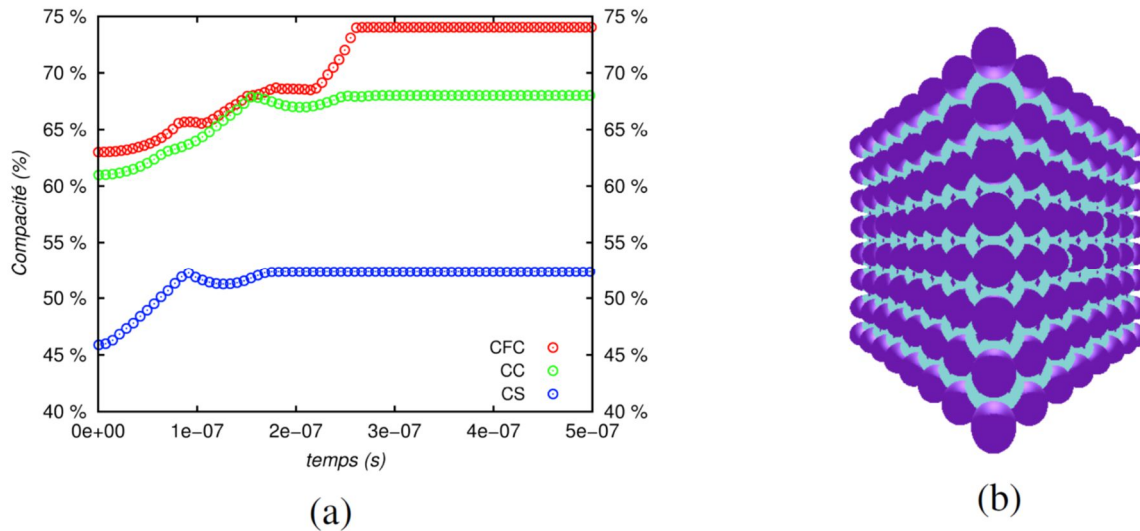


Figure V-12: (a) Evolution of the compactness of regular stacks: CS, CC and CFC - (b) Densified state of a CC stack

3.4 Mechanical behavior of powder compacts in the presence of capillary bridges

In a second time, the DEM was used to characterize the behavior of an assembly of monodisperse particles in order to study the influence of the particle size and the degree of saturation on randomly generated packing of particles. The granular packing is generated by the efficient Lubachevsky-Stillinger Algorithm (LSA) which enables to fulfill the assumptions of the Random Close Packing (RCP) [43]. Considering a constant box volume, $(10^{-4})^3 m^3$, six packings are generated with a number of particles varying in the interval $[2 \times 10^3; 2 \times 10^4]$, a particle radius ranging between $2 \mu m$ and $4 \mu m$, a constant compactness ($\approx 50\%$) and a density of $1500 kg.m^3$. The degree of saturation, S , varies within the interval $[0.64\%; 12.8\%]$.

The numerical characterization of the behavior was carried out through a simple tensile test with an imposed speed of $10^{-4} m.s^{-1}$ and a time step of $10^{-7} s$. The six stacks are solicited in simple tension in order to highlight a possible influence of the behavior as a function of particle size. It should be reminded here that the initial volume of the domain is constant regardless of the number of particles in the stack. At the beginning, when the capillary links at the contacts are created, the packing is in a state of agitation (Figure V-13(a)). Therefore, before applying the tensile stress, a stabilization phase is necessary in order to reach the equilibrium state. Figure V-13(a) provides information about the densification process of the stack with a kinetic energy close to zero when the equilibrium state is reached. Figure V-13(b) and (c) present the capillary bridges and displacement field, respectively, at the end of the

densification process. Once equilibrium state is achieved, the packing is subjected to a quasi-static tensile stress. During the test, the tensile stress, σ (Pa), is evaluated in the middle section of the packing to avoid edge effects, and the strain, ε (%), is estimated with respect to the particle radius.

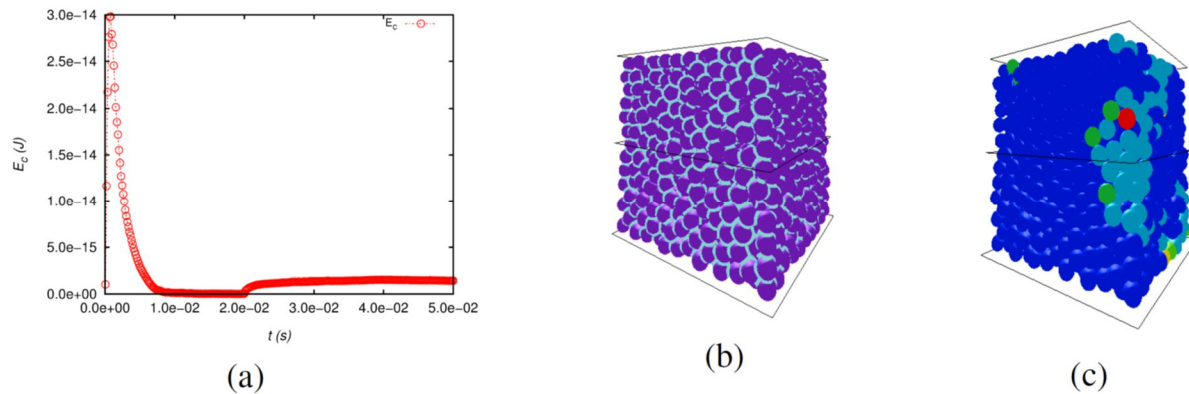


Figure V-13: Evolution of a packing of 2000 particles: (a) Kinetic energy; (b) Capillary bridges ($S = 1.28\%$); (c) Equilibrium velocity field

The curves plotted in [Figure V-14](#) show the variation of the time-weighted tensile stress as a function of the relative elongation of the packing with a water saturation rate of 10.4%. The first observation concerns the two phases that characterize the first moments of the tensile test. Indeed, the traction curve has a very steep first phase, which reflects the reaction of the stack to the load. This sharp increase is followed very quickly by a second phase of low stiffness.

The second observation is related to the relative sensitivity of the maximum stress to particle size, even though the tensile curve is less and less erratic as the number of particles increases. Finally, the stack containing 20.000 particles is the one whose tensile curve shows a decrease in the slowest stress. This behavior is partly explained by a high density of capillary links in the right section of the stack. This results in a wider flow area beyond the maximum stress.

[Figure V-14\(b\)](#) shows the evolution of a stack of 8000 particles at different times of the numerical tensile test. The wall placed at the middle of the stack allows computing with a good accuracy the tensile stress during the simulation in order to avoid a possible disturbance near the upper and lower boundaries.

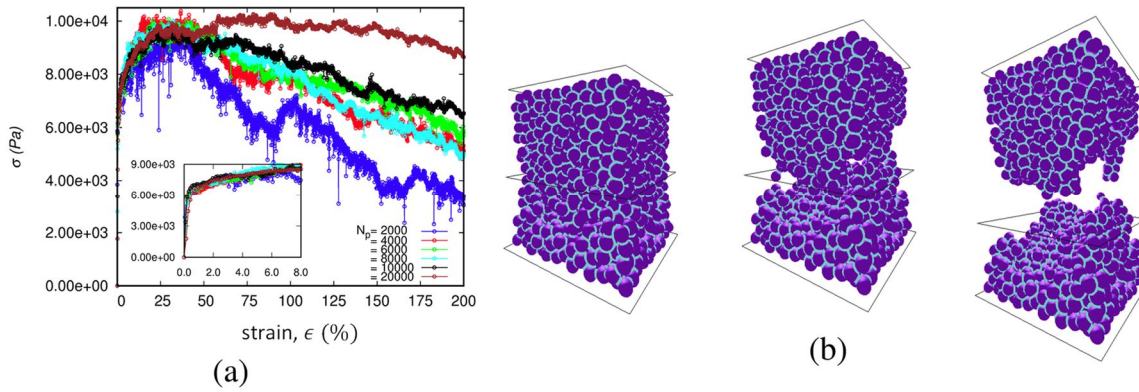


Figure V-14: variation of the time-weighted tensile stress as a function of the relative elongation of the packing

The second study focused on the influence of the water saturation rate on the tensile strength of cakes. The REV selected, among the series of stacks presented above, is the one containing 10.000 particles, which is a good compromise between accuracy and calculation time. The reference saturation rate is $S = 0.64\%$. The test protocol is identical to that described above. Figure V-15 shows a clear influence of the saturation rate on the tensile strength of the stack. This result is obviously expected, since a greater quantity of water has the effect of increasing both the intensity and the number of the capillary bonds. Indeed, this results in a coordination number, k , which increases as a function of the saturation rate (Figure V-15 (b)). This evolution is in agreement with the results of tensile tests.

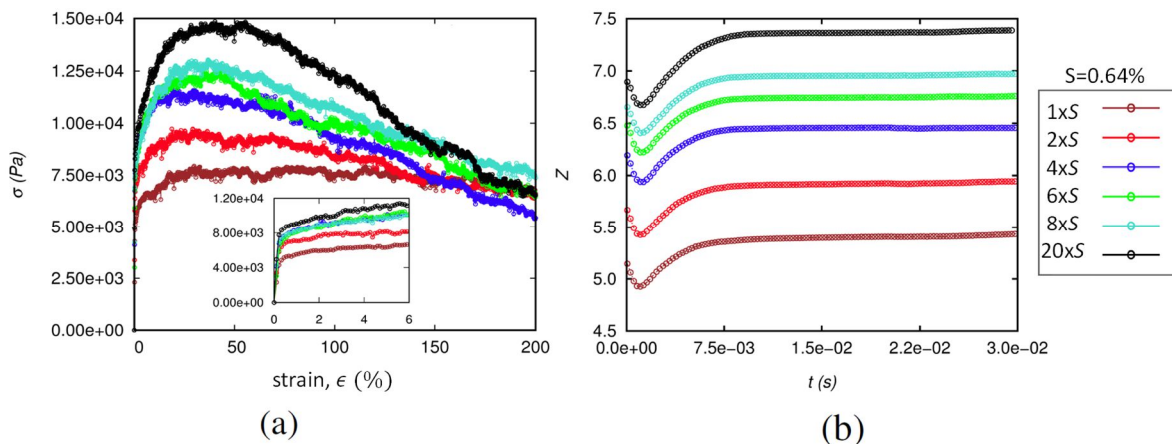


Figure V-15: (a) traction curve; (b) time evolution of the coordination number

3.5 Mechanical behavior of powder compacts in the presence of solid bridges

In this second phase of discrete modelling, we are interested in the mechanical behavior of powders containing solid bridges. In order to take into account the cohesive effect of solid

bridges at the level of elementary contacts in discrete modelling, we have introduced an Euler-Bernoulli type beam model between particles in contact. This approach has been developed by LTI/UPJV and have been described in details elsewhere [44, 45].

In this model, the solid bridges are assimilated to beams linking the particles together. The local (or microscopic) parameters that characterize the beam model are E_μ , G_μ , A_μ and L_μ , respectively the Young's modulus, the shear modulus (or Coulomb), the cross-section of the beam and the length of the beam (Figure V-16). In a matrix form, the generalized forces of cohesion induced by the beam are calculated via a matrix of stiffness (Eq. V-17) [46]. At the end of each beam element ($i; j$) are affected the degrees of freedom in translation, $u_n^{i,j}$, $u_t^{i,j}$, $u_f^{i,j}$, and in rotation $\theta_n^{i,j}$, $\theta_t^{i,j}$, $\theta_f^{i,j}$, expressed in the local base of the beam ($\vec{u}_n, \vec{u}_t, \vec{u}_f$). The subscripts n, t and f are related to the normal, tangential and bending effects, respectively.

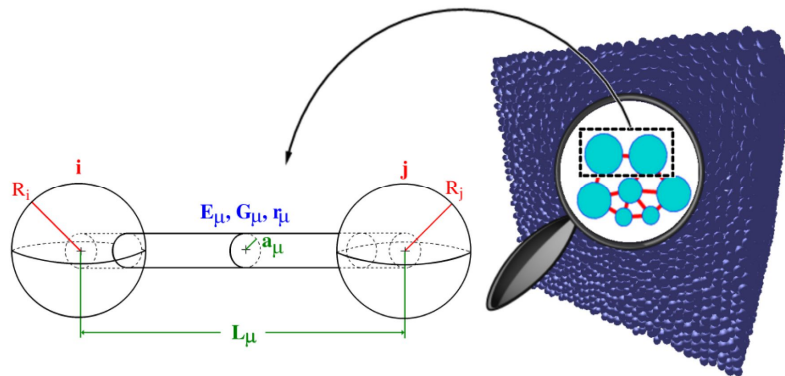


Figure V-16: Euler-Bernoulli beam type cohesion model [42]

The cohesion forces between two particles, i and j , are represented by the following system:

$$\begin{bmatrix} F_n^{j \rightarrow i} \\ F_t^{j \rightarrow i} \\ F_f^{j \rightarrow i} \\ M_n^{j \rightarrow i} \\ M_t^{j \rightarrow i} \\ M_f^{j \rightarrow i} \end{bmatrix} = \begin{bmatrix} k_n & 0 & 0 & 0 & 0 & 0 & 0 & 0 \\ 0 & k_t & 0 & 0 & 0 & 0 & \frac{k_t L_\mu}{2} & \frac{k_t L_\mu}{2} \\ 0 & 0 & k_t & 0 & -\frac{k_t L_\mu}{2} & -\frac{k_t L_\mu}{2} & 0 & 0 \\ 0 & 0 & 0 & s_n & 0 & 0 & 0 & 0 \\ 0 & 0 & -\frac{k_t L_\mu}{2} & 0 & \frac{k_t L_\mu^2}{3} & \frac{k_t L_\mu^2}{6} & 0 & 0 \\ 0 & \frac{k_t L_\mu}{2} & 0 & 0 & 0 & 0 & \frac{k_t L_\mu^2}{3} & \frac{k_t L_\mu^2}{6} \end{bmatrix} \begin{bmatrix} u_n^i - u_n^j \\ u_t^i - u_t^j \\ u_f^i - u_f^j \\ \theta_n^i - \theta_n^j \\ \theta_t^i \\ \theta_t^j \\ \theta_f^i \\ \theta_f^j \end{bmatrix} \quad (V-17)$$

where $F_n^{j \rightarrow i}$, $F_t^{j \rightarrow i}$, $F_f^{j \rightarrow i}$, $M_n^{j \rightarrow i}$, $M_t^{j \rightarrow i}$ and $M_f^{j \rightarrow i}$ are the components of the vector of generalized forces of cohesion expressed in the local base of the beam and k_n , k_t and S_n of the matrix are the local stiffnesses, with: $K_n = \frac{E_\mu A_\mu}{L_\mu}$, $K_t = \frac{12E_\mu I}{L_\mu^3}$ and $S_n = \frac{2G_\mu I_\mu}{L_\mu}$. I_μ is the quadratic moment.

Note that the radius a_μ of the cross section A_μ of the beam depends on a dimensionless parameter r_μ , such that: $a_\mu = r_\mu \frac{R_i + R_j}{2}$. The behavior of the beam is therefore a function of the local Young's modulus E_μ and the dimensionless parameter, $r_\mu \in]0,1]$.

3.5.1 Calibration of beam properties and stress state at particle scale

The identification of the local properties of the beam, namely its normal and transverse rigidities (E_μ ; G_μ) are obtained by means of a calibration technique, which makes it possible to link the macroscopic properties of a compacted powder compact to the local parameters of the strong interparticle links.

Thus, it is possible from numerically obtained abacuses (Figure V-17) to identify the microscopic properties of the beam element in order to reproduce the behavior of a caked powder whose macroscopic properties have been experimentally characterized [42, 47]. At the end of the calibration process, local properties are thus assigned to the solid bonds of a caked powder, in order to reproduce numerically the desired macroscopic behavior. Mechanical tests of indirect tensile (Brazilian test) and shear tests were carried out using the MULTICOR3D ++ discrete element simulation tool [42] on compacts of anhydrous lactose powder. The experimental characterization tests were carried out at UTC.

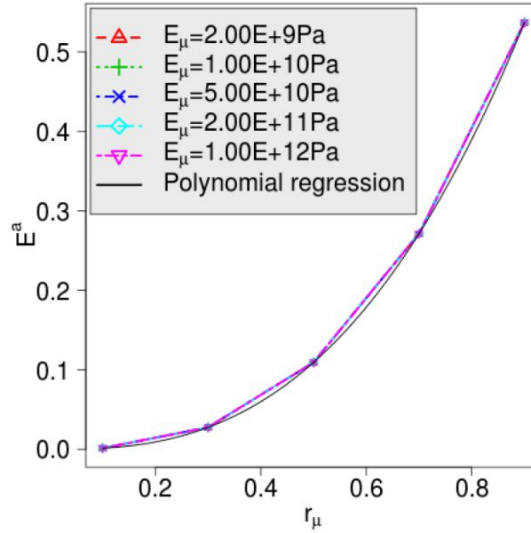


Figure V-17: Abacus of E_a as function of r_μ with E_a the ratio of macroscopic Young's modulus E_M to microscopic Young's modulus E_μ

The damage occurred during the mechanical tests in the specimen is taken into account by means of an appropriate failure criterion depending on the stress state in the particle. The cohesive links of a given particle fail when the material strength is reached. Two criteria are considered for the simulated mechanical tests. For Brazilian and shear tests, we have considered criteria based on hydrostatic stress and Mohr Coulomb model, respectively. In the case of discrete material, the virial stress does not characterize the measure for mechanical force between material points and cannot be considered as a measure for mechanical stress. Hence, we determine the stress state at the particle scale by using an equivalent Cauchy stress tensor $\bar{\sigma}_p^i$. This tensor was proposed by Zhou [48] for molecular dynamic simulations, and was used in DEM lately by Jebahi *et al.*[49]. The stress tensor is given by the following equation:

$$\bar{\sigma}_p^i = \frac{1}{2V_i} \sum_{j \in Z_i} \frac{1}{2} (d_{ij} \otimes f_{ij} + f_{ij} \otimes d_{ij}) \quad (\text{V-18})$$

with V_i the volume of the particle i , Z_i the coordination number of the particle i , d_{ij} the position vector connecting the center of the particles i and j and f_{ij} the cohesive force vector acting on the particles i and j .

The mechanical tests were conducted on samples of cylindrical shape, of diameter $D=40$ mm, thickness $e=16$ mm and volume density $\rho_v = 64\%$. The simulated compacts consist of 10^4 particles, with a mean diameter of $d_m=675$ μm . The indirect tensile and shear tests are controlled at a speed of amplitude of 1 $\text{mm}\cdot\text{min}^{-1}$. The sample sizes and the test conditions were then identical to those imposed during the experimental campaign.

3.5.2 Brazilian test

Before performing numerical the brazilian test, we have ajusted E_μ , for a given r_μ ($r_\mu \approx 0.7$), to calibrate the macroscopic mechanical behavior of the caked powder, in terms of macroscopic Young's modulus, E_M and Poisson ratio, ν_M . The solid bridges at particle scale fail when the positive hydrostatic stress exceeds the uniaxial tensile strength of the material [42]. [Figure V-18\(a\)](#) compares the numerical and experimental curves obtained in a Brazilian test. The mechanical response of the compact powder follows fairly well the experimental curve. In addition, the ultimate load reached by the sample is substantially close to that obtained during the experimental test. Also [Figure V- 18\(b\)](#) shows clearly a concentration of the tensile stress in the central zone of the sample. This type of mechanical test makes it possible to characterize the tensile strength of brittle materials. Finally, [Figure V- 17\(c\)](#) qualitatively shows the presence of particles (particles colored blue) whose interparticle bonds are broken.

This first trial demonstrated the ability of the simulation tools developed to reproduce the mechanical behavior of a cohesive multicontact system. The quality of the results obtained is, however, conditioned by the calibration step discussed previously, hence the importance of a rigorous identification of the mechanical and geometric parameters of the solid bridges. Taking into account the breaking of solid bridges, using a rupture criterion based on the hydrostatic stress measured at the particle scale [47], it was possible to simulate and follow the state of mechanical degradation of the sample at the particle scale.

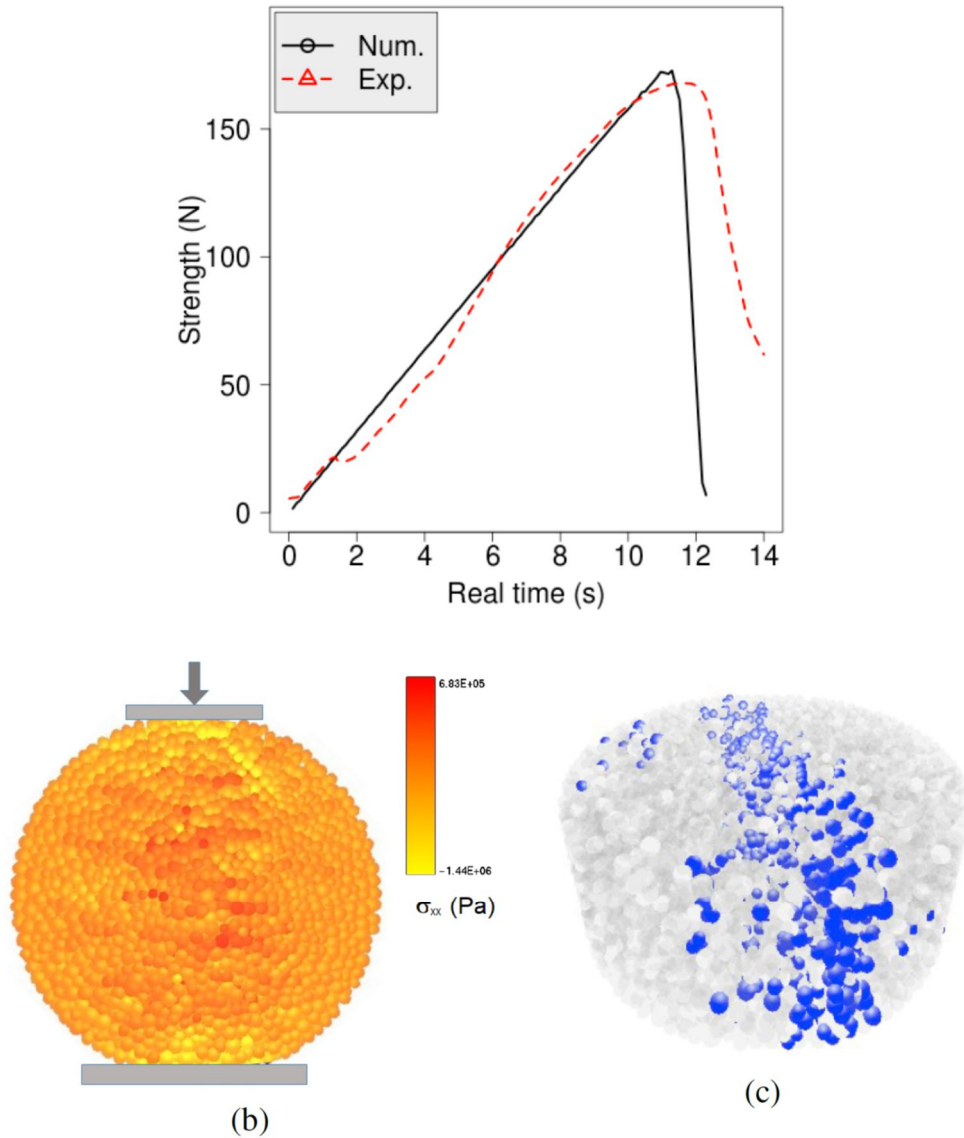


Figure V-18: (a) Comparison of the numerical and experimental compression curves; (b) tensile stress; (c) qualitative representation of the fracture during the Brazilian test

3.5.3 Shear test

The second type of simulated behavior was that obtained during a shear test on a cylindrical compact as explained in chapter II. The diameter of the sample is identical to that considered in the case of indirect traction. The particle size of the caked powder also remains unchanged, namely an average diameter of the order of 675 microns. The shear test was simulated with a speed of $1 \text{ mm} \cdot \text{mn}^{-1}$ during the mechanical test. In the case of shear test, the solid bridges created between particles fail when the Mohr Coulomb criterion is not fulfilled.

Here we just recall that the Mohr Coulomb criterion is expressed by means of a combination of shear and normal stresses, depending on the minor and major principal stresses.

The results are shown in [Figure V-19](#).

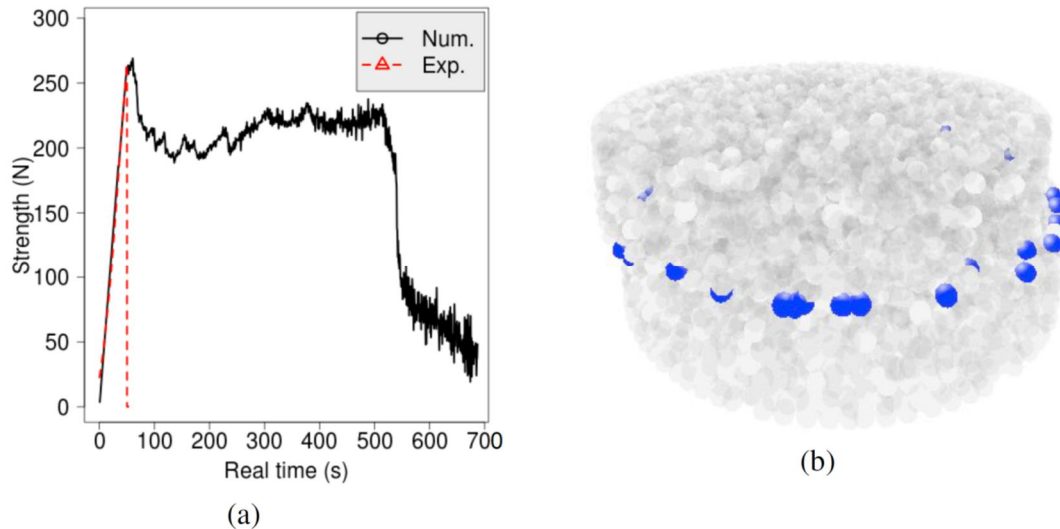


Figure V-19: (a) Comparison of the numerical and experimental shear curves; (b) Qualitative representation of the rupture during the shear test

It appears that the shear behavior obtained numerically partially reproduces that observed experimentally ([Figure V-19\(a\)](#)). Indeed, the simulated load stage is substantially close to the experimental results. Nevertheless, when the resistance capacity of the compact decreases, the behavior of the compact obtained by simulation differs significantly from that recorded during the experimental test. This difference can be caused by several factors, such as: the boundary conditions, the criteria of rupture chosen or the number of particles in the sample. The implementation of other numerical simulations would make it possible to discriminate the most influencing parameters. Further investigation is required to improve this promising method. Finally, a qualitative representation of the breaking of solid bridges is given in [Figure V-19\(b\)](#).

4 Conclusion

In this chapter, we presented the results of a study on modelling and numerical simulation of mechanical resistance of caked samples. The numerical simulations were carried out based on Discrete Element Method (DEM). The global objective of the study was to

simulate the behavior of the caked samples subjected to a mechanical, compressive or shear, stress.

First, a phenomenological model was established based on a combination of the fundamental Kelvin and Laplace laws and Rumpf model for granular media. This model allows to describe theoretically the relationships between the water activity, particle size and the packing properties on the one hand, and the degree of saturation and tensile stress on the other hand.

Then, the problem of powder caking was approached by DEM simulations. First, simulations were performed on an assembly of particles subjected to capillary forces. The phenomenological model was used as a reference to validate the numerical simulation results. After validation, numerical simulations were used to study the mechanical behavior of wet or dry cakes subjected to compression. These results constitute an important step in the description of the mechanisms activated by the relative humidity, which are at the origin of the caking of the powders. An extension to the powders in the presence of cohesive bonds in solid form was also proposed. The use of an Euler-Bernoulli beam to model the solid cohesive links and powerful numerical tools made it possible to characterize the mechanical behavior of a powder compact. The comparison of experimental results obtained by brazilian and shear tests with the numerical predictions from DEM simulations showed a good overall match between experimental behavior and simulations. These very encouraging results clearly demonstrate that the choice of a discrete approach is fully justified, on the one hand, by the intrinsic nature (granular character) of the powders, and on the other hand, by a modeling of the mechanisms of rupture at cohesive links.

References

1. Fisher, L.R. and J.N. Israelachvili, *Direct experimental verification of the Kelvin equation for capillary condensation*. *Nature*, 1979. **277**: p. 548.
2. Fisher, L.R. and J.N. Israelachvili, *Direct measurement of the effect of meniscus forces on adhesion: A study of the applicability of macroscopic thermodynamics to microscopic liquid interfaces*. *Colloids and Surfaces*, 1981. **3**(4): p. 303-319.
3. Tselishchev, Y.G. and V.A. Val'tsifer, *Influence of the Type of Contact between Particles Joined by a Liquid Bridge on the Capillary Cohesive Forces*. *Colloid Journal*, 2003. **65**(3): p. 385-389.
4. Mehrotra, V.P. and K.V.S. Sastry, *Pendular bond strength between unequal-sized spherical particles*. *Powder Technology*, 1980. **25**(2): p. 203-214.
5. Rumpf, H., *The strength of granules and agglomerates*, in *Agglomeration*, W.A. Knepper, Editor. 1962, John Wiley: New York. p. 379-418.
6. Lian, G., C. Thornton and M.J. Adams, *A Theoretical Study of the Liquid Bridge Forces between Two Rigid Spherical Bodies*. *Journal of Colloid and Interface Science*, 1993. **161**(1): p. 138-147.
7. Schubert, H., W. Herrmann and H. Rumpf, *Deformation behaviour of agglomerates under tensile stress*. *Powder Technology*, 1975. **11**(2): p. 121-131.
8. Willett, C.D., S.A. Johnson, M.J. Adams and J.P.K. Seville, *Chapter 28 Pendular capillary bridges*, in *Handbook of Powder Technology*, A.D. Salman, M.J. Hounslow, and J.P.K. Seville, Editors. 2007, Elsevier Science B.V. p. 1317-1351.
9. Shinohara, K., *Fundamental and Rheological Properties of Powders*, in *Handbook of Powder Science & Technology*, M.E. Fayed and L. Otten, Editors. 1997, Springer US: Boston, MA. p. 96-145.
10. Meissner, H.P., A.S. Michaels and R. Kaiser, *Crushing Strength of Zinc Oxide Agglomerates*. *Industrial & Engineering Chemistry Process Design and Development*, 1964. **3**(3): p. 202-205.
11. Ridgway, K. and K.J. Tarbuck, *Voidage fluctuations in randomly-packed beds of spheres adjacent to a containing wall*. *Chemical Engineering Science*, 1968. **23**(9): p. 1147-1155.
12. Lazghab, M., K. Saleh, I. Pezron, P. Guigon and L. Komunjer, *Wettability assessment of finely divided solids*. *Powder Technology*, 2005. **157**(1-3): p. 79-91.
13. D Lubachevsky, B., *How to Simulate Billiards and Similar Systems*. Vol. 94. 1991. 255-283.
14. Luding, S., *Collisions & Contacts between Two Particles*, in *Physics of Dry Granular Media*, H.J. Herrmann, J.P. Hovi, and S. Luding, Editors. 1998, Springer Netherlands: Dordrecht. p. 285-304.
15. Miller, S. and S. Luding, *Event-driven molecular dynamics in parallel*. *Journal of Computational Physics*, 2004. **193**(1): p. 306-316.
16. Cundall, P.A. and O. Strack, *A discrete numerical model for granular assemblies*. *Geotechnique*, 1979. **29**: p. 47-65.
17. Bashir, Y.M. and J.D. Goddard, *A novel simulation method for the quasi-static mechanics of granular assemblages*. *Journal of Rheology*, 1991. **35**(5): p. 849-885.
18. Lätzel, M., S. Luding, H.J. Herrmann, D.W. Howell and R.P. Behringer, *Comparing simulation and experiment of a 2D granular Couette shear device*. *The European Physical Journal E*, 2003. **11**(4): p. 325-333.
19. Kruggel-Emden, H., S. Wirtz, E. Simsek and V. Scherer, *Modeling of Granular Flow and Combined Heat Transfer in Hoppers by the Discrete Element Method (DEM)*. Vol. 128. 2006.
20. Thornton, C., S.J. Cummins and P.W. Cleary, *An investigation of the comparative behaviour of alternative contact force models during elastic collisions*. *Powder Technology*, 2011. **210**(3): p. 189-197.
21. Thornton, C., S.J. Cummins and P.W. Cleary, *An investigation of the comparative behaviour of alternative contact force models during inelastic collisions*. *Powder Technology*, 2013. **233**: p. 30-46.
22. R. Walton, O., *Explicit particle-dynamics model for granular materials*. Vol. -1. 1982.
23. Campbell, C., *Rapid Granular Flows*. Vol. 22. 2003. 57-90.

24. Gröger, T., U. Tüzün and D.M. Heyes, *Modelling and measuring of cohesion in wet granular materials*. Powder Technology, 2003. **133**(1): p. 203-215.
25. Jaeger, H.M., S.R. Nagel and R.P. Behringer, *Granular solids, liquids, and gases*. 1996.
26. M. Jaeger, H., S. R. Nagel and R. P. Behringer, *The Physics of Granular Materials*. Vol. 49. 1996.
27. Cleary, P.W. and M.L. Sawley. *Three-Dimensional Modelling of Industrial Granular Flows*. in *Second International Conference on CFD in the Minerals and Process Industries*. 1999. Melbourne.
28. Cleary, P.W. and M.L. Sawley, *DEM modelling of industrial granular flows: 3D case studies and the effect of particle shape on hopper discharge*. Applied Mathematical Modelling, 2002. **26**(2): p. 89-111.
29. Langston, P.A., U. Tüzün and D.M. Heyes, *Discrete element simulation of granular flow in 2D and 3D hoppers: Dependence of discharge rate and wall stress on particle interactions*. Chemical Engineering Science, 1995. **50**(6): p. 967-987.
30. Langston, P.A., U. Tüzün and D.M. Heyes, *Discrete element simulation of internal stress and flow fields in funnel flow hoppers*. Powder Technology, 1995. **85**(2): p. 153-169.
31. LANGSTON, P.A. and U. TUZUN, *Continuous potential discrete particle simulations of stress and velocity fields in hoppers: transition from fluid to granular flow*. Chemical Engineering Science, 1994. **49**(8): p. 1259-1275.
32. Langston, P.A., M.A. Al-Awamleh, F.Y. Fraige and B.N. Asmar, *Distinct element modelling of non-spherical frictionless particle flow*. Chemical Engineering Science, 2004. **59**(2): p. 425-435.
33. Balevičius, R., R. Kačianauskas, Z. Mróz and I. Sielamowicz, *Discrete-particle investigation of friction effect in filling and unsteady/steady discharge in three-dimensional wedge-shaped hopper*. Powder Technology, 2008. **187**(2): p. 159-174.
34. Ketterhagen, W.R., J.S. Curtis, C.R. Wassgren and B.C. Hancock, *Predicting the flow mode from hoppers using the discrete element method*. Powder Technology, 2009. **195**(1): p. 1-10.
35. Ketterhagen, W.R., J.S. Curtis, C.R. Wassgren and B.C. Hancock, *Modeling granular segregation in flow from quasi-three-dimensional, wedge-shaped hoppers*. Powder Technology, 2008. **179**(3): p. 126-143.
36. Ketterhagen, W., J. Curtis and C. Wassgren. *Modeling granular segregation during hopper discharge via discrete element methods*. in *AIChE Annual Meeting, Conference Proceedings*. 2006.
37. Norourzi, H., R. Zarghami, R. Sotudeh-Gharebagh and N. Mostoufi, *Coupled CFD-DEM Modeling: Formulation, Implementation and Application to Multiphase Flows*. 2016.
38. Golshan, S., R. Zarghami, H. Norourzi and N. Mostoufi, *Granular mixing in nauta blenders*. Vol. 305. 2016.
39. Delenne, J.Y., F. Soulié, M.S. El Youssoufi and F. Radjai, *Compressive strength of an unsaturated granular material during cementation*. Powder Technology, 2011. **208**(2): p. 308-311.
40. Kim, B.S., S.W. Park and S. Kato, *DEM simulation of collapse behaviours of unsaturated granular materials under general stress states*. Computers and Geotechnics, 2012. **42**: p. 52-61.
41. Martin, S., M. Guessasma, J. Léchelle, J. Fortin, K. Saleh and F. Adenot, *Simulation of sintering using a Non Smooth Discrete Element Method. Application to the study of rearrangement*. Computational Materials Science, 2014. **84**: p. 31-39.
42. Leclerc, W., *Discrete element method to simulate the elastic behavior of 3D heterogeneous continuous media*. International Journal of Solids and Structures, 2017. **121**: p. 86-102.
43. Lubachevsky, B.D. and F.H. Stillinger, *Geometric properties of random disk packings*. Journal of Statistical Physics, 1990. **60**(5): p. 561-583.
44. André, D., I. Iordanoff, J.-I. Charles and J. Néauport, *Discrete element method to simulate continuous material by using the cohesive beam model*. Computer Methods in Applied Mechanics and Engineering, 2012. **213-216**: p. 113-125.

45. Haddad, H., M. Guessasma and J. Fortin, *A DEM–FEM coupling based approach simulating thermomechanical behaviour of frictional bodies with interface layer*. International Journal of Solids and Structures, 2016. **81**: p. 203-218.
46. Gagneux, G. and O. Millet, *Analytic Calculation of Capillary Bridge Properties Deduced as an Inverse Problem from Experimental Data*. Transport in Porous Media, 2014. **105**(1): p. 117-139.
47. Leclerc, W., H. Haddad and M. Guessasma, *On the suitability of a Discrete Element Method to simulate cracks initiation and propagation in heterogeneous media*. International Journal of Solids and Structures, 2017. **108**: p. 98-114.
48. Zhou, M., *A new look at the atomic level virial stress: on continuum-molecular system equivalence*. Proceedings of the Royal Society of London. Series A: Mathematical, Physical and Engineering Sciences, 2003. **459**(2037): p. 2347-2392.
49. Jebahi, M., D. André, F. Dau, J.-l. Charles and I. Iordanoff, *Simulation of Vickers indentation of silica glass*. Journal of Non-Crystalline Solids, 2013. **378**: p. 15-24.

General conclusions and perspectives

In this work we studied the caking of polymorphic powders following the different phase changes that may occur within the particles or the granular medium. Lactose was used as a representative model of polymorphic products. Despite its relatively simple chemical formula and well-established molecular structure, lactose is a complex product with at least five solid polymorphs and many possible phase transitions. The initial objective of this work was to study and model the caking process of amorphous powders (or containing an amorphous phase fraction) following the phenomenon of creeping that can take place above the glass transition temperature. This phenomenon has recently been described in the literature as the main cause of caking of this category of products. However, the phenomena involved found to be much more complex than just creeping. More precisely, our study has highlighted the preponderant role of the crystallization phenomenon and the transitions taking place between the different polymorphs of lactose. Thus, emphasis has been placed on the role of crystallization phenomena and phase transition on the advent of lactose powder caking. Two cases attracted particular attention:

- lactose monohydrate powders containing a fraction of amorphous particles
- anhydrous powder samples composed of α and β anomers of lactose.

In both cases, the caking was induced by exposure of the samples to moist air, either in a Dynamic Vapor Sorption device (SPS) or in accelerated caking tests using two home-made equipment (CLAIR & OLAF). Our results showed that in both cases, the main cause of caking was the formation of lactose monohydrate, which is the most stable form among all lactose polymorphs. However, the elementary mechanisms, the limiting steps and the kinetics of the transformation process are different in each case.

Chapter I of the manuscript introduced the main powder characteristics and the basic mechanisms responsible for caking of powders. The main categories of caking and the associated underlying mechanisms were described in detail in this chapter. The literature survey carried out on the structure of materials has highlighted the complexity of phase transition phenomena and the crucial role of the glass transition phenomenon in the caking process of polymeric materials. The focus was then put more specifically on lactose and its

properties. It follows that this molecule, a priori simple, has an impressive polymorphism that can be declined in 5 (and even 7 according to some authors) different forms. The last part of this chapter deals with the methods of caking assessment reported in literature.

In Chapter II, we presented the set of materials and methods used to characterize the properties of the tested products, fresh or caked, as well as the experimental devices designed and assembled specifically for the needs of the study. Given the complexity of the products and the phenomena involved, a large number of instruments and tests was necessary to draw clear and relevant conclusions on the evolution of powders during caking. Since there is no universal caking test, the tests used and associated protocols could be adapted on a case-by-case basis.

In chapter III, we investigated the caking behavior of lactose monohydrate powders containing small amounts of amorphous lactose. The objective of this study was to point out the role of the crystallization of amorphous lactose on the caking ability of powder mixtures. In this objective, an accelerated caking test was used to investigate the caking behavior of binary mixtures consisting of amorphous lactose and α -lactose monohydrate. Because it is almost impossible to produce powders with controlled amount of amorphous phase, the amorphous lactose samples were prepared using both freeze-drying and spray-drying techniques and then mixed with lactose monohydrate samples. Two caking devices were used to characterize the caking ability of powders. The effect of amorphous content, relative humidity, temperature and pressure on the caking behavior of samples was investigated. The results showed that the presence of even small amounts of amorphous lactose (as low as 0.125%) leads to caking. The more influencing parameters were the relative humidity and the temperature whereas the pressure has no significant effect. The yield stress of caked samples was closely linked with crystallization extent and kinetics. A dimensionless time based on the ratio of real time and characteristic time of crystallization (according to Avrami's model for crystallization rate) was defined allowing unifying the experimental data.

Chapter IV dealt with the phase transition of anhydrous Lactose in solid-state due to humidification and subsequent crystallization of anhydrous lactose when exposed at humid atmospheres. Experimental evidence was brought that anhydrous lactose is converted to lactose monohydrate when exposed to ambient moisture. The conversion rate and the kinetics of the lactose transformation from anhydrous to monohydrate state was then

investigated at various temperatures and RH varying between 15 and 40°C and 70% to 95% RH, respectively. The results showed that the kinetic rate and consequently the fractional conversion of anhydrous lactose increases with the increase of the relative humidity and the temperature. A phenomenological model to describe the rate of transformation was also developed and a kinetic law based on the comparison between the experimental data and the model was established. Further analysis of experimental data showed that the limiting step of the transformation process was the solid-state crystallization of anhydrous β -lactose. Apparent rate constants of crystallization at different temperatures as well as the activation energy of the reaction were calculated. In the second part of this chapter, the effect of storage conditions on the caking behavior and kinetics of anhydrous lactose in relation with its solid-phase crystallization were studied. The results showed that crystallization was the main factor influencing the caking of anhydrous lactose powders. Four major categories of caking were distinguished, namely, non-caking, very soft caking, soft caking and hard caking. The key parameter regarding the extent of caking was the fractional conversion of anhydrous lactose. Hard cakes were obtained at fractional conversion higher than about 8%. Their yield strength increased steadily until it reached a conversion of about 15-17%, then stagnated beyond that limit. As for soft cakes, they appear beyond 4% conversion.

Chapter V presented the results of numerical simulation (based on Discrete Element Method: DEM) of mechanical resistance of caked samples. The aim of this part was to simulate the behavior of the caked samples subjected to compressive or tractive mechanical stresses. First, a phenomenological model to describe the role of capillary condensation phenomenon on caking was established. DEM simulations were then carried out considering an assembly of particles subjected to capillary forces. The simulation results were validated by comparing them with those obtained by the phenomenological model for a wet cake subjected to a tensile stress. Once validated, numerical simulations were used to study the mechanical behavior of wet or dry cakes subjected to compression. The stress-strain curves were then simulated and compared to the results of failure tests on lactose samples. A good qualitative agreement between simulation and experimental data was found.

To complete this work, several areas of development can be suggested for further studies:

- Regarding the experimental caking devices, the implementation of smaller cells, requiring a smaller amount of sample while remaining representative, may allow to adapt the device to areas for which there is little product (e.g. the pharmaceutical field). The OLAF device is equipped with a level measuring probe to follow the evolution of sample consolidation during caking as well as pressure, temperature and relative humidity sensors to measure the pressure drop of the bed as well as T and RH conditions at the entry and exit of the bed of powder. In this work, we have not been able to take advantage of all the capabilities of this equipment. However, it is obvious that such data is a valuable source of information that deserves to be analyzed and exploited later.
- As for the yield strength test, other compact geometries or compression tips should be designed for better repeatability of the results. Indeed, the diametric test, however widely used in the literature, suffers from a lack of sensitivity and repeatability. This is due to the small contact interface between the compacts and the compression plates (limited to a contact line at the beginning of the test) as well as the random nature of the appearance of the cracks, which initiate the rupture of the compact. The use of a flattened geometry (at the top and at the bottom) for the compacts or the use of punches having an incurved shape (conforming to the shape of the compacts) instead of flat plates then makes it possible to increase the surface of contact and improve the repeatability of measurements. According to the literature, the use of a crown geometry (instead of disc) also leads to more reproducible results due to a better control of the appearance of cracks.
- Similarly, the use of the RAMAN probe during the DVS tests could provide very useful information on the evolution of the molecular structure of samples. Nevertheless, it is a very special technique, requiring in-depth knowledge of the subject in order to be able to interpret conveniently the RAMAN spectra.
- Finally, in the case of caking of amorphous products by creeping, Dynamic Mechanical Thermal Analysis (DTMA) can provide a valuable help in quantifying the

viscoelastic characteristics of the product and thus contribute to a better understanding and a more reliable modeling of the phenomena involved.

- As regards the caking of lactose containing a quantity of amorphous phase, it is necessary to study the caking phenomenon below the glass transition but under conditions where crystallization cannot take place. According to the lactose phase diagram, there is a restricted range of operating conditions (T and RH) where this condition can be met. This then makes it possible to study the caking phenomenon due to the creep mechanism alone.
- In addition, in this work, the influence of the amount of amorphous lactose has been studied by incorporating artificially pure amorphous lactose into binary mixtures of amorphous and monohydrate lactose. In practice, amorphous lactose is found in small amounts on the surface of solid particles. It is indeed difficult, if not impossible, to prepare lactose samples with a peripheral layer of the amorphous phase of controlled thickness. However, it is conceivable to coat inert particles (glass beads or sand, for example) with an amorphous layer of lactose (by immersion in a concentrated solution and freeze-drying). Since lactose monohydrate is stable, caking results exclusively because of the amorphous phase and its replacement by inert particles should not influence the phenomena. This procedure makes it possible to avoid the dissolution of the support during the imbibition but also the interference of XRD and RAMAN spectra.
- It would be interesting and useful to study the influence of temperature and relative humidity on the kinetics of crystallization over a wider range than that used in our study. It will then be possible to study and simulate the behavior of powder at conditions different from those used.
- As for the caking of anhydrous lactose, it remains to elucidate the reasons for the rapid rise in conversion at the beginning of the operation. Indeed, the in-depth analysis of our data shows that the most plausible hypothesis to explain this initial increase is the

crystallization of the α anomere, much less stable than the form β . Nevertheless, the amount of lactose converted remains lower than the theoretical amount of the α anomere. Then, the amount of phase α at the interface should be distinguished from that existing within the particles. Low-depth chemical analyzes should confirm or refute this hypothesis.

- The kinetic laws and associated constants established in chapter IV correspond to an global (apparent) kinetics of the transformation process. They do not take into account the intrinsic kinetics of the mechanisms and phenomena coming in play (diffusion, adsorption, crystallization, evaporation, etc.). A phenomenological modeling of the process integrating all these phenomena is necessary to evaluate their relative importance under given conditions. This modeling work was started and well advanced but not sufficiently finalized yet at the time of this writing. It will be the subject of a post-thesis article.
- Regarding the numerical simulation, the first results are promising. After having been validated on the case of capillary bridges, it was applied for dry cakes (solid bridges). The results are in fairly good agreement with the experiment for the linear part of the compression curve. On the other hand, they do not allow predicting the behavior of the cakes after the first rupture. This is a point that needs to be addressed in future work. This numerical model is an excellent tool to compare the different compression tests (diametral, uniaxial, shearing) to bring improvements on the experimental protocol or on the geometry of compacts. It becomes also possible to study the influence of local heterogeneities (scale of the particle) on the response of these tests.

Appendix A

MorphologiG3:



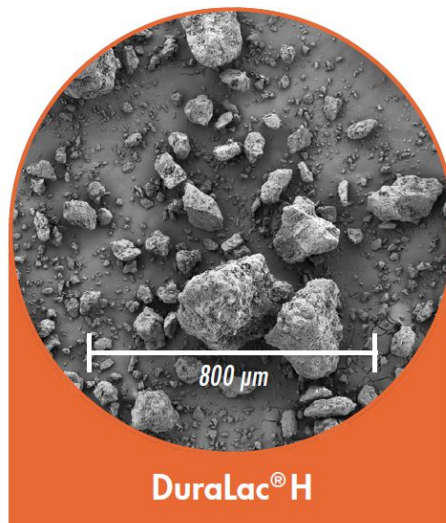
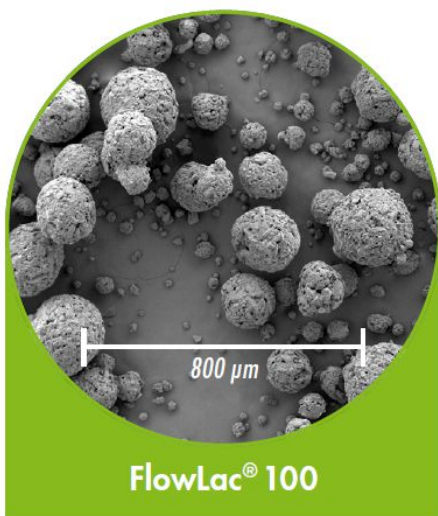
An excerpt from the "User Manual" from
Malvern Pananalytical

Appendix B

Technical Brochures of lactose samples from
Meggles:

FlowLac® 100

DuraLac® H



Appendix C

Technical Data:

BÜCHI

Mini Spray Dryer B-290

